# ADVANCES IN SELECTIVE CATIONIC α-DIIMINE NICKEL CATALYSTS: ACCESS TO POLYOLEFIN MATERIALS AND MECHANISTIC INSIGHTS INTO CHAIN WALKING POLYMERIZATION

A Dissertation

Presented to the Faculty of the Graduate School

of Cornell University

In Partial Fulfillment of the Requirements for the Degree of

Doctor of Philosophy

by

Kyle Seamus Joseph O'Connor

August 2017

# ADVANCES IN SELECTIVE CATIONIC α-DIIMINE NICKEL CATALYSTS: ACCESS TO POLYOLEFIN MATERIALS AND MECHANISTIC INSIGHTS INTO CHAIN WALKING POLYMERIZATION

Kyle Seamus Joseph O'Connor, Ph. D.

Cornell University 2017

Karl Ziegler and Giulio Natta's landmark discovery of heterogeneous catalysts for olefin polymerization ushered in a new era of polymer chemistry. Materials such as polyethylene, isotactic polypropylene, and polyolefin elastomers were commercialized from their new technology and have drastically impacted modern life. Following Ziegler and Natta's discovery, researchers made significant strides in developing single site homogenous catalysts that exhibit superior control over polymer molecular weight, tacticity, and block architecture.

One class of homogenous catalysts that has received much attention over the past two decades are the α-diimine late metal systems based on nickel and palladium. A unique mechanistic feature to late metal catalysts is a phenomenon known as "chain walking," where β-hydride elimination and metal-hydride reinsertion events move the catalyst along the growing polymer chain. This mechanism allows for a wide variety of architectures to be accessed from simple olefin feedstocks. Chapter one discusses the development of late metal complexes, focusing primarily on regioselective nickel systems that can "chain-straighten" α-olefins into linear "polyethylene," and understanding the polymerization mechanism.

Chapter two focuses on the utilization of a 2,1-regioselective nickel complex capable of forming block copolymer thermoplastic elastomers from ethylene and α-olefins. The effect of block architecture, polymerization solvent, and the ratio of α-olefin versus ethylene incorporation on the resulting polymer tensile properties is studied. The mechanism behind the loss of elastic recovery after strain deformation is also discussed.

Chapter three discusses the mechanistic analysis of branch incorporation through the study of $^{13}$C-labeled poly(α-olefins) produced using a variety of α-diimine nickel catalysts. A mathematical model is developed to deconvolute and quantify the resulting spectra. Eight unique insertion pathways are identified, quantified, and discussed. The effect of catalyst and polymerization conditions on the ratios of the eight insertion pathways are studied.

Chapter four focuses on the development and use of α-diimine nickel catalysts capable of the regio- and isoselective polymerization of 1-butene, yielding new semicrystalline polyolefins. The effect of catalyst and polymerization conditions on the properties of the resulting polymer is studied. The rationale for the observed isoselectivity is also discussed.

## BIOGRAPHICAL SKETCH

Kyle Seamus Joseph O'Connor was born on November 3rd, 1990 in Huntington Hospital on Long Island, NY. At the early age of three, before he could even read, Kyle was completing video games on the NES (Legend of Zelda and Super Mario 2 being the earliest games he conquered), forging a life-long love for the entertainment medium. In retrospect, his parents probably should have limited his screen time at that age, but it did instill a powerful desire in Kyle to take on increasingly more difficult challenges (also, a mild obsession with Nintendo).

At the beginning of 3rd grade, Kyle and his family moved to a small town on the north shore called Rocky Point, where he spent most of his formative years. With the beach a mere five-minute walk from his childhood home, he developed a love of the sea at an early age. He developed an interest in music, playing the trumpet in marching and concert band throughout middle and high school, and eventually leading the Mellophone section of the band in college. He also became a runner, joining the track and cross-country teams in high school. Kyle managed to run a 5:09 mile in his last race of senior year (and has never been able to match that time since).

Kyle's interest in chemistry developed more slowly. Oddly, it was after he received a 69 on his first chemistry exam in high school, the worst grade he had ever received at that point, that he became interested in the subject (this masochistic dedication to overcoming hurdles in chemistry would become essential in his grad school days). His future career path was truly decided, though, when his high school chemistry teacher, Mr. Nobre, dropped a gummy bear in a molten solution of potassium chlorate, generating a mini-firework show of combustion. Kyle wanted to learn the secrets of this sorcery.

Kyle continued pursuing chemistry knowledge at Stony Brook University, but, as he was a somewhat typical 18-year-old, he had absolutely no idea what he really

wanted to do with his life. It was then that Kyle met his long-time partner, Molly (who was equally clueless about what to do with her life, but knew that she wanted Kyle in it, wherever that took her) who has stuck by him through the best and worst of the grad school experience. He was on the pre-med track for a couple of years when it dawned on him that he wasn't passionate about medical school or the terrible debt it would bring. Though he briefly considered switching to a music major, at this point, Kyle was introduced to organic chemistry for the first time and found himself truly captivated. He became a teaching assistant for the course in his junior year and ended up performing research for the first time with Professor Lauher in his senior year.

Although he was a little late to the research game, Kyle found himself enjoying lab work and wanted to continue his academic pursuit of chemistry. That is when he found out about graduate school and how it was not only free to attend, but most programs paid the student to attend (for STEM majors, as his Liberal-Arts girlfriend is always quick to remind him)! Kyle applied to several graduate programs; while he was accepted to all of them, he was most excited to be accepted to Cornell University.

Kyle accepted Cornell's offer and travelled upstate to Ithaca, NY. As a native Long Islander, one of his earliest Ithaca lessons was learning that anything north of Manhattan was not necessarily "upstate," (Ithaca is central NY. NY is a big place!). After confronting the fact that his previous academic work was a breeze compared to graduate school, he joined the Coates group in 2012 and learned more about chemistry than he ever thought possible. In between the long hours in lab, he enjoys exploring the natural beauty of Ithaca, eating and drinking in one of Ithaca's many excellent restaurants, and dancing up a storm with friends and Molly (or strangers—in dancing, Kyle doesn't discriminate). He is immensely grateful for the opportunity to study and work at Cornell University and looks forward to the future ahead.

Dedicated to my partner in crime, Molly

ACKNOWLEDGMENTS

First, I would like to thank my advisor Geoff Coates for his support throughout graduate school. He gave me the freedom to intellectually grow and pursue curiosity-driven projects. He also taught me how to critically assess research and present my work in a way that is visually stimulating and easily accessible. I will always be grateful for having the opportunity to work in his group. I would also like to thank both my committee members, Brett Fors and Kyle Lancaster for their presence and support throughout graduate school. Additionally, I would like to thank my former A-exam committee member, Will Dichtel, who was a rock star at Cornell and will certainly continue to be so at Northwestern.

I want to thank my funding source for the past few years, the Center for Sustainable Polymers. It was likely luck that got me funded through the center, but I am very grateful it worked out this way. I had the opportunity to meet and collaborate with great people at the University of Minnesota (Annabelle Watts, Angelika Neitzel, and Marc Hillmyer). Being part of the Center gave me the opportunity to present my work to a broader audience and helped develop my communication skills. Also at Cornell, very many thanks to Ivan Keresztes for his boundless NMR knowledge and assistance.

Thanks so much to my whole family for their support during my time at Cornell. I didn't appreciate how much pride you guys had in me for being the first scientist in the family until recently. To all my siblings, Kelly, Courtney, James, Kaitlyn, and Madeline, I feel incredibly lucky to be your brother–and I also feel so lucky to be an uncle to Eve, William, Edie and Imogen, four of the brightest kids (and future scientists!?) I know. Mom and Dad, you liked to say I would be a doctor someday, though you probably weren't expecting this kind of doctor! And to my second parents, John and Loretta, you both have always made me feel so welcome in your home. Thank you for your support throughout grad school.

I want to thank Nate Van Zee for doing a great job hosting me on visitation weekend and convincing me to come to Cornell. We ended up not only being group mates, but 562 lab mates (I promise I wasn't stalking him). He taught me Schlenk technique and a lot of basic lab knowledge that I still use to this day. Thanks to Angie DiCiccio for always being so cheerful and making me feel completely welcome in the group in my first year. She left candy and chocolate on my desk with a note wishing me luck on my first day of giving group meeting. Such kindness was well appreciated.

I want to thank Kristina Hugar as well. My graduate school experience was really enriched by her presence as my lab mate, colleague, and friend. We danced it up like nobody's business in and out of the lab, ran many miles together, and discussed all matters of things. Speaking of dancing, I also must thank Tulaza Vaidya, my "dancing enantiomer." Her contributions as a post-doc in the Coates group laid the ground work for much of my thesis, which I will always be grateful for.

I'm not sure if she knows it, but Jessica Lamb has consistently inspired me to work harder throughout grad school. I have met few people in my life as intelligent and motivated as her, traits that were beyond helpful in writing that mechanism paper together! She also helped me get on Geoff's radar by suggesting I would be a good fit in the group. Every bit counts, so thank you for doing that.

Then there's Dave Vaccarello. We lived together for the first year of grad school, commiserating with each other on how hard things were while watching Beast Wars at night in our minimally furnished apartment. We had discussions throughout the years (usually when things in lab weren't going particularly well) about opening a Chemistry-themed bar called "The Laboratory" or opening a private-tutoring business. I think we did a good job motivating each other and making it to the finish line. Thanks Dave, and who knows, maybe we will pursue those small business dreams someday!

Thanks to Kelly Case for keeping the lab running and always being a great person to talk to (and watch videos of panda bears with). Many great conversations about science and life with Maria Sanford, the hardest working person in the Coates group (no joke, she's the best). Thanks to Anne LaPointe for being a bastion of knowledge and experience, proving to be immensely helpful throughout grad school. James Eagan is a genuinely impressive person and a role model for me in many ways (especially those karaoke skills). Thanks to the entirety of the 562 office: Omar Padilla Velez, Ting-Wei Liu, and Bryce Lipinski. You young punks are all awesome and represent the future of the Coates group! And you, Omar, are the future of team polyolefins (you got this, dude)! And thank you Ahmed Ahmed, the Rhodes Scholar, my undergrad, the dude that brought such positive energy to the lab. It was an honor being your mentor and I look forward to seeing the impact you have on the world.

There are also a few inanimate things in life that kept me animated throughout grad school. For the most part, those things were food, beverages, and entertainment platforms. In no particular order: Sony, Nintendo, Martha's (best chicken spinners), Manndibles Café (that Indian curry), ~~covfefe~~ coffee, Agava (countless trivia nights, margaritas, and their burgers), Ithaca Beer Company (a rather beautiful place to drink outside), whiskey, Planet Fitness, nature, Anime (proudly a nerd), streaming services, Chapter House (RIP), Silky Jones, Turquoise Jeep, slack lining, running, and Wegmans!

Last but not least, I would like to thank my partner of 7+ years, Molly Gelinas. I genuinely don't think I would have completed the Ph.D. without her love and support. She has witnessed the ups and downs of this crazy thing called grad school and she has stuck by me through it all. Life is so much brighter with her in it. There are few words to express my love and gratitude for her. I am beyond excited to start our next adventure together in Stamford, Connecticut!

## TABLE OF CONTENTS

## LIST OF FIGURES

## LIST OF SCHEMES

## LIST OF TABLES

# CHAPTER 1

# DEVELOPMENT OF CATIONIC LATE METAL CATALYSTS FOR THE REGIOSELECTIVE POLYMERIZATION OF α-OLEFINS

## *1.1 Introduction*

Polyolefins dominate the global market share for commodity polymers, with polyethylene (PE) and isotactic polypropylene (*i*PP) representing the world's number one and number two polymers by volume, respectively.[1] Karl Ziegler[2] and Giulio Natta's[3] landmark discovery in 1955 of heterogenous mixtures of metal alkyls and transition metal salts capable of the polymerization of ethylene and propylene ushered in a new era of polymer chemistry. Their discovery sparked vast economic growth, inspired intensive research programs worldwide, and resulted in the production of new commercial thermoplastics and elastomeric materials that have drastically impacted modern life.[4]

In the decades following Ziegler and Natta's discovery, significant strides were made by researchers toward the development of single site *homogenous* catalysts for

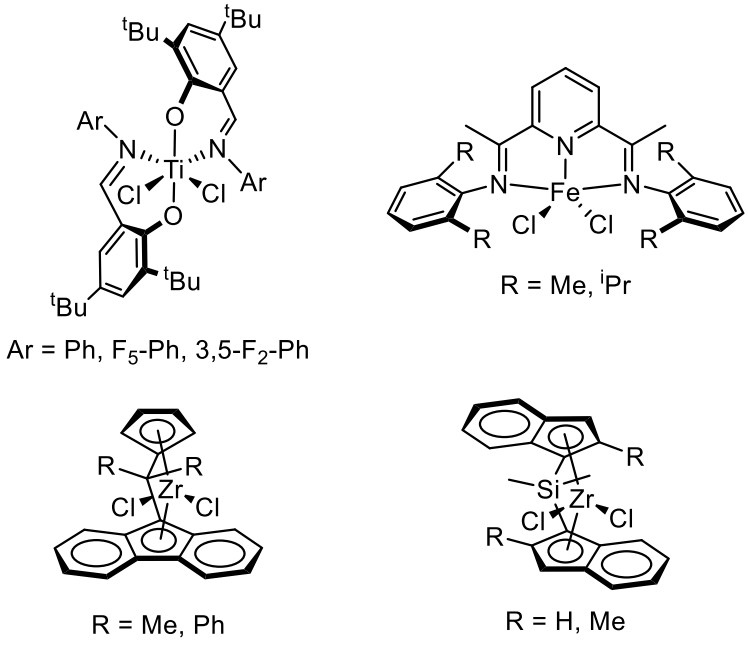


**Figure 1.1** Representative single site catalysts used for the stereoselective polymerization of propylene.

olefin polymerization.[5] These systems offer advantages over traditional Ziegler/Natta *heterogenous* catalyst systems in terms of control over molecular weight, tacticity, and overall polymer microstructure (Figure 1.1).[6] The earliest advancements in single site olefin polymerizations were realized with the advent of methylaluminoxane (MAO) activated[7] metallocene catalysts. The development and application of these metallocene systems for the synthesis of polypropylenes with tacticity, as well as block copolymers have been extensively reviewed.[8] Additionally, several post-metallocene catalyst systems have also been extensively explored.[9]

Late transition metal catalysts based on nickel and palladium were later studied for olefin polymerization. In the late 1970s, Royal Dutch Shell commercialized a process for the synthesis of α-olefins from ethylene using a nickel-based catalyst, known

**Scheme 1.1** Shell Higher Olefin Process (SHOP) Catalytic Cycle

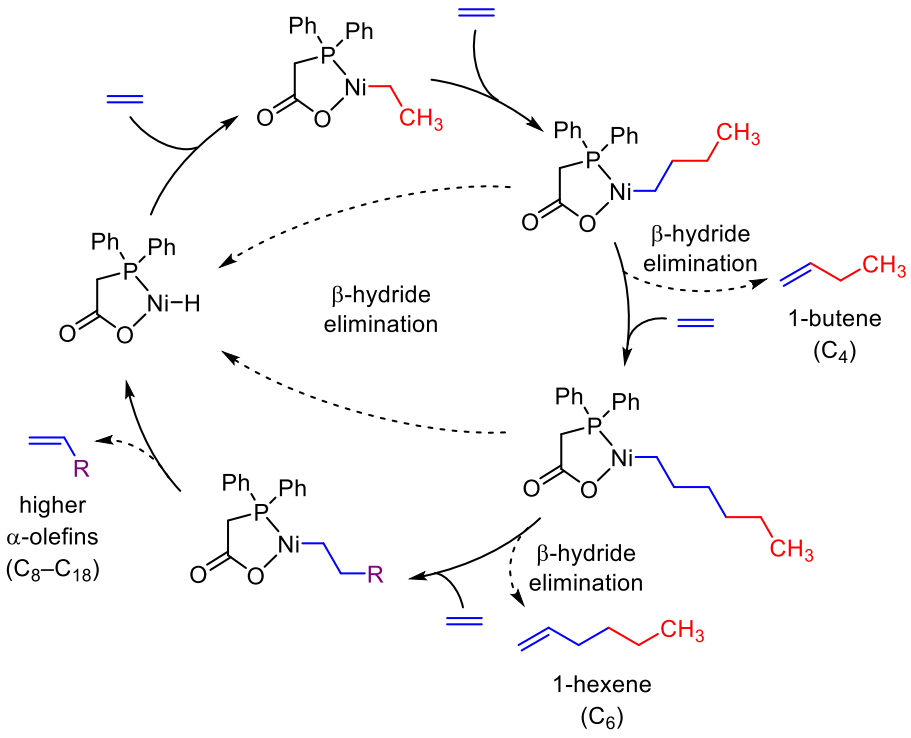

as Shell's Higher Olefin Process (SHOP).[10] Short oligomers ($C_4$–$C_{18}$), as opposed to polymeric materials, are efficiently produced due to a rapid β-hydride elimination and dissociation event that occurs during propagation (Scheme 1.1). This catalytic cycle is important for the production of α-olefins that can further be used as comonomers in ethylene polymerizations[11] or converted into precursors for plasticizers and detergents through subsequent processes.[12] However, by nature of the rapid β-hydride elimination event and dissociation of the α-olefin, this system cannot access high molecular weight polymers.

## *1.2 Discovery of Late Metal Catalysts for Olefin Polymerization*

In 1995, Brookhart and coworkers published their seminal discovery of cationic nickel(II) and palladium(II) catalysts capable of the polymerization of ethylene and α-olefins to produce high molecular weight polymers.[13] Critical to their success was in the design of the α-diimine ligand framework. Brookhart found that α-diimine catalysts with sterically bulky isopropyl substituents were effective at producing high molecular weight polymers. In contrast, catalysts that possessed less sterically bulky methyl substituents were only capable of producing low molecular weight oligomers. It was rationalized that sufficient steric bulk in the axial sites of the metal center prevented associative displacement of the olefin-metal-hydride species with exogenous monomer (Scheme 1.2). Reinsertion of the metal alkyl after β-hydride elimination can subsequently occur, allowing for continued polymer propagation.[14] Over the past two decades since their discovery, late metal olefin polymerization catalysts have been

intensely studied and used for the synthesis of a wide range of polymer architectures with interesting properties.[15]

**Scheme 1.2** Associative Displacement of Growing Polymer Chain with Sterically Unhindered α-Diimine Catalysts

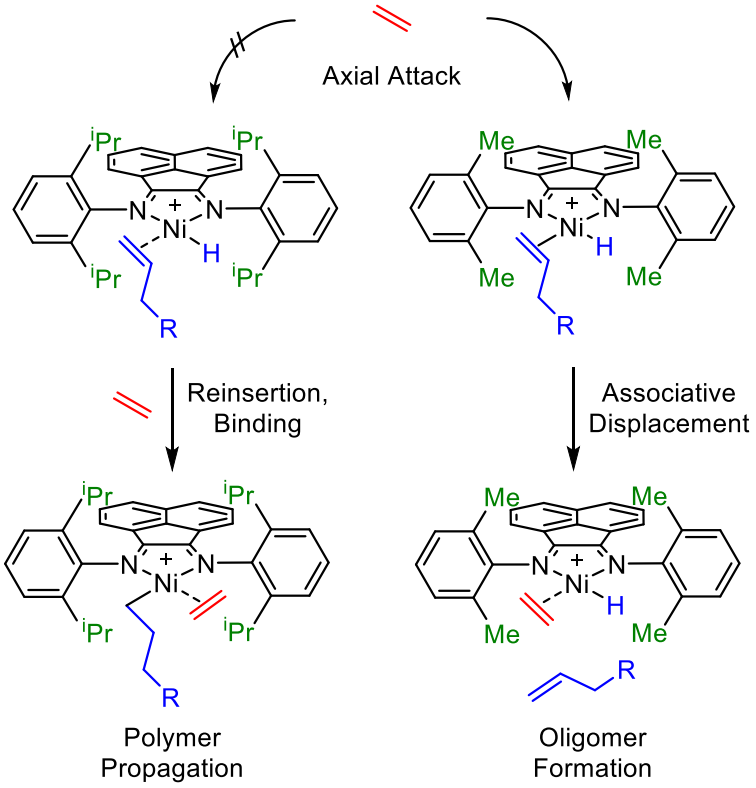


## *1.3 Chain Walking Polymerization*

One of the key mechanistic features of olefin polymerizations using late metal catalysts is an isomerization even known as "chain walking." This phenomenon was first reported by Möhring and Fink in the late 1980s, using an iminophosphonamide nickel complex for α-olefin polymerization.[16] Contrary to early metal catalyst systems (Ti, Zr, Hf) which do not readily undergo β-hydride elimination, late metal catalyst systems (Ni, Pd) perform facile β-hydride elimination. With sufficient blocking of the

axial substituents, the olefin remains bound to the metal hydride species and can subsequently reinsert into the growing polymer chain. Rotation of the olefin before reinsertion can result in the metal center positioned one carbon over from its original position before the initial β-hydride elimination (Scheme 1.3). This process can repeat many times before the next monomer insertion event, which effectively moves the metal center to various positions along the polymer backbone. Depending on the relative rates of chain migration vs olefin insertion, various microstructures can be generated from simple olefin feedstocks.[17] For example, high pressures (or concentrations) of monomer will increase the rate of insertion over chain isomerization, leading to more linear materials. Conversely, low pressures (or concentrations) of monomer will increase the relative rate of chain isomerization over insertion, potentially leading to highly branches or even hyperbranched materials (Scheme 1.4).

**Scheme 1.3** Chain Isomerization in Late Metal Catalysts

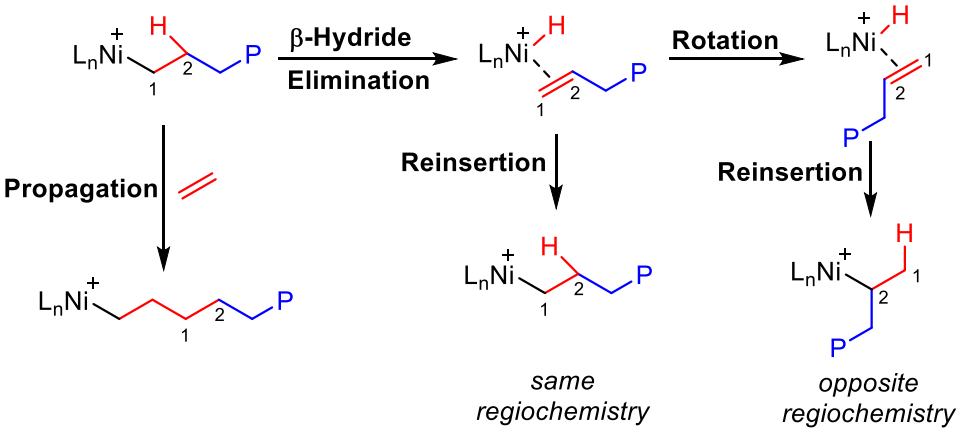

**Scheme 1.4** Examples of Possible Architectures from Chain Walking Polymerization (Image Adapted from Reference 17a)

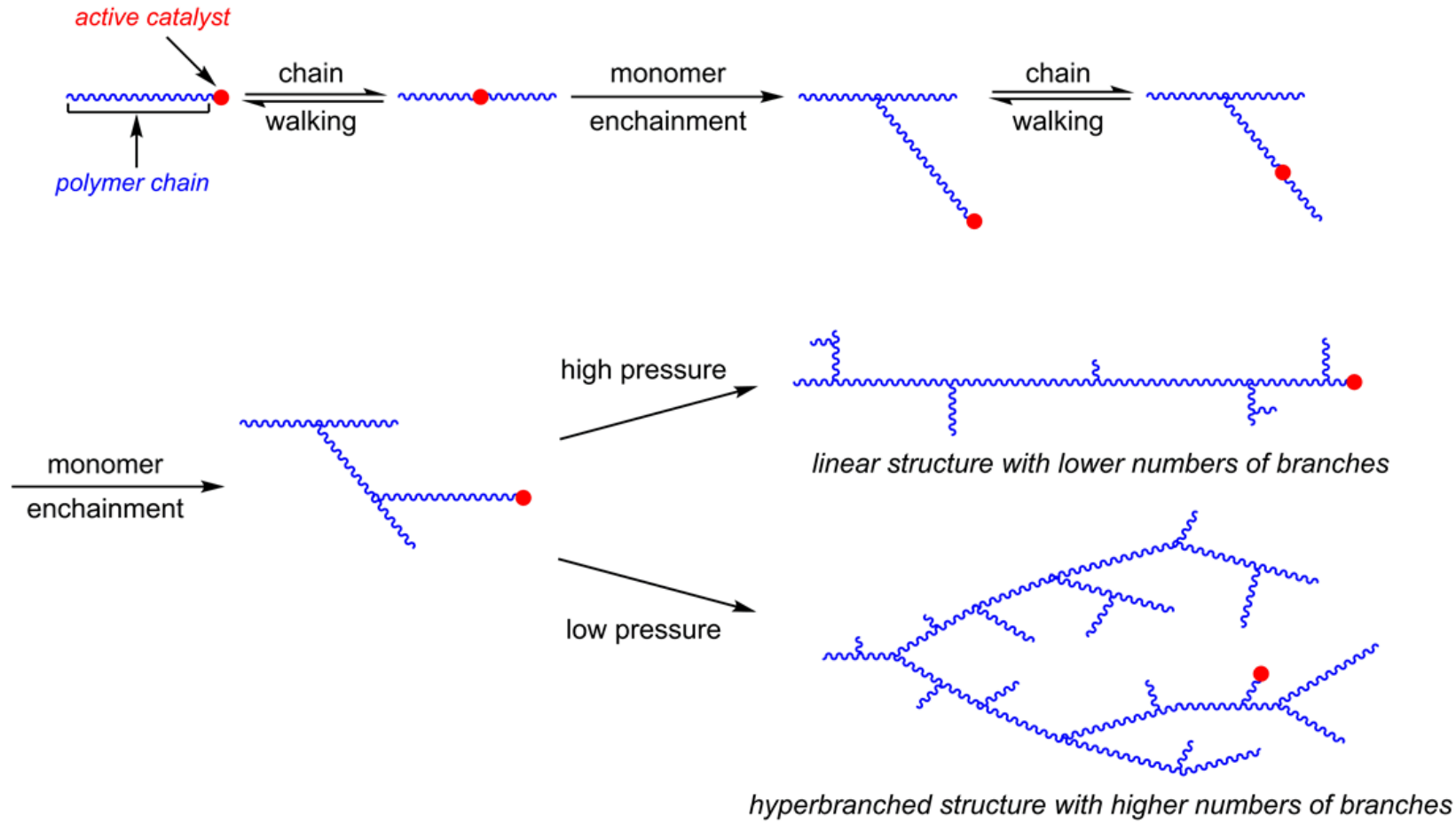

## *1.4 Mechanistic Studies of Ethylene Polymerization using Late Metal Catalysts*

### *1.4.1 Ethylene Polymerization using α-Diimine Palladium Complexes*

Brookhart pioneered several detailed mechanistic studies on the chain walking polymerization of ethylene using α-diimine late metal catalysts, the first major study focusing on well-defined palladium alkyl complexes.[18] It was determined that the catalyst resting state is the alkyl–palladium–ethylene complex, suggesting that turn over frequency (TOF) is controlled by the rate of migratory insertion of these species (Figure 1.2). For that reason, the rate of chain growth is independent of the concentration of ethylene in solution. Dynamic β-agostic interactions from the alkyl–palladium complex were also observed by variable temperature $^{1}$H NMR spectroscopy. Brookhart measured the energetic differences between chain isomerization and migratory insertion and discovered a 2.5–3.0 kcal/mol difference in favor of chain isomerization.[18] Interpretation of this difference suggests that a palladium catalyst will perform an average of 100 chain isomerizations before migratory insertion, which explains why polyethylene produced by palladium α-diimines is so highly branched (>100 branches/1000 carbons). Hyperbranched polyethylene structures can even be achieved using low pressures of ethylene, allowing access to complex polymer architectures with interesting properties.[19]

### *1.4.2 Ethylene Polymerization using α-Diimine Nickel Complexes*

Mechanistic analysis of ethylene polymerization using nickel α-diimine catalysts was performed by Brookhart and coworkers in 2003, after challenges in the synthesis of a stable well-defined nickel-alkyl species was overcome.[20] Through this study, several interesting comparisons were made between the nickel and palladium α-diimine systems. First, the migratory insertion barrier for nickel α-diimine complexes is 4–5 kcal/mol lower than the palladium analogs, accounting for the significantly increased TOFs in nickel systems. Second, the β-hydride elimination barrier in nickel systems is significantly higher (14 kcal/mol) than in palladium systems (≈ 7 kcal/mol).[21] The slower migration of nickel along the polymer backbone allows for conditions such as monomer concentration and temperature to affect the resulting number of branches. Increasing the concentration of ethylene promotes monomer trapping, thus favoring migratory insertion over chain isomerization which results in fewer branches. Typically for nickel systems, increasing the temperature of the polymerization increases the first-order rate of β-elimination faster than the second-order rate of monomer trapping, thus leading to more chain walking and increased branching.[20] At higher temperatures, there is some dependence on the rate of chain growth vs monomer concentration, suggesting

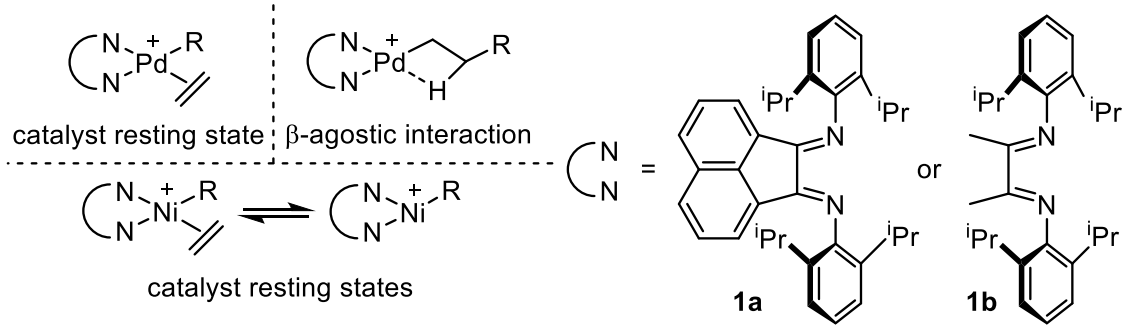


**Figure 1.2** Late metal catalyst resting states in ethylene polymerization.

that the catalyst resting state is a mixture of the cationic alkyl–nickel–ethylene adduct and the cationic nickel–alkyl adduct (Figure 1.2).

## *1.5 Mechanistic Studies of α-Olefin Polymerization using Late Metal Catalysts*

### *1.5.1 Opening Remarks*

Shortly after Brookhart's seminal discovery of late metal olefin polymerization catalysts, there was focus on using these systems for the homopolymerization of α-olefins. Brookhart demonstrated the feasibility of this transformation in his initial work with propylene and 1-hexene, obtaining high molecular weight polymers (>100 kDa) with highly branched architectures.[13] Shortly thereafter, a follow-up report highlighted the potential of α-olefin polymerizations using late metal systems.[22] In this study, α-olefins ranging from propylene (C3) to 1-octadecene (C18) were polymerized, resulting in materials with branching numbers ranging from 279/1000C (C3) all the way down to 33/1000C (C18). It was discovered that longer α-olefins at lower concentrations could result in materials with lower branching densities and higher melting temperatures up to 78 °C. Additionally, polymerizations performed at low temperatures (−10 °C) resulted in living behavior, with resulting polymers exhibiting low molecular weight distributions ($M_w/M_n$ = 1.1) allowing for the synthesis of α-olefin block copolymers. Undoubtingly, this report inspired research groups to further explore late metal–α-olefin polymerization systems and better understand both the mechanism of polymerization

and the possibilities of different types of materials and microstructures that could potentially be accessed.

### *1.5.2 Propylene Polymerization using α-Diimine Palladium Complexes*

**Scheme 1.5** 2,1- and 1,2-Regioinsertions of Propylene

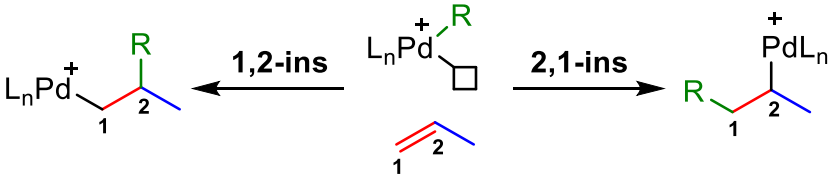


The polymerization of propylene with late metal palladium catalysts was studied in detail by Brookhart and coworkers.[23] Through analysis of the resulting polypropylene branching structure via 1D and 2D NMR spectroscopy techniques, several "rules" of polymerization were developed. First, both 1,2- and 2,1- insertion into propylene can occur, giving rise to specific branching structures. Second, the catalyst can chain walk both forward *and* backward along the newly added monomer, and this chain isomerization is faster than olefin insertion. Third, palladium catalysts do not perform insertions off secondary positions on the polymer backbone, meaning that isomerization after a 2,1-insertion to the polymer chain end *must occur* before the next monomer insertion. This particular rule results in a phenomenon known as "chain straightening," where linear segments of "polyethylene" form (Scheme 1.6). Additionally, palladium catalysts can chain walk past a methine, but cannot "walk" past a quaternary center.

**Scheme 1.6** Chain Straightening Polymerization of Propylene

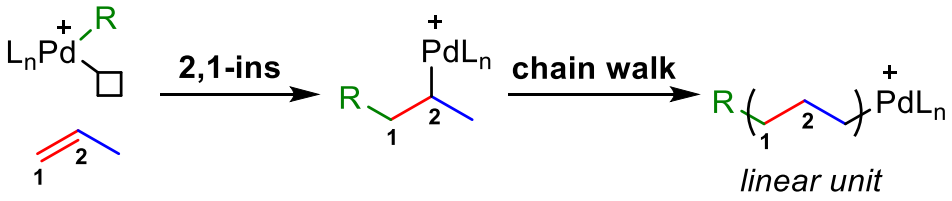


### *1.5.3 Propylene Polymerization using α-Diimine Nickel Complexes*

The polymerization of propylene using nickel-based systems was studied in detail. A key mechanistic difference was observed for nickel compared to palladium, where insertions off secondary positions along the polymer backbone occur.[23,24] Head-to-head methyl branches were observed by $^{13}C$ NMR spectroscopy, sequences that can only arise from 1,2-insertion off a secondary position (Scheme 1.7). In fact, the nickel complex with ligand **1a** (Figure 1.2) was reported to perform 1,2-insertion on a secondary position 66% of the time after an initial 2,1-insertion without chain walking. About 57% of the time after a nickel catalyst performs 2,1-insertion, it "chain straightens" to give a linear unit. Intermediate sized branches were not observed in this study (e.g. ethyl, propyl), suggesting that insertions off secondary positions further into the backbone are energetically unfavorable.

**Scheme 1.7** Head-to-Head Methyl Branches from Insertion off Secondary Positions

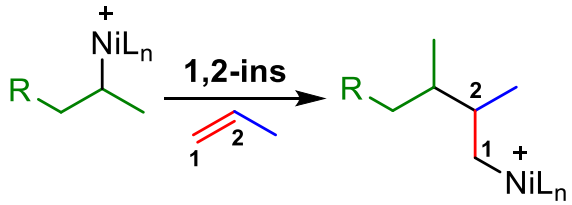

### *1.5.4 Higher α-Olefin Polymerization using α-Diimine Late Metal Complexes*

The polymerization of higher α-olefins (**C6** and higher) using palladium and nickel α-diimines behave similarly to their respective polymerizations with propylene. The most detailed study of these systems was previously performed by Ittel and Brookhart.[25] The same mechanistic rules that applied to propylene polymerizations are also active in higher α-olefin polymerizations with palladium, specifically that 2,1- and 1,2-insertions are operative and that insertions off secondary positions along the polymer backbone do not occur with palladium. The resulting microstructure of poly(α-olefins) produced by palladium complexes consists primarily of linear segments, methyl branches, and alkyl branches (6 carbons or longer) (Figure 1.3). In the case of 1-hexene polymerization, butyl branches (4 carbons) are also observed, which arise from insertions off methyl branches installed after a 1,2-insertion and no chain isomerization. Ittel and Brookhart also performed a study using $^{13}$C-labeled 1-hexene in order to better understanding the insertion pathways active in α-olefin polymerization. They determined that there are two distinct insertion pathways for installing methyl branches, either 1,2-insertion off the primary chain end or 2,1-insertion off the second to last carbon on the chain end (also referred to as the penultimate chain end). Additionally,

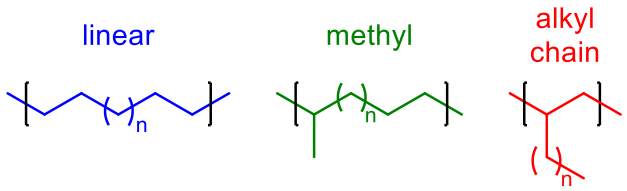


**Figure 1.3** Common branching structures in poly(α-olefins) produced by late metal catalysts.

insertions off secondary positions along the polymer backbone were rationalized not to occur since intermediate branches (e.g. ethyl, propyl) were not observed.

## *1.6 Chain Straightening Polymerization of α-Olefins*

As mentioned *vida supra*, a phenomenon known as "chain straightening" can occur for the polymerization of α-olefins, where 2,1-insertion followed by isomerization to the polymer chain end with subsequent insertion results in a linear unit (Scheme 1.6).[22] With careful ligand design and control over polymerization conditions, semicrystalline polymers that structurally resemble polyethylene can be produced from linear α-olefins. Brookhart and Gottfried previously demonstrated that the palladium-catalyzed polymerization of 1-octadecene at low concentrations produces semicrystalline "polyethylene" with a melting temperature ($T_m$) of 86.1 °C.[26] Although an important first step, this system exhibits multiple insertion pathways that result in branching defects that decrease the maximum $T_m$ obtainable (~135 °C for perfectly linear polyethylene). One of the major goals in designing late transition metal catalysts (or any metal-mediated polymerization system) is to access exclusive selectivity in order to target materials with specific properties.[27] For the case of chain straightening, this means exclusive 2,1-insertion and complete isomerization to the chain end after each α-olefin insertion (ω,1-enchainment).

### *1.6.1 Development of Chain Straightening Late Metal Catalysts*

#### *1.6.1.1 Cyclophane-based Nickel Catalyst*

In 2004, Guan and coworkers reported a novel α-diimine nickel system based on a cyclophane ligand structure intended to reduce chain transfer and increase thermal stability of the catalytic system for the polymerization of ethylene. These goals were achieved using complex **1.2** shown in Figure 1.4, where high molecular weight polyethylene could be achieved even at temperatures up to 90 °C upon activation with MAO.[28] The rigid, cyclic structure of the ligand prevents free rotation from the axial sites at elevated temperatures, thus displaying significant improvement in thermal stability over acyclic complexes.[29] The cyclophane-based catalysts were applied to the polymerization of α-olefins such as 1-hexene, displaying similar thermal stability and high activities for polymerization up to 75 °C.[30]

Interestingly, poly(1-hexene) produced by the cyclophane-based catalyst at 75 °C exhibited melting temperatures up to 62 °C. Conversely, when the original Brookhart

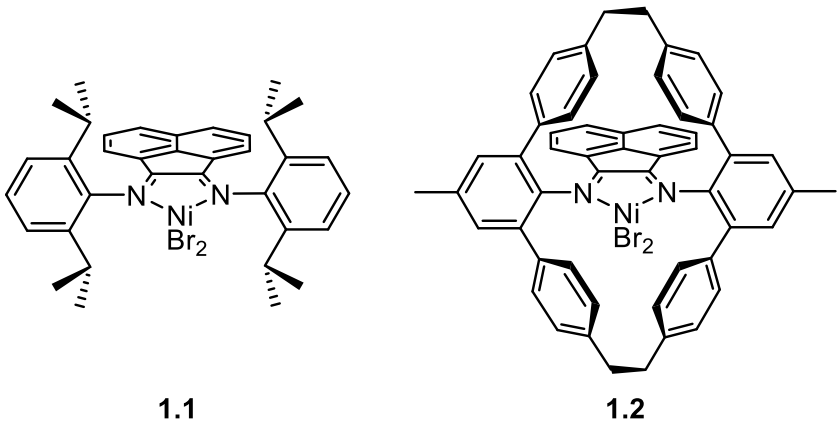


**1.1** **1.2**

**Figure 1.4** Comparison of original Brookhart complex (**1.1**) and Guan's cyclophane-based complex (**1.2**).

nickel complex (Figure 1.4, **1.1**) was used under these conditions, lower molecular weight, amorphous polymers were generated (Table 1.1). The difference in thermal properties could be explained by both the insertion mode and the chain walking mechanism. Guan rationalized that an increase in 2,1-insertion and ω,2-enchainment in **1.2** resulted in more linear segments of poly(α-olefin), and thus improved thermal properties. Guan went further and stated that the increased "chain straightening" could not solely be from a change in the relative rates of olefin insertion vs chain walking. Since 1,2-insertions always install a methyl branch and decrease crystallinity even with abundant chain isomerization, Guan rationalized that the increased thermal properties must arise from an improvement in 2,1-regioselectivity. He was unable to specifically rationalize the reason for the improvement, other than presuming that the unusual steric environment of the cyclophane structure decreases the activation barrier for 2,1-insertion.[31]

**Table 1.1** Polymerization Data for 1-Hexene from Reference 30[a]

| entry | catalyst | temp (°C) | time (h) | $M_n$[b] (kDa) | $M_w/M_n$[b] | branches/ 1000C[c] | thermal anal.[d] (°C) |
|---|---|---|---|---|---|---|---|
| 1 | **1.1** | 25 | 3 | 543 | 1.50 | 108 | −54 ($T_g$) |
| 2 | **1.1** | 50 | 3 | 461 | 1.45 | 110 | −57 ($T_g$) |
| 3 | **1.1** | 75 | 3 | 279 | 1.49 | 111 | −53 ($T_g$) |
| 4 | **1.2** | 25 | 3 | 510 | 1.22 | 57 | −34 ($T_g$), 62 ($T_m$) |
| 5 | **1.2** | 50 | 3 | 647 | 1.13 | 58 | −38 ($T_g$), 58 ($T_m$) |
| 6 | **1.2** | 75 | 3 | 529 | 1.17 | 52 | −47 ($T_g$), 58 ($T_m$) |

[a]Polymerization condition: catalyst **1.1** or **1.2** (0.005 mmol) activated with 2000 equiv of MMAO; toluene (total volume of toluene and monomer equals 50 mL), 1-hexene concentration 2.66 M. [b]Molecular weight data was determined by GPC using polystyrene standards. [c]Total branching was determined by $^1$H NMR spectroscopy. [d]$T_m$ and $T_g$ were determined by differential scanning calorimetry (DSC).

### *1.6.1.2 Nickel Catalyst with Camphyl Backbone*

In 2009, Wu and coworkers reported a novel α-diimine nickel complex with a camphyl backbone that could produce highly branched polyethylene (~220/1000C) at high reaction temperatures (80 °C).[32] A few years later in 2012, the same group applied their camphyl catalyst system (Figure 1.5, **1.4**) to the polymerization of 1-hexene, producing polymers with long methylene sequences that resulted in crystallinity.[33] Melting temperatures were modest, however, with the maximum $T_m$ at 64 °C. Inspection of the differential scanning calorimetry (DSC) traces of these polymers reveals broad endotherms with multiple melting transitions.

Further analysis revealed relatively high numbers of branches (~80/1000C) in the resulting polymers over a range of polymerization temperatures, albeit lower than the theoretical number of branches if chain straightening was not occurring (~167/1000C). Wu rationalized that the unique microenvironment of the camphyl backbone, specifically the methyl group lying on the side of the bicyclic structure (in blue), leads to an increased barrier to 1,2-insertion, thus increasing the relative amounts

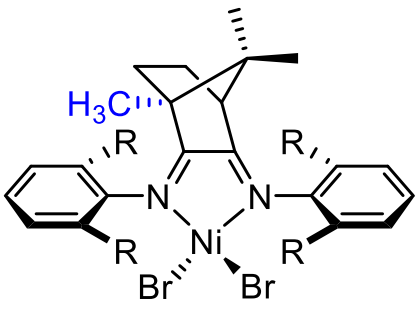


**1.3**. R = Me
**1.4**. R = $^{i}$Pr

**Figure 1.5** α-Diimine nickel complex with camphyl backbone developed by Wu.

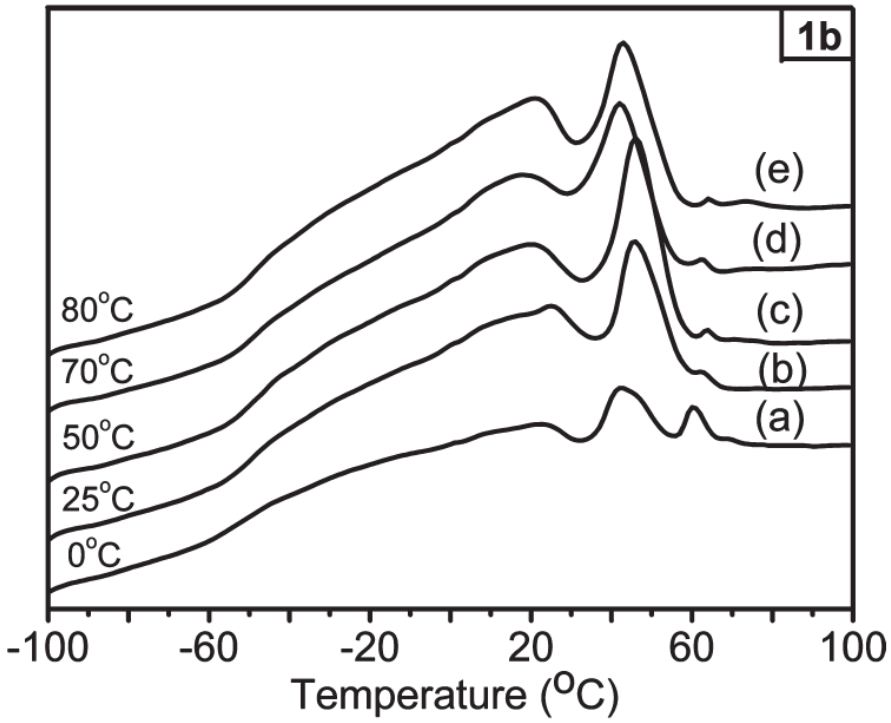


**Figure 1.6** Differential scanning calorimetry (DSC) traces of poly(1-hexene) produced by MAO-activated **1.4** (**1b** in original report) with the endotherm in the positive direction. DSC traces reproduced from reference 33a.

of 2,1-insertion and complete chain isomerization.[34] Wu also reported that although the branching density does not change over a range of temperatures, the relative number of methyl branches vs butyl branches shifts, where higher temperatures lead to increased methyl branching and decreased butyl branching. Wu suggested that this observation is caused by an increase in 1,2-insertion and complete chain walking as a function of increased temperature.

### *1.6.1.3 Aryl Naphthyl α-Diimine "Sandwich" Nickel Catalysts*

Development of palladium-catalyzed arylations of amide-protected naphthylamines by Daugulis allowed access to a new class of sterically encumbered

"sandwich" anilines.[35] In 2013, Brookhart and Daugulis utilized these anilines and introduced a new "sandwich" type nickel catalyst system for the polymerization of ethylene (**1.5**, Figure 1.7).[36] Molecular weights and branching densities of the resulting polyethylenes could be tuned by reaction temperature. High molecular weight materials (>1000 kDa) with branching densities around 80/1000C were produced at ambient temperatures (25 °C), while lower molecular weight materials (~100 kDa) with high branching densities (~150/1000C) were produced at higher temperatures (75 °C) Inspection of the crystal structure revealed a C2-symmetric species with the aryl groups of the ligand positioned in both axial sites of the metal complex, capping the nickel center in a "sandwich" fashion. This strategic blocking of the axial sites allows for increased thermal stability and a decrease in associative chain transfer reactions.

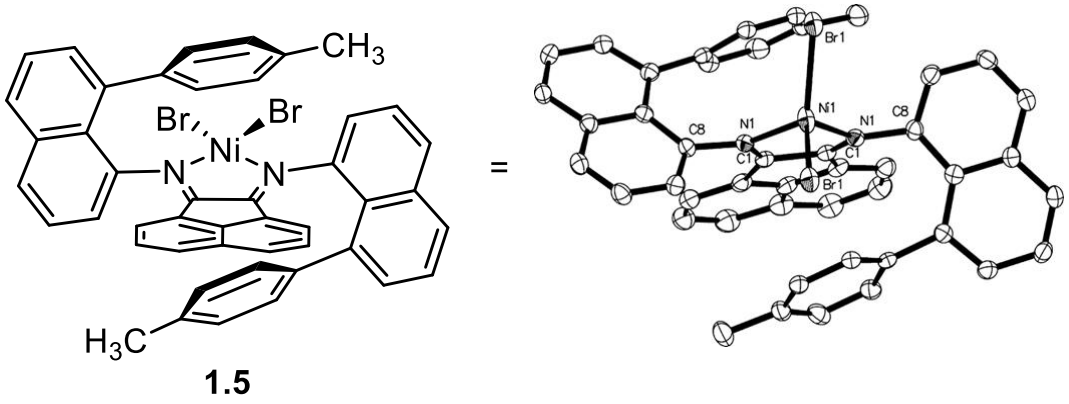


**Figure 1.7** "Sandwich" nickel complex developed by Brookhart and Daugulis. Selected bond lengths (Å) and angles (deg): Ni1–Br1 2.363(5), Ni1–N1 2.028(2), N1–C1 1.277(4), Br1–Ni1–Br1 112.3(3), N1–Ni1–N1 82.5(14), C1–N1–Ni1 111.7(19). Crystal structure reproduced from reference 36.

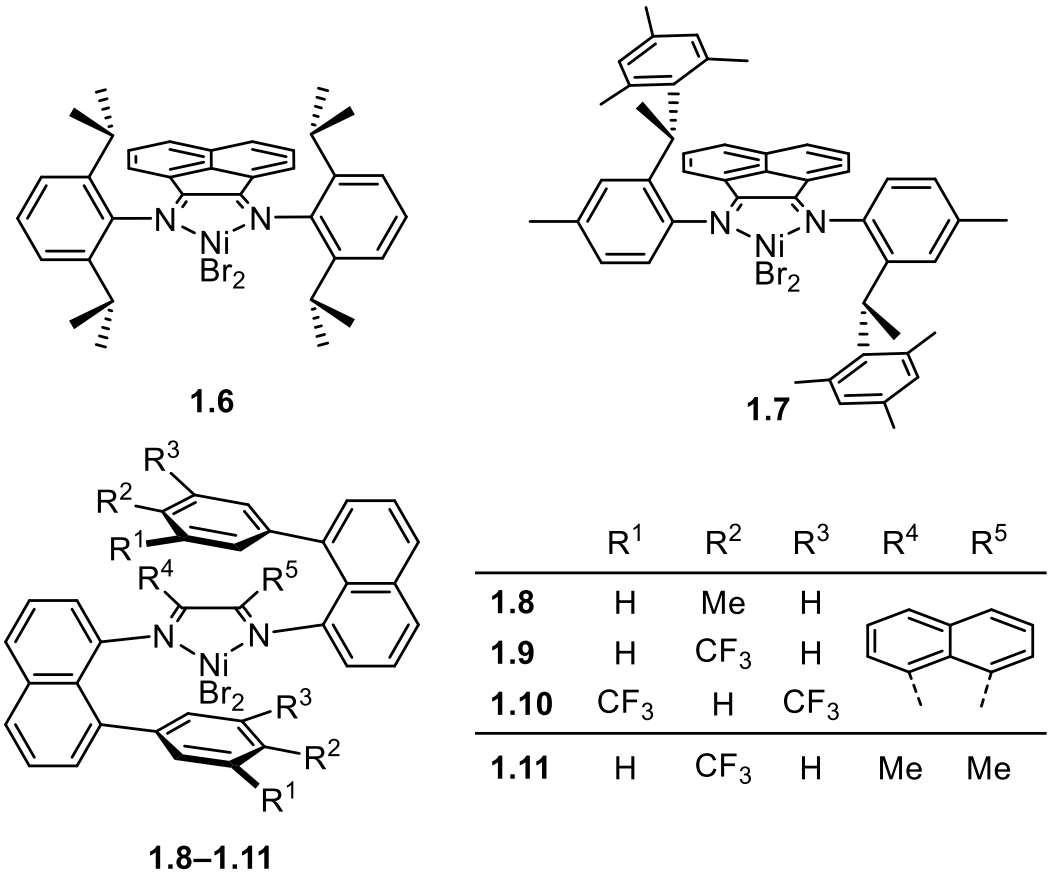


**Figure 1.8** α-Diimine nickel complexes studied in reference 37.

In 2014, Coates and Daugulis applied these "sandwich" type α-diimine nickel complexes to the polymerization of α-olefins.[37] Interestingly, the *p*-tolyl-sandwich complex (**1.5/1.8**) depicted in Figure 1.7. activated with MAO produced chain-straightened poly(1-decene) with a $T_m$ of 96 °C. Further catalyst optimization led to the synthesis of the *p*-trifluoromethyl-sandwich complex (**1.9** Figure 1.8). Polymerization of 1-decene at low concentrations (0.1 M) using complex **1.9** resulted in chain-straightened poly(1-decene) with a $T_m$ of 106 °C, the highest reported at that time. It was rationalized that the specific steric environment from the "sandwich" complex favored 2,1-insertions, and that the low concentration of monomer allowed for complete

isomerization to the chain end before the next insertion event, resulting in highly efficient chain straightening. Analysis of the resulting materials by $^{1}$H NMR spectroscopy corroborated these findings, revealing a much higher mole fraction of linear units in the materials produced by "sandwich" type catalysts compared to those produced by the original Brookhart catalyst (**1.6**, Table 1.2). Changing the catalyst backbone from the acenapthene to the dimethyl (**1.11**, Figure 1.8) resulted in access to materials with a slight improvement in melting temperature (109 °C).

Additionally, the rate of polymerization versus the length of the α-olefin (**C6** to **C18**) was studied using complex **1.9**/PMAO. Interestingly, the polymerization of shorter α-olefins such as 1-hexene exhibited higher TOFs than the polymerization of longer α-olefins such as 1-octadecene (8 $h^{-1}$ vs 2 $h^{-1}$). The decreased rate using longer α-olefins suggests that it takes the nickel catalyst longer to find the polymer chain end, which is reasonable since there are more carbons to chain walk through. These "sandwich" type catalysts were an important advance for the production of chain straightened materials from α-olefins.

**Table 1.2** Polymerization of 1-Decene by α-Diimine Nickel (II) Complexes (Table Reproduced from Reference 37)[a]

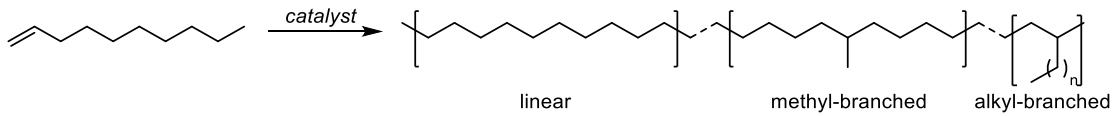


| | | | | | | | | | mole fraction of $C_{10}$ units ($\chi$)[d] | | | |
|---|---|---|---|---|---|---|---|---|---|---|---|---|
| entry | cat. | [1-decene] (M) | toluene (mL) | $t_{rxn}$ (h) | yield (g) | TON[b] | $M_n$[c] (kg/mol) | $M_w/M_n$[c] | linear ($\chi_L$) | methyl-branched ($\chi_M$) | alkyl-branched ($\chi_A$) | $T_m$[e] (°C) |
| 1 | **1.6** | 3.53 | 0.0 | 0.2 | 1.31 | 1868 | 148 | 1.7 | 0.32 | 0.15 | 0.53 | – |
| 2 | **1.6** | 2.07 | 5.0 | 0.2 | 0.51 | 727 | 86 | 1.8 | 0.43 | 0.25 | 0.32 | – |
| 3 | **1.7** | 3.53 | 0.0 | 1.0 | 1.06 | 1517 | 131 | 1.5 | 0.30 | 0.20 | 0.50 | – |
| 4 | **1.7** | 2.07 | 5.0 | 1.0 | 0.63 | 903 | 100 | 1.8 | 0.34 | 0.29 | 0.37 | – |
| 5 | **1.8** | 3.53 | 0.0 | 2.0 | 0.29 | 415 | 58 | 1.1 | 0.54 | 0.24 | 0.22 | 60[g] |
| 6 | **1.8** | 2.07 | 5.0 | 3.0 | 0.33 | 472 | 69 | 1.1 | 0.59 | 0.22 | 0.19 | 69[g] |
| 7 | **1.8** | 0.10 | 37.0 | 24.0 | 0.09 | 128 | 21 | 1.4 | 0.68 | 0.21 | 0.11 | 96[g] |
| 8 | **1.9** | 3.53 | 0.0 | 2.0 | 0.30 | 431 | 70 | 1.1 | 0.52 | 0.18 | 0.30 | 63[g] |
| 9 | **1.9** | 2.07 | 5.0 | 3.0 | 0.25 | 361 | 76 | 1.1 | 0.65 | 0.16 | 0.19 | 75[g] |
| 10 | **1.9** | 1.13 | 15.0 | 24.0 | 0.43 | 612 | 151 | 1.1 | 0.68 | 0.17 | 0.15 | 84[g] |
| 11 | **1.9** | 0.10 | 37.0 | 24.0 | 0.06 | 86 | 32 | 1.2 | 0.77 | 0.16 | 0.07 | 106 |
| 12 | **1.9** | 0.05 | 38.0 | 48.0 | 0.06 | 81 | 25 | 1.3 | 0.77 | 0.17 | 0.06 | 106 |
| 13 | **1.10** | 0.10 | 37.0 | 24.0 | 0.02 | 8 | 8 | 1.2 | 0.74 | –[i] | –[i] | 108 |
| 14 | **1.11** | 0.10 | 37.0 | 24.0 | 0.05 | 22 | 10 | 1.3 | 0.76 | 0.15 | 0.09 | 109 |

[a]Polymerization conditions: Ni = 5 $\mu$mol in chlorobenzene (2 mL), [MAO]/[Ni] = 200, $T_{rxn}$ = 22 °C, toluene. [b]TON (turnover number) = (mol 1-decene consumed) / (mol Ni). [c]Determined using gel permeation chromatography (GPC) in 1,2,4-trichlorobenzene at 150 °C vs polyethylene standards. [d]Determined using $^1$H NMR spectroscopy. [e]Peak melting point (second heat) determined using DSC. [f]No $T_m$. [g]Broad endotherm. [h]Ni = 17 $\mu$mol. [i]$\chi_M + \chi_A$ = 0.26, overlapping NMR signals.

#### *1.6.1.4 Amine-Imine Nickel Catalysts*

In 2015, Wu and coworkers developed a nickel-based system using a mixed ligand species possessing both an amine and an imine.[38] Interestingly, the nature of the substituents on the ligand had a dramatic effect on the regioselectivity of the catalysts for α-olefin polymerization. For example, the polymerization of 1-hexene using MAO-activated **1.12** led to chain-straightened poly(1-hexene) with melting temperatures up to 107 °C. Conversely, utilization of **1.13** resulted in amorphous poly(1-hexene) with a high degree of methyl branches. Wu rationalized the difference with a coordination-insertion model of the four possible transition states for olefin insertion in C1-symmetric catalysts (Figure 1.9). He showed that **1.12** possessing a gem-dimethyl backbone creates a steric environment where only one transition state is favored, resulting in 2,1-insertion and chain straightening behavior. For **1.13** possessing a *tert*-butyl substituent in the backbone, the steric environment favors one specific transition state that results in 1,2-insertion and thus a high degree of methyl branches. The coordination-insertion model for rationalizing regiochemistry of insertion is a potentially important tool for designing future catalyst systems with the desired 2,1-regioselectivity for chain straightening.

**Coordination-Insertion Model for Catalyst 1.12**

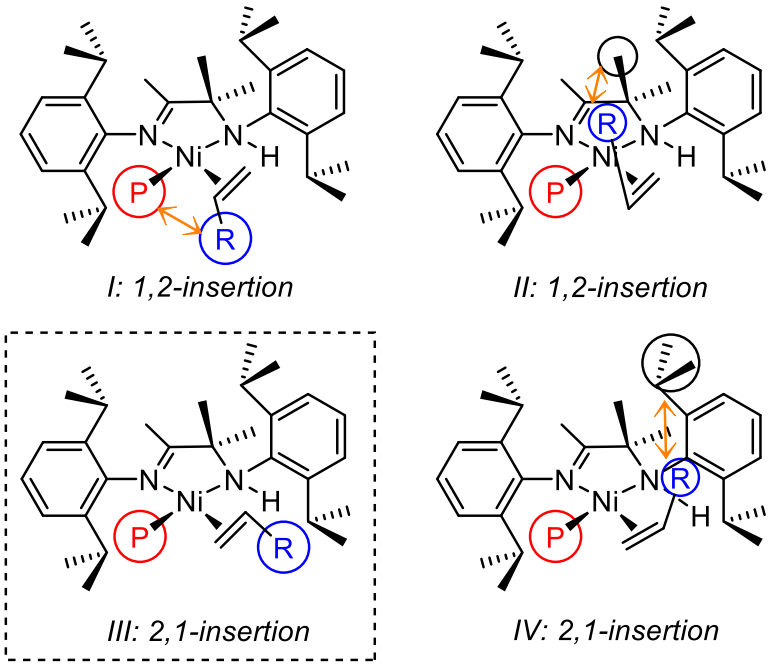


**Coordination-Insertion Model for Catalyst 1.13**

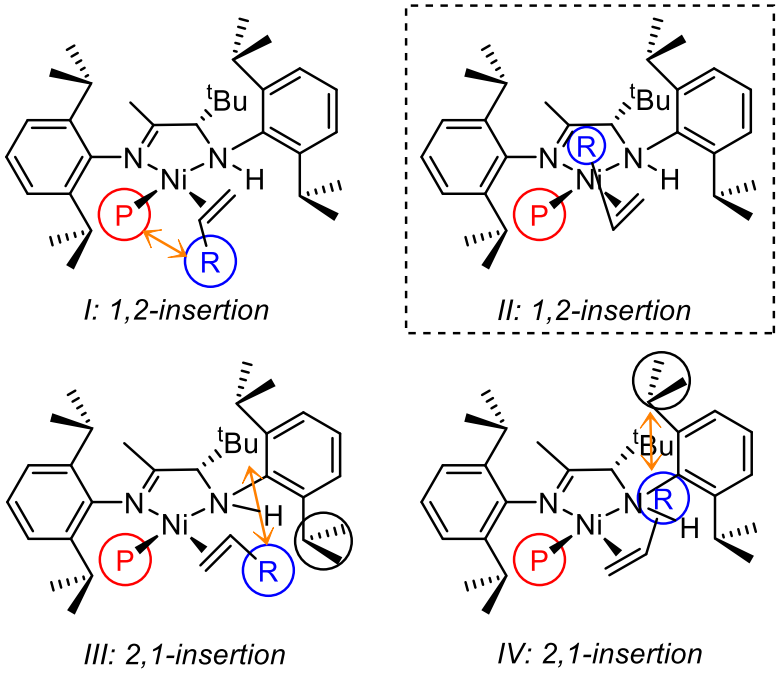


**Figure 1.9** Coordination-insertion model for mixed amine-imine nickel catalysts **1.12** (top) and **1.13** (bottom). Favored binding transition states are noted with dashed boxes. Image adapted from reference 38.

### *1.6.1.5 Double-Decker Xanthum-Bridged Palladium Catalysts*

**Scheme 1.8** Polymerization of 1-Hexene using Double-Decker Palladium Complex

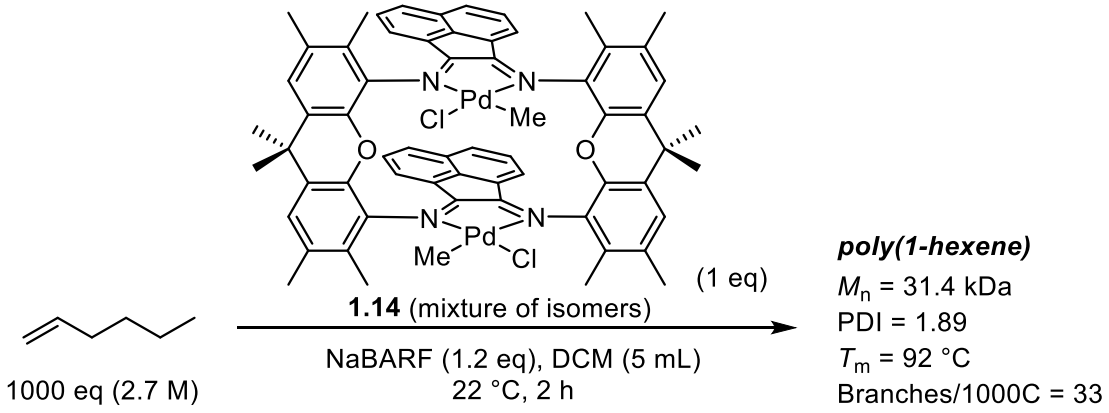


Although there are far less examples in the literature, palladium-based chain straightening catalysts have recently been explored as viable options for producing semicrystalline polymers from α-olefins. In 2015, Takeuchi and coworkers reported a bimetallic "double-decker" palladium complex that exhibited high selectivity for chain straightening α-olefins (**1.14**, Scheme 1.8).[39,40] These bimetallic complexes performed better in terms of higher molecular weights and improved selectivity for producing chain straightened poly(α-olefins) than their monometallic counterparts. At high concentrations of 1-hexene, polymers with modest molecular weights and high melting temperatures were produced (Scheme 1.8). Typically with nickel systems, lower concentrations of monomer are necessary in order to produce chain straightened materials. Palladium catalysts are known to preferentially insert off primary carbons based on Brookhart's "rules" of polymerization,[23] so design of a highly 2,1-regioselective palladium system may lead to highly chain straightened materials as Takeuchi reported.

### *1.6.1.6 Iminopyridyl Nickel-based Catalysts*

**Scheme 1.9** New "Sandwich" Aniline for New Highly Active Iminopyridyl Nickel Catalysts

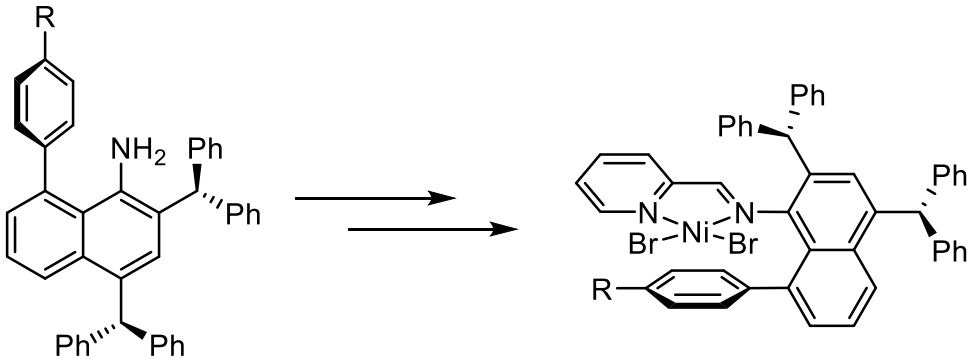


R = Me (**1.15**), H (**1.16**), Ph (**1.17**)

In 2016, Chen and coworkers utilized the palladium-catalyzed arylation chemistry developed by Daugulis[35] and synthesized a new iminopyridyl nickel catalyst for the polymerization of ethylene and α-olefins.[41] Previous attempts at using the iminopyridyl backbone have resulted in systems that produce low molecular weight polyethylene (<20 kDa), likely due to insufficient steric shielding of the axial metal sites resulting in chain transfer side reactions.[42] The new nickel catalyst depicted in Scheme 1.9 (complex **1.17**) can generate polyethylene from ethylene with high molecular weights up to 1,000 kDa. Application to the polymerization of α-olefins resulted in chain straightened poly(α-olefins) with melting temperatures up to 106 °C (Table 1.3). Similar to the "sandwich" aryl-naphthyl catalysts used by Coates and Daugulis, high melting temperatures are achieved using low monomer concentrations and ambient polymerization temperature (Table 1.3, entry 7). Additionally, longer α-olefins (**C10**) produced more crystalline materials than shorter α-olefins (**C6**) under similar reaction

conditions, presumably due to the higher probability of producing longer sequences of methylene branches from longer α-olefins.

**Table 1.3** Polymerization of α-Olefins by Ni(II) Complexes **1.15**–**1.17** (Reproduced from Reference 41)[a]

| Ent. | Cat. | α-Olefin[b] | Yield (mg) | Act.[c] | $M_n$[d] (x $10^{-4}$) | PDI[d] | $B$[e] | $T_m$[f] (°C) |
|---|---|---|---|---|---|---|---|---|
| 1 | **1.15** | **C6** | 587 | 19.6 | 1.7 | 1.78 | 64 | 49.7 |
| 2 | **1.15** | **C8** | 372 | 12.4 | 1.4 | 1.73 | 46 | 70.0 |
| 3 | **1.15** | **C10** | 430 | 14.3 | 2.1 | 1.61 | 32 | 89.0 |
| 4 | **1.16** | **C6** | 171 | 5.7 | 3.6 | 2.01 | 75 | 39.3 |
| 5 | **1.17** | **C6** | 291 | 9.7 | 1.0 | 1.76 | 70 | 56.5 |
| 6 | **1.15** | **C10** | 64 | 0.26 | 1.4 | 1.52 | 29 | 97.9 |
| 7 | **1.17** | **C10** | 45 | 0.19 | 1.3 | 1.49 | 26 | 105.5 |

[a]Conditions: 10 μmol pre-catalyst, 200 eq. $Et_2AlCl$ (cocatalyst), 1.0 M α-olefin. 2 mL $CHCl_3$, total volume 20 mL, 3 h. [b]**C6** = 1-hexene, **C8** = 1-octene, **C10** = 1-decene. [c]Activity (Act.) = $10^3$ g (mol Ni h)$^{-1}$. [d]Molecular weight was determined by GPC using polystyrene standards. [e]*B* = branches per 1000 carbon atoms, determined by $^1$H NMR analysis. [f]Determined by DSC. [g]0.1 M **C10** for 24 h.

## *1.7 Diimine Nickel Catalysts with 1,2-Regioselectivity*

Ligand structure and reaction conditions can also be tuned to produce catalyst systems that exhibit high 1,2-regioselectivity for α-olefin polymerization. In contrast to chain straightening catalysts that exhibit 2,1-regioselectivity and produce poly(α-olefins) with long methylene sequences, 1,2-selective catalysts install methyl branches throughout the polymer repeat units, leading to rare architectures difficult to access from α-olefins by other methods.[43]

### *1.7.1 C2-Symmetric α-Diimine Nickel Catalysts (rac-**1**)*

In 2005, Coates and coworkers reported an α-diimine nickel catalyst with C2-symmetry capable of the regio- and isoselective polymerization of propylene to produce isotactic polypropylene.[44] A highly significant temperature effect was observed on the selectivity of the resulting polymerization. Under ambient conditions, *rac*-**1**/MAO produced regioirregular polypropylene with a low $T_g$, whereas at low reaction temperatures (< −60 °C), *rac*-**1**/MAO produced isotactic polypropylene with a high $T_m$ (Scheme 1.10). Living behavior and precise control over the polymer microstructure with temperature allowed for the synthesis of polypropylene block copolymers with elastomeric properties.

**Scheme 1.10** Effect of Temperature on the Polymerization of Propylene using *rac*-**1**

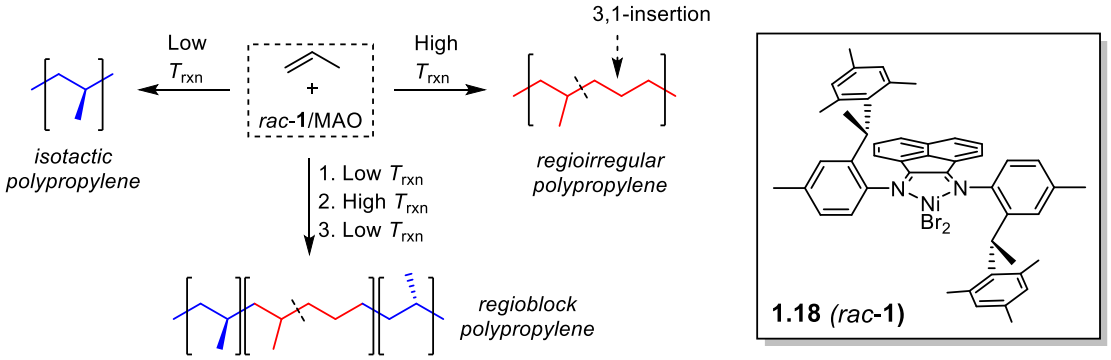


In 2006, Coates and coworkers expanded their study of the *rac*-**1** catalyst system to higher α-olefins beyond propylene.[45] Using a highly 1,2-regioselective catalyst and varying the length of the α-olefin (**C4**–**C8**), "ethylene-propylene" (EP) copolymer equivalents were accessed with tailored molecular weights and "ethylene" content. ω,2-Enchainment, where 1,2-insertion followed by isomerization to the chain end before subsequent insertion, is necessary for the desired EP copolymer. ω,1-Enchainment is

**Scheme 1.11** Comparison of Major Enchainment Types in α-Olefin Polymerization

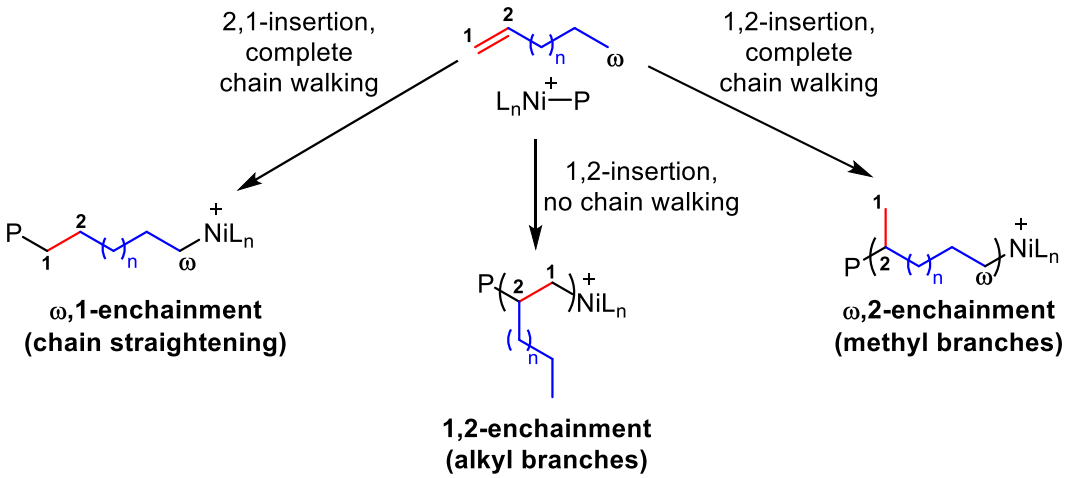


observed as a side reaction and leads to chain straightened segments which is not desired in this system. 1,2-Enchainment, which occurs from 1,2-insertion and subsequent insertion off the methyl branch can also be observed in all poly(α-olefins) beyond poly(1-butene) (Scheme 1.11). For the *rac*-**1** catalyst system,[46] as the length of the α-olefin increased, the amount of ω,2-enchainment decreased in favor of 1,2-enchainment pathways (Table 1.4). Interestingly, the amount of ω,1-enchainment remained relatively constant between α-olefins with even numbers of carbons (e.g. **C4**, **C6**, **C8**, ~0.05) but dropped to less than 1% of the enchainments of odd-numbered α-olefins (**C5**, **C7**). The reason for this was unclear and not commented on in the original manuscript.

**Table 1.4** Polymerization of α-Olefins using *rac*-**1** under Optimized Conditions[a]

| | | | | enchainment type (mole fraction) | | | | |
|---|---|---|---|---|---|---|---|---|
| entry | α-olefin | $M_n$[b] (kDa) | $M_w/M_n$[b] | ω,2[c] | ω,1[d] | $C_2$[c] branch | $C_3$[c] branch | $C_{\geq 4}$[c] branch |
| 1 | 1-butene | 66.1 | 1.26 | 0.96 | 0.04 | 0.00 | 0.00 | 0.00 |
| 2 | 1-pentene | 26.7 | 1.21 | 0.92 | 0.00 | 0.04 | 0.04 | 0.00 |
| 3 | 1-hexene | 31.0 | 1.14 | 0.84 | 0.05 | 0.02 | 0.04 | 0.05 |
| 4 | 1-heptene | 21.2 | 1.14 | 0.78 | 0.01 | 0.02 | 0.05 | 0.14 |
| 5 | 1-octene | 33.4 | 1.06 | 0.70 | 0.06 | 0.01 | 0.04 | 0.19 |

[a]Polymerization conditions: Ni = 10 $\mu$mol, [Al]/[Ni] = 100, $T_{rxn}$ = −40 °C, $t_{rxn}$ = 24 h. [b]Determined using gel permeation chromatography in 1,2,4,-$C_6H_3Cl_3$ at 140 °C versus polyethylene standards. [c]Determined by $^{13}$C NMR spectroscopy. [d]Determined by the equation $\chi_{\omega,1} = [(1 - NR)/1 + 2R)]$, where N = (ω – 2); R = $[CH_3]/[CH_2]$, determined by $^1$H NMR spectroscopy.

### *1.7.2 α-Keto-β-Diimine Nickel Catalysts*

In 2009, Bazan and coworkers reported a cationic nickel catalyst system based on a β-diimine ligand structure with an α-keto group in the backbone (**1.19**, Scheme 1.12).[47] Structurally analogous β-diimine nickel catalysts without the α-keto group had previously been synthesized and utilized for the polymerization of ethylene, but exhibited low activities (TOF ~ 514 $h^{-1}$).[48] The additional of an α-keto moiety resulted in an extremely significant increase in activity for ethylene polymerization (TOF ~ 207,000 $h^{-1}$). Bazan proposed that the exo-cyclic carbonyl group provided electronic delocalization extending from the cationic nickel center through the Lewis acid activator (e.g. MAO) bound through the carbonyl lone pairs, effectively removing more electron density from the active metal center (Scheme 1.12).

**Scheme 1.12** α-Keto-β-Diimine Nickel Catalyst and the Proposed Active Species

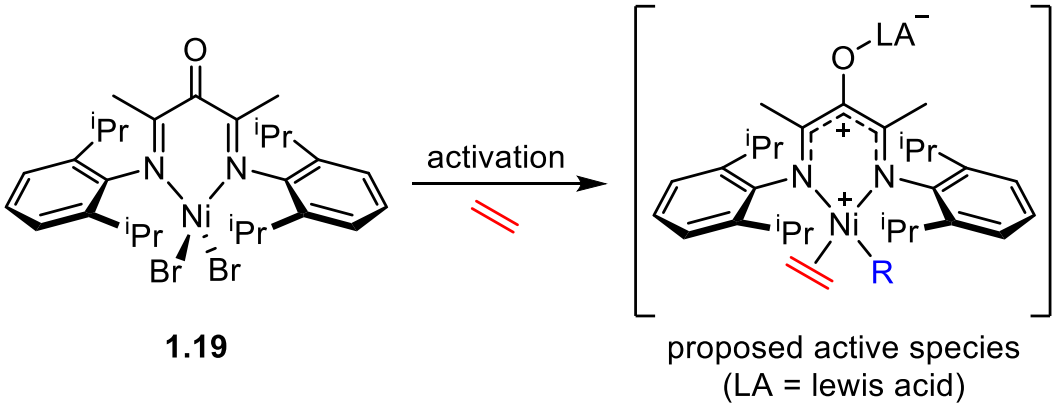


**1.19**

proposed active species
(LA = lewis acid)

Similar to the *rac*-**1** catalyst system, the α-keto-β-diimine system (**1.19**) polymerizes propylene with a significant temperature dependence on the structure of the resulting polymer.[49] Under ambient conditions, regioirregular amorphous polypropylene forms from **1.19**/MAO. However, isotactic polypropylene ([*mmmm*] = 0.85)[50] is readily synthesized at low temperatures (−60 °C), exhibiting high melting temperatures of 134 °C. Isotacticity was determined to occur through an enantiomorphic site control mechanism.[51] The source for 1,2-selectivity is difficult to rationalize as there is no clear coordination-insertion model that would suggest preference for a specific binding mode in this system (refer to Figure 1.9).

Application of **1.19** to the polymerization of 1-hexene (0.8 M) at low temperature (−10 °C) resulted in low dispersity high molecular weight poly(1-hexene) ($M_n$ = 120 kDa, PDI = 1.05) with an unusually high amount of butyl branches compared to methyl branches (76.5% versus 16.5%). This catalytic behavior is strikingly different from cationic α-diimine systems, where methyl branches are typically the predominant branching structure.[15a] Bazan claimed that $^{13}$C NMR signatures consistent with 2,1-

insertion pathways were not observed for the polymerization of 1-hexene using **1.19**.[47b] Although in truth, it is difficult to make this assertion accurately,[52] the large amount of butyl branches present are indicative of 1,2-enchainment (Scheme 1.11) which must initially arise from 1,2-insertion. Additionally, the resulting poly(1-hexene) produced by **1.19** is atactic.

## *1.8 Synthesis of Thermoplastic Elastomers using Late Metal Catalysts*

Researchers over the years have applied late metal systems to the synthesis of polyolefin thermoplastic elastomers. As early as 1996, Brookhart demonstrated that block copolymers with elastic properties could be produced from ethylene and α-olefins using α-diimine nickel catalysts.[22] In this system, α-olefins are polymerized at low concentration to create semicrystalline "hard" segments, while ethylene is polymerized to give amorphous "soft" segments.[53] In early metal systems, α-olefins are typically used to introduce branching and decrease crystallinity in materials.[54] The chain walking mechanism present in late metal systems, however, allows for this reversal in monomer selectivity. Coates and coworkers have also utilized C2 symmetric nickel complexes to produce regioblock polypropylenes that behave as elastomers (as described in Section 1.7.1).[45]

The approach of using α-olefins as semicrystalline "hard" segments in thermoplastic elastomers has been underutilized, likely due to a lack of selectivity in the original Brookhart systems. It was almost two decades later that the next report surfaced that used this approach to make thermoplastic elastomers. In 2015, Ricci and coworkers

produced block copolymers from complex **1.20** activated with diethylaluminum chloride ($Et_2AlCl$) using 1-dodecene as the "hard" segment and ethylene as the "soft" segment (Scheme 1.13).[55] They accessed diblock and triblock copolymers, reporting elastic behavior in terms of low Young's moduli, high elastic strains before break, and modest stress before break (Table 1.5). The triblock copolymer architecture exhibited the highest strength in terms of stress before break.

**Scheme 1.13** Synthesis of Block Copolymer Thermoplastic Elastomer

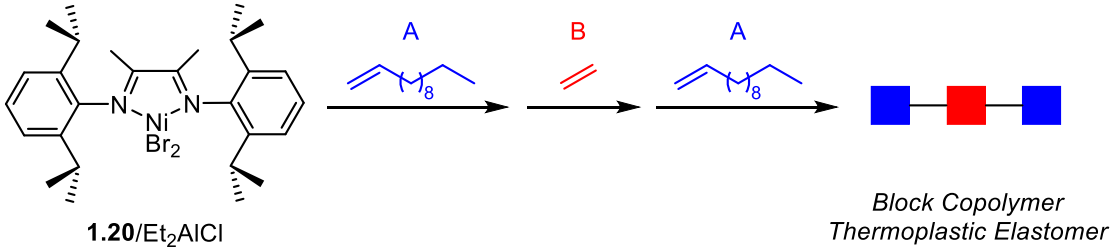


One of the major drawbacks to these materials is their limited elastic recovery. Hysteresis experiments where samples are cycled through ten iterations of 300% strain deformation and relaxation exhibit only 25% shape recovery.[55] Since activated **1.20** is likely regiorandom with respect to α-olefin insertion,[23] the thermal properties of the poly(1-dodecene) using as the "hard" segments in these materials are not robust and may provide poor anchorage necessary for elastic recovery.[56]

**Table 1.5** Synthesis and Mechanical Properties of Block Copolymers (Reproduced from Reference 55)[a]

| entry | polymer | $M_n$[b] (kDa) | $M_w/M_n$[b] | $T_m$[c] (°C) | ΔH[c] (J/g) | $E$[d] (MPa) | $\sigma$[e] (MPa) | $\varepsilon$[f] (%) |
|---|---|---|---|---|---|---|---|---|
| 1 | A | 70.9 | 1.20 | 78 | 52 | 42.9 | 12.4 | 664 |
| 2 | A–B | 84.4 | 1.23 | 77 | 37 | 22.9 | 4.1 | 657 |
| 3 | A–B | 109.7 | 1.29 | 79 | 29 | 21.5 | 6.1 | 968 |
| 4 | A–B–A | 96.8 | 1.33 | 77 | 36 | 28.2 | 18.3 | 994 |

[a]Polymerization conditions: toluene, Ni complex **1.20**, 10 μmol; $Et_2AlCl$/Ni molar ratio, 200; temperature, 22 °C. [b]From SEC. [c]From DSC (second heating) ($T_m$ at peak maximum). [d]$E$ = Young's modulus, [e]$\sigma$ = ultimate tensile strength, and [f]$\varepsilon$ = elongation at break.

Ricci and Leone studied the homopolymerization of 1-octene using **1.20** in a follow-up report.[57] The effect of monomer concentration, temperature, and catalyst activator (MAO versus $Et_2AlCl$) using **1.20** were studied. Interestingly, materials with higher numbers of alkyl branches relative to methyl branches could be achieved with **1.20** using $Et_2AlCl$ as the activator and high concentrations of 1-octene (1.0 M – 3.0 M). The mechanical properties of the resulting materials were superior to their previous ethylene/1-dodecene block copolymers, with elastic strains up to 1300% and elastic strain recoveries up to 82% (Figure 1.10). An unfortunate drawback to these materials, however, is their relatively low melting temperatures ($T_m$ = 43 °C). Due to the high numbers of alkyl branches (41/1000C), the resulting polymer thermal properties are poor which limits many practical applications for these materials.

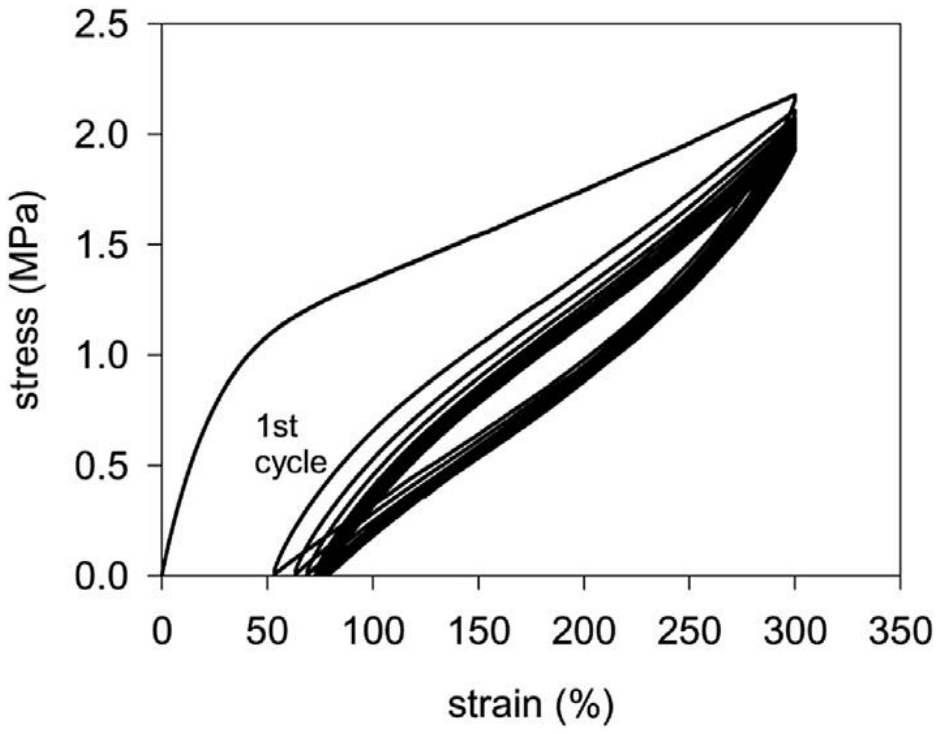


**Figure 1.10** Hysteresis curve of poly(1-octene) produced by **1.20**/$Et_2AlCl$. Sample was cycled ten times at 300% strain, showing 82% elastic strain recovery. Image reproduced from reference 57.

Homopolymers of polyethylene produced by late metal catalyst have also shown elastomeric properties. In 2016, Sun and co-workers produced elastomeric polyethylenes using asymmetric, sterically bulky α-diimine nickel catalysts (Figure 1.11).[58] Reaction temperature played a critical role in modulating the resulting polymer thermal properties, mechanical properties, and branching densities. Under ambient conditions, materials with lower branching densities (106/1000C) and higher melting temperatures (96 °C) were achieved. At higher reaction temperatures (i.e. 80 °C), the resulting materials were described as hyperbranched (171/1000C) with much lower melting temperatures (20 °C). In terms of the mechanical properties, the more highly branched materials exhibited higher elongations before break (731%) compared to materials produced under ambient conditions (218%). This system shows promise

towards achieving all-ethylene-elastomers, but improvements in polymer thermal properties will again be necessary for practical applications.

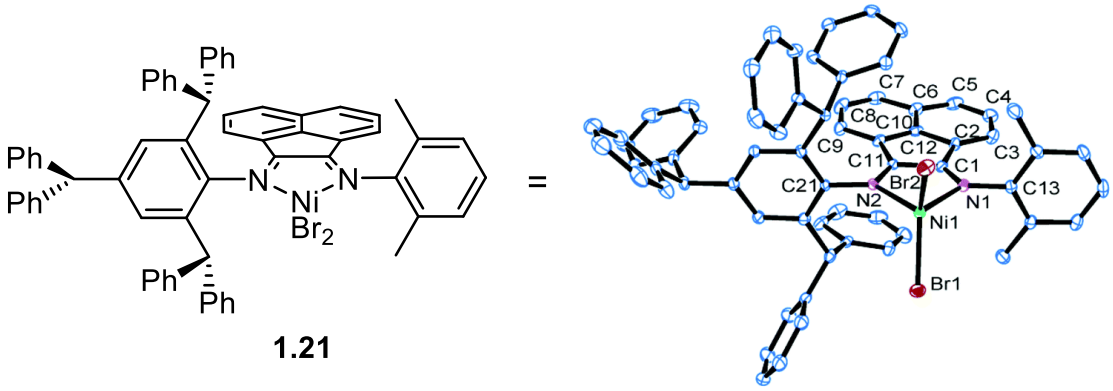


**Figure 1.11** α-Diimine nickel complex used for the synthesis of hyperbranched, elastomeric polyethylenes. Crystal structure reproduced from reference 58.

## *1.9 Conclusions*

For over the past two decades, cationic late metal catalysts have been studied for the polymerization of ethylene and α-olefins. Due to the chain walking mechanism, materials with widely variable branching structures can be accessed from simple monomer feedstocks. Brookhart and coworkers pioneered this field with the introduction of the α-diimine late metal complex for olefin polymerization. Brookhart's mechanistic analysis allowed for the development of polymerization "rules" to help better understand how late metal systems behave, especially in regards to α-olefin polymerizations.

Recent efforts have focused on the chain straightening polymerization of α-olefins for the synthesis of semicrystalline "polyethylene." Several nickel catalysts have been introduced that can perform chain straightening, with the best systems to date producing linear low density polyethylene equivalents ($T_m$ up to 113 °C). There are

fewer examples of effective palladium chain straightening catalysts, but considering Brookhart's "rules" of polymerization that palladium complexes do not readily insert off secondary positions, a highly 2,1-regioselective palladium catalyst should be effective at producing linear polymers from α-olefins. Progress still needs to be made in developing catalysts with perfect selectivity for ω,1-enchainment which would result in high density polyethylene ($T_m$ = 135 °C). Additionally, a better understanding of the nature of the ligand framework and the resulting selectivity would be beneficial in performing future targeted ligand syntheses.

Beyond chain straightening, there has also been focus on using late metal catalysis to introduce precision branching throughout a polymer. The *rac*-**1** catalyst system can introduce precision methyl branches in poly(α-olefins). The α-keto-β-diimine nickel catalyst system also exhibits high selectivity for 1,2-insertion, allowing access to isotactic polypropylene at low temperatures and highly branches poly(α-olefins) under ambient conditions.

Late metal catalysts have also been used for the synthesis of polyolefin thermoplastic elastomers from ethylene and α-olefins. Block copolymers and hyperbranched materials with elastic properties have been accessed. Although materials with impressive elongations and elastic recoveries have been achieved, there is still much work to be done in accessing polymers with improved thermal properties that can be used in practical applications.

## REFERENCES

(1) Galli, P.; Vecellio, G. *J. Polym. Sci. Part A: Polym. Chem.* **2004**, *42*, 396–415.

(2) Ziegler, K.; Holzkamp, E.; Breil, H.; Martin, H. *Angew. Chem.* **1955**, *67*, 426–426.

(3) Natta, G,; Pino, P.; Corradini, P.; Danusso. F.; Mantica, E.; Mazzanti, G. *J. Am. Chem. Soc*. **1955**, *77*, 1708–1710.

(4) Bohm, L. L. *Angew. Chem. Int. Ed.* **2003**, *42*, 5010–5130.

(5) Coates, G. W. *Chem. Rev.* **2000**, *100*, 1223–1252.

(6) Heterogenous catalysis also have advantages over homogenous catalysis in terms of catalyst recyclability and reusability, significant for industrial applications. However, there are several practical issues with studying heterogenous systems. Please refer to Pino, P.; Mülhaupt, R. *Angew. Chem., Int. Ed. Engl.* **1980**, *19*, 857–875

(7) Sinn, H.; Kaminsky, W. *Adv. Organomet. Chem.* **1980**, *18*, 99–149.

(8) (a) Britzinger, H. H.; Fischer, D.; Mülhaupt, R.; Rieger, B.; Waymouth, R. M. *Angew. Chem., Int. Ed.* **1995**, *34*, 1143–1170. (b) Kaminsky, W. *Macromol. Chem. Phys.* **1996**, *197*, 3907–3945. (c) Bochman, M. *J. Chem. Soc. Dalton Trans.* **1996**, 255–270. (d) Hamielec, A. E.; Soares, J. B. P. *Prog. Polym. Sci.* **1996**, *21*, 651–706. (e) Hlatky, G. G. *Coord. Chem. Rev.* **1999**, *181*, 243–296.

(9) (a) Stephan, D. W.; Guérin, F.; Spence, R. E. v. H.; Koch, L.; Gao, X.; Brown, S. J.; Swabey, J. W.; Wang, Q.; Xu, W.; Zoricak, P.; Harrison, D. G. *Organometallics* **1999**,

*18*, 2046–2048. (b) Makio, H.; Kashiwa, N.; Fujita, T. *Adv. Synth. Catal.* **2002**, *344*, 477–493. (c) Hustad, P. D.; Tian, J.; Coates, G. W. *J. Am. Chem. Soc.* **2002**, *124*, 3614–3621.

(10) Reuben, B.; Wittcoff, H. *J. Chem. Educ.* **1988**, *65*, 605–607.

(11) Stadler, F. J.; Piel, C.; Klimke, K.; Kaschta, J.; Parkinson, M.; Wilhelm, M.; Kaminsky, W.; Münstedt, H. *Macromolecules* **2006**, *39*, 1474–1482.

(12) Marquis, D. M.; Sharman, S. H.; House, R.; Sweeney, W. A. *J. Am. Oil Chem. Soc.* **1966**, *43*, 607–614.

(13) Johnson, L. K.; Killian, C. M.; Brookhart, M. *J. Am. Chem. Soc.* **1995**, *117*, 6414–6415.

(14) Brookhart describes a discrete, olefin–hydride intermediate undergoing associative displacement, however, β-hydride transfer through a concerted process with an olefin–hydride - like transition state has been theoretically proposed. For more details, please refer to (a) Deng, L.; Margl, P.; Ziegler, T. *J. Am. Chem. Soc.* **1997**, *119*, 1094–1100. (b) Deng, L.; Woo, T. K.; Cavallo, L.; Margl, P. M.; Ziegler, T. *J. Am. Chem. Soc.* **1997**, *119*, 6177–6186.

(15) (a) Ittel, S. D.; Johnson, L. K. *Chem. Rev.* **2000**, *100*, 1169–1203. (b) Simon, L. C.; Soares, J. B. P.; De Souza, R. F. *AIChE J.* **2000**, *46*, 1234–1240. (c) Zhu, F.; Xu, W.; Liu, X.; Lin, S. *J. Appl. Polym. Sci.* **2002**, *83*, 1123–1132. (d) Popeney, C.; Guan, Z. *Organometallics* **2005**, *24*, 1145–1155. (e) Meinhard, D.; Rieger, B. *Chem. Asian J.* **2007**, *2*, 386–392. (f) Leung, D. H.; Ziller, J. W.; Guan, Z. *J. Am. Chem Soc.* **2008**, *130*,

7538–7539. (g) Xu, Y.; Xiang, P.; Ye, Z.; Wang, W.-J. *Macromolecules* **2010**, *43*, 8026–8038. (h) Wang, f.; Yuan, J.; Li, Q.; Tanaka, R.; Nakayama, Y.; Shiono, T. *Appl. Organometal. Chem.* **2014**, *28*, 477–483. (i) Losio, S; Leone, G.; Bertini, F.; Ricci, G.; Sacchi, M. C.; Boccia, A. C. *Polym. Chem.* **2014**, *5*, 2065–2075. (j) He, Z.; Liang, Y.; Yang, W.; Uchino, H.; Yu, J.; Sun, W.-H.; Han, C. C. *Polymer* **2015**, *56*, 119–122.

(16) Möhring, V. M.; Fink, G., *Angew. Chem., Int. Ed.* **1985**, *24*, 1001–1003.

(17) (a) Guan, Z.; Cotts, P. M.; McCord, E. F.; McClain, S. J. *Science* **1999**, *283*, 2059–2062. (b) Guan Z.; *Chem. Eur. J.* **2002**, *8*, 3087–3092.

(18) Tempel, D. J.; Johnson, L. K.; Huff, R. L.; White, P. S.; Brookhart, M. *J. Am. Chem. Soc.* **2000**, *122*, 6686–6700.

(19) (a) Jianli, W.; Zhang, K.; Ye, Z. *Macromolecules* **2008**, *41*, 2290–2293. (b) Xiao, A.; Wang, Li.; Liu, Q.; Yu, H.; Wang, J.; Huo, J.; Tan, Q.; Ding, J.; Ding, W.; Amin, A. M. *Macromolecules* **2009**, *42*, 1834–1837. (c) Xu, Y.; Ziang, P.; Ye, Z.; Wang, W. *Macromolecules* **2010**, *43*, 8026–8038. (d) Sun, G.; Hentschel, J.; Guan, Z. *ACS Macro. Lett.* **2012**, *1*, 585–588.

(20) Leatherman, M. D.; Svejda, S. A.; Johnson, L. K.; Brookhart, M. *J. Am. Chem. Soc.* **2003**, *125*, 3068–3081.

(21) (a) Shultz, L. H.; Tempel, D. J.; Brookhart, M. *J. Am. Chem. Soc.* **2001**, *123*, 11539–11555. (b) Shultz, L. H.; Brookhart, M. *Organometallics* **2001**, *20*, 3975–3982.

(22) Killian, C. M.; Tempel, D. J.; Johnson, L. K.; Brookhart, M. *J. Am. Chem. Soc.* **1996**, *118*, 11664–11665.

(23) McCord, E. F.; McLain, S. J.; Nelson, L. T. J.; Arthur, S. D.; Coughlin, E. B.; Ittel, S. D.; Johnson, L. K.; Tempel, D.; Killian, C. M.; Brookhart, M. *Macromolecules* **2001**, *34*, 362–371.

(24) Subramanyam, U.; Rajamohanan, P. R.; Sivaram, S. *Polymer* **2004**, *45*, 4063–4076.

(25) McCord, E. F.; McLain, S. J.; Nelson, L. T. J.; Ittel, S. D.; Tempel, D.; Killian, C. M.; Johnson, L. K.; Brookhart, M. *Macromolecules* **2007**, *40*, 410–420.

(26) Gottfriend, A. C.; Brookhart, M. *Macromolecules* **2003**, *36*, 3085–3100.

(27) Camacho, D. H.; Guan, Z. *Chem. Commun.* **2010**, *46*, 7879–7893.

(28) Camacho, D. H.; Salo E, V.; Ziller, J. W.; Guan, Z. *Angew. Chem., Int. Ed.* **2004**, *43*, 1821–1825.

(29) Gates, D. P.; Svejda, S. A.; Oñate, E.; Killian, C. M.; Johnson, L. K.; White, P. S.; Brookhart, M. *Macromolecules* **2000**, *33*, 2320–2334.

(30) Camacho, D. H.; Guan, Z. *Macromolecules* **2005**, *38*, 2544–2546.

(31) Guan and coworkers also designed an alkane-bridged macrocyclic ligand as an analog to their cyclophane- system. Interestingly, the alkane-bridged ligand was not an active catalyst. Please refer to Camacho, D. H.; Salo, E. V.; Guan, Z.; Ziller, J. W. *Organometallics* **2005**, *24*, 4933–4939.

(32) Liu, F.; Hu, H.; Xu, Y.; Guo, L.; Zai, S.; Song, K.; Gao, H.; Zhang, L.; Zhu, F.; Wu, Q. *Macromolecules* **2009**, *42*, 7789–7796.

(33) (a) Liu, F.; Gao, H.; Hu, Z.; Hu, H.; Zhu, F.; Wu, Q. *J. Polym. Sci. Part A: Polym. Chem.* **2012**, *50*, 3859–3866. (b) Liu, J.; Chen, D.; Wu, H.; Xiao, Z.; Gao, H.; Zhu, F.; Wu, Q. *Macromolecules* **2014**, *47*, 3325–3331.

(34) Wu depicted a coordination-insertion model for 1-hexene insertion into the camphyl-based nickel catalyst in order to explain the observed 1,2-selectivity, but the depiction was not clear and was thus not reproduced in this text. The relatively high numbers of branches observed suggests a small difference in energetics between 2,1- and 1,2- insertion.

(35) Nadres, E. T.; Santos, G. I. F.; Shabashov, D.; Daugulis, O. *J. Org. Chem.* **2013**, *78*, 9689–9714.

(36) Zhang, D.; Nadres, E. T.; Brookhart, M.; Daugulis, O. *Organometallics* **2013**, *32*, 5136–5143.

(37) Vaidya, T.; Klimovica, K.; LaPointe, A. M.; Keresztes, I.; Lobkovsky, E. B.; Daugulis, O.; Coates, G. W. *J. Am. Chem. Soc.* **2014**, *136*, 7213−7216.

(38) Hu, H.; Gao, H.; Chen, D.; Li, G.; Tan, Y.; Liang, G.; Zhu, F.; Wu, Q. *ACS Catal.* **2015**, *5*, 122–128.

(39) Takano, S.; Takeuchi, D.; Osakada, K. *Chem. Eur. J.* **2015**, *21*, 16209–16218.

(40) The “double-decker” palladium catalyst was initially reported for the copolymerization of ethylene and polar comonomers: Takano, S.; Takeuchi, D.; Osakada, K.; Akamatsu, N.; Shishido, A.; *Angew. Chem.* **2014**, *126*, 9400–9404.

(41) Dai, S.; Sui, X.; Chen, C. *Chem. Commun.* **2016**, *52*, 9113–9116.

(42) (a) Laine, T. V.; Lappalainen, K.; Liimatta, J.; Aitola, E.; Löfgren, B.; Leskelä, M. *Macromol. Rapid Commun.* **1999**, *20*, 487–491. (b) Yue, E.; Zhang, L.; Xing, Q.; Cao, X.; Hao, X.; Redshaw, C.; Sun, W. *Dalton Trans.* **2014**, *43*, 423–431.

(43) Ring opening metathesis polymerization (ROMP) and acyclic diene metathesis (ADMET) have been employed to access architectures with precision branching. Refer to (a) Bielawski, C. W.; Grubbs, R. H. *Angew. Chem., Int. Ed.* **2000**, *39*, 2903–2906. (b) Wu, Z.; Grubbs, R. H. *Macromolecules* **1995**, *28*, 3502–3508. (c) Konzelman, J.; Wagener, K. B.; *Macromolecules* **1996**, *29*, 7657–7660. (d) Wagener, K. B.; Valenti, D.; Hahn, S. F. *Macromolecules* **1997**, *30*, 6688–6690.

(44) Cherian, A. E.; Rose, J. M.; Lobkovsky, E. B.; Coates, G. W. *J. Am. Chem. Soc.* **2005**, *127*, 13770–13771.

(45) Rose, J. M.; Cherian, A. E.; Coates, G. W. *J. Am. Chem. Soc.* **2006**, *128*, 4186–4187.

(46) In the original publication (reference 44), *rac*-**1** is referred to as *rac*-**3**, but it is the same catalyst system. For consistency, it was referred to as *rac*-**1** in this text.

(47) (a) Azoulay, J. D.; Schneider, Y.; Galland, G. B.; Bazan, G. C. *Chem. Commun.* **2009**, 6177–6179. (b) Azoulay, J. D.; Rojas, R. S.; Serrano, A. V.; Ohtaki, H.; Galland, G. B.; Wu, G.; Bazan, G. C. *Angew. Chem., Int. Ed.* **2009**, *48*, 1089–1092.

(48) Feldman, J.; McLain, S. J.; Parthasarathy, A.; Marshall, W. J.; Calabrese, J. C.; Arthur, S. D. *Organometallics* **1997**, *16*, 1514–1516.

(49) Azoulay, J. D.; Gao, H.; Koretz, Z. A.; Kehr, G.; Erker, G.; Shimizu, F.; Galland, G. B.; Bazan, G. C. *Macromolecules* **2012**, *45*, 4487–4493.

(50) Pentad structures can be observed in the $^{13}C$ NMR spectrum for polypropylene. [*mmmm*] refers to five successive isotactic repeat units of propylene.

(51) (a) Shelden, R. A.; Fueno, T.; Tsunetsugu, T.; Furukawa, J. *J. Polym. Sci., Polym. Lett.* **1965**, *3*, 23–26. (b) Odian, G. Principles of Polymerization, 4th ed.; John Wiley & Sons: New York, 2004; p 711.

(52) About 16.5% of the branches observed in poly(1-hexene) from **1.19** are methyl branches. These can arise from either 1,2-insertion off the primary chain end carbon *or* 2,1-insertion off the penultimate chain end carbon. For more information, please refer to Chapter 3 of this thesis.

(53) A more in-depth discussion on thermoplastic elastomers can be found in Chapter 2 of this thesis.

(54) Arriola, D. J.; Carnahan, E. M.; Hustad, P. D.; Kuhlman, R. L.; Wenzel, T. T. *Science* **2006**, *312*, 714−719.

(55) Leone, G.; Mauri, M.; Bertini, F.; Canetti, M.; Piovani, D.; Ricci, G. *Macromolecules* **2015**, *48*, 1304–1312.

(56) Wang, H. P.; Chum, S. P.; Hiltner, A.; Baer, E. *J. Appl. Polym. Sci.* **2009**, *113*, 3236−3244.

(57) Leone, G.; Mauri, M.; Pierro, I.; Ricci, G.; Canetti, M.; Bertini, F. *Polymer* **2016**, *100*, 37–44.

(58) Wang, X.; Fan, L.; Ma, Y.; Guo, C-Y.; Solan, G. A.; Sun, Y.; Sun, W-H. *Polym. Chem.* **2017**, *8*, 2785–2795.

# CHAPTER 2

# CONTROLLED CHAIN WALKING FOR THE SYNTHESIS OF THERMOPLASTIC POLYOLEFIN ELASTOMERS: SYNTHESIS, STRUCTURE, AND PROPERTIES

Adapted with permission from O'Connor, K. S.; Watts, A.; Vaidya, T.; LaPointe, A. M.; Hillmyer, M. A.; Coates, G. W. *Macromolecules* **2016**, *49,* 6743–6751.

## *2.1 Introduction*

Elastomers are an important class of polymeric materials with commercial applications spanning tires, rubbers, clothing, and insulators.[1] Typical thermoset elastomers, such as vulcanized rubber, are amorphous polymers that have been chemically crosslinked.[2] These crosslinks provide excellent mechanical properties, allowing for nearly perfect elastic recovery after strain-induced deformation, though they result in materials that are not easily recycled, reprocessed, or reused.[3] Thermoplastic elastomers (TPEs) are a desirable alternative to thermoset materials because they contain physical crosslinks that can similarly resist strain-induced deformation, while maintaining the ability to be reprocessed.[4] Elasticity of TPEs is derived from a polymer microstructure containing alternating hard segments with either high melting points ($T_m$) or high glass transition temperatures ($T_g$) and soft, low $T_g$ segments. The soft segments elongate upon strain-induced deformation, while the hard segments create anchoring points needed for elastic recovery.[4] Typically, at least two glassy or semicrystalline segments and one amorphous segment are required to achieve good elastic behavior, so ABA triblock or $(AB)_n$ multiblock copolymer architectures are generally targeted.[5,6,7]

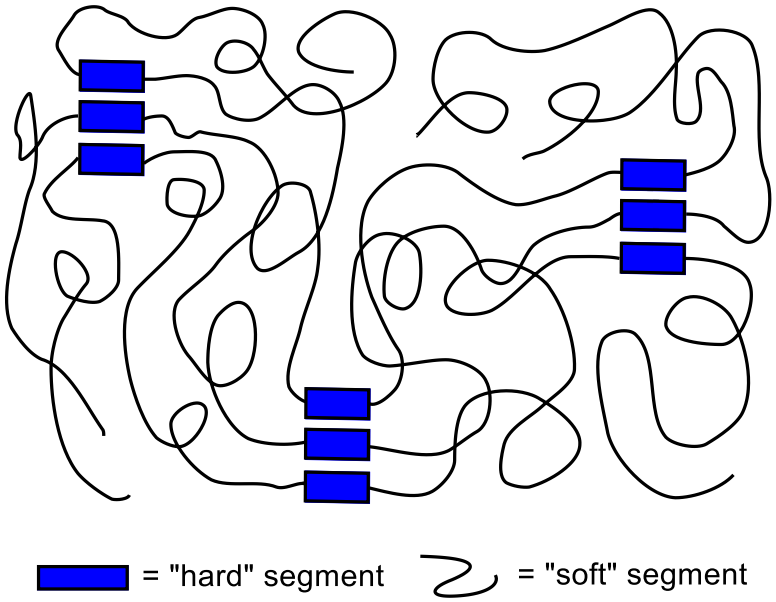


**Figure 2.1** Simplified structure of triblock copolymer thermoplastic elastomer.

Polystyrene is commonly used as the hard segment with rubbery polydienes as the soft segment in commercial triblock TPEs, which are synthesized via living anionic polymerization. Although this robust system can access materials with predictable molar mass and narrow molar mass distributions,[8,9] there has been increasing interest in exploring new systems capable of incorporating different feedstocks from styrene and dienes, monomers primarily derived from fossil fuel sources.[10,11] TPEs derived entirely from olefinic feedstocks, specifically ethylene and α-olefins, represent an attractive alternative to styrene-based materials due to the high abundance, low cost, and potential biorenewability of the monomers. Ethylene can be renewably sourced through the dehydration of bioethanol,[12] whereas α-olefins can be renewably accessed through ethylene oligomerization[13] and ethenolysis of fatty acids.[14] Anionic polymerization cannot efficiently enchain ethylene and α-olefins, however, so a different polymerization strategy is required.

There are a number of methods known for generating elastic materials from olefinic building blocks. In 2006, Dow Chemical Company developed a remarkable chain-shuttling strategy for synthesizing multiblock TPEs from ethylene and α-olefins.[15] In this one-pot procedure, two catalysts with different α-olefin affinities individually operate to polymerize ethylene or copolymerize ethylene and 1-octene. A shuttling agent transfers the growing polymer chains between catalysts, giving an $(AB)_n$ multiblock copolymer with alternating semicrystalline and amorphous segments. This commercial technology is capable of synthesizing TPEs, but the ability to study the effects of number and size of blocks on elastic properties is challenging with this catalyst platform. Another methodology for the generation of polyolefin elastomers was recently developed by Coates and co-workers involving the synthesis of elastomeric graft copolymers. In this system, a hafnium catalyst is utilized to incorporate semicrystalline allyl-terminated polypropylene macromonomers into an amorphous ethylene/1-octene copolymer backbone.[16] The resulting graft materials exhibit exceptional tensile properties and elastic recovery; however, the synthesis of the graft copolymers requires a two-step polymerization process.

Group IV metallocene complexes were some of the earliest examples used to access TPEs from olefins, specifically propylene, through living coordination polymerization, with the capability of controlling molar mass and block structure. Coates and Waymouth developed an oscillating zirconocene catalyst that changes its geometry during the course of the polymerization, generating multiblock copolymers consisting of alternating isotactic and atactic polypropylene segments.[17] Sita and coworkers developed a zirconocene catalyst that changes polymerization behavior by

adjusting the stoichiometry of the borate activator, allowing access to alternating hard-soft block structures.[18] The materials synthesized through these systems have elastic properties at room temperature, but their elasticity suffers below the $T_g$ of the soft atactic polypropylene segment (~0 °C), thereby limiting low temperature applications. Propylene-based materials with lower $T_g$'s can be synthesized using late transition metal catalysts. A chiral nickel α-diimine complex was shown to produce well-defined elastomeric materials from propylene by adjusting the temperature over the course of the polymerization.[19] Reactions performed at low temperatures produced highly crystalline isotactic polypropylene, whereas elevated temperatures produced a microstructure resembling an ethylene/propylene copolymer, which has a lower $T_g$ (−44 °C) than atactic polypropylene.

The difference in polymer microstructure obtained between the zirconocene and nickel α-diimine complexes can be explained by a phenomenon known as "chain walking." This process, common to late transition metal catalysts, involves rapid β-hydride elimination and reinsertion into the propagating polymer chain, which can position the active catalyst at numerous sites along the polymer backbone (Scheme 2.1). Insertion of monomer off the backbone produces branches of various lengths, a property that has been reported to modulate with monomer concentration and reaction temperature.[20] Since the seminal discovery of α-diimine nickel complexes for olefin polymerization over two decades ago,[21] many studies have been performed to better understand the chain walking polymerization mechanism for both ethylene and α-olefins.[22,23,24] One of the earliest nickel complexes developed by Brookhart and coworkers (**2.1**, Scheme 2.1) generally gave highly branched, amorphous polymers

from ethylene but more linear materials could be accessed at high pressures and low temperatures. For the polymerization of α-olefins, a "chain straightening" phenomenon can occur, where 2,1-insertion followed by complete chain walking to the ω-position of the growing polymer chain before subsequent monomer insertion (ω-1 enchainment) leads to linear regions of "polyethylene" (Scheme 2.1). Reaction conditions such as temperature and concentration of α-olefin have shown to affect the rates of chain walking relative to insertion, allowing access to various polymer structures.[25] The regiochemistry of insertion is critical for optimal chain straightening, as 1,2-insertion and complete chain walking before subsequent insertion (ω-2 enchainment) will install a methyl group on the polymer backbone, decreasing crystallinity of the polymer. Various ligand structures have been explored to control the regiochemistry of α-olefin insertion. Wu and coworkers demonstrated precise control over the regiochemistry of 1-hexene insertion by modifying the ligand structure of a nickel amine-imine complex, accessing both a 1,2-selective complex which produces amorphous polymer and a 2,1-selective complex which produces semicrystalline polymer ($T_m$ = 107 °C).[26] Chen and coworkers also developed an interesting aminopyridyl nickel complex which exhibits significant 2,1-insertion and complete chain walking of α-olefins to yield semicrystalline materials with high melting temperatures ($T_m$ = 105.5 °C).[27]

**Scheme 2.1** Modes of Enchainment for Ethylene and α-Olefins using α-Diimine Nickel Complexes

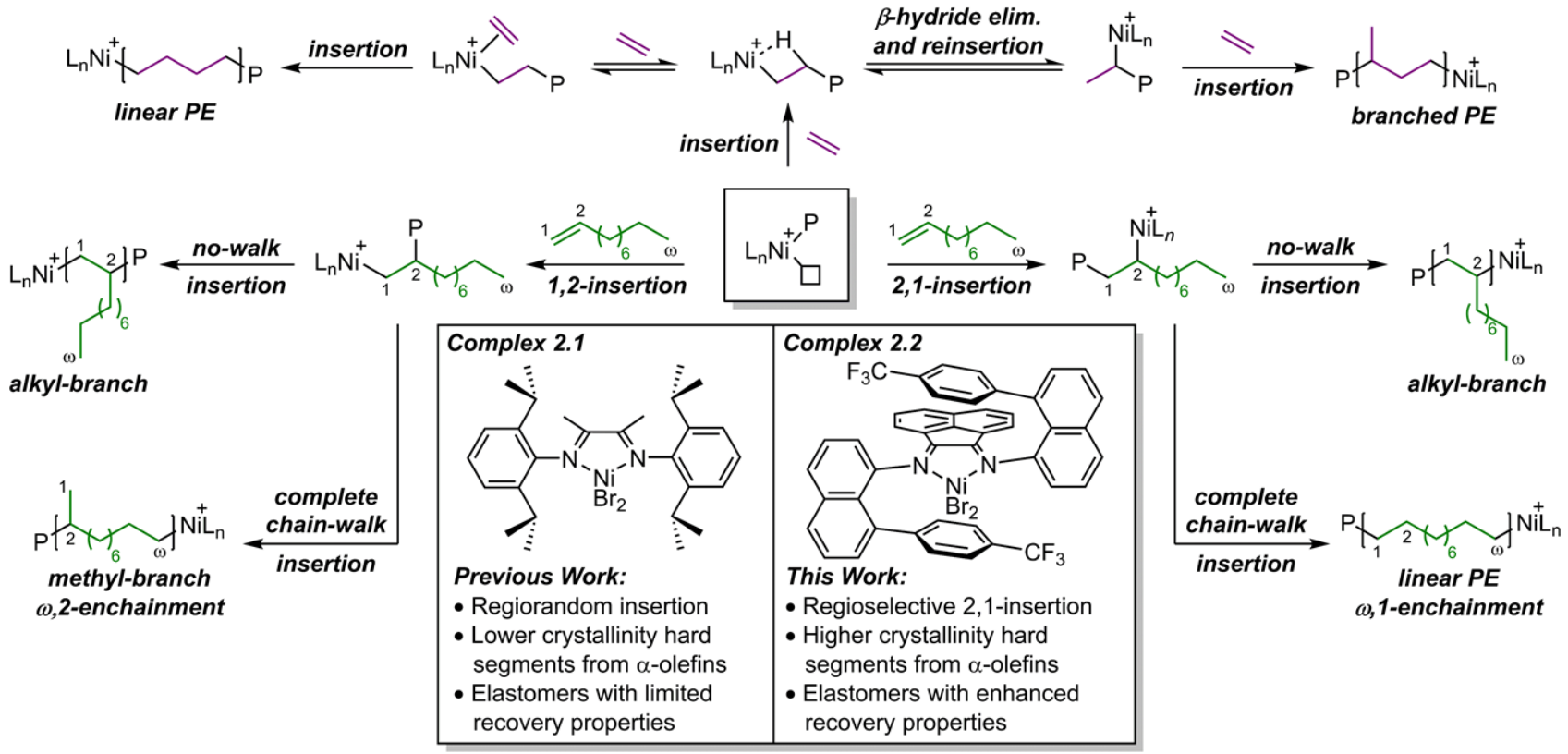

With precise control over regiochemistry of insertion and chain walking, nickel complexes can create TPEs with α-olefin semicrystalline blocks and ethylene amorphous blocks. This methodology is intriguing because it forms the hard segments using α-olefins, which are much more commonly used to introduce branching and decrease crystallinity in early metal systems. Brookhart and coworkers reported the first triblock copolymer using this methodology, with 1-octadecene and ethylene at low temperatures.[28] These materials were empirically described as elastic, but no further characterization of mechanical properties were reported. Ricci and coworkers recently employed the same approach to synthesize triblock copolymers from 1-dodecene and ethylene at room temperature[29] to give materials with strain at break values approaching 1000%. Despite these impressive strain values, the resulting polymers suffered from significant permanent deformations after stretching (~35% recovery after 10 cycles of 300% strain). These materials were synthesized using complex **2.1**, which exhibits regiorandom insertion of α-olefins, thus decreasing the degree of crystallinity in the hard segments. Coates and Daugulis recently reported an aryl-naphthyl-α-diimine Ni(II) "sandwich" complex (**2.2**, Scheme 2.1) which exhibits regioselective 2,1-insertion and complete chain walking of 1-decene at room temperature, giving polymers with low dispersities ($Đ$ = 1.2) and competitive thermal properties ($T_m$ = 106 °C).[30] A similar nickel "sandwich" complex has previously been reported[31] to give highly branched amorphous materials from low pressures of ethylene. We hypothesized that we could combine the outstanding chain straightening of 1-decene with the facile chain walking of ethylene using complex **2.2** to synthesize block copolymers in a controlled manner

with improved $T_m$ and crystallinity in the hard regions, allowing access to thermoplastic elastomers with improved mechanical properties.

Herein, we report the one-pot synthesis of thermoplastic elastomer block copolymers by polymerizing 1-decene to form hard blocks with high crystallinity and ethylene to form soft blocks with low crystallinity using complex **2.2**. A variety of block structures ranging from a diblock up to a heptablock copolymer were synthesized. Statistical copolymers of ethylene and 1-decene were also synthesized for comparison. The effects of the architecture as well as the ratio of hard to soft segments are discussed. The mechanical properties of these copolymers were explored by subjecting samples to uniaxial tension until failure and hysteresis step cycle tests. The creep behavior was also analyzed to demonstrate the resilience of the materials.

## *2.2 Results and Discussion*

### *2.2.1 Triblock Copolymer Thermoplastic Elastomers*

#### *2.2.1.1 Synthesis and Characterization*

Complex **2.2** was selected for the synthesis of block copolymer TPEs due to its ability of producing highly linear materials from α-olefins and branched materials from ethylene in a controlled and facile manner (1-Decene was chosen as the α-olefin because there are multiple renewable pathways for accessing this monomer, and it has previously been shown to give highly crystalline materials using complex **2.2**.[32] Triblock architectures were synthesized by first polymerizing 1-decene at low concentrations using **2.2** activated with methylaluminoxane (MAO) to generate the initial hard block.

A dilute solution of 1-decene was necessary to maximize chain straightening for high $T_m$ and crystallinity.[30] After the appropriate amount of time, ethylene was pressurized directly into the reaction vessel to grow the subsequent soft block. Due to the faster polymerization rate of ethylene compared to 1-decene and the low concentration of α-olefin present in the reaction mixture, 1-decene consumption was negligible during the polymerization of ethylene.[28,35]

**Scheme 2.2** General Procedure for Synthesis of Block Copolymer Thermoplastic Elastomers

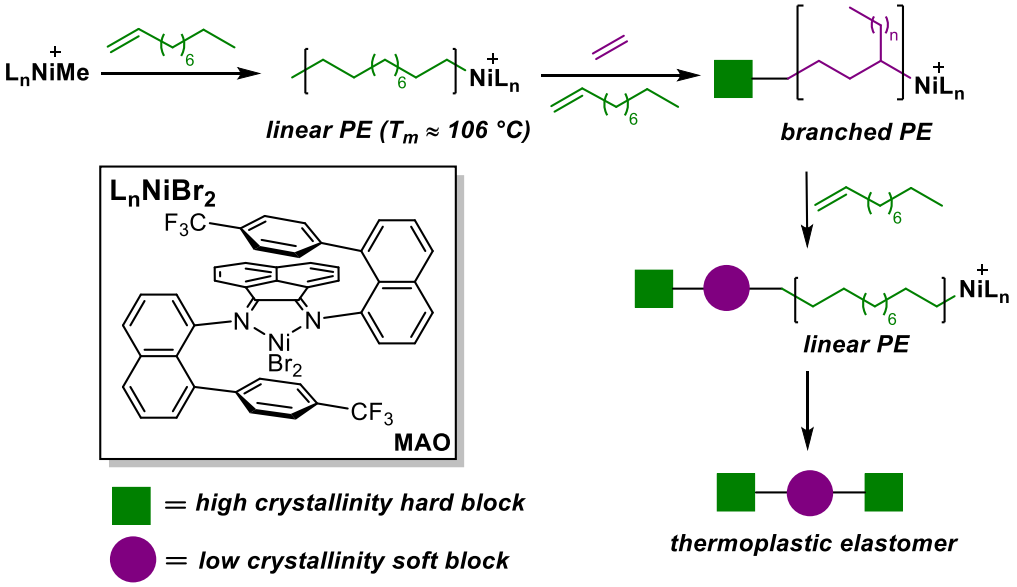


After growing the soft block to the intended length, excess ethylene was exchanged with a nitrogen atmosphere. In the absence of ethylene, 1-decene polymerization resumed, generating the next hard block (Scheme 2.2). This strategy is convenient because it does not require complete consumption of 1-decene before adding ethylene, unlike other sequential addition strategies which generally require full consumption of initial monomer before adding the next monomer to access well-defined

blocks. Aliquots were taken after the growth of each block to analyze molar mass and thermal properties.

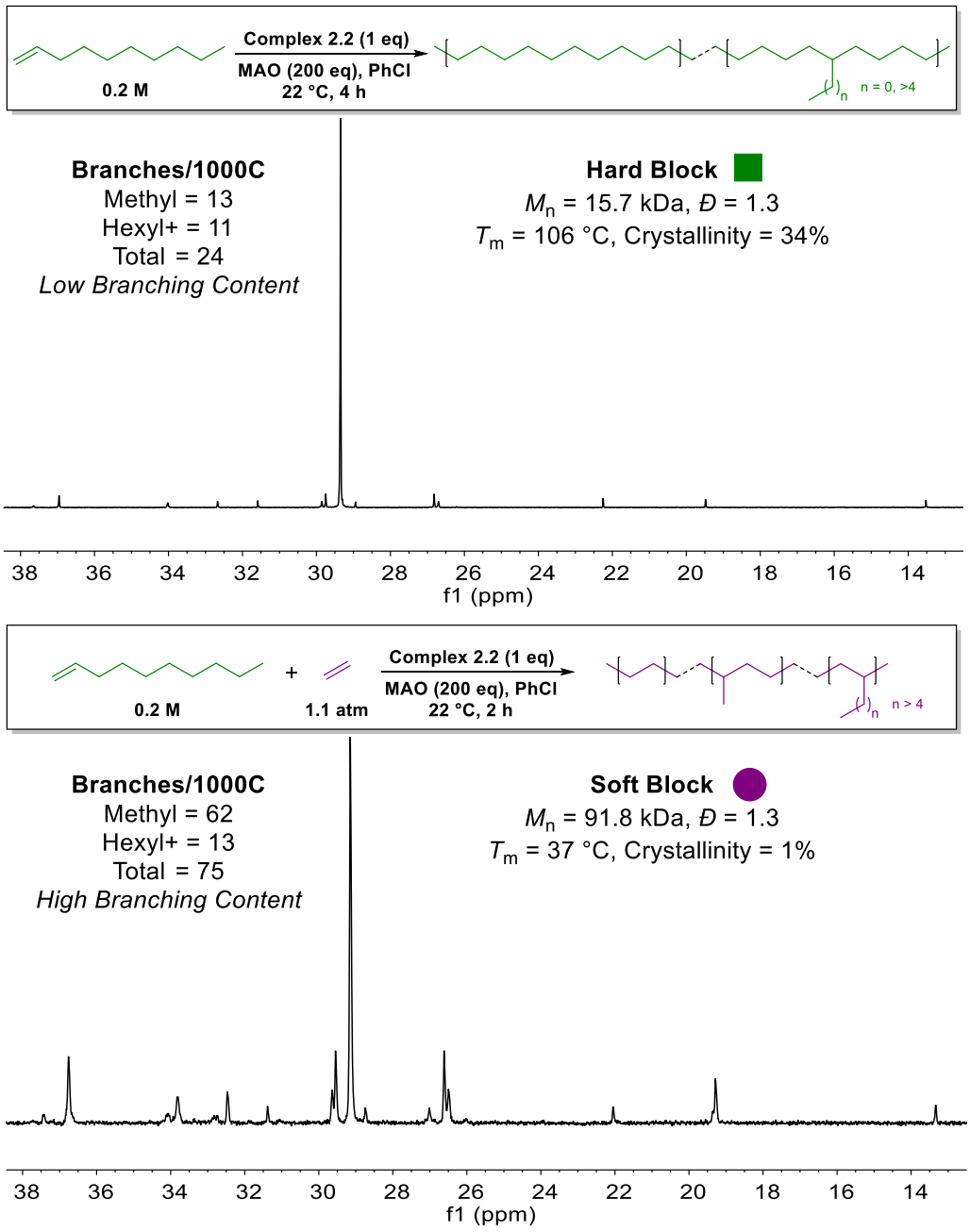


**Figure 2.2** $^{13}$C NMR spectra of a representative hard block from 1-decene (top) and soft block from ethylene/1-decene (bottom) using complex **2.2**.

ABA triblock copolymers grown in toluene demonstrated modest control of molar mass, with dispersities ranging from 1.4 to 1.6 (Table 2.1, entries 1–4). Polymer molar masses were kept relatively constant, while the ratio of hard segments incorporated was varied (Table 2.1, entries 1–3). A lower molar mass sample was also synthesized for comparison (Table 2.1, entry 4). Gel permeation chromatography (GPC) traces displayed a clear shift in molar mass distribution for each aliquot, which was indicative of successful block copolymer growth (Figure 2.3). The dispersity after growth of the first 1-decene block was generally low (1.2 to 1.3), though broadening was observed during the polymerization of the ethylene block. This broadening was likely due to chain transfer reactions with trace trimethylaluminum present from the MAO activator,[33] or from associative chain transfer of the growing polymer chain via ethylene. These undesired chain transfer events can be mitigated by performing the polymerization in the more polar solvent chlorobenzene, producing materials with better control over molar mass and lower dispersities (1.3) (Table 2.1, entries 5–6). It appears the additional polarity of chlorobenzene compared to toluene has a beneficial effect on the ion pair of complex **2.2** and MAO in limiting chain transfer, though the exact mechanism is unclear.[34] A number of samples with higher molar mass exhibited a shoulder in the molar mass distribution. While we cannot confirm the cause for this second distribution, we suspect that a low pressure of ethylene coupled with increasing viscosity of the reaction mixture causes a heterogeneity in the overall ethylene concentration in solution, which may generate two distributions. At lower molar masses (lower viscosity), the distributions are unimodal.[35]

**Table 2.1** Effect of Solvent and Hard Content on Synthesis and Mechanical Properties of Triblock Copolymers[a]

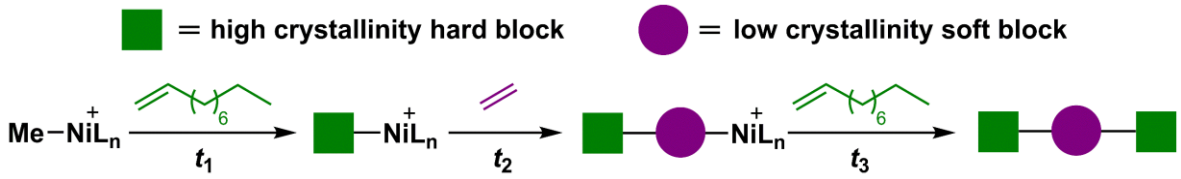


| entry | solvent | $t_1$–$t_2$–$t_3$ (h) | block lengths[b] (kDa) | $M_n$ total[b] (kDa) | $Đ$[b] | wt. % of hard blocks[c] | $T_m$[d] (°C) | $X$[d] (%) | ε[e] (%) | σ[e] (MPa) | E[f] (MPa) | SR[g] (%) |
|---|---|---|---|---|---|---|---|---|---|---|---|---|
| 1 | PhMe | 2.0–0.8–4.5 | 5–90–5 | 100 | 1.4 | 10 | 40, 89 | 1.1 | 630 ± 10 | 12.8 ± 1.1 | 8.1 ± 0.7 | 77 |
| 2 | PhMe | 5.5–0.8–16.5 | 12–95–10 | 117 | 1.5 | 19 | 42, 99 | 4.2 | 640 ± 50 | 18.1 ± 2.2 | 16.5 ± 1.2 | 72 |
| 3 | PhMe | 15.0–0.9–33.0 | 22–73–18 | 113 | 1.6 | 35 | 98 | 6.6 | 670 ± 10 | 29.7 ± 2.5 | 26.0 ± 1.5 | 61 |
| 4 | PhMe | 7.5–0.5–24.0 | 14–43–17 | 74 | 1.5 | 42 | 99 | 6.9 | 750 ± 10 | 23.3 ± 2.6 | 38.4 ± 1.3 | 59 |
| 5 | PhCl | 7.0–1.0–20.0 | 14–66–11 | 91 | 1.3 | 27 | 23, 97 | 3.0 | 680 ± 30 | 19.8 ± 3.2 | 9.8 ± 0.2 | 85 |
| 6[h] | PhCl | 3.0–0.8–5.0 | 13–53–12 | 78 | 1.3 | 32 | 25, 98 | 4.6 | 710 ± 10 | 23.9 ± 1.1 | 14.4 ± 0.3 | 80 |

[a]Polymerization conditions: [**2.2**] = 5.7 mM in PhCl, [MAO] / [**2.2**] = 200, [1-decene] = 0.1 M, ethylene pressure = 1.1 atm, solvent = 72 mL, 22 °C. [b]Determined using gel permeation chromatography (GPC) in 1,2,4-trichlorobenzene at 150 °C vs polyethylene standards. [c]Wt. % of hard blocks = ($\Sigma M_{n,hard}/M_{n,total}$). [d]Determined using differential scanning calorimetry (DSC), melting endotherm of second heat. Crystallinity ($X$) was calculated using the reference enthalpy of fusion (293.6 J $g^{-1}$) for fully crystalline polyethylene. [e]Strain at break, ε, and stress at break, σ, determined at fracture using uniaxial tensile test. [f]Young's modulus, E, is the initial slope of the stress vs strain curve in the linear region ($0 < \varepsilon < 0.05$) and was calculated from the average of at least 5 monotonic curves. [g]Strain recovery, SR, determined by a 300% strain step cycle test using equation $100(\varepsilon_a - \varepsilon_r)/\varepsilon_a$, where $\varepsilon_a$ = applied strain and $\varepsilon_r$ = strain at zero load after 10$^{th}$ cycle. [h][1-decene] = 0.2 M.

Utilizing differential scanning calorimetry (DSC), the thermal transitions were analyzed for each aliquot of every elastomer sample (Figure 2.4). The hard block from 1-decene (red) was highly crystalline, displaying melting temperatures ≥106 °C for samples above 10 kDa and crystallinities ≥30%.[36] Hard block samples with molar masses below 10 kDa exhibited broader and lower $T_m$'s (103 °C, entry 1). The degree of crystallinity and the melting temperature in the sample decreased after growth of the second block, consistent with the branched polyethylene block inhibiting some crystallization of the chain straightened 1-decene block. The final triblock sample (blue) exhibited a similar $T_m$ and slightly enhanced crystallinity in comparison to the diblock, which is consistent with enchaining more hard segment. For triblock samples with higher ethylene incorporation, a lower melting endotherm can be observed from 30–60 °C (Table 2.1, entries 1–2). This melting endotherm suggested that the soft polyethylene segment is not completely amorphous, but possesses regions of crystallinity. This lower melting endotherm could also be seen in triblock copolymers synthesized in chlorobenzene (Table 2.1, entries 5–6) at a lower melting range of 20–45 °C. These polymers have highly crystalline regions from the chain straightened 1-decene end blocks connected by a slightly crystalline (~1%) polyethylene midblock, providing an architecture suitable for TPEs.

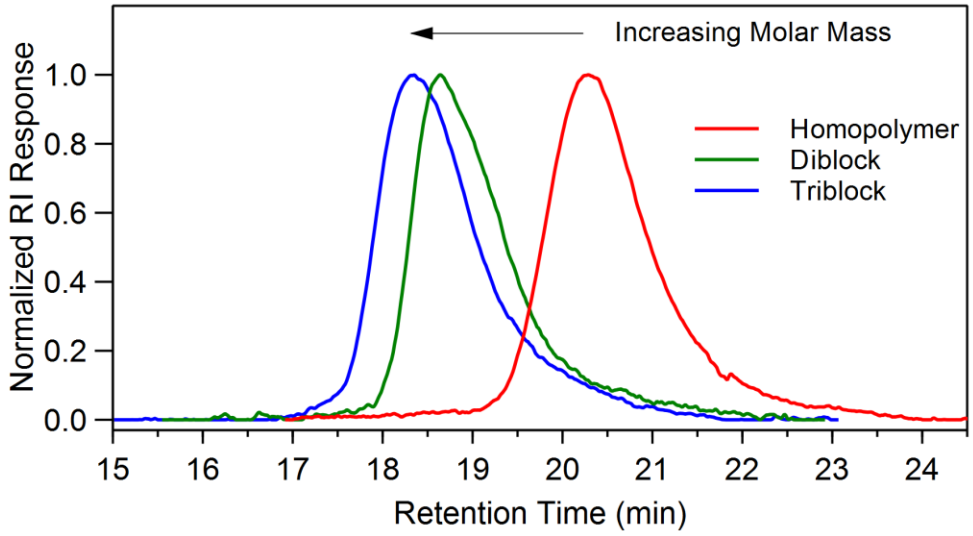


**Figure 2.3** GPC trace of successive blocks of a triblock copolymer (Table 2.1, entry 4).

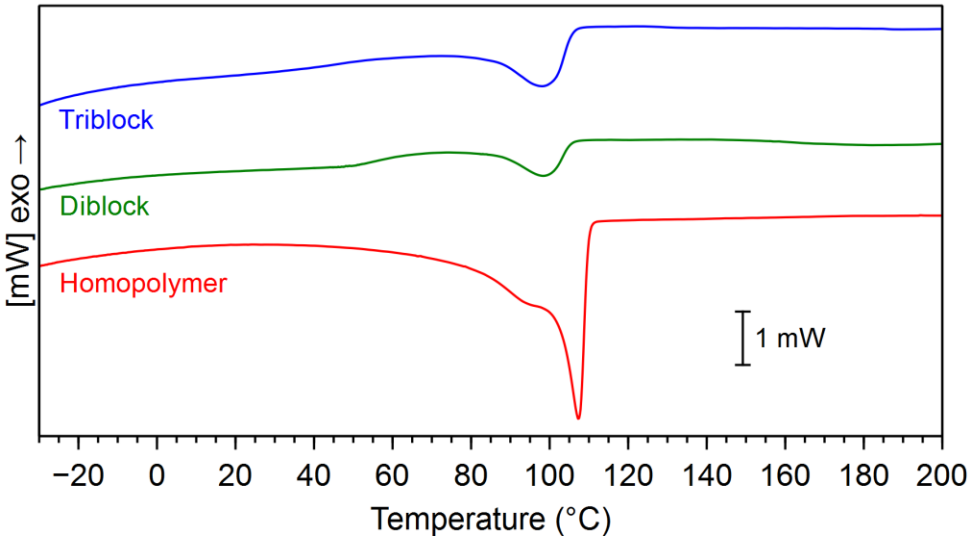


**Figure 2.4** DSC analysis of polymers at successive stages of a triblock copolymer (Table 2.1, entry 4). Melting endotherms from second heating cycles are reported (heating rate = 10 °C/min).

### *2.2.1.2 Mechanical Properties*

Polymer films were melt-pressed at 110 °C under a pressure of 5.2 MPa for 15 minutes and cooled at a rate of ~6 °C/min to 22 °C. These films were subsequently cut into tensile bars for analysis of mechanical properties. Tensile strength was measured for all elastomer samples and Figure 2.5 shows representative tensile strength curves for entries 1–3 (Table 2.1). The slope of the tensile strength curve increases on approach to break, suggesting strain hardening.[37] These samples exhibited strain at break values ranging from 630–670%, a property that did not vary considerably by adjusting the ratio of hard content in the triblock copolymer. The lower molar mass sample (Table 2.1, entry 4) experienced somewhat higher elongations at break (750%). Stress at break and Young's modulus, however, showed an increase with increasing hard content in the triblock copolymer (Figure 2.5), indicating that increasing hard content increases ultimate tensile strength and tensile toughness of the material. The sample with the lowest hard content (entry 1, 10%) showed stress at break values of 13 MPa and a Young's modulus of 8.1 MPa. The sample with 35% hard content (entry 3) showed stress at break values of 30 MPa and a Young's modulus of 26 MPa. Triblock copolymers grown in chlorobenzene (entries 5–6) display slightly elevated strain at break values (680–710%), comparable stress at break values (20–24 MPa), and lower Young's moduli (9.8–14.4 MPa) than samples grown in toluene of similar hard content (entry 3).

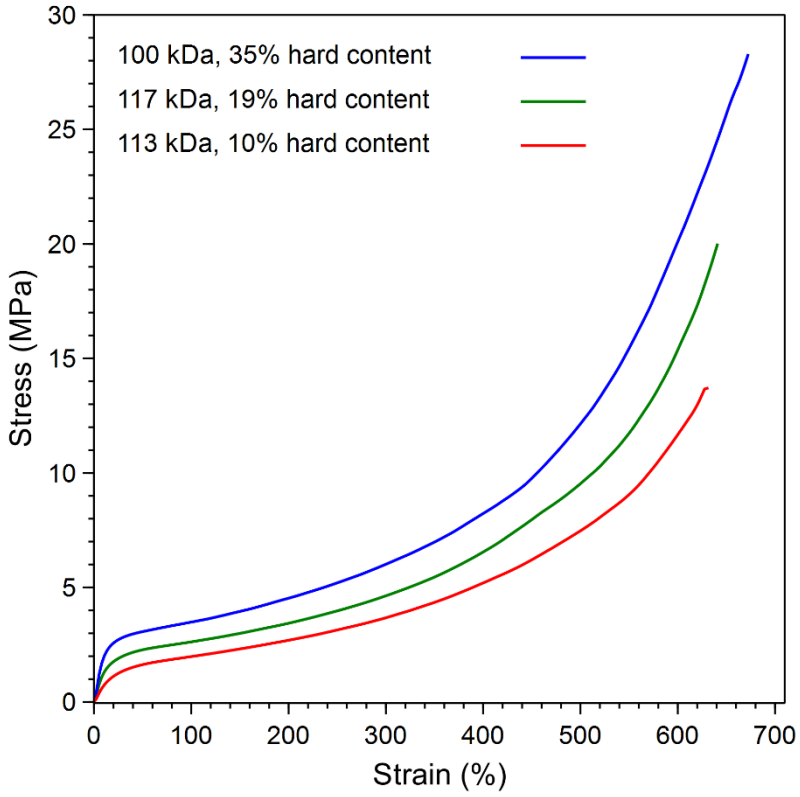


**Figure 2.5** Representative tensile strength curves for triblock copolymers with increasing hard content (Table 2.1, entries 1–3). End of curve represents point of polymer breaking.

Polymer samples were also subjected to hysteresis testing where each sample was extended to 300% strain over 10 cycles to determine the elastic recovery. This was calculated by comparing the strain recovered after cycle 10 to the tensile bar's original length (Table 2.1). The first cycle resulted in the most significant amount of permanent deformation, followed by minimal deformation on subsequent cycles (Figure 2.6). For samples grown in toluene, as the crystallinity of the material increased, the amount of permanent deformation also increased. Entry 1 (Table 2.1, 10% hard content) showed an elastic strain recovery of 77%, compared to entry 3 (Table 2.1, 35% hard content) which only showed a strain recovery of 61%. For samples grown in chlorobenzene

(Table 2.1, entries 5–6), recoveries were substantially improved (80–85%) compared to toluene-grown samples of similar soft content. We suspected that the reduced $T_m$ and crystallinity of the soft block observed for samples synthesized in chlorobenzene compared to toluene improves the recovery properties.

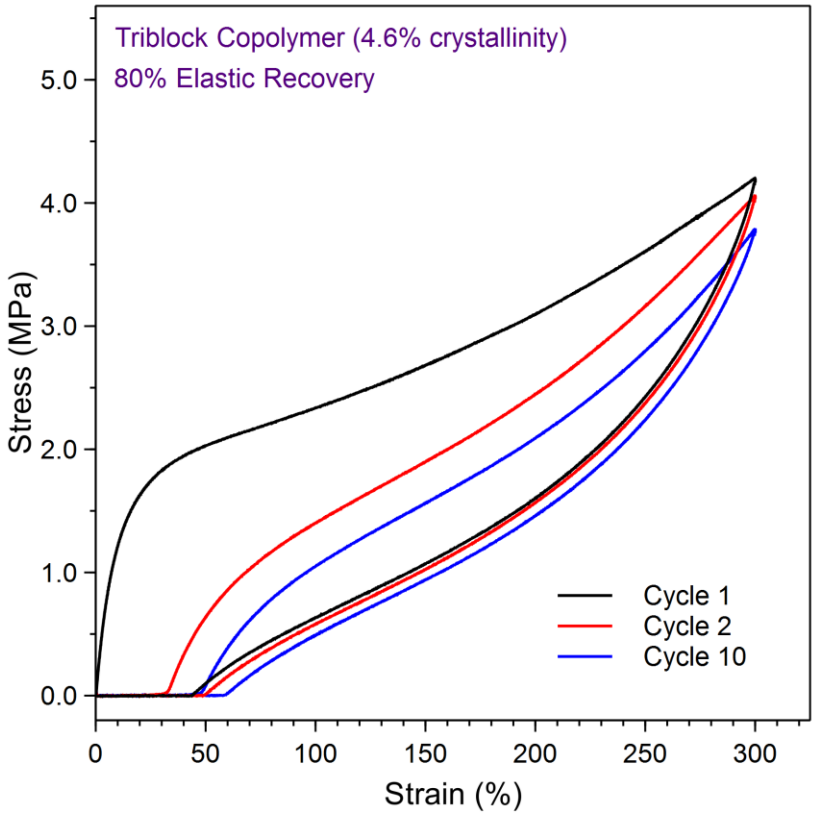


**Figure 2.6** Representative hysteresis experiment for a triblock copolymer (Table 2.1, entry 6). Ten cycles at 300% strain were performed.

It is known that elastomers such as vulcanized rubber can experience strain-induced crystallization after deformation,[38,39] where soft segments can align and crystallize (Figure 2.7). Samples with less crystallinity in the soft blocks could potentially exhibit less strain-induced crystallization, giving materials with improved elastic recovery. We also cannot rule out the possibility that triblock copolymers grown

in toluene have a greater amount of diblock copolymer side product than samples grown in chlorobenzene due to increased chain transfer events during the course of the polymerization, which could have a detrimental effect on elastic recovery.

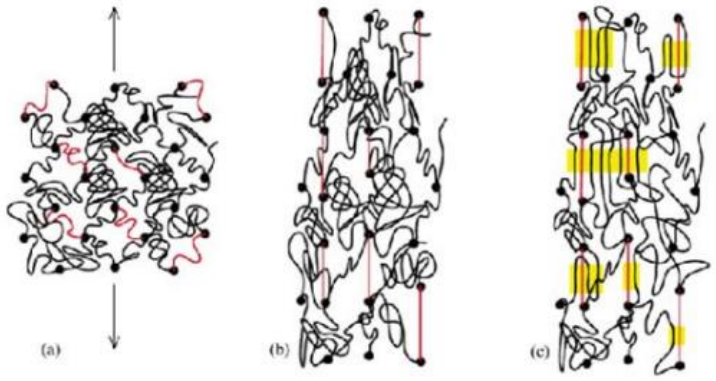


**Figure 2.7** Depiction of strain-induced crystallization occurring after elongation of a cross-linked polymer (image reproduced from reference 39).

### *2.2.2 Higher Order Block Copolymers*

#### *2.2.2.1 Synthesis and Characterization*

Since higher order block copolymers have been shown to exhibit improved mechanical properties compared to triblock copolymers,[40,41] we subsequently targeted pentablock and heptablock structures. To successfully access these materials, three parameters were adjusted. First, all polymerizations were carried out in chlorobenzene to maintain the molar mass control necessary to achieve these structures. Second, the concentration of 1-decene was increased from 0.1 M to 0.2 M in order to reproducibly complete the synthesis.[42] Third, the individual block sizes for the hard and soft segments were decreased in comparison to the triblock copolymers in order to maintain the same overall molar mass. Attempts were made to access polymer molar masses above 120

kDa, but were ultimately unsuccessful due to the high viscosity of the solution and precipitation of the growing polymer chain. Development of thermally stable nickel complexes for the controlled synthesis of thermoplastic elastomers block copolymers will be necessary to combat the viscosity issue and improve molecular weights.

With these modifications, pentablock and heptablock structures were successfully synthesized with hard content varying from 24% to 42% (Table 2.2). Overall molar masses ranged from 83–117 kDa, with a relatively constant $Đ$ of 1.3 maintained throughout the majority of the polymerization, until the final block, where a slight broadening from 1.3 to 1.4 occurred (Figure 2.8). DSC showed similar trends to the triblock structures, where the high hard block $T_m$ decreased sharply after addition of the soft block. As previously observed with the triblock copolymers, the crystallinity of each aliquot increased slightly with the enchainment of 1-decene and decreased slightly with the enchainment of ethylene/1-decene throughout the polymerization.[43] For the heptablock copolymer, the overall crystallinity and melting temperature were lower than expected considering the amount of 1-decene incorporation, suggesting that the individual lengths of the hard blocks are more important than the overall incorporation of hard content in terms of increasing $T_m$ and crystallinity.

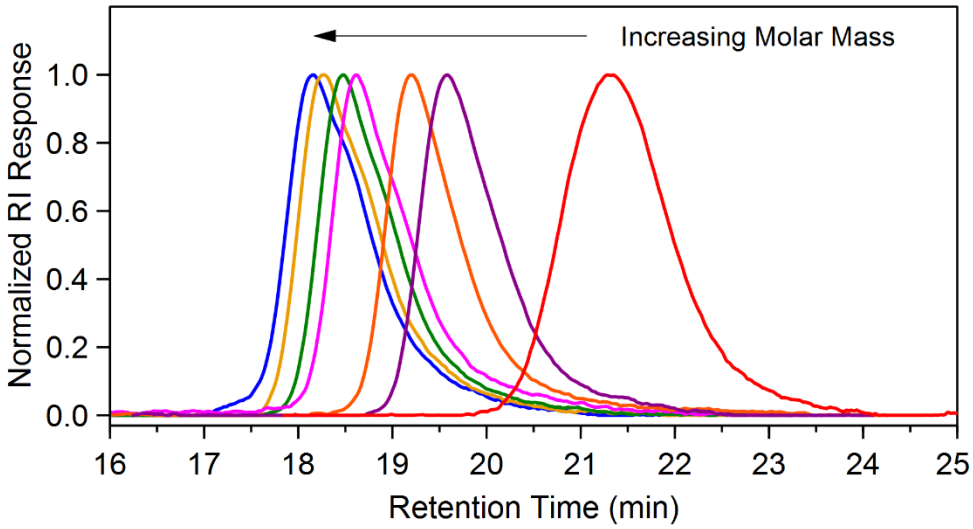


**Figure 2.8** GPC trace of successive blocks of a heptablock copolymer (Table 2.2, entry 4).

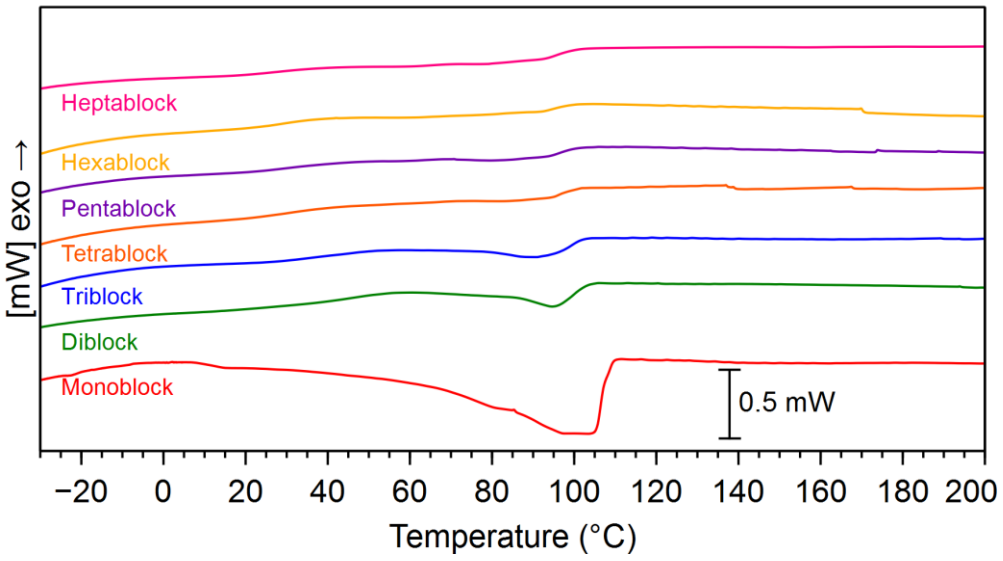


**Figure 2.9** DSC trace of successive blocks of a heptablock copolymer (Table 2.2, entry 4). Melting endotherms from second heat are reported.

**Table 2.2** Synthesis and Characterization of Higher Order Block Copolymers[a]

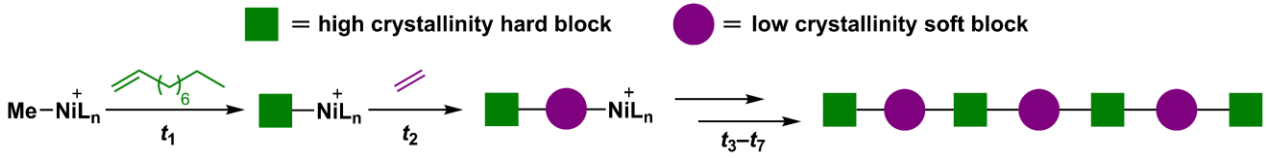


| entry | $t_1$–$t_2$–$t_3$–$t_4$–$t_5$–$t_6$–$t_7$ (h) | block lengths[b] (kDa) | $M_n$ total[b] (kDa) | $Đ$[b] | wt. % of hard blocks[c] | $T_m$[d] (°C) | $X$[d] (%) | ε[e] (%) | σ[e] (MPa) | E[f] (MPa) | SR[g] (%) |
|---|---|---|---|---|---|---|---|---|---|---|---|
| 1[h] | 6.0–0.7–14.5–0.7–14.5 | 11–40–6–42–17 | 117 | 1.4 | 29 | 24, 98 | 5.6 | 630 ± 20 | 29.1 ± 1.9 | 18.6 ± 0.3 | 77 |
| 2 | 2.0–0.7–3.0–0.7–5.0 | 9–48–9–33–8 | 107 | 1.4 | 24 | 25, 94 | 2.8 | 570 ± 10 | 16.9 ± 1.3 | 10.2 ± 0.4 | 80 |
| 3 | 4.0–0.7–6.0–0.7–10.0 | 16–43–19–25–14 | 116 | 1.4 | 42 | 22, 96 | 4.4 | 620 ± 10 | 19.8 ± 0.6 | 14.2 ± 0.1 | 78 |
| 4 | 1.5–0.3–2.0–0.3–3.0–0.4–6.0 | 6–18–11–20–10–12–6 | 83 | 1.4 | 40 | 91 | 2.0 | 670 ± 40 | 28.8 ± 6.0 | 14.9 ± 0.7 | 80 |

[a]Polymerization conditions: [**2.2**] = 5.7 mM in PhCl, [MAO] / [**2.2**] = 200, [1-decene] = 0.2 M, ethylene pressure = 1.1 atm, PhCl = 72 mL, 22 °C. [b]Determined using gel permeation chromatography (GPC) in 1,2,4-trichlorobenzene at 150 °C vs polyethylene standards. [c]Wt. % of 1-decene = ($\Sigma$ $M_{n,hard}/M_{n,total}$). [d]Determined using differential scanning calorimetry (DSC), melting endotherm of second heat. Crystallinity ($X$) was calculated using the reference enthalpy of fusion (293.6 J g$^{-1}$) for fully crystalline polyethylene. [e]Strain at break, ε, and stress at break, σ, determined at fracture using uniaxial tensile test. [f]Young's modulus, E, is the initial slope of the nominal stress vs nominal strain curve in the linear region ($0 < \varepsilon < 0.05$) and was calculated from the average of 5 monotonic curves. [g]Strain recovery, SR, determined by a 300% strain step cycle test using equation $100(\varepsilon_a - \varepsilon_r)/\varepsilon_a$, where $\varepsilon_a$ = applied strain and $\varepsilon_r$ = strain at zero load after 10$^{th}$ cycle. [h][1-decene] = 0.1 M.

#### *2.2.2.2 Mechanical Properties*

The mechanical properties of these higher order block copolymers were tested and compared to the original triblock samples. Interestingly, these materials (Table 2.2, entries 1–3) generally exhibited similar mechanical properties to the triblock copolymers in terms of tensile strength and elastic recovery (Table 2.1, entries 5–6). One particular pentablock structure (Table 2.2, entry 2) even exhibited slightly lower strain at break values compared to the triblock copolymers. This is potentially due to the short length of the soft segments, reducing the amount the polymer chain can extend, resulting in lower strain at break values. There was also no discernable trend in hard block composition vs mechanical properties when comparing two pentablock copolymers (Table 2.2, entries 2 and 3), with both samples exhibiting similar tensile properties and elastic return. These results strongly suggest that there is limited benefit in producing higher order block copolymers beyond the triblock architecture in regards to improving mechanical properties.

### *2.2.3 Diblock and Statistical Copolymers*

#### *2.2.3.1 Synthesis and Mechanical Properties*

To understand how a soft segment with a low degree of crystallinity contributes to the elastic properties of the resulting TPEs, AB diblock copolymers consisting of one hard and one soft segment were synthesized and their mechanical properties were tested. Diblock copolymers were grown in both toluene and chlorobenzene with hard ratios of 10–30% for comparison to their triblock counterparts (Table 2.3). After performing tensile strength and hysteresis experiments, we were surprised to observe that all

samples exhibited elastic properties. While the diblock copolymers (Table 2.3, entries 1–3) exhibited similar stress at break and elastic recovery values compared to the triblock copolymers of similar molar mass and hard content, they displayed higher elongation at break values than the previously tested copolymers (780–970%). We observed consistent trends for the triblock and diblock samples; materials grown in chlorobenzene experienced higher strain at break values than samples grown in toluene when controlling for molar mass and hard content, and elastic recovery suffered as the ratio of hard content increased (Table 2.3, entries 2–3). A second $T_m$ in the low melting region could not readily be observed for entry 3, presumably due to the large amount of crystallinity from the hard segment overshadowing the melting transition in the low melting region.

### *2.2.4 Comparison of Mechanical Properties*

These results indicated that the crystalline regions of the soft block contribute to the elastic behavior of the diblock copolymers by providing sufficient anchoring domains. Therefore, statistical copolymers of ethylene and 1-decene were synthesized to study materials with compositions mimicking that of the soft blocks in the TPE samples (Table 2.3, entries 4–5). Since 1-decene consumption was negligible, the resulting materials are essentially homopolymers of ethylene. These materials had narrow dispersities (1.2–1.3), and exhibited low $T_m$'s (42–49 °C) with low levels of crystallinity (1.4–2.2%). The mechanical properties were surprisingly impressive as the elongations were upwards of 1100%,[44] longer than any of the block copolymer samples. It appeared that block architecture had a significant detrimental effect on the maximum

**Table 2.3** Synthesis and Characterization of Diblock and Statistical Copolymers[a]

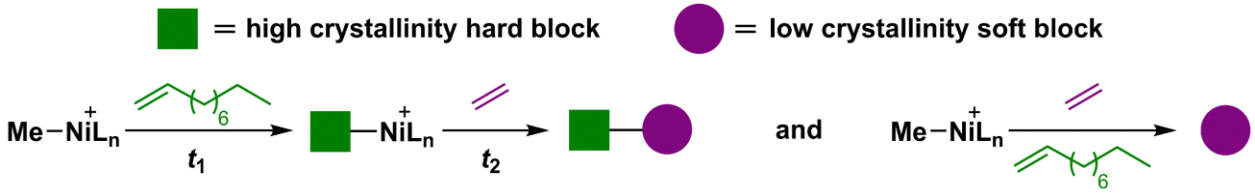


| entry | solvent | $t_1$–$t_2$ (h) | block lengths[b] (kDa) | $M_n$ total[b] (kDa) | $Đ$[b] | wt. % of hard blocks[c] | $T_m$[d] (°C) | $X$[d] (%) | ε[e] (%) | σ[e] (MPa) | E[f] (MPa) | SR[g] (%) |
|---|---|---|---|---|---|---|---|---|---|---|---|---|
| 1[h] | PhMe | 7.5–0.7 | 14–115 | 128 | 1.5 | 11 | 50, 97 | 3.1 | 780 ± 10 | 19.2 ± 1.8 | 9.8 ± 0.2 | 70 |
| 2 | PhCl | 3.5–1.5 | 15–107 | 122 | 1.4 | 10 | 36, 97 | 3.6 | 870 ± 10 | 26.1 ± 1.1 | 8.6 ± 0.2 | 78 |
| 3 | PhCl | 8.0–0.3 | 25–59 | 84 | 1.3 | 30 | 100 | 5.4 | 970 ± 40 | 24.4 ± 1.8 | 18.0 ± 0.2 | 58 |
| 4 | PhMe | 1.0 | 102 | 102 | 1.3 | n/a | 49 | 2.2 | 1100 ± 20 | 17.6 ± 2.2 | 5.9 ± 0.3 | 66 |
| 5 | PhCl | 2.0 | 102 | 102 | 1.2 | n/a | 41 | 1.4 | 1120 ± 30 | 11.6 ± 1.7 | 3.8 ± 0.2 | 77 |

[a]Polymerization conditions: [**2.2**] = 5.7 mM in PhCl, [MAO] / [**2.2**] = 200, [1-decene] = 0.2 M, ethylene pressure = 1.1 atm, solvent = 72 mL, 22 °C. [b]Determined using gel permeation chromatography (GPC) in 1,2,4-trichlorobenzene at 150 °C vs polyethylene standards. [c]Wt. % of hard blocks = ($\Sigma$ $M_{n,hard}/M_{n,total}$). [d]Determined using differential scanning calorimetry (DSC), melting endotherm of second heat. Crystallinity ($X$) was calculated using the reference enthalpy of fusion (293.6 J g$^{-1}$) for fully crystalline polyethylene. [e]Strain at break, ε, and stress at break, σ, determined at fracture using uniaxial tensile test. [f]Young's modulus, E, is the initial slope of the nominal stress vs nominal strain curve in the linear region ($0 < \varepsilon < 0.05$) and was calculated from the average of 5 monotonic curves. [g]Strain recovery, SR, determined by a 300% strain step cycle test using equation $100(\varepsilon_a - \varepsilon_r)/\varepsilon_a$, where $\varepsilon_a$ = applied strain and $\varepsilon_r$ = strain at zero load after 10$^{th}$ cycle. [h][1-decene] = 0.1 M.

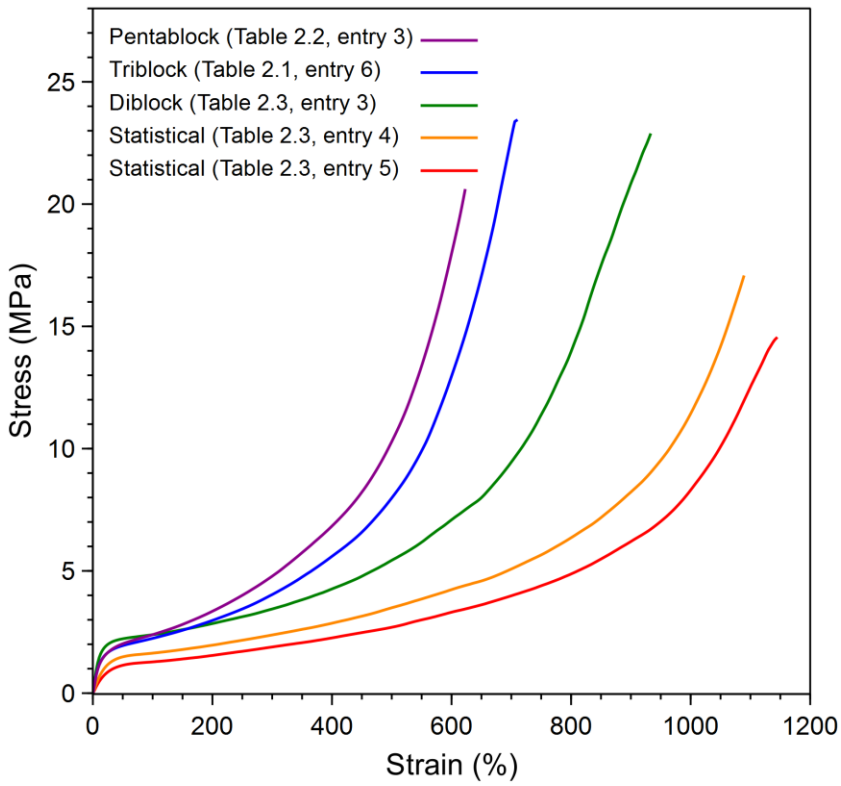


**Figure 2.10** Representative tensile strength curves for various block architectures, from pentablock to statistical copolymers.

elongation possible. As the number of blocks decreased, the maximum strain at break increased (Figure 2.10). The Young's moduli were also lower than the other samples (3.8 and 5.9 MPa). Most surprisingly, the statistical copolymer samples displayed comparable elastic recovery to all other materials tested. The statistical copolymer grown in toluene exhibited lower elastic recovery (66%) than the statistical copolymer grown in chlorobenzene (77%), corresponding to differences in the crystallinity of the soft segment as previously observed.

### *2.2.5 Creep Analysis of Block and Statistical Copolymers*

To explain why all of the polymers synthesized, regardless of block architecture, behaved as elastomers, we posit that the crystalline regions of the soft block are significant enough to act as physical cross-links, allowing elastic recovery to occur. To test this hypothesis, the creep behavior of these polymers was studied. Samples with various architectures were elongated to 300% strain and kept at a constant stress for 3 hours.[35] We suspect that elasticity in these materials is derived not from phase separation of the individual blocks into well-ordered structures, but rather crystallizable domains embedded in an amorphous matrix behaving as anchoring units.[45,46] If low melting crystallites are responsible for the elastic recovery seen in diblock and statistical copolymers, then a constant force could disrupt these interactions and pull the polymer chains apart. Conversely, triblock and pentablock copolymers with the conventional hard-soft-hard architecture have larger proportions of crystalline domains that should better resist strain-induced deformation.

The results of the creep experiment support our hypothesis, showing that higher numbers of blocks result in less deformation under constant force conditions (Figure 2.11) after 3 hours. Statistical copolymers (Table 2.2, entries 4–5) resulted in the greatest deformation over time, particularly the sample grown in chlorobenzene (entry 5), which has the lowest crystallinity. The diblock copolymer (Table 2.3, entry 3) experienced improved resistance to creep compared to the statistical copolymers, but triblock (Table 2.1, entry 6) and pentablock copolymers (Table 2.2, entry 3) exhibited the least amount of deformation. Since both the triblock and pentablock structures displayed virtually the same amount of creep over the given time, it appears that again

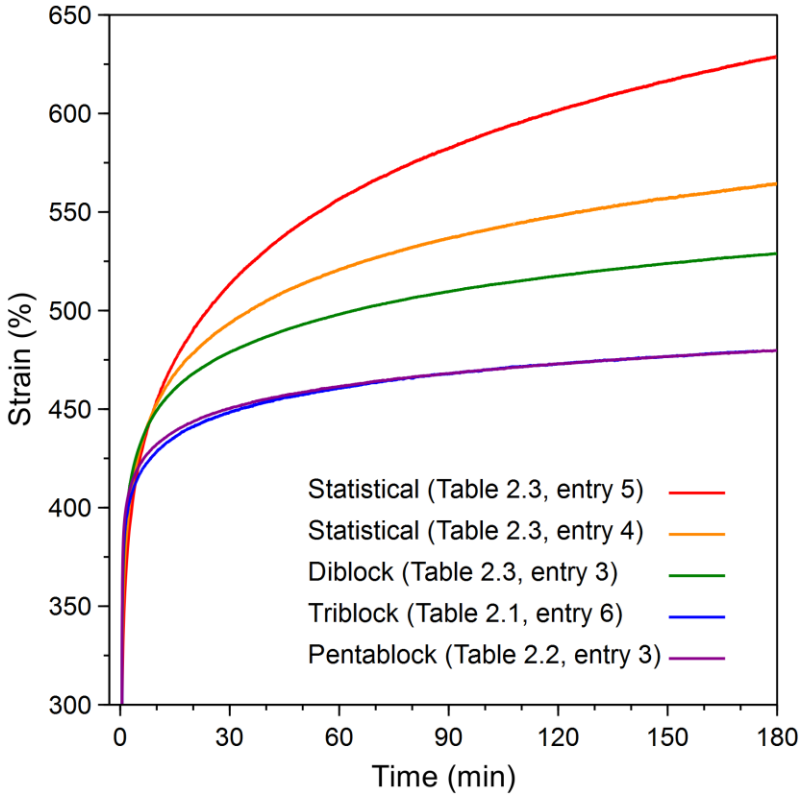


**Figure 2.11** Creep results for various block architectures, from pentablock to statistical copolymers. Samples were strained to 300% and held at constant force over a period of 3 hours. The change in strain over time is reported.

no benefit was gained through the synthesis of higher order multiblocks. These results show that although all samples generated with this catalyst system behave as elastomers, materials with two or more hard blocks are better suited for performance applications, as diblock and statistical copolymers more rapidly lose elasticity over longer periods of extension.

### *2.2.6 Mechanical Properties of Hard Block*

A sample of chain straightened poly(1-decene) was produced using complex **2.2** and the mechanical properties of the resulting material were analyzed in order to

understand the nature of the hard block. As expected, the semicrystalline hard block homopolymer behaved much differently than the block copolymers and the statistical copolymers. The material displayed a high Young's modulus (180.5 MPa) and plastic deformation during tensile testing. No elastic recovery was observed for this sample, underscoring the fact that the hard segment does not behave as an elastomer (Figure 2.12). The significance of the hard segment is in its ability to create anchoring units in the block copolymer matrix for elastic recovery and creep resistance.

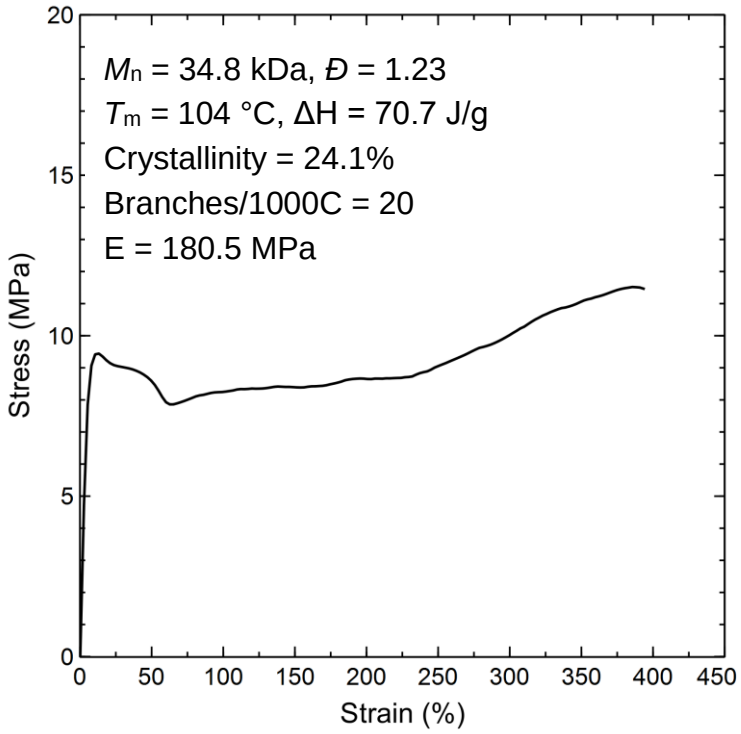


**Figure 2.12** Characterization and mechanical properties of poly(1-decene) produced by complex **2.2**. Synthesis can be found in the experimental section.

### *2.2.7 Dependence of Elastic Recovery on Cycling Rate*

All elastomer samples analyzed in this study were tested at the same cycling speed of 50 mm/min (~100% strain/min). This relatively fast cycling rate is convenient for

efficiently testing samples, but we were curious if the rate of hysteresis had a significant effect on the observed elastic recovery properties. Therefore, we tested both a triblock (Table 2.1, entry 6) and a statistical copolymer (Table 2.3, entry 5) at 5 mm/min (10% strain/min). We hypothesized that a slower rate of stretching may adversely affect the recovery properties of the statistical copolymer since it is more susceptible to creep under prolonged strain compared to the triblock copolymer. Surprisingly, the elastic recoveries observed under slow cycling conditions for *both* the triblock and the statistical copolymer samples were identical to those observed under standard cycling conditions. These results highlight that the standard hysteresis conditions used to measure elastic recovery in this work are valid.

### *2.2.8 Strain-Induced Crystallization of Statistical Copolymer*

Earlier in this work, we posited that strain-induced crystallization may be responsible for the loss of elastic recovery observed in TPE samples. To support this hypothesis, we performed a study using differential scanning calorimetry, where two tensile bars cut from the same film (Table 2.3, entry 4) were analyzed and compared. One bar was left unstrained, while the other bar was rapidly stretched to ~300% strain and relaxed about 15 times over the course of 30 seconds. A piece of the center gauge from each bar was removed and subjected to thermal analysis. The *first heating traces* were compared since we were specifically interested in sample history (strained vs unstrained). The unstrained sample showed a single melting endotherm at 43 °C, while the strained sample showed broadening, with two identifiable endotherms at 39 °C and

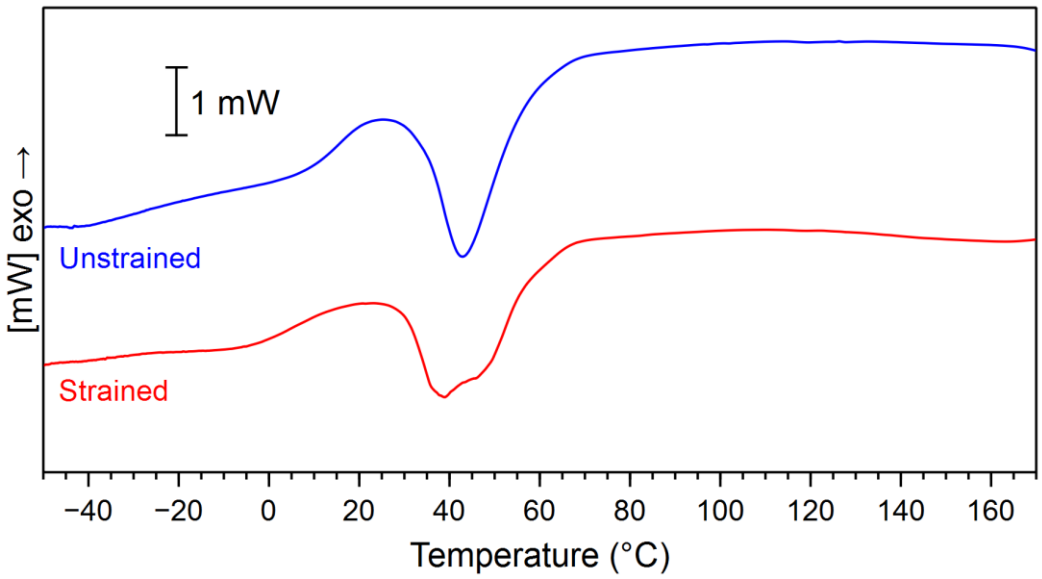


**Figure 2.13** DSC traces for unstrained and strained statistical copolymer, with *first heat* reported. Two peaks can be observed for strained sample.

46 °C. These results suggest that the crystallinity of the material changes after strain-induced deformation, potentially due to strain-induced crystallization.

For the block copolymers, there are two crystalline domains that give rise to the observed thermal properties; a high melting domain from the hard segment (~100 °C) and a low melting domain from the soft segment (~25–45 °C). Strain-induced crystallization is a phenomenon that occurs specifically in the soft segments of elastomers. We were interested what would happen to a block copolymer if it was heated above its low melting domain, but below its high melting domain. For this experiment, we used a film of a triblock copolymer (Table 2.1, entry 6) that had previously experienced strain-induced deformation and submerged it in a 70 °C water bath. Excitingly, the material experienced an immediate change back to the original shape before deformation (Figure 2.14). This suggests that strain-induced crystallites are primarily responsible for the loss in elastic recovery after strain induced deformation.

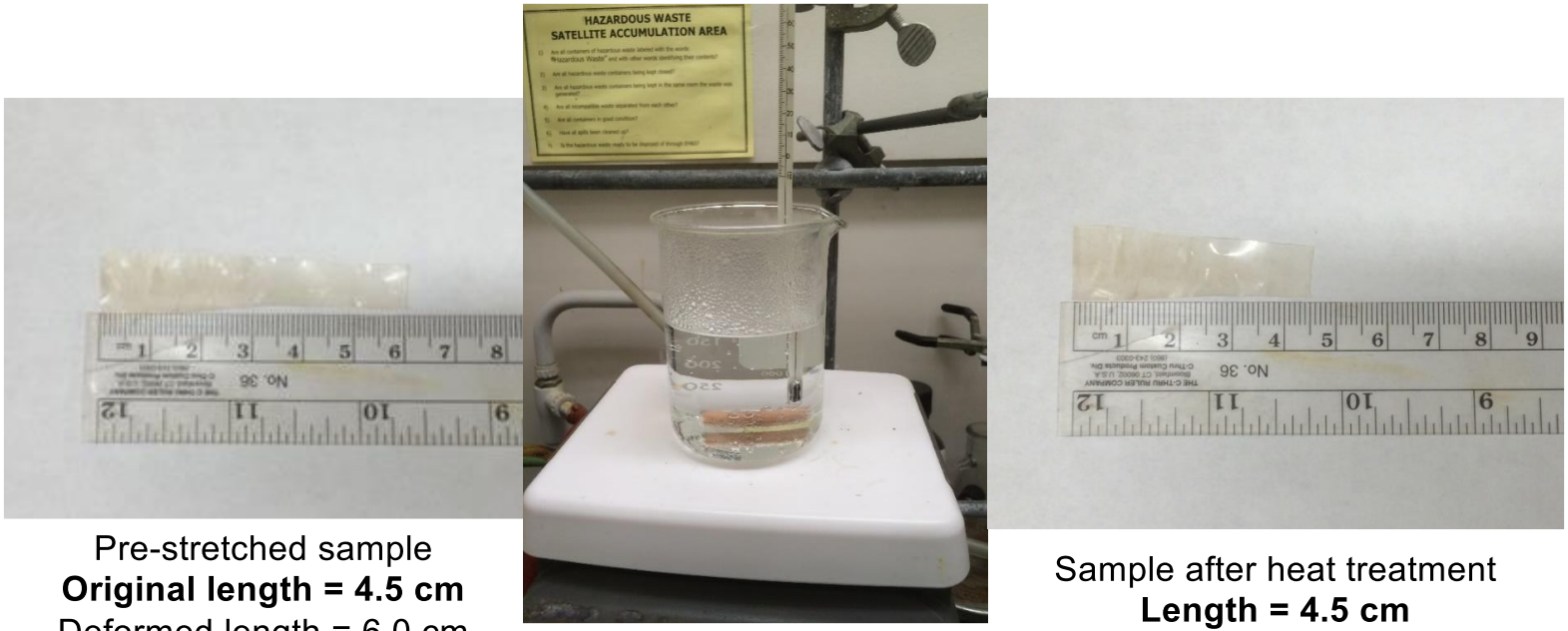


**Figure 2.14** Selective heating experiment of a thermoplastic elastomer block copolymer. Sample returns to original shape instantaneously upon heating to 70 °C.

## *2.3 Conclusions*

We report a chain walking strategy for the synthesis of thermoplastic elastomer block copolymers from inexpensive, potentially biorenewable feedstocks, where 1-decene is utilized as the hard segment and ethylene is utilized as the soft segment. Modest control of molar mass can be maintained by growing these samples in toluene, yielding triblock copolymers with mechanical properties that can be modulated by varying the ratio of the hard and soft blocks. Switching the solvent to chlorobenzene was pivotal for accessing improved triblock materials with low $Đ$ (1.3), high elongations before break (680–710%), low Young's moduli (9.8–14.4 MPa), and improved elastic recovery (80–85%). This additional control of block length allowed for higher order block copolymers to be synthesized, which displayed similar mechanical properties to triblock copolymers, albeit with lower overall elongations before break (570–630%). Diblock and statistical copolymers were synthesized and exhibited comparable elastic properties to triblock and pentablock copolymers, with even higher elongations before break (780–1120%). By performing a creep experiment, which maintained a constant force and measured change in strain over time, we observed that samples with higher numbers of blocks (triblock, pentablock) were more resistant to deformation compared to samples with lower numbers of blocks (diblock, statistical).

Our system allows access to a variety of elastic materials with tunable properties that can be modulated based on block architecture and ratio of hard content. Materials with lower numbers of blocks can elongate further before breaking, but elasticity is lost under sustained force. Conversely, materials with increased hard content are stronger but also show a decrease in elastic recovery. The TPEs accessed by our system have the

best mechanical properties to date when using α-olefins as the hard segments and ethylene as the soft segments, as well as comparable properties to other ethylene/1-octene block and statistical copolymers.[47] Promisingly, these materials have similar tensile strength and elastic recovery values to Dow's commercial olefin block copolymers. However, chemically cross-linked materials such as vulcanized rubber are still dominant in terms of their near perfect elastic recovery. Further catalyst optimization has the potential to improve upon the elastic recovery of the reported materials by modulating the chain walking process to obtain more crystalline hard segments and completely amorphous soft segments. In order to realize this goal, mechanistic studies of complex **2.2** and other related nickel species have been performed and will be discussed in the following chapter. This system demonstrates great promise due to the low cost and accessibility of the monomer feedstocks, along with the sustainability and reusability of the resulting materials.

## *2.4 Experimental*

### *2.4.1 General Considerations*

Air and/or moisture sensitive compounds were manipulated under an atmosphere of nitrogen using standard Schlenk techniques or an MBraun Labmaster glovebox. Flash column chromatography was performed using silica gel (particle size 40–64 μm, 230–400 mesh).

The $^{1}$H NMR, $^{13}$C{$^{1}$H} NMR spectra were recorded on Varian INOVA 500, Varian INOVA 600, or Varian INOVA 400 using the residual non-deuterated solvent signal as a reference. Polymers were analyzed using quantitative $^{1}$H and $^{13}$C NMR

spectroscopy in $Cl_2CDCDCl_2$ ($d_2$-TCE) at 135 °C. $Cr(acac)_3$ (acac=acetylacetonate) from Sigma Aldrich was added for quantitative $^{13}C$ NMR analysis of select samples (17 mg of $Cr(acac)_3$ in 0.5 mL of $d_2$-TCE, 0.1 M).[48] MestReNova software was used to process the NMR spectra.

High temperature gel permeation chromatography (GPC) was performed on Agilent PL-GPC 220 equipped with a refractive index (RI) detector and three PL-Gel Mixed B columns. GPC columns were eluted at 1.0 mL/min with 1,2,4-trichlorobenzene (TCB) containing 0.01 wt. % di-*tert*-butylhydroxytoluene (BHT) at 150 °C. The samples were prepared in TCB (with BHT) at a concentration of 1.0 mg/mL and heated at 150 °C for at least 1 hour prior to injection. GPC data calibration was done with monomodal polyethylene standards from Polymer Standards Service and Agilent.

Differential scanning calorimetry (DSC) measurements were performed on Mettler-Toledo Polymer DSC instrument equipped with an automated sampler. Polymer samples in crimped aluminum pans were analyzed under nitrogen at a heating rate of 10 °C/min from −70 to 200 °C. STARe software was used to process the collected data and melting points ($T_m$) were obtained and reported from the second heating run.

### *2.4.2 Materials*

Acenaphthenequinone (Sigma), triphenyl phosphite (Sigma), zinc chloride (Strem), nickel bromide dimethoxyethane adduct (Strem), palladium acetate (Acros), 1-naphthylamine (AK Scientific), silver acetate (AK Scientific), potassium hydroxide (Macron), acetic acid (Macron), 2-picolinic acid (Alfa Aesar), potassium oxalate (Alfa

Aesar), 4-iodobenzotrifluoride (Oakwood Chemical) and pyridine (Fisher Scientific) were used as received.

Anhydrous chlorobenzene was purchased from Sigma Aldrich, sparged with nitrogen for 40 minutes and stored over activated 4 Å molecular sieves. 1-Decene was purchased from Acros Chemicals (95% purity), distilled and stored over activated 4 Å molecular sieves prior to use. Ethylene was from Airgas, Inc. Methylaluminoxane (MAO) was generously donated by Albemarle Corporation (30 wt. % in toluene) and dried by removing volatiles (toluene and trace trialkylaluminum) under vacuum and heating at 40 °C for at least 8 hours. Anhydrous toluene, hexanes, and dichloromethane (HPLC) were purchased from Fisher Scientific, sparged with nitrogen for 40 minutes, and purified over solvent columns. NMR solvents were purchased from Cambridge Isotope Laboratories and stored over activated 4 Å molecular sieves.

### *2.4.3 Complex Synthesis*

Complex **2.2** was previously reported and synthesized according to literature procedures.[30] A basic schematic of the synthesis can be viewed below. The resulting dark red crystals were stored in a vial inside a glovebox and crushed into a fine powder immediately before use.

**Scheme 2.3** General Synthesis of Complex **2.2**

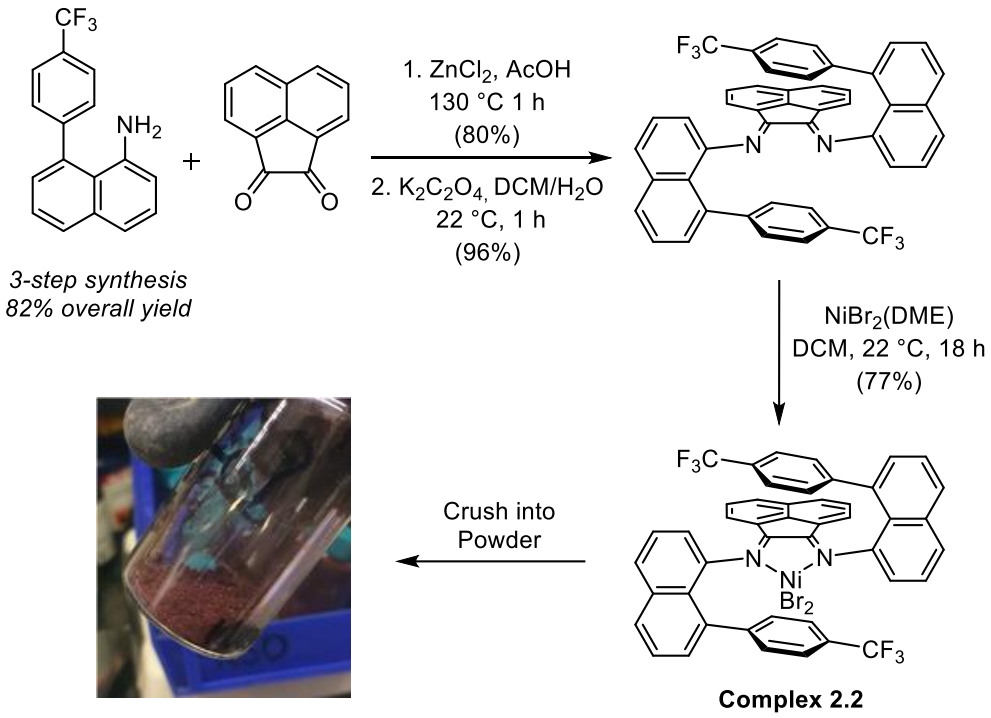


### *2.4.4 General Polymerization Scheme (Synthesis of Block Copolymers)*

All polymerizations were set up in a MBraun Labmaster glovebox. An oven-dried 200 mL Fisher-Porter bottle (Andrews Glass) equipped with a magnetic stir bar was charged with MAO (200 eq, 6.79 mmol), solvent (72 mL of toluene or chlorobenzene) and 1-decene (0.1 M, 1.6 mL or 0.2 M, 3.2 mL). The vessel was sealed with a Swagelok reactor head. Complex **2.2** (1 eq, 34.1 μmol) was dissolved in chlorobenzene (6 mL) and drawn into a gas tight syringe equipped with a stainless-steel needle, then sealed at the tip using a rubber septum. The vessel and syringe were removed from the glovebox. The vessel was submerged in a water bath, connected to a nitrogen inlet and pressurized to 20 psig (1.4 atm). Under this pressure, the catalyst solution was injected. The polymerization was run for the appropriate time to grow the first hard block from 1-decene. An aliquot was removed (8 mL) and precipitated into

acidic methanol (5 % HCl v/v, ~50 ml) for future analysis. The nitrogen atmosphere was then exchanged with ethylene (16 psig, 1.1 atm) by cycling ethylene into the bottle and releasing pressure through the top valve via a syringe needle inserted through a rubber septum at least 3 times. The ethylene inlet was left open for a given amount of time to grow the soft block, after which the ethylene atmosphere was replaced with nitrogen by cycling nitrogen into the bottle and releasing pressure through the top valve at least 8 times. An aliquot was removed (3 mL) and precipitated into acidic methanol for future analysis. For triblock copolymers, the polymerization was quenched after the given time by reducing pressure through the top valve and injecting 10 mL of methanol into the vessel with vigorous stirring. The polymer solution was then precipitated into a solution of acidic methanol (5 % HCl v/v ~500 mL), and stirred for at least 4 hours. All polymers were filtered, washed with methanol and dried under vacuum at 45 °C until constant weight. For higher order block copolymers, additional cycles were repeated until the desired block architecture was achieved.

### *2.4.5 Synthesis of Statistical Copolymers*

An oven-dried 200 mL Fisher-Porter bottle equipped with a magnetic stir bar was charged with MAO (200 eq, 6.79 mmol), appropriate solvent (72 mL of toluene or chlorobenzene) and 1-decene (0.2 M, 3.2 mL). Complex **2.2** was dissolved in chlorobenzene (6 mL) and drawn into a gas tight syringe equipped with a stainless-steel needle, sealed at the tip using a rubber septum. The vessel and syringe were removed from the glovebox. The vessel was submerged in a water bath and connected to an ethylene inlet (1.1 atm), cycling 3 times to exchange the nitrogen environment. While

open to ethylene, the catalyst was immediately injected into the reaction vessel. After the desired polymerization time, the pressure was reduced through the top valve and the reaction mixture was quenched with methanol (10 mL) under vigorous stirring. The polymer solution was precipitated into acidic methanol (5% HCl v/v, ~500 mL), and stirred for at least 4 hours. The resulting polymers were filtered, washed with methanol and dried in vacuo until constant weight.

### *2.4.6 Synthesis of Chain Straightened Poly(1-Decene)*

An oven-dried 500 mL Fisher-Porter bottle equipped with a magnetic stir bar was charged with MAO (200 eq, 18.1 mmol), chlorobenzene (210 mL), and 1-decene (0.2 M, 8.57 mL). Complex **2.2** (1 eq, 90.5 μmol) was slurried in chlorobenzene (7 mL) and drawn into a gas tight syringe equipped with a stainless-steel needle, sealed at the tip using a rubber septum. The vessel and syringe were removed from the glovebox, with the vessel submerged in a water bath and pressurized with 1.1 atm of $N_2$. After temperature equilibration (~15 minutes), the slurry of complex **2.2** was injected under positive pressure. After 22 hours, the reaction was quenched with methanol (10 mL) and precipitated into acidic methanol (5% HCl v/v, ~1000 mL), and stirred for at least 7 hours. The resulting polymer was filtered, washed with methanol and dried in vacuo until constant weight, yielding 2.45 g of a white, powdery material.

### *2.4.7 Casting Polymer Films*

All polymer samples were melt-casted using a Carver Press hot plate. Each sample was loaded into a rectangular stainless steel mold (92 mm x 30 mm x 0.5 mm) sandwiched between two Mylar sheets and two stainless steel sheets and pressed under a pressure of ~52 MPa at 110 °C for 15 minutes. At this pressure, the sample was cooled to 22 °C at a rate of 6 °C/min over a period of 20 minutes. The rectangular film was removed from the mold and excess polymer around the edges was removed with a razor blade. The film was subsequently cut into tensile bars using a stainless-steel polymer die (gauge length = 16 mm, gauge width = 3 mm, gauge thickness = 0.6 mm) to give polymer bars which were rubbery, clear and easy to handle.

### *2.4.8 Mechanical Studies*

Mechanical studies were performed using a Shimadzu Autograph AGS-X Series tensile tester. For tensile strength and hysteresis experiments, a crosshead velocity of 50 mm/min was used for each sample. For tensile strength experiments, tensile bars were elongated until break. At least five tensile bars were tested for each

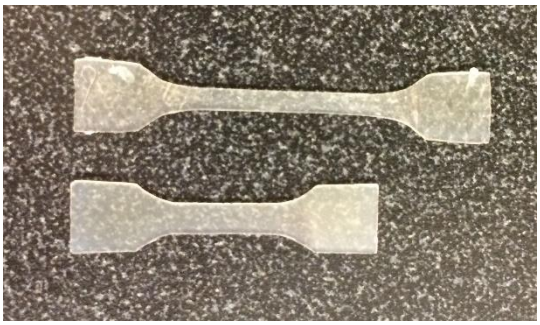

**Figure 2.15** Representative image of tensile bars. Top bar has been stretched and exhibits shape deformation.

individual sample. For hysteresis experiments, tensile bars were cycled ten times to 300% strain. Three tensile bars were tested for each individual sample to ensure reproducibility.

### *2.4.9 $^{1}H$ NMR and $^{13}C$ NMR Analysis of Samples*

All samples were analyzed by $^{1}H$ NMR to obtain the basic branching/1000C metric commonly used in the literature. The equation used to determine branching was developed by Rieger et. al.[49] and is displayed below:

$$\text{total branching/1000C} = \frac{\frac{1}{3} I_{CH_3}}{\frac{\left(I_{CH_2} - \left(\frac{1}{3} I_{CH_3}\right)\right)}{2} + \frac{1}{3} I_{CH_3}} \times 1000$$

Select samples were analyzed by quantitative $^{13}C$ NMR spectroscopy in order to determine the specific branching distribution. Signals were assigned based on previous literature reports.[30,50] All signals were integrated, with the total integral value set to 1000. Branching values were then calculated based on the follow simplified equations described below in Figure 2.18. Only methyl and branches six carbons and longer were observed in these systems, which is typical for α-diimine nickel catalyst systems.

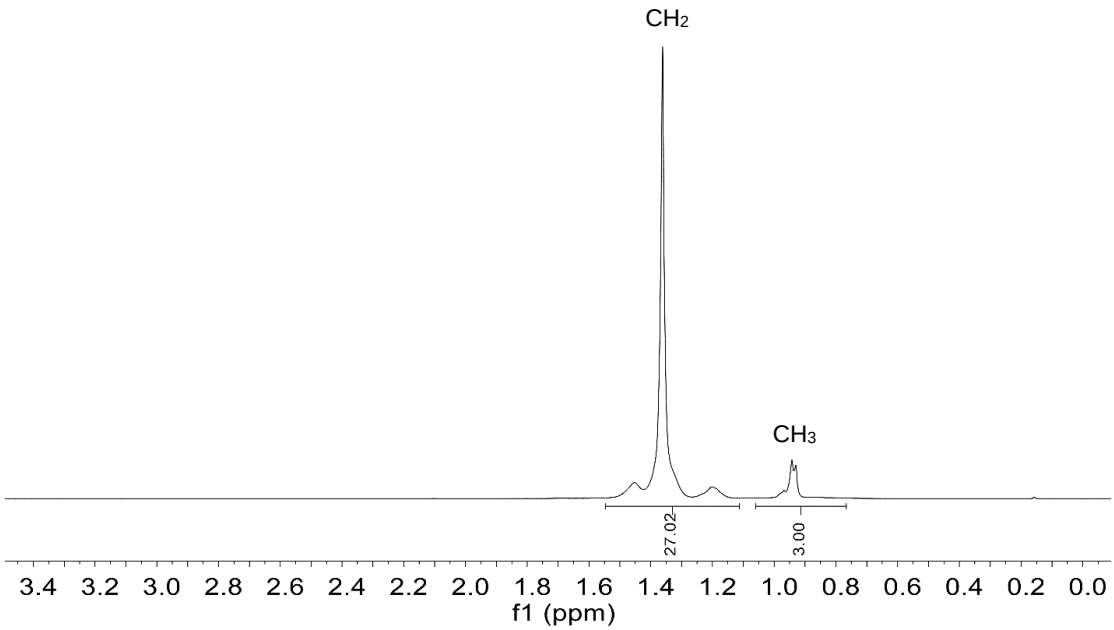


**Figure 2.16** Representative $^{1}$H NMR spectrum of a pentablock copolymer (Table 2.2, entry 1).

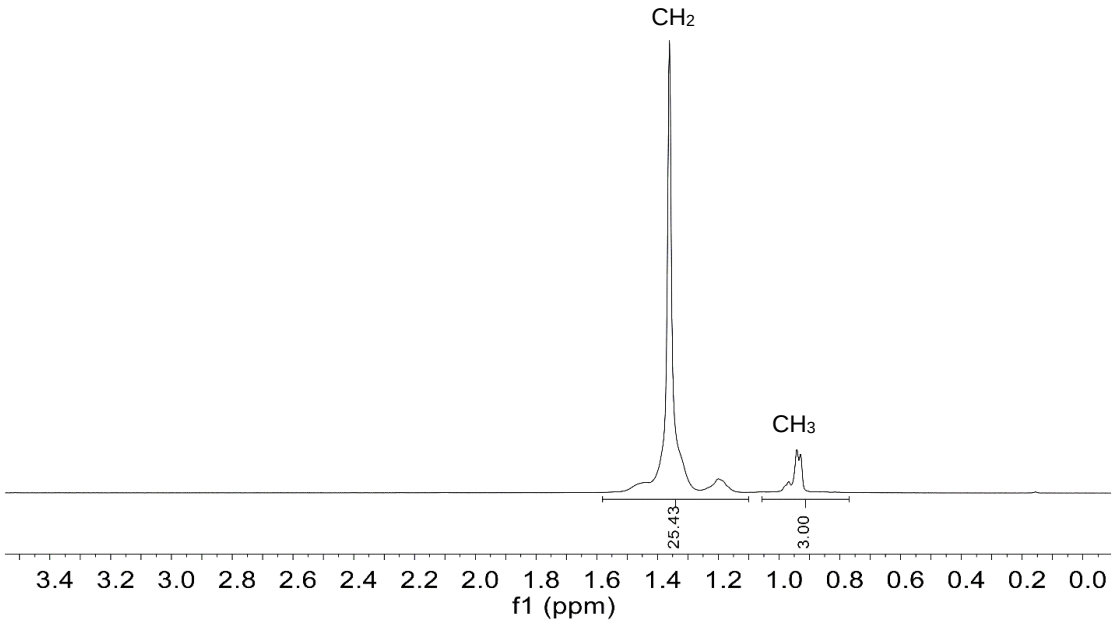


**Figure 2.17** Representative $^{1}$H NMR spectrum of a statistical copolymer (Table 2.3, entry 5).

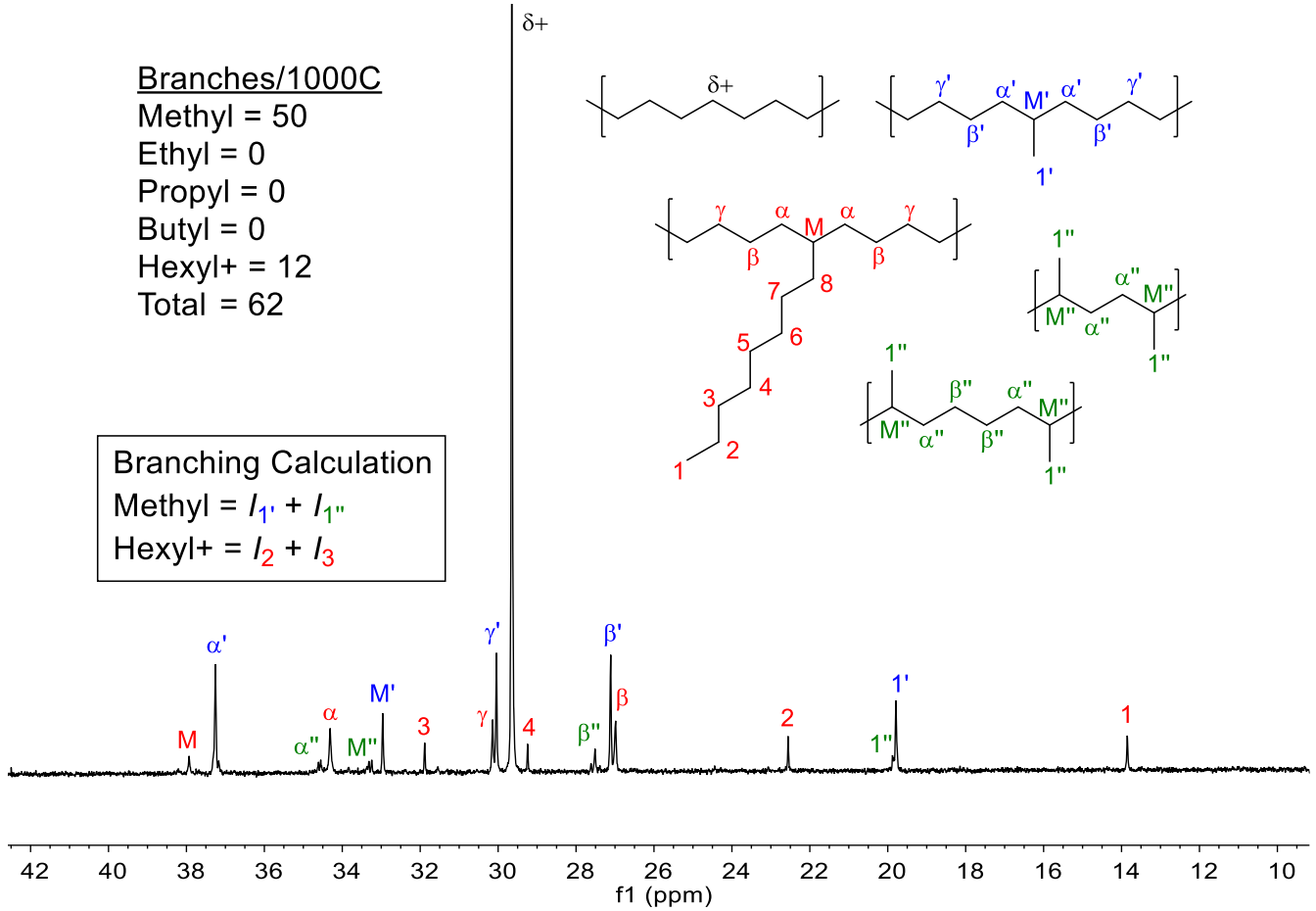


**Figure 2.18** $^{13}$C NMR spectrum with assignments and branching numbers for a triblock copolymer (Table 2.1, entry 6).

### *2.4.10 Additional Data for TPE Samples*

**Table 2.4** Yields and Branching Numbers for all TPE Samples Previously Discussed in Chapter 2

| Table | Entry | Block Structure | Yield (g) | Branches/1000C[a] |
|---|---|---|---|---|
| 2.1 | 1 | Tri- | 1.64 | 69 |
| 2.1 | 2 | Tri- | 2.08 | 65 |
| 2.1 | 3 | Tri- | 2.49 | 57 |
| 2.1 | 4 | Tri- | 1.34 | 60 |
| 2.1 | 5 | Tri- | 2.38 | 74 |
| 2.1 | 6 | Tri- | 2.39 | 70 |
| 2.2 | 1 | Penta- | 3.25 | 65 |
| 2.2 | 2 | Penta- | 2.97 | 68 |
| 2.2 | 3 | Penta- | 3.24 | 64 |
| 2.2 | 4 | Hepta- | 2.32 | 65 |
| 2.3 | 1 | Di- | 2.54 | 70 |
| 2.3 | 2 | Di- | 2.43 | 72 |
| 2.3 | 3 | Di- | 1.93 | 62 |
| 2.3 | 4 | Stat. | 2.33 | 72 |
| 2.3 | 5 | Stat. | 3.44 | 83 |

[a]Determined by $^{1}$H NMR using the equation described in Section 2.4.9.

### *2.4.11 GPC Traces of Select TPE Samples Exhibiting Bimodality*

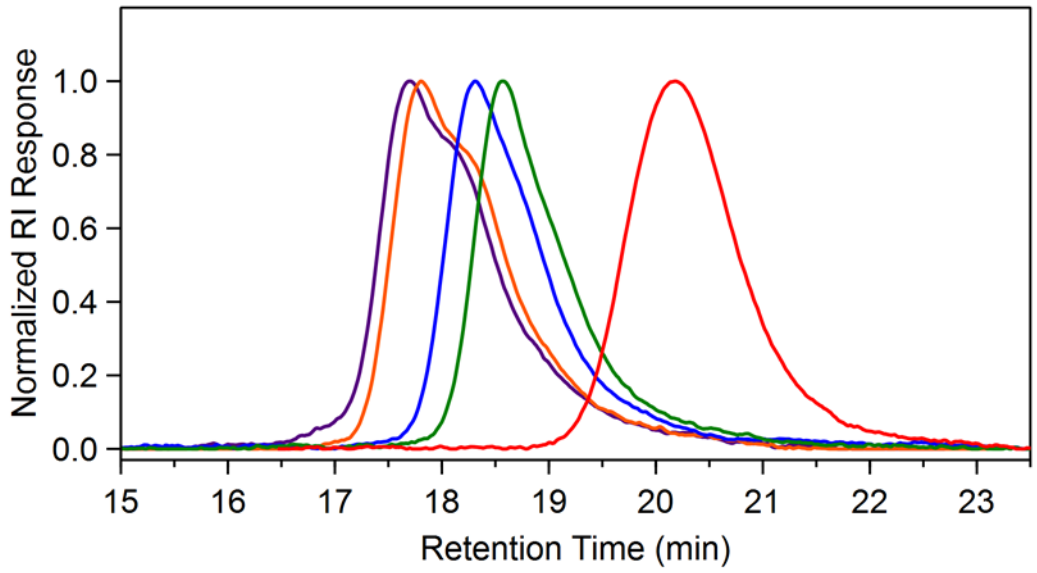


**Figure 2.19** GPC trace of successive blocks of a pentablock copolymer (Table 2.2, entry 3).

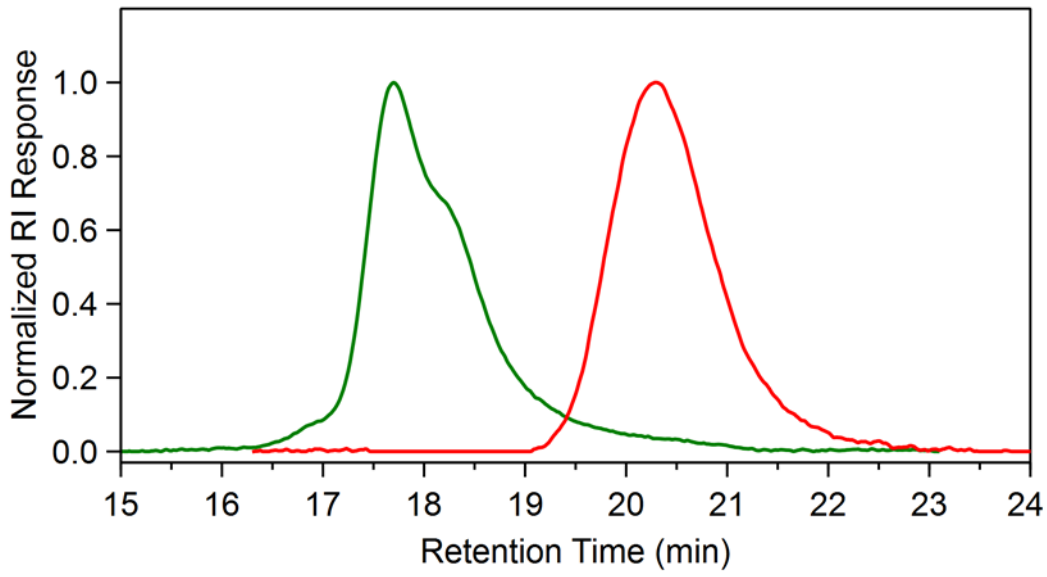


**Figure 2.20** GPC trace of successive blocks of a diblock copolymer (Table 2.3, entry 2).

## REFERENCES


(1) Craver, C.; Carraher, C.; Applied Polymer Science: 21st Century, Elsevier Science: Oxford, 2000.

(2) Akiba, M.; Hashim, A. S. *Prog. Polym. Sci.* **1997**, *22*, 475–521.

(3) Adhikari, B.; De, D.; Maiti, S. *Prog. Polym. Sci.* **2000**, *25*, 909–948.

(4) (a) Holden, G.; Kricheldorf, H. R.; Quirk, R. P. Thermoplastic Elastomers, 3rd ed.; Hanser Publishers: Munich, 2004. (b) Brobny, J.G. Handbook of Thermoplastic Elastomers; William Andrews: New York, 2007.

(5) Koo, C. M.; Hillmyer, M. A.; Bates, F. S. *Macromolecules* **2006**, *39*, 667–677.

(6) Schneiderman, D. K.; Hill, E. M.; Martello, M. T.; Hillmyer, M. A. *Polym. Chem.* **2015**, *6*, 3641–3651.

(7) Ocando, C.; Fernández, R.; Tercjak, A.; Mondragon, I.; Eceiza, *Macromolecules* **2013**, *46*, 3444–3451.

(8) Hirao, A.; Goseki, R.; Ishizone, T. *Macromolecules* **2014**, *47*, 1883–1905.

(9) Morton, M.; McGrath, J. E.; Juliano, P. C. *J. Polym. Sci., Part C: Polym. Symp.* **1969**, *26*, 99–115.

(10) Weisz, P. B. *Physics Today* **2004**, *57*, 47–52.

(11) Robertson, M. L; Hillmyer, M. A.; Mortamet, A. -C.; Ryan, A. J. *MRS Bull.* **2010**, *35*, 194–200.

(12) Takahara, I.; Saito, M.; Inaba, M.; Murata, K. *Catal. Lett.* **2005**, *105*, 249−252.

(13) Small, B. L.; Brookhart, M. *J. Am. Chem. Soc.* **1998**, *120*, 7143–7144.

(14) Thomas, R. M.; Keitz, B. K.; Champagne, T. M.; Grubbs, R. H. *J. Am. Chem. Soc.* **2011**, *133*, 7490−7496.

(15) Arriola, D. J.; Carnahan, E. M.; Hustad, P. D.; Kuhlman, R. L.; Wenzel, T. T. *Science* **2006**, *312*, 714−719.

(16) (a) Ohtaki, H.; Deplace, F.; Vo, G. D.; LaPointe, A. M.; Shimizu, F.; Sugano, T.; Kramer, E. J.; Fredrickson, G. H.; Coates, G. W. *Macromolecules* **2015**, *48*, 7489–7494. (b) Ohtaki, H; Shimizu, F; Coates, G. W.; Fredrickson, G. H. *PCT Int. Appl.* WO 2013061974 A1 20130502, 2013.

(17) Coates, G. W.; Waymouth, R. M. *Science* **1995**, *267*, 217−219.

(18) Harney, M. B.; Zhang, Y.; Sita, L. R. *Angew. Chem. Int. Ed.* **2006**, *45*, 2400−2404.

(19) Rose, J. M.; Deplace, F.; Lynd, N. A.; Wang, Z.; Hotta, A.; Lobkovsky, E. B.; Kramer, E. J.; Coates, G. W. *Macromolecules* **2008**, *41*, 9548−9555.

(20) Subramanyam, U.; Sivaram, S. *J. Polym. Sci., Part A: Polym. Chem*. **2007**, *45*, 191−210.

(21) Johnson, L. K.; Killian, C. M.; Brookhart, M. *J. Am. Chem. Soc.* **1995**, *117*, 6414−6415.

(22) McCord, E. F.; McLain, S. J.; Nelson, L. T. J.; Ittel, S. D.; Tempel, D.; Killian, C. M.; Johnson, L. K.; Brookhart, M. *Macromolecules* **2007**, *40*, 410−420.

(23) Tempel, D. J.; Johnson, L. K.; Huff, L. R.; White, P. S.; Brookhart, M. *J. Am. Chem. Soc.* **2000**, *122*, 6686−6700.

(24) For a recent perspective on chain walking polymerization with late transition metal complexes: Guo, L.; Dai, S.; Sui, X.; Chen, C. *ACS Catal.* **2016**, *6*, 428−441.

(25) Bomfim, J. A. S.; Dias, M. L.; Filgueiras, C. A. L.; Peruch, F.; Deffieux, A. *Catal. Today* **2008**, *133-135*, 879−885.

(26) Hu, H.; Gao, H.; Chen, D.; Li, G.; Tan, Y.; Liang, G.; Zhu, F.; Wu, Q. *ACS Catal.*, **2015**, *5*, 122−128.

(27) Dai, S.; Sui, X.; Chen, C. *Chem. Commun.* **2016**, *52*, 9113−9116.

(28) Killian, C. M.; Tempel, D. J.; Johnson, L. K.; Brookhart, M. *J. Am. Chem. Soc.* **1996**, *118*, 11664−11665.

(29) Leone, G.; Mauri, M.; Bertini, F.; Canetti, M.; Piovani, D.; Ricci, G. *Macromolecules* **2015**, *48*, 1304−1312.

(30) Vaidya, T.; Klimovica, K.; LaPointe, A. M.; Keresztes, I.; Lobkovsky, E. B.; Daugulis, O.; Coates, G. W. *J. Am. Chem. Soc.* **2014**, *136*, 7213−7216.

(31) Zhang, D.; Nadres, E. T.; Brookhart, M.; Daugulis, O. *Organometallics* **2013**, *32*, 5136−5143.

(32) This system can also be utilized with different length α-olefins other than 1-decene to produce thermoplastic elastomers. Complex **2.2** (and other α-diimine nickel complexes) are known to polymerize longer chain α-olefins (such as 1-octadecene) and access materials with higher melting temperatures than those found using shorter chain α-olefins. Varying the length of the α-olefins could potentially modulate the properties of the resulting materials. However, since 1-decene can be accessed renewably not only through bioethylene oligomerization but also the ethenolysis of fatty acids, we chose to focus our studies using 1-decene as the hard segment.

(33) Busico, V.; Cipullo, R.; Cutillo, F.; Friederichs, N.; Ronca, S.; Wang, B. *J. Am. Chem. Soc.* **2003**, *125*, 12402−12403.

(34) Detailed studies on ion pairing in late transition metal complexes are limited, but ion pairing in early transition metal complexes are well documented. For zirconium metallocene complexes, the nature of the ion pair can affect catalyst activity and stability, as well as polymer molecular weight, tacticity, and branching content. For an informative review on ion pairing, please refer to: Macchioni, A. *Chem. Rev.* **2005**, *105*, 2039−2074.

(35) See experimental section for more details.

(36) The maximum $T_m$ of the 1-decene hard block measures at 106 °C, but a smaller endotherm can be observed at 95 °C in Figure 2.4. We suspect this endotherm is due to branching defects in the hard block, possibly from the melting of long side chains.

(37) Ayoub, G.; Zaïri, F.; Fréderix, C.; Gloaguen, J. M.; Naït-Abdelaziz, M.; Seguela, R.; Lefebvre, J. M. *Int. J. Plast.* **2011**, *27*, 492−511.

(38) Toki, S.; Fujimaki, T.; Okuyama, M. *Polymer J.* **2000**, *41*, 5423−5429.

(39) Thien-Nga, L.; Guilie, J.; Le Tallec, P. *European Congress on Computational Methods in Applied Sciences and Engineering* **2012**, 10.

(40) Hotta, A.; Cochran, E.; Ruokolainen, J.; Khanna, V.; Fredrickson, G. H.; Kramer, E. J.; Shin, Y. W.; Shimizu, F.; Cherian, A. E.; Hustad, P. D.; Rose, J. M.; Coates, G. W. *Proc. Natl. Acad. Sci. USA* **2006**, *103*, 15327−15332.

(41) Bates, F. S.; Fredrickson, G. H.; Hucul, D.; Hahn, S. F. *AlChE J.* **2001**, *47*, 762−765.

(42) Growing the final hard block was prohibitively challenging at 0.1 M, likely due to increased viscosity and low free monomer concentration at the end of polymerization. This issue was originally circumvented by injecting additional 1-decene for the growth of the final block (Table 2.2, entry 1), but this procedure requires estimating the amount of 1-decene consumed in the reaction in order to add the correct amount of monomer to return the concentration to 0.1 M. To avoid issues with reproducibility, polymerizations were performed at 0.2 M.

(43) The sample synthesized as described in Table 2.2, entry 4 was an exception to this trend, where crystallinity did not predictably change between enchaining hard and soft segments.

(44) Table 2.3, entry 5 (produced in chlorobenzene) is an underestimate of the true strain at break for the sample. During tensile strength testing, samples broke near the grips as opposed to the gauge area of the tensile bar. Two tensile bars tested broke in the gauge area at elongations beyond 1300% before break. These samples were omitted from the average calculations, but they are likely more indicative of the true properties of this material.

(45) Poon, B. C.; Dias. P.; Ansems, P.; Chum, S. P.; Hiltner, A.; Baer, E. *J. Appl. Polym. Sci.* **2007**, *104*, 489−499.

(46) Wang, H. P.; Khariwala, D. U.; Cheung, W.; Chum, S. P.; Hiltner, A.; Baer, E. *Macromolecules* **2007**, *40*, 2852−2862.

(47) Wang, H. P.; Chum, S. P.; Hiltner, A.; Baer, E. *J. Appl. Polym. Sci.* **2009**, *113*, 3236−3244.

(48) Prasad, J. V.; Rao, P. V. C.; Garg, V. N. *Eur. Polym. J.* **1991**, *27*, 251−254.

(49) Meinhard D.; Wegner, M.; Kipiani, G.; Hearley, A.; Reuter, P.; Fischer, S.; Marti, O.; Rieger, B. New Nickel (II) Diimine Complexes and the Control of Polyethylene Microstructure by Catalyst Design. *J. Am. Chem. Soc.* **2007**, *129*, 9182−9191.

(50) Azoulay, J. D.; Bazan, G. C.; Galland, G. B. *Macromolecules* **2010**, *43*, 2794−2800.

# CHAPTER 3

# UNDERSTANDING THE INSERTION PATHWAYS AND CHAIN WALKING MECHANISMS OF α-DIIMINE NICKEL CATALYSTS FOR α-OLEFIN POLYMERIZATION: A $^{13}C$ NMR SPECTROSCOPIC INVESTIGATION

Adapted with permission from O'Connor, K. S.; Lamb, J. R.; Vaidya, T.; Keresztes, I.; Klimovica, K.; LaPointe, A. M.; Daugulis, O.; Coates, G. W. *Macromolecules*, **2017**, *Accepted.*

## *3.1 Introduction*

Brookhart's discovery of late transition metal α-diimine complexes for the polymerization of ethylene and α-olefins has sparked widespread experimental and theoretical study over the past two decades.[1] Cationic nickel(II) and palladium(II) α-diimine complexes are capable of producing polyolefins from ethylene and α-olefins with variable branching densities and polymer microstructures. This diversity allows access to materials with a broad range of thermal, mechanical, and rheological properties.[2] The structural diversity stems primarily from a competitive reaction between olefin insertion and a catalyst isomerization event known as "chain walking." Chain walking involves β-hydride elimination followed by metal hydride reinsertion into the growing polymer chain with opposite regiochemistry (Scheme 3.1). Metal migration along the polymer backbone allows propagation to occur at sites beyond the position generated in the initial insertion. For α-olefin polymerization, the regiochemistry of the initial olefin insertion paired with the position of the next insertion event dictates the overall branching structure (Scheme 3.2). For example, performing a 2,1-insertion followed by complete chain walking and insertion off the chain end (ω,1-enchainment) results in a "chain straightened" segment with repeated methylene units. In contrast, 1,2-insertion followed by complete chain walking and insertion (ω,2-

**Scheme 3.1** Simplified Chain Walking Isomerization Pathway

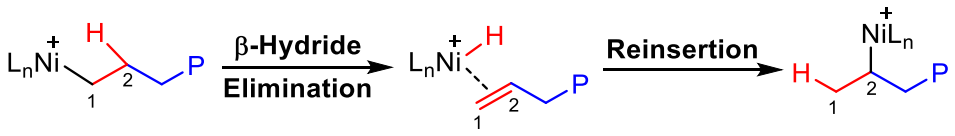

enchainment) installs a methyl branch. The numerous combinations of insertion and chain walking pathways that can occur give rise to unique polyolefin microstructures.

Higher α-olefins are highly abundant, inexpensive monomers that are interesting to consider for polymerization. α-Olefins are primarily derived from the oligomerization of ethylene [3] but can also be sourced from renewable feedstocks via the ethenolysis of fatty acid derivatives.[4] In industrial polymerizations, α-olefins are primarily used as comonomers for ethylene polymerizations to introduce branching and decrease crystallinity.[5,6] The early metal catalysts used in industry limit poly(α-olefins) to highly branched, amorphous materials because these catalysts do not readily chain walk. Late

**Scheme 3.2** Possible Insertion Pathways for α-Olefins using α-Diimine Nickel Catalysts, with the Green Pathway Resulting in Chain Straightened Materials

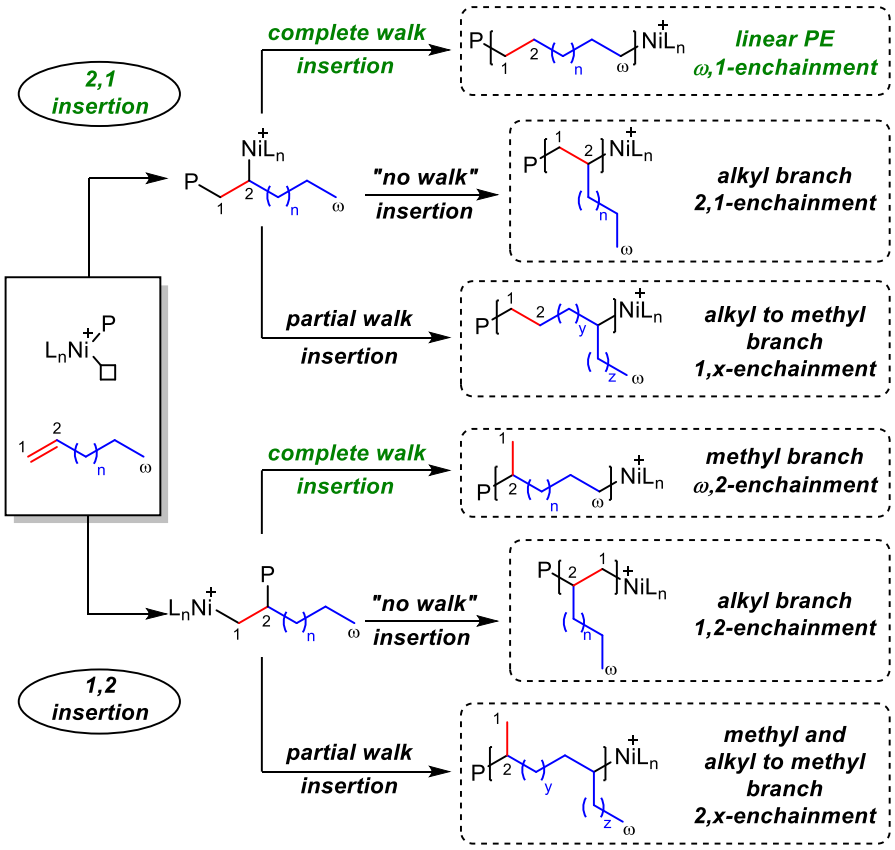

metal catalysts, however, easily undergo chain walking, which allows for a broad range of structures and properties for poly(α-olefins).

One of the primary challenges in α-olefin polymerization using late transition metal catalysts is exhibiting precise control over both the regiochemistry of olefin insertion and the location of the next insertion event after chain walking. There are several distinct positions where a nickel complex can insert on a growing polymer chain that will lead to specific branching structures (Figure 3.1). Generally, catalysts that combine indiscriminate insertion regioselectivity and random chain walking produce highly branched materials with low melting temperatures and low crystallinity. Conversely, catalysts with high selectivity for ω,1-enchainment produce chain-straightened poly(α-olefins) with high melting temperatures and high crystallinity.

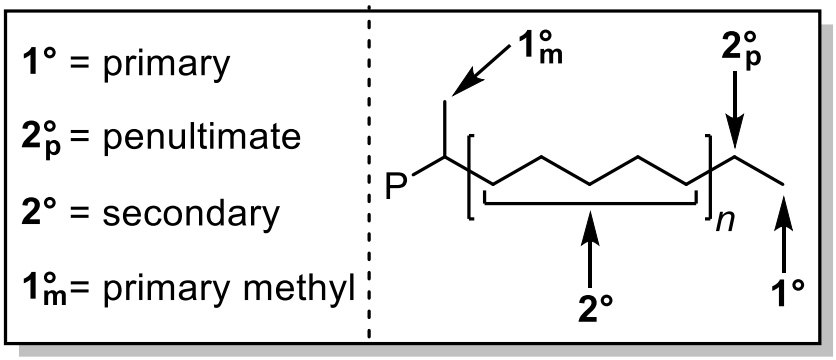


**Figure 3.1** Nomenclature for possible positions where a nickel complex can insert on a growing polymer chain.

The selectivity for a given polymerization is determined by both the identity of the catalyst and the polymerization conditions, such as monomer concentration. Coates/Daugulis,[7] Merna,[8] and Shiono[9] demonstrated that lower α-olefin concentrations generally result in polymers with fewer branches and improved thermal properties. Lower branching is likely due to a decreased rate in monomer trapping relative to the

rate of chain walking, allowing for more instances of complete chain walking before the next insertion event. For certain α-diimine nickel systems, however, the specific change in branch type is more pronounced than the change in the overall number of branches. Ricci[2h] and Leone[2i] systematically showed that higher α-olefin concentrations did not have a significant effect on the overall branching numbers in their resulting poly(α-olefins), but there was a clear increase in the ratio of alkyl branches compared to methyl branches. The effect of temperature on catalyst selectivity is also profound. An α-diimine nickel complex with a bulky camphyl backbone[10] and a nickel complex with a cyclophane-based structure[11] produce more linear materials at higher polymerization temperatures. Coates and coworkers have developed a chiral C2-symmetric nickel catalyst that shows highly selective 1,2-insertion of α-olefins at low temperatures, resulting in precise ω,2-enchainment.[1g, 12]

Further catalyst development has resulted in some of the highest selectivities for ω,1-enchainment in α-olefin polymerization under ambient conditions. Wu and coworkers demonstrated that high 2,1- or 1,2-selectivity for 1-hexene polymerization could be dictated by the ligand substitution pattern of a mixed imine-amine nickel complex.[13] Chen and coworkers have reported an effective iminopyridyl nickel catalyst with good selectivity for chain straightening 1-hexene, resulting in polymers with melting temperatures near 106 °C.[14] Coates and Daugulis have shown that arylnaphthyl-α-diimine nickel "sandwich" complexes produce chain straightened poly(α-olefins) with the highest melting temperatures reported up-to-date. Polymers with melting points up to 113 °C were produced.[7]

**Scheme 3.3** 1st Generation Mechanistic Explanation of Enchainments for α-Olefin Polymerizations Using α-Diimine Nickel Catalysts

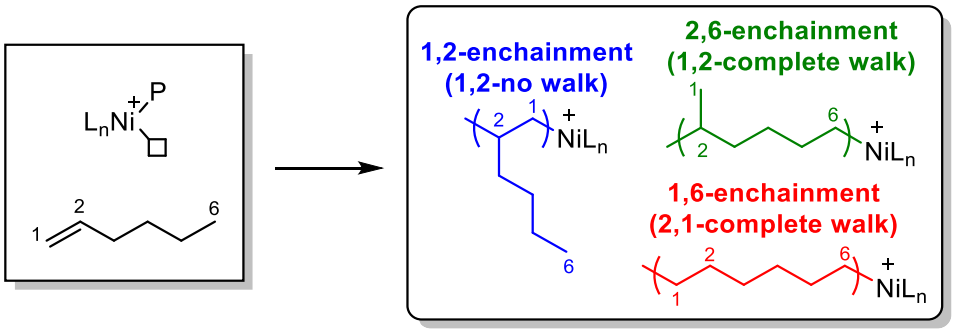


Despite the advances in nickel catalyzed α-olefin polymerizations, a system with "perfect" selectivity for ω,1-enchainment has not been developed. Such a system would result in a high density polyethylene-equivalent polymer with a $T_m$ near 135 °C. To achieve this, a catalyst system must have perfect 2,1-insertion selectivity followed by efficient chain-running to the end of polymer chain coupled with an exclusive migratory insertion off the primary chain end position. If we can better appreciate how the catalyst and reaction conditions affect the nature of the mechanistic errors during α-olefin polymerization, we can improve our overall understanding of these systems. We believe a more complete understanding of α-olefin polymerization with α-diimine nickel complexes will ultimately allow for the development of improved catalysts that exhibit the desired selectivity.[15]

Impressive microstructural characterizations and mechanistic studies of poly(α-olefins) produced by nickel catalysts have expanded the understanding of these polymerizations.[16] Initially, it was assumed that the vast majority of insertions occurred off primary carbons, meaning 1,2-insertions installed branches and 2,1-insertions installed linear units (Scheme 3.3). This assumption allowed for the simple calculation of regioselectivity through $^1$H NMR spectroscopy using eq (3.1), below, where $B$ = the

number of branches as determined by the $^{1}$H NMR spectrum and $x$ = the number of insertions necessary to produce a polymer with 1000 carbons (which is dependent on the length of the α-olefin).

$$\%(1,2) = \frac{B \text{ branches}}{1000 \text{ C}} \frac{1 \text{ (1,2)}}{1 \text{ branch } x \text{ insertions}} \frac{1000 \text{ C}}{} * 100 \quad (3.1)$$

In 2004, Subramanyam and coworkers used $^{13}$C NMR spectroscopy to confirm the presence of head-to-head methyl branches in their analysis of poly(1-hexene), a branching unit that can only occur through 1,2-insertion off a secondary penultimate carbon.[17] Even though these branching units were small compared to the rest of the signal, this work showed that the polymerizations are more complicated than the 1$^{st}$ generation mechanistic model predicted.

Ittel and Brookhart examined the polymerization of $^{13}$C-labeled 1-hexene using nickel α-diimine catalysts.[18] They demonstrated that both 1,2-insertion off a primary carbon and 2,1-insertion off a secondary penultimate carbon were active pathways for installing methyl branches. This invalidated the 1$^{st}$ generation model for calculating regioselectivity because 2,1-insertion can produce both linear and branched units. A revised model for calculating regioselectivity using the $^{13}$C-labeled polymers was developed (see eq ((3.2)), where the values for "methine" and "methylene" are determined by the integrations from the $^{13}$C NMR spectrum):

$$\%(1,2) = \frac{\Sigma(methine)}{\Sigma(methine+methylene)} * 100 \quad (3.2)$$

Quantification of the number of branches was also performed using $^{13}$C NMR spectroscopy as described in eq ((3.3)), where %(1,2) is the percent of the total

**Scheme 3.4** Insertion off a Secondary Position Leading to a $^{13}$C-Labeled α* Signal

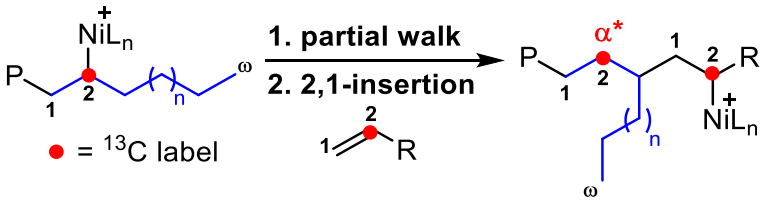


integration arising from all $^{13}$C-labeled methines and %(2°-2,1) is the percent of the total integration arising from all $^{13}$C-labels β to branching points:

$$\frac{B \text{ branches}}{1000 \text{ C}} = \frac{\%(1,2)+\%(2°/2,1)}{100 \text{ insertions}} \frac{x \text{ insertions}}{1000 \text{ C}} \tag{3.3}$$

Since ethyl and propyl branches are not observed in their system, Ittel and Brookhart suggested that insertions off secondary carbons occur exclusively at the penultimate position to produce methyl branches. This is a viable explanation explaining the lack of intermediate branches in polymer derived from 1-hexene in α-diimine nickel systems. Close inspection of their $^{13}$C NMR spectrum reveal a signal that can potentially be assigned to a $^{13}$C-labeled carbon alpha to a long branch (**α***) that is accessible through 2,1-insertion off a non-penultimate secondary position (Scheme 3.4). Although this signal was small in comparison to the other signals, it indicates other pathways may be operative in α-olefin polymerization. A 3$^{rd}$ generation model is necessary to account for these additional secondary pathways. While improving the accuracy of the analysis, these additional insertion modes increase the complexity, requiring the development of a mathematical model capable of capturing the intricacies of the system.

Herein, we performed a detailed study using $^{13}$C-labeled α-olefins to determine the specific mechanistic pathways that lead to branching defects.[19] Two different $^{13}$C-

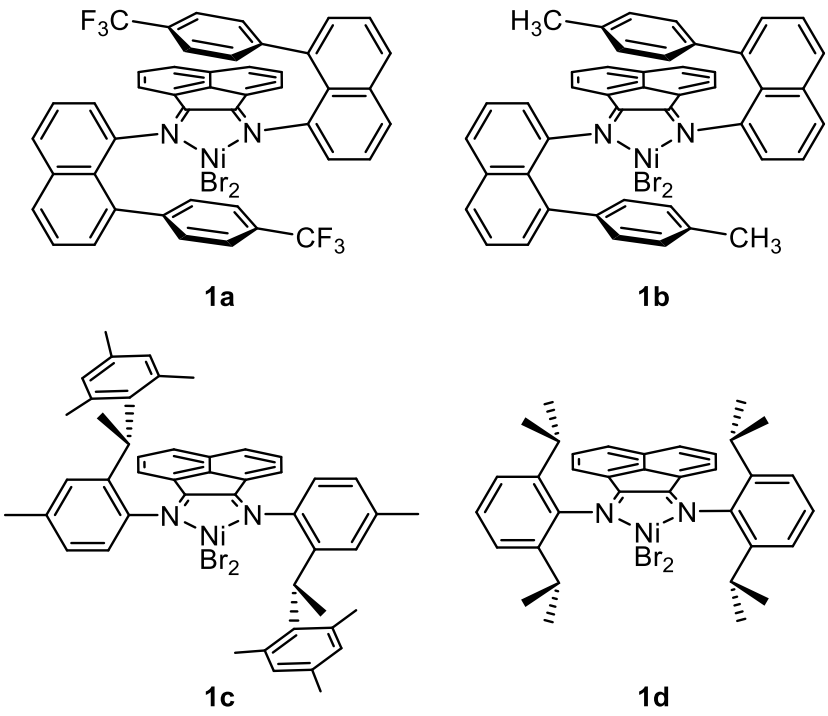


**Figure 3.2** α-Diimine nickel complexes studied in this work.

labeled monomers were synthesized – with the $^{13}$C-label either at the C2-position (1-decene) or the ω-position (1-dodecene) – in order to compare the types of mechanistic data that can be derived. With the advent of highly selective chain straightening nickel complexes, we focused our attention on the nickel "sandwich" arylnaphthyl-α-diimines (Figure 3.2, **1a** and **1b**) and compared their performance to less ω,1-selective complexes (Figure 3.2, **1c** and **1d**).[20] We report a detailed, quantitative model that uses the data from the resulting $^{13}$C NMR spectra to differentiate between eight unique insertion pathways. Beyond providing accurate quantification of the overall regiochemistry of olefin insertion as well as the general preference for primary vs secondary insertion, the additional detail allows us to specifically compare how different catalyst systems install branching defects.

## 3.2 Experimental Design

### 3.2.1 Opening Remarks

For this work, two $^{13}$C-labeled α-olefin monomers were subjected to "chain straightening" conditions to form predominantly linear "polyethylene," with branching defects that were quantified by $^{13}$C NMR spectroscopy. The identity of the branching defects and the position of the $^{13}$C-labels aid in differentiating eight mechanistic pathways, such that the propensity of different catalysts and reaction conditions to generate defects from 1,2-insertion (regioerror) versus incomplete chain walking can be quantified.

### 3.2.2 Naming Convention

Because there are numerous insertion pathways that can position the $^{13}$C-label in various locations in the resulting polymer, the label naming convention shown in Figure 3.3 will be used.[21] The position (methine, α, β, γ, etc.) of the label relative to the nearest branch (associated branch) will be denoted, followed by a superscript to indicate the number of carbons in the associated branch. Since branches with ≥ 5 carbons cannot

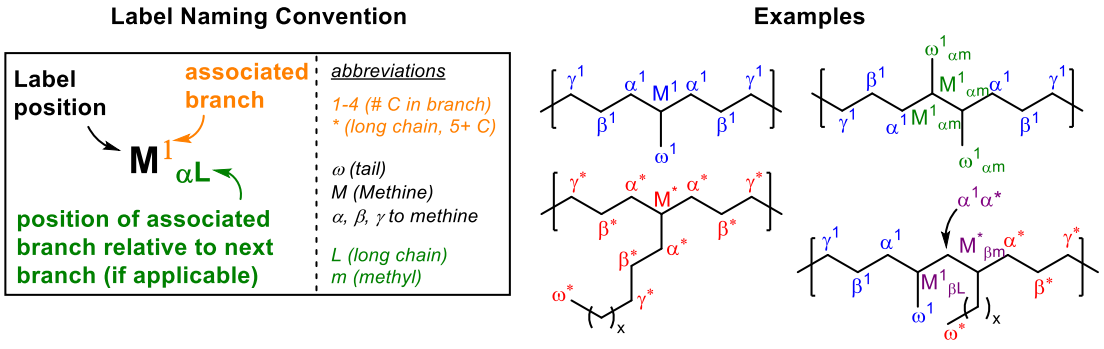


**Figure 3.3** Label convention used for this study.

be differentiated by $^{13}$C NMR spectroscopy using this model,[22] an alkyl branch (≥ 5 carbons) will be denoted with an asterisk. For example, **α¹** designates a $^{13}$C-labeled methylene carbon that is alpha (one carbon) from a one carbon branch (methyl branch). Conversely, **α*** designates a methylene carbon alpha from a branch that is ≥ 5 carbons (alkyl branch). The superscript will be followed by a subscript if another branch is in close enough proximity to the associated branch to cause a change in chemical shift. For example, **M*$_{βm}$** designates the methine carbon of a alkyl branch that is beta (two carbons) from a methyl branch. New labels will only be used when a different chemical shift is observed in the $^{13}$C NMR spectrum. Thus, the labels **β*$_{γm}$** and **β²** are not used because those signals cannot be differentiated from the far more prevalent **β***. In some cases, relative stereochemistry lead to multiple peaks in the $^{13}$C NMR spectrum for the same position. For example, **ω¹$_{αm}$** consists of three signals, two where the adjacent methyls are *meso* and one where the two adjacent methyls are *racemo*. In this case, all signals are added together to give the total integration for **ω¹$_{αm}$**. If a label is between two branches such that it is associated with both, the position relative to each branch will be used. For example, **β¹γ*** indicates that the label is beta (two carbons) from a methyl branch and gamma (three carbons) from an alkyl branch. If the label is on the backbone > 3 carbons away from the nearest branch, then it will contribute to the main linear signal denoted by **δ+**.

To fully elucidate the mechanistic pathways that give rise to branching defects, we must consider both the position of the nickel catalyst prior to the next monomer insertion and whether the insertion mode is 2,1 or 1,2. If the nickel catalyst walks to the end of the polymer chain, the next monomer inserted will undergo “primary” (1°)

insertion. If the nickel catalyst does not get to the end of the chain, the next monomer will undergo "secondary" (2°) insertion. A special case of secondary insertion that is particularly relevant is when the catalyst gets to the penultimate carbon before inserting the next monomer, which we refer to as "penultimate" ($2^{\circ}_{p}$) insertion. A primary insertion off a methyl branch defect ($1^{\circ}_{m}$), as opposed to the end of the polymer chain, is also significant enough to warrant its own label. From each of these four positions, the olefin can react either via the desired 2,1-insertion or undesired 1,2-insertion, resulting in a total of eight mechanistic pathways (A–H) that are considered in our model.

### *3.2.3 Assumptions Made for Mechanistic Model*

#### *3.2.3.1 Fast Chain Walking*

Throughout this analysis, it is necessary to make certain assumptions in order to most accurately assign some $^{13}C$ NMR signals to different pathways. We mostly made use of two, well-established assumptions in the literature for olefin polymerization by α-diimine complexes. The first is that chain walking is "fast" relative to insertion.

The most extensive studies have been done on (α-diimine)Pd(II) complexes for ethylene polymerization. In these cases, the barrier to chain walking (via β-H elimination, olefin rotation, and reinsertion) is significantly lower (6–7 kcal/mol) than the barrier to olefin insertion.[1e, 23] The result of this energy difference is that the position of the palladium along the polymer chain *completely equilibrates prior to insertion*. This claim was supported by low-temperature NMR studies of isolated palladium complexes. Subsequent mechanistic studies by Brookhart and coworkers[19b] on (α-

diimine)Ni(II) complexes for ethylene polymerization were more problematic due to the difficult synthesis of the highly-sensitive β-agostic complexes. Ultimately, they found that, at low temperatures, chain walking is slower for nickel compared to palladium due to an increased barrier for β-hydrogen elimination, while ethylene polymerization is faster for nickel. As the temperature was increased, the rate of chain walking increased (because of first-order β-hydrogen elimination) compared to olefin insertion (because of second-order ethylene trapping). In addition, it was shown that the resting state of the catalyst was the β-agostic interaction, such that migratory insertion is fast after the olefin binds to nickel.

Some mechanistic insights on α-olefin polymerizations using (α-diimine)Pd(II) complexes have been reported. In a Brookhart paper,[24] it was rationalized that, compared to ethylene, trapping of an α-olefin by a Pd alkyl complex is slower, dissociation is faster, and insertion rates are slower. All of these factors combined favor chain walking over migratory insertion. Even though direct analysis of chain walking vs. α-olefin insertion is limited, a similar rationale can be applied to (α-diimine)Ni(II) complexes. In 2007, Brookhart and coworkers used this same assumption in their 2$^{nd}$ generation mechanistic model,[18] stating "Mechanistic studies have shown that, in the case of Ni aryldiimine systems, the catalyst resting state is the alkyl agostic species and that there is substantial chain-walking prior to insertion. Thus, just as in the case of the Pd systems, the alkyl olefin complexes will equilibrate prior to insertion, and the relative ratios of insertion pathways will depend on both the equilibrium ratios of the various olefin complexes as well as their rates of insertion (Curtin-Hammett kinetics)."

For all of the reasons stated above, we generally think the assumption of fast chain walking is good at low concentrations of α-olefin and using sterically bulkier polymerization catalysts (**1a**–**b**). If this model is used for a catalyst that has an increased rate of insertion relative to chain walking, this assumption will not hold. In some cases, small satellites in the $^{13}C$ NMR spectra due to splitting between a labeled $^{13}C$ and an adjacent natural abundance $^{13}C$, we observed some discrepancies that indicate this assumption may not be completely accurate. We observed that 2° insertion seems to occur more often on a labeled carbon (to give **M***) and one carbon away from the label (to give **α***) than expected, which could happen if insertion occasionally occurs quickly (before many chain walking events can equilibrate the position of the nickel). In order to fully understand this phenomenon, a more in-depth understanding of the kinetics of nickel chain walking and α-olefin insertion are necessary, which was deemed beyond the scope of this work. The amount of error this adds into the model will vary depending on the catalyst and conditions.

One result of this assumption is that "no chain walk" actually means "effectively no chain walk." We use the phrase "no chain walk" to mean that the nickel inserts the next monomer from the same position it was in after the previous insertion, but it is possible that the metal has chain walked to a new position and then returned to its initial position.

#### *3.2.3.2 Primary over Secondary Insertion Pathways*

The second assumption is that insertions off primary carbons are more favorable than insertions off secondary carbons, such that if a specific primary and secondary

insertion pathway could both lead to the same signal in $^{13}C$ NMR, it is assumed that the primary insertion pathway is more likely occurring.

Major contributions to this assumption stem from experimental analysis of the branching structure of poly(α-olefins) produced by (α-diimine)Ni(II) complexes.[25] For example, Subramanyam performed $^{13}C$ NMR analysis on poly(1-hexene) and observed no signals associated with ethyl or propyl branches, suggesting that insertion off secondary carbons is energetically unfavorable compared to insertion off primary carbons. He does reveal that insertion off the penultimate carbon to produce head-to-head methyl branches occur, but even this special case of secondary insertion is low compared to the other insertion pathways. Other groups have studied the effect of monomer length on branching structure, finding that poly(α-olefins) produced from 1-octene and higher α-olefins consist primarily of methyl and alkyl branches.[2e] For 1-hexene polymerization, butyl branches are commonly found, but this is presumed to occur through successive 1,2-insertions off primary carbons. The implication here is that most alkyl branches for higher α-olefins occur through insertions off primary methyl groups previously installed by 1,2-insertion. Brookhart also emphasizes this assumption in his mechanism paper, highlighting the unfavorable steric interactions of inserting an α-olefin into a secondary nickel alkyl complex, making this pathway unfavorable.[18] His assumption goes one step further, though, saying that insertion off secondary carbons beyond the penultimate carbon does not occur for 1-hexene polymerization. We know for our studies with 1-decene and 1-dodecene that these secondary pathways do indeed occur, albeit at a lower frequency than primary insertion pathways.

**Scheme 3.5** Additional Pathways G and H from Insertions off Primary Methyls

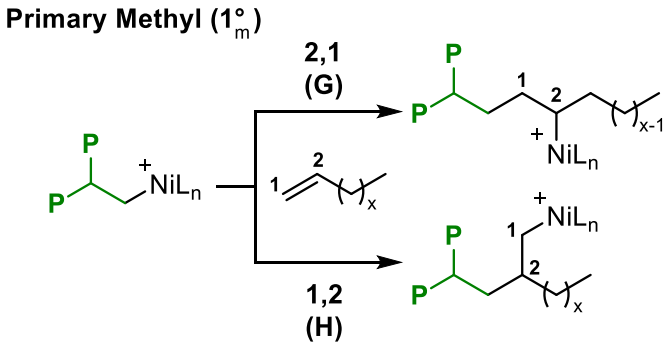


One of the consequences of this assumption is that primary insertion off a methyl branch is more likely than secondary insertion for the formation of various signals. Unfortunately, insertions off methyl branches produce the longest branching defects, which affect the crystallinity more than shorter branches. Since these primary insertions are different from the desired primary insertions off the end of the polymer chain, we decided to create pathways G and H, which correspond to primary insertion off a methyl ($1^{\circ}_{m}$) with a 2,1- and 1,2-insertion mode, respectively (Scheme 3.5). The labels that arise from these pathways are dependent on the monomer used (C2- vs ω-labeled) and the pathway from which the methyl was initially installed. The signals are further discussed in the appropriate sections below.

### *3.2.4 C2-Labeled Monomer*

For 1-decene with a $^{13}$C-label in the 2-position, the label on the *incoming monomer* was used to track the mechanistic pathway because this label should be in closest proximity to the current insertion event. Scheme 3.6 shows eight unique insertion pathways, as well as the observed $^{13}$C-label under the assumption that the catalyst fully chain walks away after the current insertion. The next paragraph will elaborate on the

details of this model in the absence of this assumption. The desired pathway for chain straightening is 2,1-insertion off a primary position at the chain end (pathway A), such that the label will contribute to **δ+** after chain walking (ω,1-enchainment). Performing a 1,2-insertion off the chain end installs a methyl branch defect (pathway B), where the $^{13}$C-label ends up on the methine of this methyl branch (**M$^{1}$**) after chain walking. 2,1-Insertion off the penultimate position (pathway C) also gives a methyl branch defect but results in a **β$^{1}$** label. Without the presence of the $^{13}$C-label, it is impossible to distinguish pathways B and C since they both result in the same branching defect. 1,2-Insertion off the penultimate position can also occur (pathway D), resulting in head-to-head methyl branches with an **M$^{1}_{\alpha m}$** label installed. Insertion off a secondary (non-penultimate) position results in an alkyl branch and yields a **β*** label from 2,1-insertion (pathway E) or **M$^{1}_{\alpha L}$** from 1,2-insertion (pathway F). Lastly, insertion off the primary position of a previously installed methyl branch can occur, converting a methyl branch into an alkyl branch, such that the $^{13}$C-label ends up as **γ*** from 2,1-insertion (pathway G) or **M$^{1}_{\beta L}$** from 1,2-insertion (pathway H).

**Scheme 3.6** Insertion Pathways and Possible $^{13}$C-Labels Arising from the Analysis of Incoming C2-Monomer (red label) Assuming Full Chain Walking after Initial Insertion

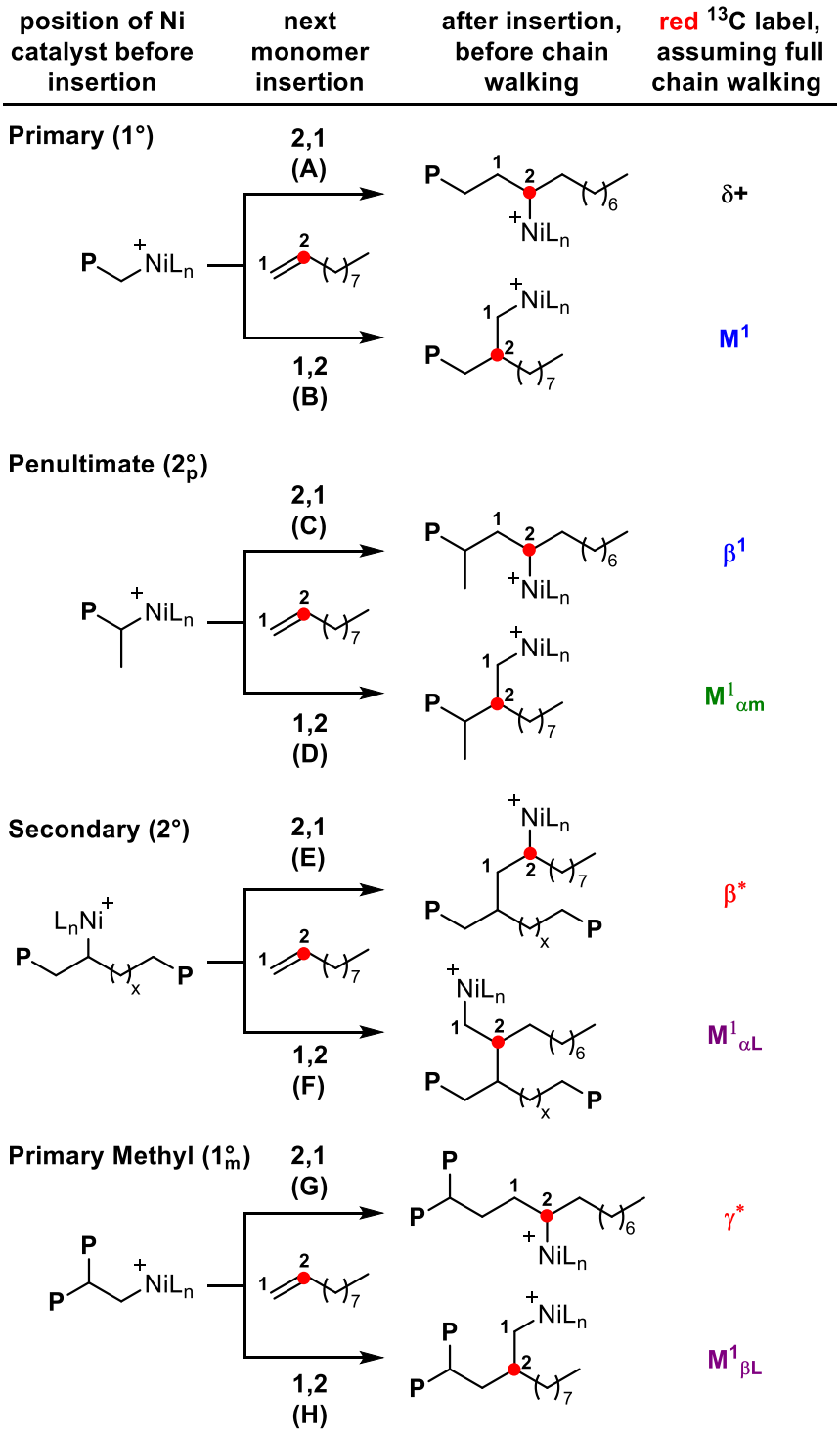

In terms of the types of signals observed, Scheme 3.6 represents the most simplified view of the C2-labeled monomer because it fails to consider complications that arise from incomplete chain walking following the current insertion event. One common example is shown in Scheme 3.7, where a label installed via pathway A (red label) – and thus should contribute to the **δ+** signal according to Scheme 3.6 – actually contributes to the **β*** signal because of 2° insertion (pathway E) two carbons away from the label. Secondary insertion could occur at any carbon along the polymer backbone distant from branching defects, so this sequence could also give rise to **M***, **α***, and **γ*** signals. Since the label installed via pathway E (Scheme 3.7, purple label) also contributes to the **β*** signal, **β*** is broken up into the components **β*(A)** and **β*(E)** to designate the pathway from which that signal originated. This and other pathways necessitate the calculation of component signals so that the integration of each $^{13}$C NMR signal is properly split between the contributing pathways (see Section 3.6 for schemes of relevant pathways and derivations of each component).

**Scheme 3.7** Complications Arising from Partial Chain Walking

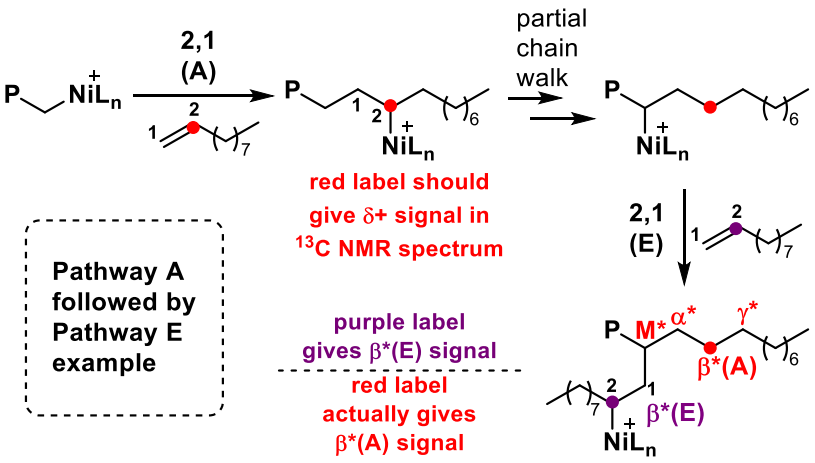

Additionally, a few pathway sequences with incomplete chain walking lead to completely new signals that must be added into the calculation to fully account for the contribution of each pathway. The percent contribution from each pathway can be calculated from the sum of the appropriate (1) signals shown in Scheme 3.6, (2) components derived from incomplete chain walking, and (3) the additional signals divided by the sum of the integrations for all signals. Thus, the percent contribution for each pathway can be calculated from the C2-labeled $^{13}$C NMR integrations by eqs (3.4) –(3.11), where $\sum I$ is the sum of all $^{13}$C NMR integrations (see Section 3.6 for derivation). Note that equation (3.12) encompasses a few very small signals that were unassignable, *P*(U). The integrations of these unassigned signals are included in $\sum I$:

$$P(\mathrm{A}) = \frac{(\delta+) + 3.5\alpha^*}{\sum I} \tag{3.4}$$

$$P(\mathrm{B}) = \frac{\mathrm{M}^1 + \mathrm{M}^* - 0.5\alpha^* + \mathrm{M}^*_{\beta\mathrm{m}} + \mathrm{M}^*_{\beta\mathrm{L}}}{\sum I} \tag{3.5}$$

$$P(\mathrm{C}) = \frac{\beta^1 + \gamma^* - \mathrm{M}^* - 0.5\alpha^* - \mathrm{M}^*_{\alpha\mathrm{m}} - 0.5\mathrm{M}^1_{\alpha\mathrm{L}} - \mathrm{M}^*_{\alpha\mathrm{L}} + \mathrm{M}^1_{\beta\mathrm{L}} - \mathrm{M}^*_{\beta\mathrm{m}} - \mathrm{M}^*_{\beta\mathrm{L}} + \beta^1\alpha^* + \beta^1\beta^* + \beta^1\gamma^*}{\sum I} \tag{3.6}$$

$$P(\mathrm{D}) = \frac{\mathrm{M}^1_{\alpha\mathrm{m}} + \mathrm{M}^*\alpha\mathrm{m} + 0.5\mathrm{M}^1_{\alpha\mathrm{L}}}{\sum I} \tag{3.7}$$

$$P(\mathrm{E}) = \frac{\beta^* - \gamma^* + \mathrm{M}^* - 0.5\alpha^* + \mathrm{M}^*_{\alpha\mathrm{m}} + 0.5\mathrm{M}^1_{\alpha\mathrm{L}} + \mathrm{M}^*_{\alpha\mathrm{L}} - \mathrm{M}^1_{\beta\mathrm{L}} + \mathrm{M}^*_{\beta\mathrm{m}} + \mathrm{M}^*_{\beta\mathrm{L}}}{\sum I} \tag{3.8}$$

$$P(\mathrm{F}) = \frac{0.5\mathrm{M}^1_{\alpha\mathrm{L}} + \mathrm{M}^*_{\alpha\mathrm{L}}}{\sum I} \tag{3.9}$$

$$P(\mathrm{G}) = \frac{\gamma^* - \alpha^*}{\sum I} \tag{3.10}$$

$$P(\mathrm{H}) = \frac{\mathrm{M}^1_{\beta\mathrm{L}} + \mathrm{M}^*_{\beta\mathrm{m}\beta\mathrm{L}} + \mathrm{M}^*_{\beta\mathrm{L}\beta\mathrm{L}}}{\sum I} \tag{3.11}$$

$$P(\mathrm{U}) = \frac{\mathrm{M}^{\mathrm{x}} + \mathrm{CH}_2 + \mathrm{others}}{\sum I} \tag{3.12}$$

### *3.2.5 ω-Labeled Monomer*

For 1-dodecene with a $^{13}$C-label in the ω-position, a similar analysis to the C2-labeled monomer can be made. The simple interpretation with the assumption of full chain walking after the current insertion is shown in Scheme 3.8. For this monomer, the label closest to the next insertion event is the *last monomer on the polymer chain* (green), so it is this label – and not the label on the incoming monomer (purple) – that is used to track the mechanistic pathway for the current insertion. Again, the desired 1°-2,1 pathway A (ω,1-enchainment) installs a label on the backbone of the polymer and contributes to the linear **δ+** $^{13}$C NMR signal. Pathway B installs a methyl branch, but the different label position results in an $\boldsymbol{\alpha^1}$ signal as opposed to the $\mathbf{M^1}$ signal observed for the C2-labeled monomer. Penultimate enchainment (pathways C and D) gives $\boldsymbol{\omega^1}$ and $\boldsymbol{\omega^1_{\omega m}}$ signals from 2,1- and 1,2-insertion, respectively. One disadvantage of using the ω-labeled monomer is highlighted in the secondary insertion pathways; this monomer is unable to distinguish pathways E and F because both place the label at the end of an alkyl branch (**ω***). Thus, a broader percentage for secondary insertion, *P*(E+F), can be calculated, but the regioselectivity information is lost. Additionally, the $^{13}$C-label installed from pathways G and H varies depending on the source of the initial methyl branch. Because the ω-labeled monomer cannot properly correct for pathways E–H where the $^{13}$C-label ends up far away from the backbone of the polymer, the result is an overestimation of pathways E+F and underestimation of pathways G and H. Fortunately, these pathways are typically the least common, but it is an additional source of error to consider.

**Scheme 3.8** Possible $^{13}$C-Labels Arising from the Analysis of the Last ω-Labeled Monomer on Polymer Chain (green label) Assuming Full Chain Walking After Initial Insertion

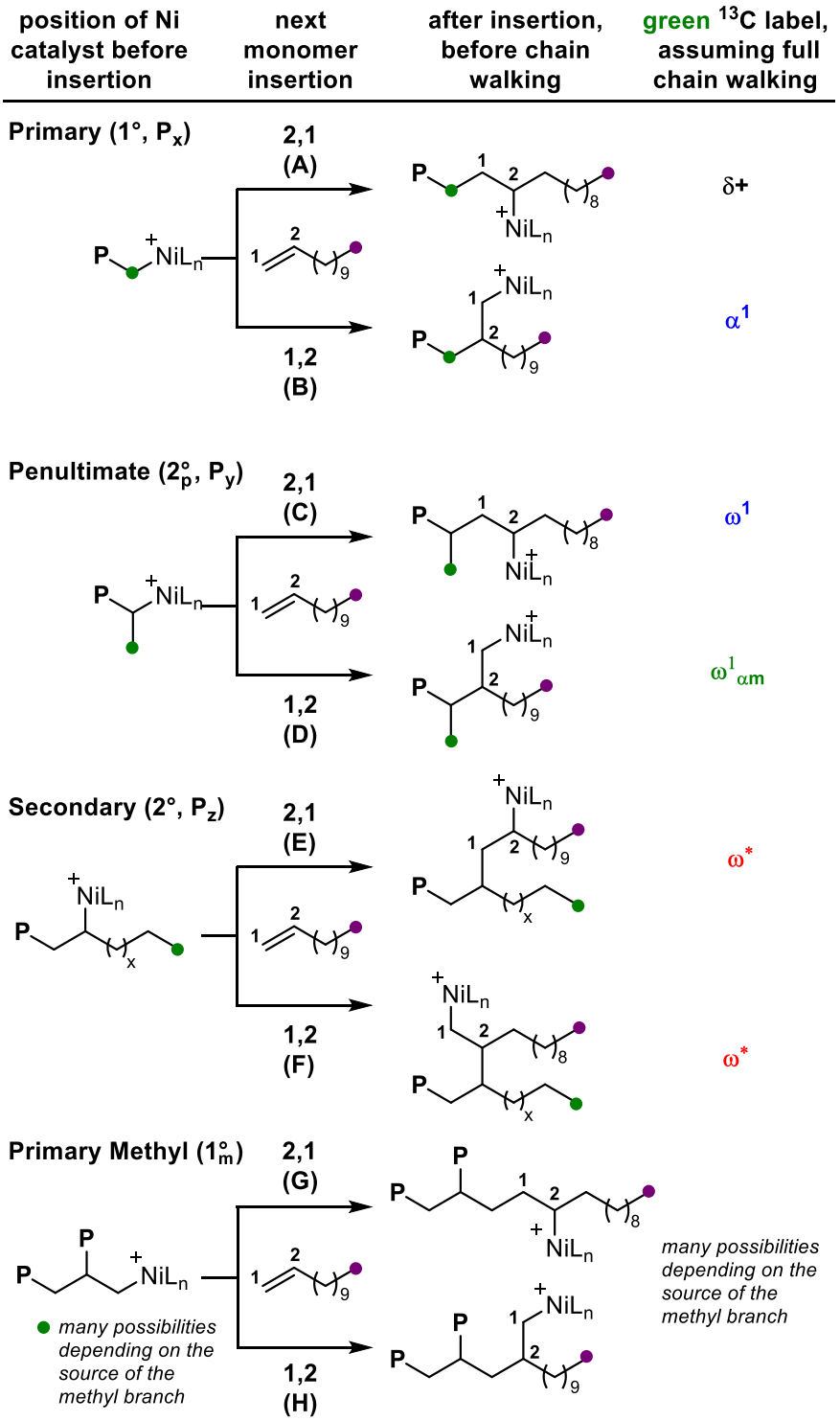

Secondary insertion close to a previously installed label on the backbone (pathway A followed by E, similar to Scheme 3.7) is also applicable for the ω-labeled monomer. For these cases, a label from pathway A will contribute to **M***, **α***, **β***, or **γ***. The same partial chain walk pathways give rise to component signals that must be considered (see Section 3.6 for the derivation of the component signals for the ω-labeled monomer).

Comparable to the C2-labeled monomer analysis, the percentage of each pathway can be calculated from the following equations:

$$P(\mathrm{A}) = \frac{(\delta+) + 3\mathrm{M}^* + \beta^* + \gamma^* + \mathrm{M}^*_{\alpha\mathrm{m}}}{\sum I} \tag{3.13}$$

$$P(\mathrm{B}) = \frac{\alpha^1 + ½\alpha^* - \mathrm{M}^*}{\sum I} \tag{3.14}$$

$$P(\mathrm{C}) = \frac{\omega^1 + ½\alpha^* - \mathrm{M}^* + \alpha^*\alpha^1 + \alpha^*\alpha^* + \omega^1_{\beta\mathrm{L}}}{\sum I} \tag{3.15}$$

$$P(\mathrm{D}) = \frac{\omega^1_{\alpha\mathrm{m}} + \omega^1_{\alpha\mathrm{L}}}{\sum I} \tag{3.16}$$

$$P(\mathrm{E{+}F}) = \frac{\omega^* - \alpha^* + 2\mathrm{M}^* - \alpha^*\alpha^1 - 2\alpha^*\alpha^* + \omega^{2-4} + \omega^{\mathrm{X}}}{\sum I} \tag{3.17}$$

$$P(\mathrm{G}) = \frac{\alpha^*\alpha^* + \alpha^* - 2\mathrm{M}^*}{\sum I} \tag{3.18}$$

$$P(\mathrm{H}) = \frac{\alpha^*\alpha^1 + \alpha^*\alpha^*}{\sum I} \tag{3.19}$$

$$P(\mathrm{U}) = \frac{\alpha^{\mathrm{X}} + \mathrm{CH_2} + \mathrm{others}}{\sum I} \tag{3.20}$$

### *3.2.6 Equations for Overall Regioselectivity and Insertion Evaluation*

While the individual pathways A–H give the most detailed information, it is sometimes preferable to look at the overall probability of each type of insertion mode.

To quantify regioerrors, the percent of 2,1- and 1,2-insertion can be calculated from the appropriate pathways, as shown in eqs (3.21) and (3.22), below. Note that unassigned signals are not included in these calculations (e.g. eq (3.21) gives the percent of 2,1-insertion out of *assigned signals*, not total signals). For the ω-labeled monomer where pathways E and F cannot be distinguished, we decided to omit them from equations (3.21) and (3.22) (both in the numerator and denominator).

$$P(2,1) = \frac{P(\mathrm{A})+P(\mathrm{C})+P(\mathrm{E})+P(\mathrm{G})}{P(\mathrm{A-H})} \tag{3.21}$$

$$P(1,2) = \frac{P(\mathrm{B})+P(\mathrm{D})+P(\mathrm{F})+P(\mathrm{H})}{P(\mathrm{A-H})} \tag{3.22}$$

Similarly, in order to evaluate the amount of insertion off primary and secondary positions, the following equations were used:

$$P(1° + 1^{\circ}_{\mathrm{m}}) = \frac{P(\mathrm{A})+P(\mathrm{B})+P(\mathrm{G})+P(\mathrm{H})}{P(\mathrm{A-H})} \tag{3.23}$$

$$P\left(2° + 2^{\circ}_{\mathrm{p}}\right) = \frac{P(\mathrm{C})+P(\mathrm{D})+P(\mathrm{E})+P(\mathrm{F})}{P(\mathrm{A-H})} \tag{3.24}$$

The number of branches per 1000 carbons based on the $^{13}$C NMR spectra were also calculated by evaluating the number of branches installed via each pathway: A and G result in no branches; B, C, E, and H result in one branch; and D and F result in two branches each. This can only be calculated for the C2-labeled monomer since the ω-labeled monomer cannot differentiate between pathways E and F. The number of

insertions per 1000 carbons depends on the length of the monomer used, so $n$ is the number of carbons in the monomer ($n$ = 10 for C2-labeled monomer):

$$\frac{B \text{ branches}}{1000 \text{ C}} = \frac{\%(\text{B})+\%(\text{C})+\%(\text{E})+\%(\text{H})+2[\%(\text{D})+\%(\text{F})]}{100 \text{ insertions}} * \frac{\frac{1000}{n}\text{insertions}}{1000 \text{ C}} \quad (3.25)$$

### *3.2.7 Natural Abundance Correction*

In this work, 1-decene (MW = 141 Da) or 1-dodecene (MW = 169 Da) monomers were used, which means 9–11 unlabeled carbons are enchained per monomer. The polymers made in this study are 15–30 kDa, which corresponds to approximately 100–200 monomers enchained per polymer. Therefore, at least 9 x 100 = 900 unlabeled carbons are incorporated into each chain, which, at 1.1% natural abundance, contributes $^{13}$C NMR signal equivalent of 9 carbon labels, or ≥8% of the observed signal. We rationalized that 8% was too much signal from unlabeled carbons to ignore and felt that a correction was necessary to improve the accuracy of the resulting calculations. We also observed some $^{13}$C NMR signals corresponding to positions that cannot be attributed to the labeled carbon and thus must appear due to natural abundance.

In order to correct for the natural abundance (N.A.), two identical polymerizations were run except one used labeled monomer and the other did not. Then, a $^{13}$C NMR spectrum was acquired for each run using identical acquisition parameters, concentration, etc. For the unlabeled 1-decene monomer, there are 10 carbons contributing 1.1% $^{13}$C signal from natural abundance. This means for each monomer enchained, an average of 0.11 carbons will be $^{13}$C (or 1 carbon in every 9–10 monomers), as shown in eq (3.26**)**.

$$10 \text{ carbons} * 0.011 \text{ N. A.} = 0.11 \quad (3.26)$$

For the C2-labeled 1-decene monomer, there are 9 carbons contributing 1.1% $^{13}$C signal and one carbon contributing 99% $^{13}$C signal from the label. Therefore, for each monomer enchained, an average of 1.09 carbons will be $^{13}$C, as shown in eq (3.27). Therefore, the total integration of the labeled polymer spectrum should be 9.9 times more than the unlabeled spectrum, as shown in eq (3.28).

$$(9 \text{ carbons} * 0.011 \text{ N. A.}) + (1 \text{ carbon} * 0.99 \text{ label}) = 1.09 \quad (3.27)$$

$$\frac{1.09}{0.11} = 9.9 \quad (3.28)$$

Thus, $\sum I$ (sum of all $^{13}$C NMR signals) for the labeled polymer spectrum was set to 990, $\sum I$ for the unlabeled polymer spectrum was set to 100, and then the signal from the unlabeled spectrum was subtracted from the signal from the labeled spectrum. All of the signals from positions that cannot be labeled subtracted out to 0 ± 0.4, except for $\boldsymbol{\gamma^1}$ due to overlap with the shoulder of the main **δ+** signal.

Similarly, for the unlabeled 1-dodecene monomer, there are 12 carbons contributing 1.1% $^{13}$C signal (eq (3.29)). The ω-labeled monomer has 11 carbons contributing 1.1% $^{13}$C signal and one carbon contributing 93% $^{13}$C signal from the label (eq (3.30)). This means that the total integration of the labeled polymer spectrum should be 8.0 times more than the unlabeled spectrum (eq (3.31)).

$$12 \text{ carbons} * 0.011 \text{ N. A.} = 0.132 \quad (3.29)$$

$$(11 \text{ carbons} * 0.011 \text{ N.A.}) + (1 \text{ carbon} * 0.93 \text{ label}) = 1.051 \quad (3.30)$$

$$\frac{1.051}{0.132} = 8.0 \quad (3.31)$$

Thus, $\sum I$ for the labeled polymer spectrum was set to 800, $\sum I$ for the unlabeled polymer spectrum was set to 100, and then the signal from the unlabeled spectrum was subtracted from the signal from the labeled spectrum. All of the signals from positions that cannot be labeled subtracted out to 0 ± 0.1. This analysis, subtraction procedure, and low observed error allow us to have confidence that the signals we are interpreting only arise from the $^{13}$C label and not natural abundance.

## *3.3 Results/Discussion*

### *3.3.1 C2-Labeled monomer*

#### *3.3.1.1 Complex **1a**: Standard Conditions*

We began our analysis by studying the polymerization of $^{13}$C-labeled 1-decene under standard chain straightening conditions using complex **1a** (Table 3.1). As previously reported, the polymerization of 1-decene produced semicrystalline material with a microstructure composed primarily of extended methylene sequences along with a small portion of methyl and alkyl (≥ 5 carbons) branches (Figure 3.4). The polymerization of the C2-labeled monomer produced a material with similar molecular weight, thermal properties, and number of branches to the unlabeled sample.

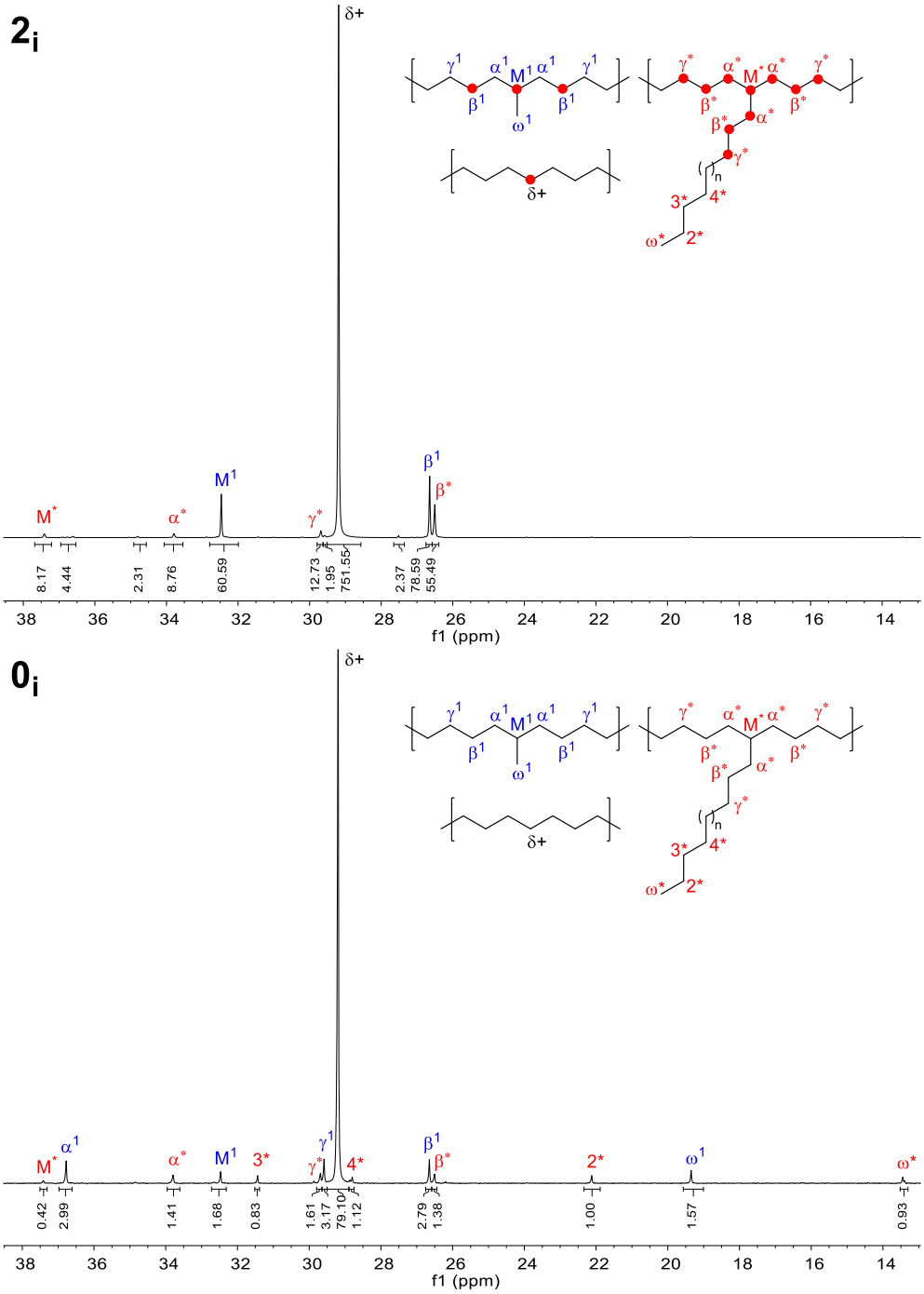


**Figure 3.4** $^{13}$C NMR spectra of poly(1-decene) produced by **1a**. The top spectrum ($2_i$) is polymer produced from $^{13}$C-labeled 1-decene (Table 3.1, entry 1), while the bottom spectrum ($0_i$) is polymer produced from unlabeled 1-decene (Table 3.1, entry 2). The red circles on the structures depicted show possible positions for a $^{13}$C-label to appear.

**Table 3.1** Polymerization of $^{13}$C-Labeled and Unlabeled 1-Decene Using **1a**[a]

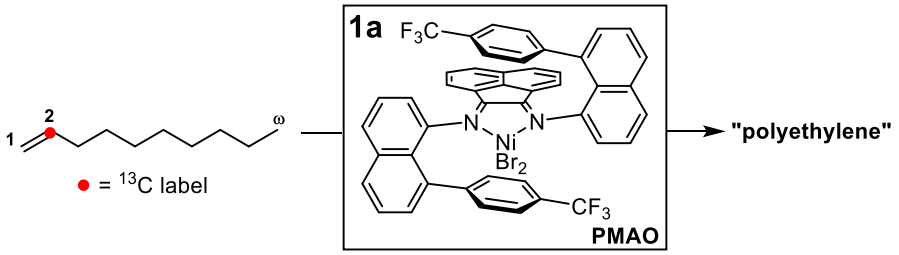


| entry (ID) | $^{13}$C-label | TOF[b] ($h^{-1}$) | $M_n$[c] (kDa) | $Đ$[c] | $T_m$[d] (°C) | ΔH[d] (J/g) | $B$[e] |
|---|---|---|---|---|---|---|---|
| 1 ($2_i$) | C2 | 4 | 24.6 | 1.4 | 106 | 84.1 | 26 |
| 2 ($0_i$) | – | 4 | 24.8 | 1.2 | 106 | 83.1 | 27 |

[a]Polymerization conditions: [**1a**] = 2.5 mM in PhCl, [monomer] = 0.1 M, [PMAO]/[**1a**] = 200, PhCl = 11.9 mL, 22 °C, 24 h. [b]Calculated using the equation: (mol monomer consumed)(mol complex)$^{-1}$(time)$^{-1}$ [c]Determined using gel permeation chromatography (GPC) in 1,2,4-trichlorobenzene at 150 °C vs polyethylene standards. [d]Determined using differential scanning calorimetry (DSC), melting endotherm of second heat. [e]Branches/1000 carbons, determined by $^1$H NMR.

Analysis of the resulting calculations showed that for the polymerization of C2-labeled 1-decene at 22 °C using **1a** (entry 1), pathway A (1°-2,1) is the major pathway at 76.5% (Table 3.2). This is expected since consecutive insertions via pathway A result in ω,1-enchainment, which is necessary for producing chain straightened poly(α-olefins). Brookhart previously reported that methyl branches can be installed through 1,2-insertion at the end of the polymer chain (pathway B) and 2,1-insertion at the penultimate position (pathway C). Using **1a**, we also observed both pathways occurring to install methyl branches, with pathway B at 7.2% and pathway C at 9.5%.

Interestingly, we observed pathway E (2°-2,1), which results in alkyl branching, occurring at 5.2%. It was previously thought this pathway does not occur significantly because ethyl and propyl branches are not observed in the $^{13}$C NMR spectra. However, pathway E is the only viable insertion mode to install the observed **α*** signal. Pathways

D and F were also observed but at a much lower frequency, comprising only 0.5% of the total signal. This suggests that 1,2-insertion off secondary carbons is energetically unfavorable in this system. A small portion of signals arising from pathways G and H was observed accounting for only 0.8% of the total signal. Consequently, insertions off previously installed methyl branches are energetically unfavorable in this system as well. Through these calculations, we determined that **1a** is predominantly 2,1-selective at 92.1% and the preference for primary insertion pathways is high at 84.8% (Table 3.3). We then used equation (3.25) to calculate the number of branches. For entry 1, this value was 23/1000C, which is comparable to the 26/1000C value determined by $^{1}$H NMR spectroscopy.

**Table 3.2** Breakdown of Insertion Pathways for the Polymerization of $^{13}$C-Labeled 1-Decene Using **1a** (Table 3.1, $2_i$)

| entry (ID) | A-1° 2,1 (%) | B-1° 1,2 (%) | C-$2^{\circ}_{p}$ 2,1 (%) | D-$2^{\circ}_{p}$ 1,2 (%) | E-2° 2,1 (%) | F-2° 1,2 (%) | G-$1^{\circ}_{m}$ 2,1 (%) | H-$1^{\circ}_{m}$ 1,2 (%) | U[a] (%) |
|---|---|---|---|---|---|---|---|---|---|
| 1 ($2_i$) | 76.5 | 7.2 | 9.5 | 0.4 | 5.2 | 0.1 | 0.6 | 0.2 | 0.3 |

[a]U refers to signals not assigned to a specific pathway but included in the total integration.

**Table 3.3** Total Values of the Insertion Pathways for the Polymerization of $^{13}$C-Labeled 1-Decene Using **1a** (Table 3.1, $2_i$)

| entry (ID) | 1°[a] (%) | 2°[b] (%) | 2,1[c] (%) | 1,2[d] (%) | *B*[e] |
|---|---|---|---|---|---|
| 1 ($2_i$) | 84.8 | 15.2 | 92.1 | 7.9 | 23 |

[a]Total primary insertion (1°), determined by eq (3.23). [b]Total secondary insertion (2°), determined by eq (3.24). [c]Total 2,1-insertion, determined by eq (3.21). [d]Total 1,2-insertion, determined by eq (3.22). [e]*B* = Branches/1000C, determined by $^{13}$C NMR spectroscopy using equation (3.25).

**Table 3.4** Comparison of Different Generation Models for Sample $2_i$

| model | 1° (%) | 2° (%) | 2,1 (%) | 1,2 (%) | *B* |
|---|---|---|---|---|---|
| 1st gen[a] | – | – | 74 | 26 | – |
| 2nd gen[b] | 85 | 15 | 92 | 8 | 24 |
| 3rd gen[c] | 86 | 14 | 92 | 8 | 23 |

[a]Regioselectivity calculated using eq (3.1). [b]Regioselectivity calculated using eq (3.2). Primary insertion (1°) calculated from sum of all $^{13}$C-labeled methines, plus the sum of all $^{13}$C-labeled methylenes minus those β to a branch, and secondary insertion (2°) calculated from sum of all $^{13}$C-labeled methylenes β to a branch (see reference 18). Branches/1000C (*B*) calculated using equation (3.3). [c]Regioselectivity calculated using equation (3.22) and (3.21). Branches/1000C (*B*) calculated using equation (3.25).

We compared the calculated regiochemistry of insertion and branching numbers from our 3rd generation mechanistic model with the previously developed models (1st and 2nd generation, Table 3.4). The 1st generation model predicts that 2,1-selectivity will be dominant at 74%, which underestimates our 3rd generation model's 2,1-selectivity by 18%. Brookhart determined regioselectivity by calculating the ratio of $^{13}$C-labeled methine integrations to $^{13}$C-labeled methylene integrations, assuming that all methines arise from 1,2-insertion and all methylenes from 2,1-insertion.[18] This model is in close agreement with our model in this case, with essentially no difference in calculated regioselectivity or total primary and secondary insertion pathways. Our model takes into account that a $^{13}$C-labeled methine can also be generated through 2,1-insertion directly off a $^{13}$C-labeled carbon, but this pathway is rare in this system. We expected that the 2nd and 3rd generation models should be very similar for **1a** because all the additional pathways considered in the new model (particularly 2° insertion) are small. The branches/1000C values calculated by these models are also similar, only differing by 1 branch.

### *3.3.1.2 Complex **1a**: Temperature Screen*

Having shown the viability of our model, we probed the effect of temperature on the chain straightening polymerization of C2-labeled 1-decene using **1a**. The polymerization was performed at three different temperatures (0 °C, 22 °C, and 50 °C) and the resulting polymers were analyzed (Table 3.5). At 0 °C (entry 1), the $T_m$ of the polymer improved slightly to 108 °C with a modest reduction in the number of branches compared to the sample obtained at 22 °C (entry 2). However, the sample produced at 50 °C demonstrated a broadening in molecular weight distribution and a marked drop in $T_m$ to 93 °C with an increase in number of branches (entry 3). Turnover frequencies (TOFs) also increased as a function of temperature. Inspection of the $^{13}C$ NMR spectra for these samples (Figure 3.5) show an increase in signals associated with alkyl branches

**Table 3.5** Temperature Effect on the Polymerization of $^{13}C$-Labeled 1-Decene Using **1a**[a]

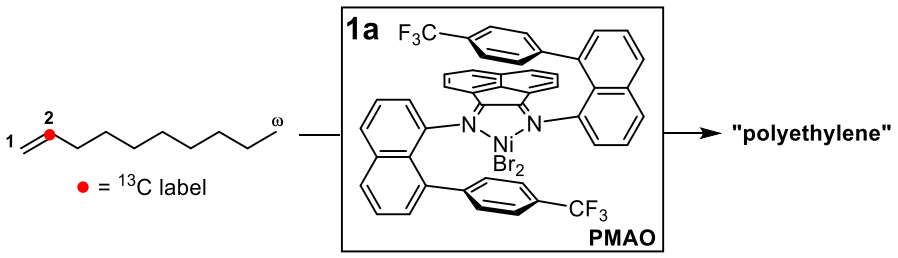


| entry (ID) | temp (°C) | time (h) | TOF[b] ($h^{-1}$) | $M_n$[c] (kDa) | $Đ$[c] | $T_m$[d] (°C) | ΔH[d] (J/g) | $B$[e] |
|---|---|---|---|---|---|---|---|---|
| 1 ($2_{ii}$) | 0 | 48 | 2 | 20.9 | 1.4 | 108 | 81.2 | 25 |
| 2 ($2_i$) | 22 | 24 | 4 | 24.6 | 1.4 | 106 | 84.1 | 26 |
| 3 ($2_{iii}$) | 50 | 15 | 11 | 12.7 | 1.6 | 93 | 51.7 | 31 |

[a]Polymerization conditions: [**1a**] = 2.5 mM in PhCl, [monomer] = 0.1 M, [PMAO]/[**1a**] = 200, PhCl = 11.9 mL. [b]Calculated using the equation: (mol monomer consumed)(mol catalyst)$^{-1}$(time)$^{-1}$. [c]Determined using gel permeation chromatography (GPC) in 1,2,4-trichlorobenzene at 150 °C vs polyethylene standards. [d]Determined using differential scanning calorimetry (DSC), melting endotherm of second heat. [e]Branches/1000 carbons, determined by $^1H$ NMR spectroscopy.

(**M***, **α***, **β***, and **γ***) as a function of increased temperature. Signals associated with methyl branches (**M**$^{\mathbf{1}}$ and **β**$^{\mathbf{1}}$) also increased as a function of temperature, but to a somewhat lesser degree.

We related these signals to the mechanistic pathways using our model and analyzed the resulting calculations (Table 3.6). As the temperature increased from 0 °C to 50 °C, pathway A decreased from 77.6% to 71.3% in favor of other competing pathways. Pathway B showed a slight increase from 6.3% to 8.0%, in addition to minor increases in pathways D and H which are associated with 1,2-insertion. Overall, the amount of 2,1-insertion only decreased by 2.3%, suggesting that temperature does not have a major effect on the regioselectivity of insertion for this system. Interestingly,

**Table 3.6** Temperature Effect on the Breakdown of Insertion Pathways of **1a** for the Polymerization of $^{13}$C-Labeled 1-Decene (Table 3.1, $2_{ii}$, $2_i$, and $2_{iii}$)[a]

| entry (°C) | A-1° 2,1 (%) | B-1° 1,2 (%) | C-$2^{\circ}_{p}$ 2,1 (%) | D-$2^{\circ}_{p}$ 1,2 (%) | E-2° 2,1 (%) | F-2° 1,2 (%) | G-$1^{\circ}_{m}$ 2,1 (%) | H-$1^{\circ}_{m}$ 1,2 (%) | U[a] (%) |
|---|---|---|---|---|---|---|---|---|---|
| 1 (0) | 77.6 | 6.3 | 10.1 | 0.3 | 4.4 | 0.1 | 0.5 | 0.4 | 0.3 |
| 2 (22) | 76.5 | 7.2 | 9.5 | 0.4 | 5.2 | 0.1 | 0.6 | 0.2 | 0.3 |
| 3 (50) | 71.3 | 8.0 | 8.8 | 0.7 | 9.6 | 0.1 | 0.6 | 0.6 | 0.3 |

[a]U refers to signals not assigned to a specific pathway but included in the total integration.

**Table 3.7** Temperature Effect on the Total Values of the Insertion Pathways for the Polymerization of $^{13}$C-Labeled 1-Decene Using **1a** (Table 3.1, $2_i$)

| entry (°C) | 1°[a] (%) | 2°[b] (%) | 2,1[c] (%) | 1,2[d] (%) | *B*[e] |
|---|---|---|---|---|---|
| 1 (0) | 85.0 | 15.0 | 92.9 | 7.1 | 22 |
| 2 (22) | 84.8 | 15.2 | 92.1 | 7.9 | 23 |
| 3 (50) | 80.7 | 19.3 | 90.6 | 9.4 | 29 |

[a]Total primary insertion (1°), determined by eq (3.23). [b]Total secondary insertion (2°), determined by eq (3.24). [c]Total 2,1-insertion, determined by eq (3.21). [d]Total 1,2-insertion, determined by eq (3.22). [e]*B* = Branches/1000C, determined by $^{13}$C NMR spectroscopy using equation (3.25).

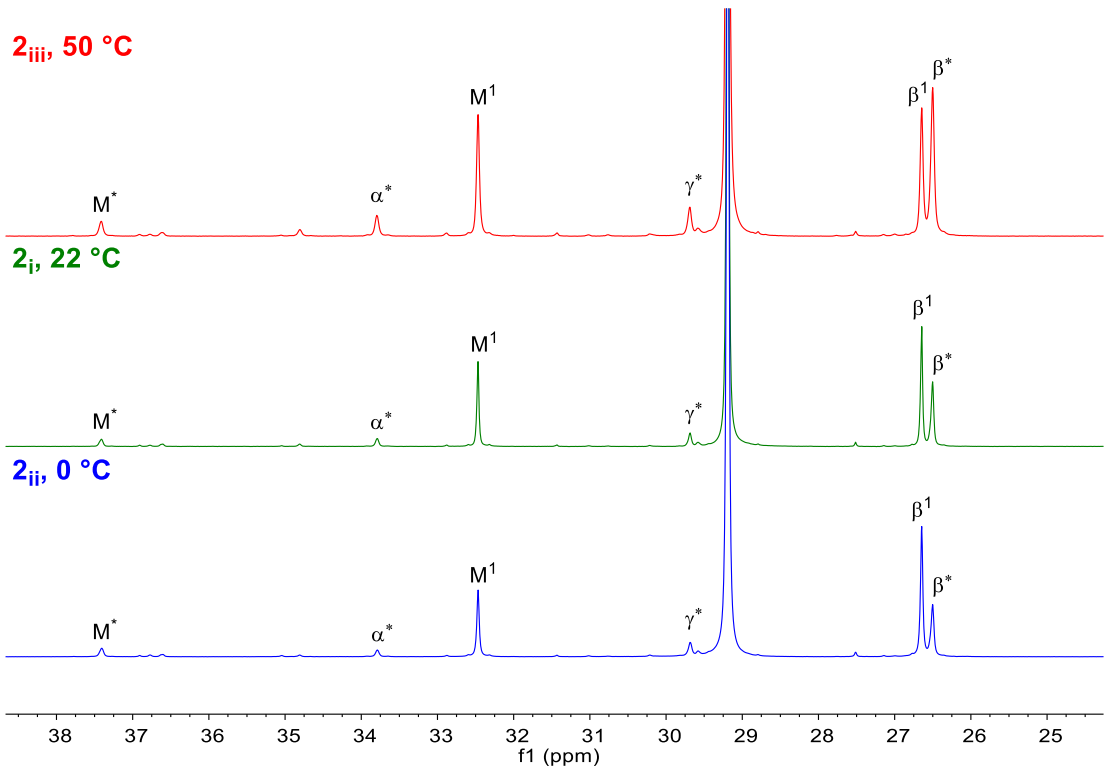


**Figure 3.5** $^{13}$C NMR spectra depicting the temperature dependence on the branching structure of $^{13}$C-labeled poly(1-decene) using **1a** (Table 3.5, $2_{iii}$, $2_i$, and $2_{ii}$).

raising the temperature from 0 °C to 50 °C had the greatest effect on pathway E, which increased from 4.4% to 9.6%. Increasing temperature should favor the unimolecular β-hydride elimination event over the bimolecular insertion event, causing increased chain walking and thus increasing the probability of the metal center residing on a secondary position before insertion. Curiously, the frequency of pathway C appeared to decrease slightly as a function of increasing temperature, suggesting that **1a** is more likely to isomerize to the primary position at higher temperatures if it can manage to chain walk to the penultimate position.

Even though increasing the reaction temperature only had a modest effect on the overall number of branches (+7/1000C), a significant effect on the $T_m$ of the resulting material was observed (108 °C to 93 °C). This contrast emphasizes the importance of

considering not only the number of branches, but also the nature of the branches. Pathway E specifically installs alkyl branches which have a more substantial impact on reducing $T_m$ and crystallinity in chain straightened poly(α-olefins) compared to methyl branches. Analysis using our mechanistic model allows for a more in-depth understanding of how the behavior of the catalyst was affected at various temperatures and demonstrated that secondary insertion pathways are more adversely affected by temperature than the regiochemistry of insertion.

### *3.3.1.3 Complex **1c** and **1d**: Standard Conditions*

**Table 3.8** Polymerization of $^{13}$C-Labeled 1-Decene Using **1c** and **1d**[a]

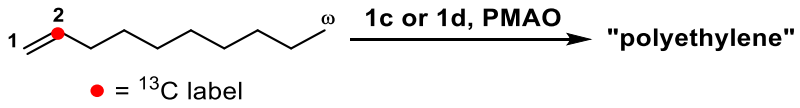


| entry (ID) | pre-cat. | TOF[b] ($h^{-1}$) | $M_n$[c] (kDa) | $Đ$[c] | $T_m$[d] (°C) | ΔH[d] (J/g) | $B$[e] |
|---|---|---|---|---|---|---|---|
| 1 ($2_{iv}$) | **1c** | 34 | 32.3 | 1.3 | 69 | 32.9 | 44 |
| 2 ($2_v$) | **1d** | 40 | 31.5 | 1.4 | 46 | 17.3 | 72 |

[a]Polymerization conditions: [**1c**] = [**1d**] = 2.5 mM in PhCl, [monomer] = 0.1 M, [PMAO]/[pre-cat.] = 200, PhCl = 11.9 mL, 22 °C, 6.5 h. [b]Calculated using the equation: (mol monomer consumed)(mol catalyst)$^{-1}$(time)$^{-1}$. [c]Determined using gel permeation chromatography (GPC) in 1,2,4-trichlorobenzene at 150 °C vs polyethylene standards. [d]Determined using differential scanning calorimetry (DSC), melting endotherm of second heat. [e]$B$ = Branches/1000 carbons, determined by $^1$H NMR spectroscopy.

We expanded our study to **1c** and **1d**, two complexes that are not competent at producing highly crystalline materials from α-olefins under typical chain straightening conditions. It is known that MAO-activated **1c** exhibits almost exclusive 1,2-selectivity for α-olefin insertion at low temperatures,[1g,12] but less is known about the regioselectivity of insertion under ambient conditions. Complex **1d** has been studied by

various groups and is known to be regiorandom with respect to α-olefin polymerization.[18] We were interested in demonstrating that our model could arrive at the same conclusions for **1d**, but also deliver additional insight into the specific pathways that lead to the observed branching defects. Polymerization of $^{13}$C-labeled 1-decene by **1c** and **1d** produced "polyethylene" with modest, broad melting temperatures and high branching numbers (Table 3.8). TOFs were improved for both complexes compared to **1a,** which could be explained by a less sterically hindered environment around the active metal center.

Analysis of the resulting $^{13}$C NMR spectra displayed materials with a more complex branching structure – particularly for **1d**, which produced polymer with signals corresponding to methines near other branching points, such as $\mathbf{M^1_{\beta L}}$, $\mathbf{M^*_{\beta m}}$, and $\mathbf{M^1_{\alpha L}}$ (Figure 3.6). These signals are indicative of a high propensity for **1d** to undergo 1,2-insertion, since every 1,2-insertion will result in the $^{13}$C-label positioned as a methine. Various methine labels were also observed for **1c**, but in much lower amounts compared to **1d**. The most abundant defect signals are $\mathbf{\beta^1}$ and **β***, which are installed by penultimate and non-penultimate secondary insertion, respectively.

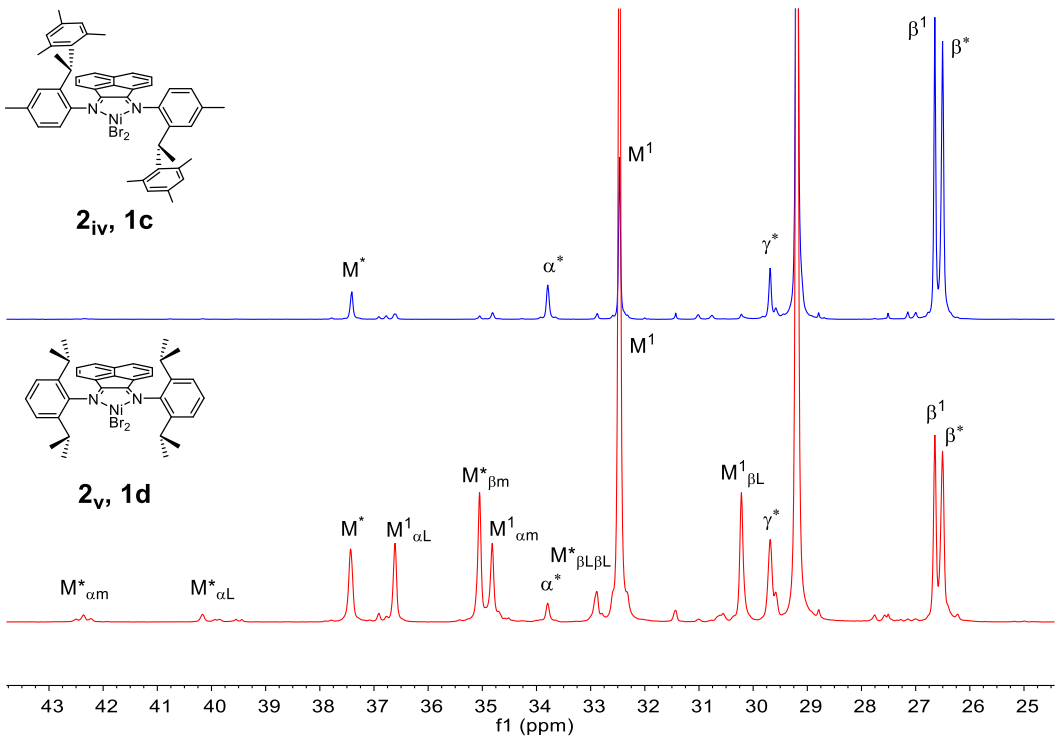


**Figure 3.6** $^{13}$C NMR spectra of the resulting polymers from the polymerization of $^{13}$C-labeled 1-decene using **1c** (top, Table 3.8, $2_{iv}$) and **1d** (bottom, Table 3.8, $2_{v}$).

We applied the model for **1c** and calculated that 2,1-regioselectivity is surprisingly high at 88.8% (Table 3.9). Most of the 1,2-regioerrors occur through pathway B at 9.1%. Primary insertion pathways, however, account for only 68.5% of the signal compared to 31.5% for secondary insertion pathways (Table 3.10). There is a large amount of secondary 2,1-insertion, with pathway C (methyl branches) and pathway E (alkyl branches) occurring at 15.6% and 14.9%, respectively. 1,2-Insertions off secondary carbons appear unfavorable in this system, accounting for only 1.0% of the total signal. Interestingly, only 1.9% stems from pathways G and H, showing that primary insertions off methyl branches are disfavored. For **1c**, it appears that, in general, secondary insertion pathways are the major contributor to the poor thermal properties of the resulting polymer.

The preceding analysis of **1c** is in stark contrast to **1d**, where primary insertion pathways were calculated to be relatively high at 81.2%. The regiochemistry of α-olefin insertion using **1d** appeared mostly regiorandom, with 2,1-insertion at 49.1% and 1,2-insertion at 50.9% (Table 3.10). This is in agreement with Brookhart's mechanistic analysis.[18] Although **1d** prefers primary insertion pathways, the regiorandom insertions lead to highly branched materials with poor thermal properties. Additionally, insertion off methyl branches is more feasible in this system, with pathway G (2,1) at 3.0% and pathway H (1,2) at 7.8%. Surprisingly, pathway H appears to be more common than pathway G despite the overall regiorandom nature of **1d**. It is also interesting to note that, under these conditions, **1d** does not readily undergo insertions via pathway C (3.0%) to install isolated methyl branches; instead, most methyl branches are generated through pathway B (35.2%). The comparison of these two complexes highlights the significance of why a system must possess *both* 2,1-regioselectivity *and* precise selectivity for insertion off the primary chain end (pathway A) to produce highly crystalline materials from α-olefins and emphasizes why it is necessary to have a model that can differentiate between these pathways.

**Table 3.9** Breakdown of the Insertion Pathways for the Polymerization of $^{13}$C-Labeled 1-Decene Using **1c** and **1d** (Table 3.8, $2_{iv}$ and $2_{v}$)

| entry (pre-cat.) | A-1° 2,1 (%) | B-1° 1,2 (%) | C-$2^{\circ}_{p}$ 2,1 (%) | D-$2^{\circ}_{p}$ 1,2 (%) | E-2° 2,1 (%) | F-2° 1,2 (%) | G-$1^{\circ}_{m}$ 2,1 (%) | H-$1^{\circ}_{m}$ 1,2 (%) | U[a] (%) |
|---|---|---|---|---|---|---|---|---|---|
| 1 (**1c**) | 57.3 | 9.1 | 15.6 | 0.8 | 14.9 | 0.2 | 0.8 | 1.1 | 0.2 |
| 2 (**1d**) | 34.4 | 35.2 | 3.0 | 5.2 | 8.2 | 2.2 | 3.0 | 7.8 | 0.9 |

[a]U refers to signals not assigned to a specific pathway but included in the total integration.

**Table 3.10** Total Values of the Insertion Pathways for the Polymerization of $^{13}$C-Labeled 1-Decene Using **1c** and **1d** (Table 3.8, $2_{iv}$ and $2_v$)

| entry (pre-cat.) | 1°[a] (%) | 2°[b] (%) | 2,1[c] (%) | 1,2[d] (%) | *B*[e] |
|---|---|---|---|---|---|
| 1 (**1c**) | 68.5 | 31.5 | 88.8 | 11.2 | 43 |
| 2 (**1d**) | 81.2 | 18.8 | 49.1 | 50.9 | 69 |

[a]Total primary insertion (1°), determined by eq (3.23). [b]Total secondary insertion (2°), determined by eq (3.24). [c]Total 2,1-insertion, determined by eq (3.21). [d]Total 1,2-insertion, determined by eq (3.22). [e]*B* = Branches/1000C, determined by $^{13}$C NMR spectroscopy using equation (3.25).

We compared the calculated regiochemistry of insertion and branching numbers for **1c** and **1d** from our model with the 1st and 2nd generation models. We observed that similarly for **1a**, the 1st generation model fails to accurately predict the amount of 2,1- and 1,2-insertion for **1c** and **1d**. The 1st generation model predicts that **1c** is essentially regiorandom with a slight preference for 1,2-insertion, while both the 2nd and 3rd generation models calculate that **1c** gives high 2,1-selectivity. For **1d**, the 1st generation model predicts a modestly 1,2-selective catalyst, whereas the regioselectivities calculated by the 2nd and 3rd generation model show a regiorandom catalyst. A more notable difference can be observed in overall primary and secondary insertion pathways between the 2nd and 3rd generation models, where the former underestimates secondary insertion pathways by 7% compared to the latter. This is reasonable because our 3rd generation model accounts for non-penultimate secondary insertion, which comprises 10.4% of total insertions for this system (pathways E and F, Table 3.9). Many of the methylene signals that contribute to pathway E were attributed to primary insertion in the 2nd generation model. The 3rd generation model calculates 69 branches/1000C from the $^{13}$C NMR spectrum, which matches more closely with the value determined by $^{1}$H NMR spectroscopy (72/1000C) compared to the 2nd generation model (62/1000C). The

**Table 3.11** Comparison of Different Generation Models for Samples from Table 3.8 (Comparison of **1c** and **1d** for the Polymerization of $^{13}$C-Labeled 1-Decene)

| model (pre-cat.) | 1° (%) | 2° (%) | 2,1 (%) | 1,2 (%) | *B* |
|---|---|---|---|---|---|
| 1st gen (**1c**)[a] | – | – | 44 | 56 | – |
| 2nd gen (**1c**)[b] | 70 | 30 | 88 | 12 | 43 |
| 3rd gen (**1c**)[c] | 68 | 32 | 89 | 11 | 42 |
| 1st gen (**1d**)[a] | – | – | 28 | 72 | – |
| 2nd gen (**1d**)[b] | 88 | 12 | 52 | 48 | 62 |
| 3rd gen (**1d**)[c] | 81 | 19 | 49 | 51 | 69 |

[a]Regioselectivity calculated using eq (3.1). [b]Regioselectivity calculated using eq (3.2). Primary insertion (1°) calculated from sum of all $^{13}$C-labeled methines, plus the sum of all $^{13}$C-labeled methylenes minus those β to a branch, and secondary insertion (2°) calculated from sum of all $^{13}$C-labeled methylenes β to a branch (see reference 18). Branches/1000C (*B*) calculated using equation (3.3). [c]Regioselectivity calculated using equation (3.22) and (3.21). Branches/1000C (*B*) calculated using equation (3.25).

major improvement in the 3rd generation model lies in its ability to accurately separate and quantify eight unique pathways that nickel α-diimine catalysts can perform during α-olefin polymerization, where previous models quantified only three pathways. Our 3rd generation model provides an enhanced picture on how catalyst choice and polymerization conditions affect the behavior of a specific catalyst system.

### *3.3.2 ω-Labeled Monomer*

#### *3.3.2.1 Complex **1a**: Standard Conditions*

We further studied **1a** by polymerizing 1-dodecene with a $^{13}$C-label in the ω-position, as opposed to the 2-position, under standard chain straightening conditions (Table 3.12, entry 1). We believe that similar mechanistic insights could be obtained even if the $^{13}$C-label was moved to a different position in the monomer. Under standard

**Table 3.12** Polymerization of $^{13}$C-Labeled 1-Dodecene and Unlabeled 1-Dodecene Using **1a**[a]

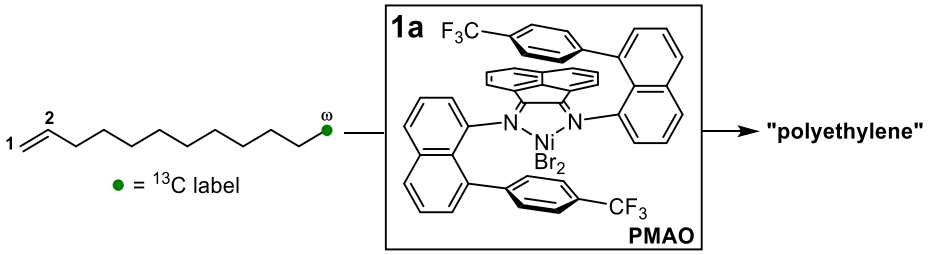


| entry (ID) | $^{13}$C-label | TOF[b] ($h^{-1}$) | $M_n$[c] (kDa) | $Đ$[c] | $T_m$[d] (°C) | ΔH[d] (J/g) | $B$[e] |
|---|---|---|---|---|---|---|---|
| 1 ($\omega_{vi}$) | ω | 2 | 13.8 | 1.5 | 107 | 94.1 | 24 |
| 2 ($0_{vi}$) | – | 4 | 31.2 | 1.3 | 108 | 91.1 | 24 |

[a]Polymerization conditions: [**1a**] = 3.1 mM in PhCl [monomer] = 0.1 M, [PMAO]/[**1a**] = 200, PhCl = 14 mL, 22 °C, 24 h. [b]Calculated using the equation: (mol monomer consumed)(mol catalyst)$^{-1}$(time)$^{-1}$. [c]Determined using gel permeation chromatography (GPC) in 1,2,4-trichlorobenzene at 150 °C vs polyethylene standards. [d]Determined using differential scanning calorimetry (DSC), melting endotherm of second heat. [e]Branches/1000 carbons, determined by $^1$H NMR spectroscopy.

conditions, MAO-activated **1a** produced chain straightened poly(1-dodecene) with a $T_m$ of 107 °C and a low number of branches (Table 3.12, entry 1). Analysis of the resulting polymer by $^{13}$C NMR spectroscopy (Figure 3.7) depicts a material composed primarily of linear methylene units and a small amount of methyl and alkyl branches. This polymer ($\omega_{vi}$) had a nearly identical structure to that of the C2-labeled polymer ($2_i$), except the types of enhanced signals have changed. Since the $^{13}$C-label is positioned at the end of the monomer chain, –$CH_3$ signals such as **ω*** and **ω$^1$** are now readily visible, while methyl methine signals such as **M$^1$** are no longer visible (Figure 3.7).

The mechanistic model was applied to calculate the prevalence of pathways A–H for the polymerization of ω-labeled 1-dodecene (Table 3.13, entry 1). For comparison purposes, insertion pathways for the polymerization of C2-labeled 1-decene using **1a** are also included (Table 3.13, entry 2). Although some information is lost – it is impossible to differentiate between pathways E and F – the ω-labeled polymer gives a similar mechanistic picture to the C2-labeled polymer. Pathway A was calculated at 74.1% for the ω-labeled polymer compared to the C2-labeled polymer at 76.5%. Pathways B, C, and D are also quite close, with variations totaling only 0.5%. The most significant deviation appears in pathways E and F with a 3.9% difference. Although pathways E and F cannot be distinguished using the ω-labeled monomer, this system can still provide accurate mechanistic insight, especially for catalysts that already

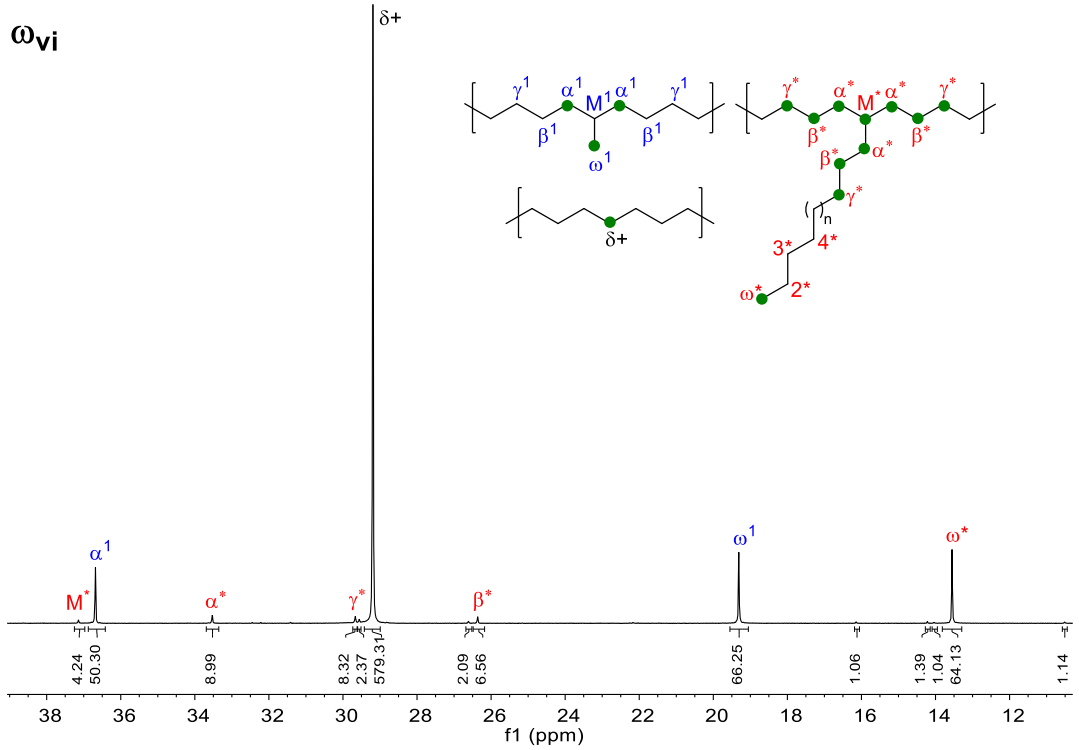


**Figure 3.7** $^{13}$C NMR spectrum of $^{13}$C-labeled poly(1-dodecene) produced by **1a** (Table 3.12, entry 1, $\omega_{vi}$). The green circles on the structures show possible positions for a $^{13}$C-label to appear.

**Table 3.13** Comparison of the Insertion Pathways for **1a** using C2-Labeled 1-Decene and ω-Labeled 1-Dodecene (Table 3.1, $2_i$ and Table 3.12, $\omega_{vi}$)

| entry (ID) | A-1° 2,1 (%) | B-1° 1,2 (%) | C-$2^{\circ}_{p}$ 2,1 (%) | D-$2^{\circ}_{p}$ 1,2 (%) | E-2° 2,1 (%) | F-2° 1,2 (%) | G-$1^{\circ}_{m}$ 2,1 (%) | H-$1^{\circ}_{m}$ 1,2 (%) | U[a] (%) |
|---|---|---|---|---|---|---|---|---|---|
| 1 ($2_i$) | 76.5 | 7.2 | 9.5 | 0.4 | 5.2 | 0.1 | 0.6 | 0.2 | 0.3 |
| 2 ($\omega_{vi}$) | 74.1 | 7.1 | 9.1 | 0.4 | 9.2 | | 0.1 | 0.0 | 0.0 |

[a]U refers to signals not assigned to a specific pathway but included in the total integration.

**Table 3.14** Comparison of the Total Values of Insertion Pathways for **1a** using C2-Labeled 1-Decene and ω-Labeled 1-Dodecene (Table 3.1, $2_i$ and Table 3.12, $\omega_{vi}$)

| entry (ID) | 1°[a] (%) | 2°[b] (%) | 2,1[c] (%) | 1,2[d] (%) | *B*[e] |
|---|---|---|---|---|---|
| 1 ($2_i$) | 84.8 | 15.2 | 92.1 | 7.9 | 23 |
| 2 ($\omega_{vi}$) | 81.3 | 18.7 | 91.8 | 8.2 | – |

[a]Total primary insertion (1°), determined by eq (3.23). [b]Total secondary insertion (2°), determined by eq (3.24). [c]Total 2,1-insertion, for C2-label: determined by eq (3.21). For ω-label: determined by the equation [A+C+G/(A+B+C+D+G+H)*100]. [d]Total 1,2-insertion, for C2-label: determined by eq (3.22). For ω-label, determined by the equation [B+D+H/(A+B+C+D+G+H)*100]. [e]*B* = Branches/1000C, determined by $^{13}$C NMR spectroscopy using equation (3.25). Cannot be determined for ω-labeled polymer.

exhibit effective chain straightening for α-olefins. These catalyst systems perform less secondary insertion pathways as well as less insertions off methyl branches which can result in complications with analysis (discussed *vida infra*), and thus allow for a relatively accurate assessment of the source of branching defects. In the case of **1a**, which is a competent chain straightening catalyst,[7] the data obtained with the ω-labeled monomer provides accurate mechanistic insights into the branching defects.

An advantage of the ω-labeled monomer using highly sensitive NMR spectrometers is that we can observe defects that cannot easily be viewed by conventional methods. In this system, we managed to observe very small signals from

ethyl and propyl branches ($\boldsymbol{\omega^2}$ and $\boldsymbol{\omega^3}$). While much smaller than the $\boldsymbol{\omega^1}$ and $\boldsymbol{\omega^*}$ signals, it shows 2° insertion near the chain end does indeed occur. It is very interesting to note that the amount of signal arising from these intermediate branches only accounts for ~0.4% of the total signal, whereas the total amount of insertion off secondary carbons (pathways E and F) is 9.2%. This prompts the question, why do insertions off secondary carbons occur more frequently off the polymer backbone as opposed to near the chain end? One explanation is that there are simply more backbone methylenes to insert off than chain end methylenes. Assuming the energetics of insertion off all methylenes beyond penultimate are similar, then it is statistically unlikely for the catalyst to insert off a methylene near the chain end to produce an intermediate branch. Another possibility is that once the catalyst is close enough to the chain end, it becomes more energetically favorable to continue walking to the primary or penultimate positions before the next monomer insertion, akin to a thermodynamic sink. Further kinetic and energetic analysis of these systems would be beneficial for better understanding the limited number of intermediate branches observed.

### *3.3.2.2 Complex **1a**: Concentration Effect*

We further utilized the ω-labeled monomer to explore the effect of higher concentration, conditions that are typically unfavorable for chain straightening. Increasing the concentration to 1.0 M caused a marked increase in rate and resulted in a higher molecular weight polymer with a lower $T_m$ of 95 °C and increased branching number (Table 3.15, entry 2). Comparing the $^{13}C$ NMR spectra for the polymers made at 0.1 M and 1.0 M (Figure 3.8) shows a clear increase in **ω¹** and **ω*** signals at 1.0 M, meaning that a larger number of both methyl and alkyl branches was produced. Analysis using the mechanistic model (Table 3.16) demonstrated a drop in pathway A from 74.1% to 65.9% in favor of an increase in the secondary insertion pathways C (9.1% to 12.1%), and E+F (9.2% to 13.9%).

**Table 3.15** Concentration Effect for the Polymerization of $^{13}C$-labeled 1-Dodecene using **1a**[a]

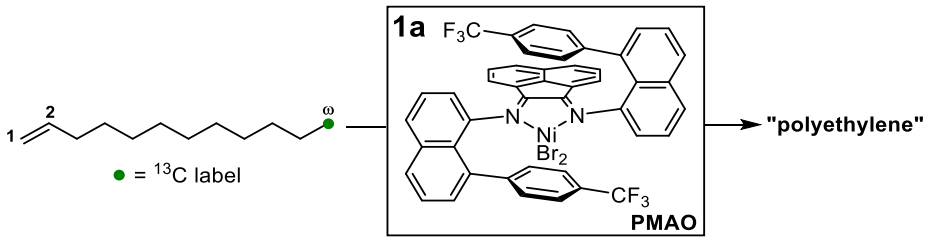


| entry (ID) | conc (M) | TOF[b] ($h^{-1}$) | $M_n$[c] (kDa) | $Đ$[c] | $T_m$[d] (°C) | ΔH[d] (J/g) | $B$[e] |
|---|---|---|---|---|---|---|---|
| 1 ($\omega_{vi}$) | 0.1 | 2 | 13.8 | 1.5 | 107 | 94.1 | 24 |
| 2 ($\omega_{vii}$) | 1.0 | 71 | 46.2 | 1.4 | 95 | 35.8 | 32 |

[a]Polymerization conditions: [**1a**] = 3.1 mM in PhCl, [PMAO]/[**1a**] = 200, 22 °C, 24 h (for $\omega_{vi}$), 3 h (for $\omega_{vii}$). [b]Calculated using the equation: (mol monomer consumed)(mol catalyst)$^{-1}$(time)$^{-1}$. [c]Determined using gel permeation chromatography (GPC) in 1,2,4-trichlorobenzene at 150 °C vs polyethylene standards. [d]Determined using differential scanning calorimetry (DSC), melting endotherm of second heat. [e]Branches/1000 carbons, determined by $^1H$ NMR spectroscopy.

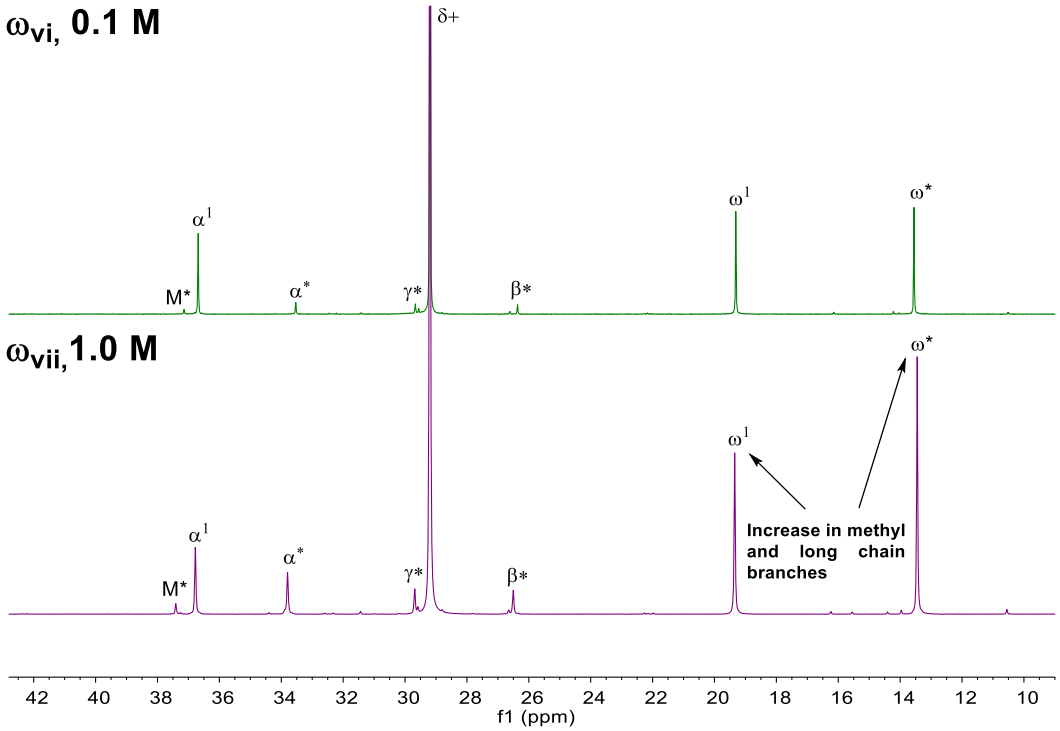


**Figure 3.8** $^{13}$C NMR spectra of $^{13}$C-labeled poly(1-dodecene) grown at 0.1 M (top, Table 3.15, $\omega_{vi}$) and 1.0 M (bottom, Table 3.15, $\omega_{vii}$) using **1a**.

These results are consistent with faster monomer trapping due to more available olefin in each catalyst's local environment, thus favoring olefin insertion over chain walking. Interestingly, pathway B appears to decrease slightly from 7.1% to 5.6% by increasing the monomer concentration. Again, pathways E and F cannot be differentiated due to the distance from the $^{13}$C-label; however, it is very likely that the

**Table 3.16** Breakdown of the Insertion Pathways for the Polymerization of $^{13}$C-Labeled 1-Dodecene using **1a** at Different Concentrations (Table 3.15, $\omega_{vi}$ and $\omega_{vii}$)

| entry (M) | A-1° 2,1 (%) | B-1° 1,2 (%) | C-2°$_p$ 2,1 (%) | D-2°$_p$ 1,2 (%) | E-2° 2,1 (%) | F-2° 1,2 (%) | G-1°$_m$ 2,1 (%) | H-1°$_m$ 1,2 (%) | U[a] (%) |
|---|---|---|---|---|---|---|---|---|---|
| 1 (0.1) | 74.1 | 7.1 | 9.1 | 0.4 | 9.2 | | 0.1 | 0.0 | 0.0 |
| 2 (1.0) | 65.9 | 5.5 | 12.0 | 0.5 | 13.9 | | 2.0 | 0.1 | 0.1 |

[a]U refers to signals not assigned to a specific pathway but included in the total integration.

**Table 3.17** Total Values of the Insertion Pathways for the Polymerization of $^{13}$C-Labeled 1-Dodecene using **1a** at Different Concentrations (Table 3.15, $\omega_{vi}$ and $\omega_{vii}$)

| entry (M) | 1°[a] (%) | 2°[b] (%) | 2,1[c] (%) | 1,2[d] (%) | *B*[e] |
|---|---|---|---|---|---|
| 1 (0.1) | 81.3 | 18.7 | 91.8 | 8.2 | – |
| 2 (1.0) | 73.6 | 26.4 | 92.9 | 7.1 | – |

[a]Total primary insertion (1°), determined by eq (3.23). [b]Total secondary insertion (2°), determined by eq (3.24). [c]Total 2,1-insertion, determined by the equation [A+C+G/(A+B+C+D+G+H)*100]. [d]Total 1,2-insertion, determined by the equation [B+D+H/(A+B+C+D+G+H)*100]. [e]*B* = Branches/1000C from $^{13}$C NMR spectroscopy cannot be determined for ω-labeled polymer.

vast majority of secondary insertions occur through pathway E given the high selectivity for 2,1-insertions.

### *3.3.2.3 Complex **1b**: Standard Conditions*

We also applied our mechanistic model to probe the differences in behavior between **1a** and **1b**, which only differ by the substituents on the capping axial aryl groups ($CF_3$ vs $CH_3$). It had been previously observed that MAO-activated **1b** ($CH_3$) is

**Table 3.18** Polymerization of $^{13}$C-Labeled 1-Dodecene using **1a** and **1b**[a]

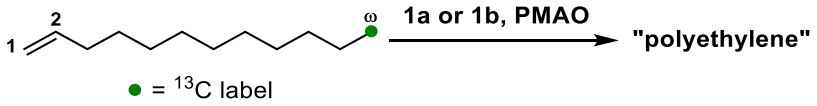


| entry (ID) | pre-cat. | TOF[b] ($h^{-1}$) | $M_n$[c] (kDa) | *Đ*[c] | $T_m$[d] (°C) | ΔH[d] (J/g) | *B*[e] |
|---|---|---|---|---|---|---|---|
| 1 ($\omega_{vi}$) | **1a** | 2 | 13.8 | 1.5 | 107 | 94.1 | 24 |
| 2 ($\omega_{viii}$) | **1b** | 3 | 28.4 | 1.3 | 100 | 78.1 | 32 |

[a]Polymerization conditions: [**1a**] = [**1b**] = 3.1 mM in PhCl, [monomer] = 0.1 M, [PMAO]/[pre-cat.] = 200, 14 mL PhCl, 22 °C, 24 h. [b]Calculated using the equation: (mol monomer consumed)(mol catalyst)$^{-1}$(time)$^{-1}$. [c]Determined using gel permeation chromatography (GPC) in 1,2,4-trichlorobenzene at 150 °C vs polyethylene standards. [d]Determined using differential scanning calorimetry (DSC), melting endotherm of second heat. [e]Branches/1000 carbons, determined by $^1$H NMR spectroscopy.

not as effective for the chain straightening polymerization of α-olefins compared to **1a** ($CF_3$), with polymers formed exhibiting somewhat lower melting temperatures and crystallinities.[7] The diminished thermal properties were due to an increase in the number of branches, however, the relative rise in 1,2-insertion and secondary insertions were unclear. Thus, **1b** was tested using the ω-labeled monomer. The resulting polymer from **1b** (Table 3.18, entry 2) was higher in molecular weight, slightly lower in melting temperature (100 °C), and had a higher branching number compared to the polymer from **1a** (entry 2).

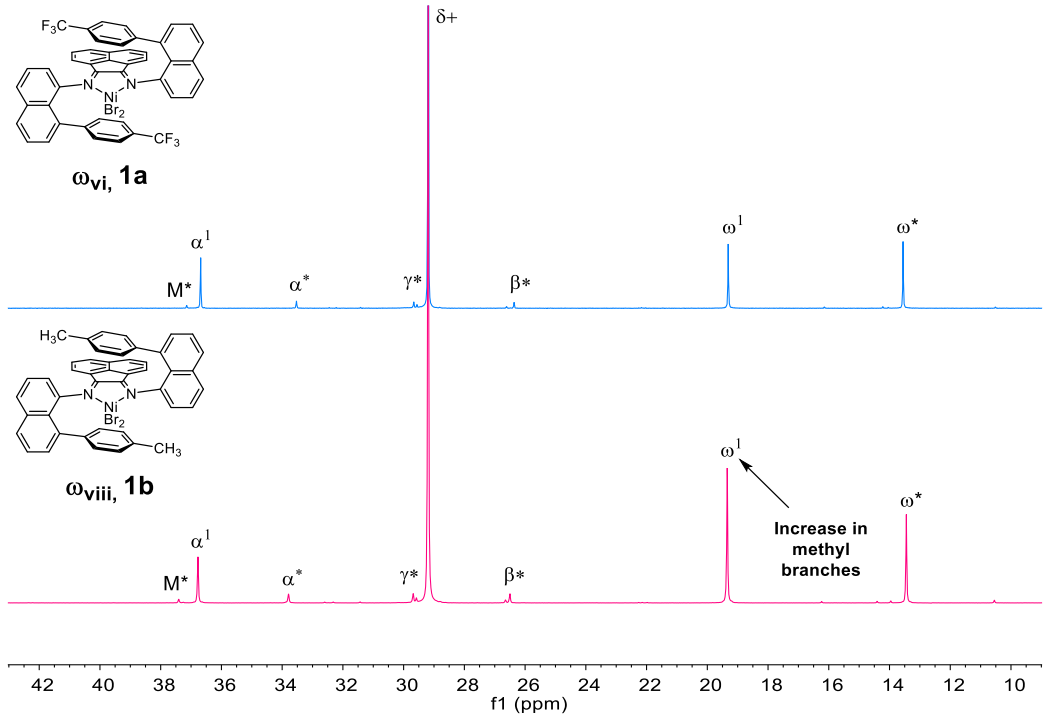


**Figure 3.9** $^{13}C$ NMR spectra of the ω-labeled polymers produced by **1a** (Table 3.18, $\omega_{vi}$) and **1b (**Table 3.18, $\omega_{viii}$).

**Table 3.20** Comparison of Insertion Pathways between **1a** (Table 3.18, $\omega_{vi}$) and **1b** (Table 3.18, $\omega_{viii}$) for the Polymerization of $^{13}$C-Labeled 1-Dodecene

| entry (pre-cat.) | A-1° 2,1 (%) | B-1° 1,2 (%) | C-2°$_p$ 2,1 (%) | D-2°$_p$ 1,2 (%) | E-2° 2,1 (%) | F-2° 1,2 (%) | G-1°$_m$ 2,1 (%) | H-1°$_m$ 1,2 (%) | U[a] (%) |
|---|---|---|---|---|---|---|---|---|---|
| 1 (**1a**) | 74.1 | 7.1 | 9.1 | 0.4 | 9.2 | | 0.1 | 0.0 | 0.0 |
| 2 (**1b**) | 65.9 | 5.5 | 12.0 | 0.5 | 13.9 | | 2.0 | 0.1 | 0.1 |

[a]U refers to signals not assigned to a specific pathway but included in the total integration.

**Table 3.19** Comparison of the Total Insertion Pathways between **1a** (Table 3.18, $\omega_{vi}$) and **1b** (Table 3.18, $\omega_{viii}$) for the Polymerization of $^{13}$C-Labeled 1-Dodecene

| entry (pre-cat.) | 1°[a] (%) | 2°[b] (%) | 2,1[c] (%) | 1,2[d] (%) | *B*[e] |
|---|---|---|---|---|---|
| 1 (**1a**) | 81.3 | 18.7 | 91.8 | 8.2 | – |
| 2 (**1b**) | 74.1 | 25.9 | 93.4 | 6.6 | – |

[a]Total primary insertion (1°), determined by eq (3.23). [b]Total secondary insertion (2°), determined by eq (3.24). [c]Total 2,1-insertion, determined by the equation [A+C+G/(A+B+C+D+G+H)*100]. [d]Total 1,2-insertion, determined by the equation [B+D+H/(A+B+C+D+G+H)*100]. [e]*B* = Branches/1000C from $^{13}$C NMR spectroscopy cannot be determined for ω-labeled polymer.

Comparison of the $^{13}$C NMR spectra of **1a** and **1b** shows that the two spectra appear quite similar in regards to the type of branches present, each resulting in a mixture of methyl and alkyl branches (Figure 3.9). A deeper look shows that, specifically, the intensity of the signal assigned as $\boldsymbol{\omega^1}$ is higher for the polymer generated by **1b**. Analysis using the mechanistic model and comparison to the previous results from **1a** shows that most pathways do not substantially change. The regioselectivity of insertion between the two systems appear close in value, with MAO-activated **1a** and **1b** displaying 91.8% and 93.4% 2,1-selectivity, respectively. Pathways E+F only experience a subtle increase from 9.2% to 9.7% between **1a** and **1b**, respectively. The most signficant difference in catalyst behavior occurs in just pathway C, penultimate

2,1-insertion (Table 3.20). The $CH_3$ catalyst exhibits 15.9% of pathway C compared to the $CF_3$ catalyst at just 9.1%. Our mechanistic model was able to quantify the specific effects of the ligand pertubation on the insertion pathways between **1a** ($CF_3$) and **1b** ($CH_3$). This targeted mechanistic knowledge is important for better understanding the relationship between ligand substituents and the nature of a given α-olefin polymerization.

### *3.3.3 $^{13}$C-Labeled Monomer Comparison using Complex **1d***

Both $^{13}$C-labeled monomers in conjunction with our model are effective at providing detailed mechanistic insights on α-olefin polymerization using cationic nickel complexes. However, it is important to emphasize the different types of mechanistic information accessible through these monomers, which is highlighted through the

**Table 3.21** Polymerization of $^{13}$C-Labeled Monomers Using **1d**

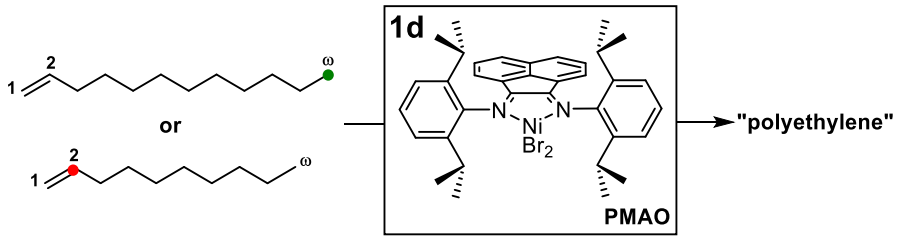


| entry (ID) | $^{13}$C-label | TOF[c] ($h^{-1}$) | $M_n$[d] (kDa) | $Đ$[d] | $T_m$[e] (°C) | ΔH[e] (J/g) | $B$[f] |
|---|---|---|---|---|---|---|---|
| 1 ($2_v$)[a] | C2 | 40 | 31.5 | 1.4 | 46 | 17.3 | 72 |
| 2 ($\omega_{ix}$)[b] | ω | 47 | 51.2 | 1.5 | 53 | 23.1 | 73 |

[a]Polymerization conditions: [**1d**] = 2.5 mM in PhCl, [monomer] = 0.1 M, [PMAO]/[**1d**] = 200, PhCl = 11.9 mL, 22 °C, 6.5 h. [b]Polymerization conditions: [**1d**] = 3.1 mM in PhCl, [monomer] = 0.1 M, [PMAO]/[**1d**] = 200, 14 mL PhCl, 22 °C, 7.0 h. [c]Calculated using the equation: (mol monomer consumed)(mol catalyst)$^{-1}$(time)$^{-1}$. [d]Determined using gel permeation chromatography (GPC) in 1,2,4-trichlorobenzene at 150 °C vs polyethylene standards. [e]Determined using differential scanning calorimetry (DSC), melting endotherm of second heat. [f]Branches/1000 carbons, determined by $^1$H NMR.

comparison of sample $2_v$ (Table 3.21, entry 1) and sample $\omega_x$ (Table 3.21, entry 2) produced using **1d**.

When using the C2-labeled monomer, the insertion pathway is described by the label of the incoming monomer. By design, the $^{13}$C-label is near the insertion event such that accurate determination of the regiochemistry of insertion can be performed. Since the label normally ends up on the polymer backbone, subtle changes in the branching environment will change the chemical shift of the label, providing additional information on subsequent insertions. Various methine signals in different branching environments can be observed and quantified, allowing for a fuller understanding of the regiochemistry of insertion and the branching structure of the polymer (Figure 3.10).

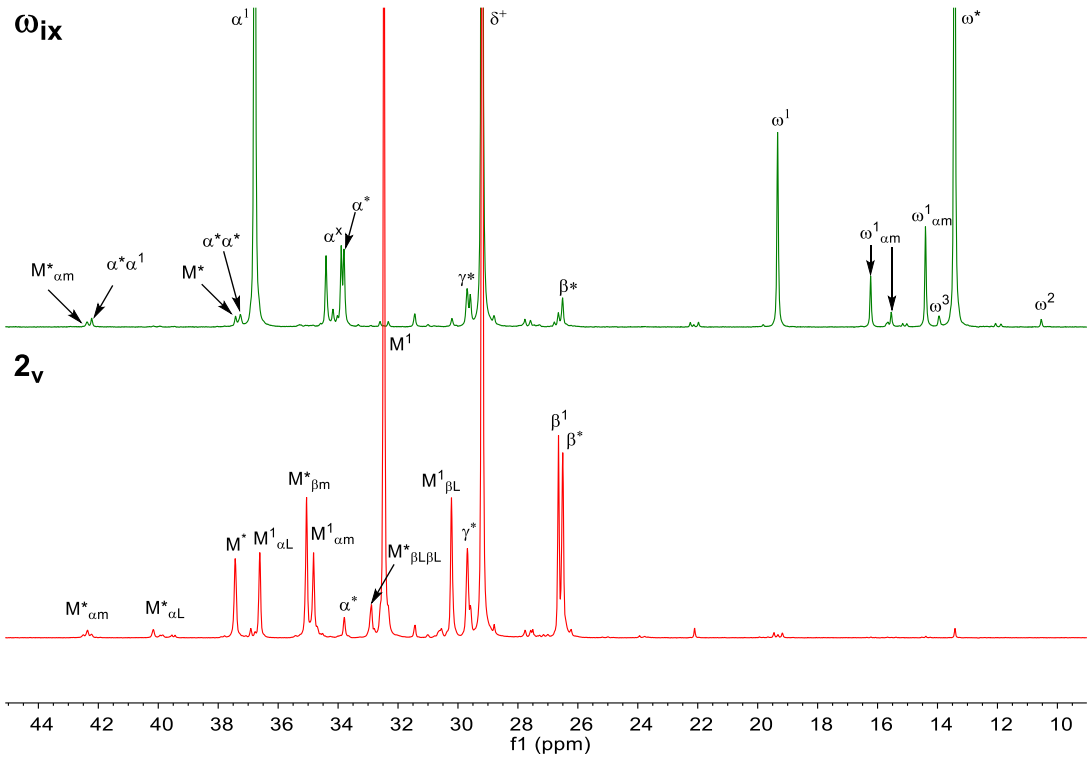


**Figure 3.10** Comparison of $^{13}$C-labeled polymers produced by **1d** using the ω-labeled monomer (top, Table 3.21, $\omega_{ix}$) and C2-labeled monomer (bottom, Table 3.21, $2_v$).

When using the ω-labeled monomer, the insertion pathway is described by the last label installed on the polymer. When the catalyst chain walks to the penultimate position or primary chain end, the label is close to its insertion event and is installed on or near the polymer backbone. However, if the catalyst inserts the next monomer far from the chain end, the last label on the polymer chain becomes the end of an alkyl branch which is too distant to capture the information of its insertion event. Therefore, catalyst systems that exhibit greater amounts of secondary insertions or insertions off methyl branches result in the loss of regiochemical information.

Because of this shortcoming of the ω-labeled monomer, major discrepancies can be observed between the two labeled polymers produced by **1d**, specifically in pathways E–H. Analysis of the ω-labeled polymer shows that secondary insertions pathways are overestimated at 20.0%, compared to 10.4% for the C2-labeled polymer. This was expected because MAO-activated **1d** readily inserts off methyl branches (pathways G and H) and can even perform successive 1,2-insertions off methyl branches without chain walking. Installing so many alkyl branches in a row makes it difficult to correct for these pathways with the ω-labeled monomer, combining signals from pathways G and H into **ω*** and thus overestimating pathways E+F. One benefit of the ω-labeled monomer though is the ability to observe intermediate branches more readily compared to the C2-labeled monomer.

## *3.4 Conclusions*

In this $^{13}$C-labeling study, we developed a new mechanistic model for quantifying eight different insertion pathways (A–H) for the polymerization of α-olefins

using cationic nickel α-diimine catalysts. We explored how various ligand structures and conditions affected the distribution of the eight pathways (Scheme 3.9). By accounting for non-penultimate secondary insertion and correcting for $^{13}C$ NMR signals arising from natural abundance, we believe this model provides the most accurate analysis to date in terms of quantifying these unique insertion pathways. We primarily focused on **1a** and demonstrated similar values for pathways A–H between the analysis of two polymers resulting from the polymerization of two different $^{13}C$-labeled monomers (C2-labeled 1-decene and ω-labeled 1-dodecene). MAO-activated **1a** displayed high 2,1-regioselectivity and preference for insertion off the primary chain end (pathway A), both of which are necessary for producing chain straightened materials. At lower temperatures (0 °C), the chain straightening of **1a** improved slightly with an increase in 2,1-selectivity and a decrease in secondary insertion pathways. Higher temperatures (50 °C) mostly affected secondary insertion pathways, which increased by 4.3%, whereas the 2,1-regioselectivity only decreased slightly by 2.3%. Although the branching number of the polymer produced at 50 °C only increased slightly, the thermal properties were significantly affected because of the higher ratio of alkyl branches. Increasing the concentration from 0.1 M to 1.0 M demonstrated higher percentages of secondary insertion pathways and a limited change in regioselectivity. We highlighted that subtle changes in ligand structure can have targeted effects on the observed insertion pathways with the comparison of **1a** ($CF_3$) and **1b** ($CH_3$). We observed that the presence of trifluoromethyl substituents in the "sandwich" ligand structure as opposed to methyl substituents, specifically decreased the amount of methyl branches occurring through pathway C.

**Scheme 3.9** Summary of Results from Mechanistic Studies

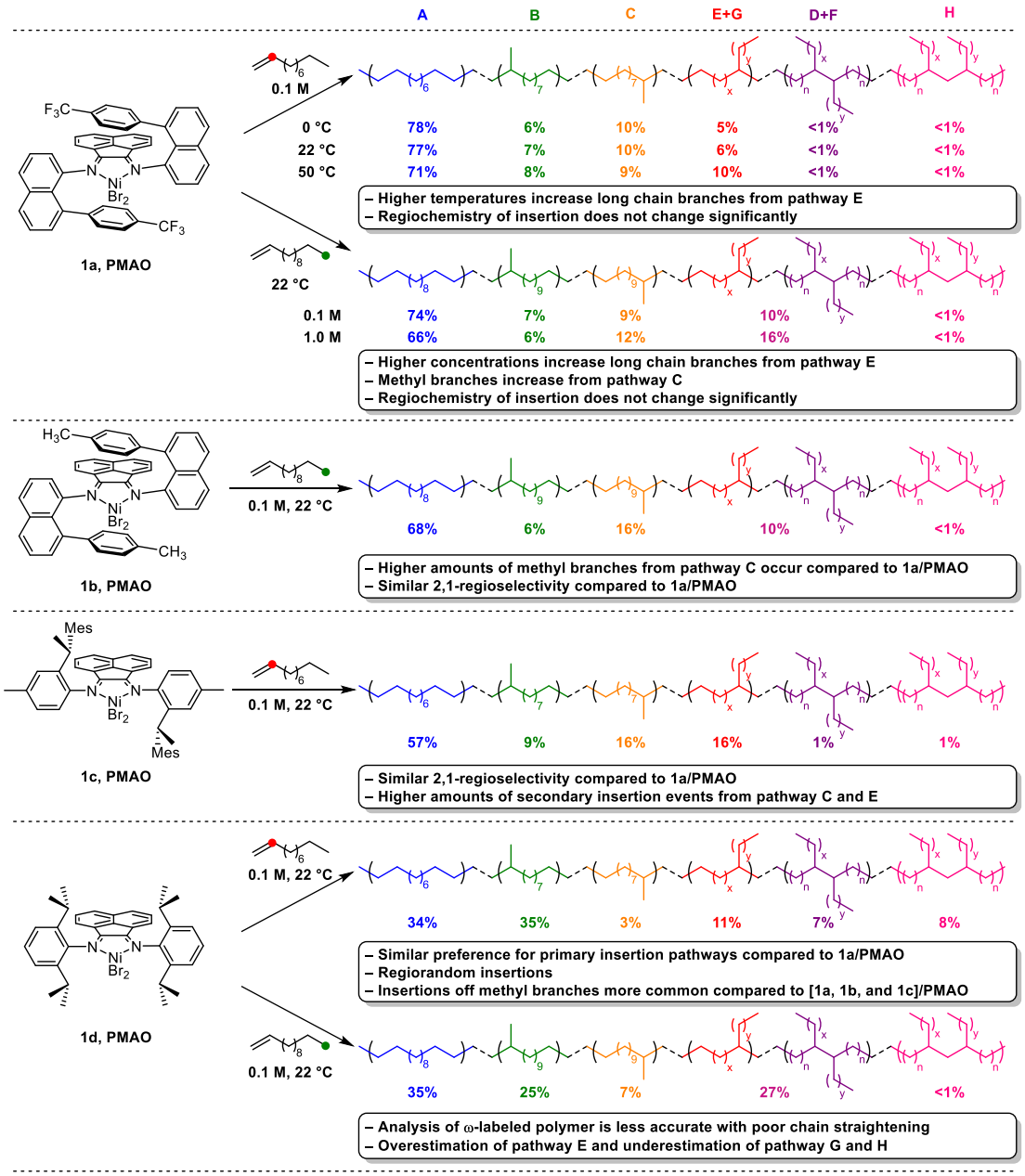


Further studies with **1c** and **1d** demonstrated the importance of having selectivity for both 2,1-insertion *and* insertion off the primary chain end (pathway A). MAO-activated **1c** was mostly 2,1-selective at 88.6%, but introduced a high number of branches through secondary insertion pathways. Conversely, MAO-activated **1d**

showed a preference for insertion off primary carbons, but introduced branching through regiorandom insertions.

With the newly developed mechanistic model, we can easily determine not only the branching distribution, but also the insertion pathways from which the branches are installed. This knowledge helps correlate changes in ligand design and reaction conditions to specific changes in the insertion modes of the catalyst. The application of this model may guide future ligand design in order to target late metal catalysts with improved selectivity for chain straightening α-olefins.

## *3.5 Experimental*

### *3.5.1 General Considerations*

Air and/or moisture sensitive compounds were manipulated under an atmosphere of nitrogen using standard Schlenk techniques or an MBraun Labmaster glovebox. Flash column chromatography was performed using silica gel (particle size 40–64 μm, 230–400 mesh).

The $^{1}H$ NMR and $^{13}C\{^{1}H\}$ NMR spectra were recorded on a 500 MHz Bruker AV III HD with broadband Prodigy Cryoprobe or a Varian INOVA 600 MHz spectrometer equipped with a switchable 5BB probe, using the residual non-deuterated solvent signal as a reference [$CDCl_3$: 7.26 ppm ($^{1}H$), 77.16 ppm ($^{13}C$), $Cl_2CDCDCl_2$ ($d_2$-TCE): 6.0 ppm ($^{1}H$), 73.78 ppm ($^{13}C$)]. All polymer samples were analyzed in $d_2$-TCE in 5mm tubes using quantitative $^{1}H$ and $^{13}C\{^{1}H\}$ NMR spectroscopy at 130 °C, using $Cr(acac)_3$ (acac=acetylacetonate) from Sigma Aldrich as a paramagnetic relaxation agent[26] to reduce NMR time (17 mg of $Cr(acac)_3$ in 0.5 mL of $d_2$-TCE, 0.1 M, ~5 wt. %

of polymer). Parameters used for quantitative $^{13}C\{^{1}H\}$ NMR using the 500 MHz Bruker were as follows: ns = 1024, d1 = 8.5 s, at = 1.5 s, for a total time of 3 hours per sample. MestreNova software was used to process the spectra. When appropriate, line fitting analysis was performed to more accurately quantify partially overlapping signals.

High temperature gel permeation chromatography (GPC) was performed on Agilent PL-GPC 220 equipped with a refractive index (RI) detector and three PL-Gel Mixed B columns. GPC columns were eluted at 1.0 mL/min with 1,2,4-trichlorobenzene (TCB) containing 0.01 wt. % di-*tert*-butylhydroxytoluene (BHT) at 150 °C. The samples were prepared in TCB (with BHT) at a concentration of 1.0 mg/mL and heated at 150 °C for at least 1 hour prior to injection. GPC data calibration was done with monomodal polyethylene standards from Polymer Standards Service.

Differential scanning calorimetry (DSC) measurements were performed on Mettler-Toledo Polymer DSC instrument equipped with an automated sampler. Polymer samples in crimped aluminum pans were analyzed under nitrogen at a heating rate of 10 °C/min from −70 to 200 °C. STARe software was used to process the collected data and melting points ($T_m$) and heats of fusion (ΔH) were obtained and reported from the second heating run.

HRMS analyses were performed on a Thermo Scientific Exactive Orbitrap MS system with an Ion Sense DART ion source, or a Hewlett-Packard 6890N GC coupled with a JEOL GCMate II dual sector mass spectrometer (ESI) in positive-ion mode. The mass axis for the latter was calibrated using high-boiling perfluorokerosene fragment ions.

### *3.5.2 Materials*

1-Decene (Acros Chemicals, 95%) and 1-dodecene (Sigma Aldrich, 95%) were distilled, degassed by three freeze-pump-thaw cycles, and stored over activated 4 Å molecular sieves before use. $^{13}$C-labeled 1-decene in the 2 position and $^{13}$C-labeled 1-dodecene in the ω position were synthesized as described in Sections 3.5.4 and 3.5.5, degassed by three freeze-pump-thaw cycles, and stored over activated 4 Å molecular sieves. Polymethylaluminoxane (PMAO-IP) was purchased from Akzo Nobel (7 wt. % in toluene) and dried by removing volatiles under vacuum and heating at 40 °C for at least 10 hours. Anhydrous chlorobenzene (Sigma Aldrich, 99.8%) was sparged with nitrogen for 40 minutes and stored over activated 4 Å molecular sieves prior to use. Diethyl ether was dried over calcium hydride and degassed by three freeze-pump-thaw cycles. $^{13}CO_2$ and $^{13}CH_3I$ were purchased from Cambridge Isotope Laboratories and used without further purification. All other reagents were purchased from commercial sources and used without further purification.

### *3.5.3 Complex Synthesis*

Complex **1a**,[7] **1b**,[2d] **1c**,[27] and **1d**[1a] have been previously reported and were synthesized according to known literature procedures. Complex **1a** and **1c** were crystallized and crushed into a fine powder before use, while complexes **1b** and **1d** were stored as a powder before use.

### *3.5.4 Synthesis of $^{13}$C-Labeled 1-Decene (2 position)*

Method developed by M. Brookhart et al. was adapted.[18]

**(1-$^{13}$C)-Nonanoic acid**

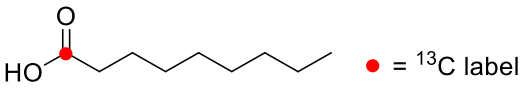


Diethyl ether (60 mL) was added into a flame dried 250 mL three-necked round bottom flask equipped with a Teflon-coated stir bar, two Schlenk adapters, and a septum. One Schlenk adapter was connected to a vacuum line. The other Schlenk adapter was connected to a Y-shaped connector by rubber tubing. One branch of the Y-shaped connector was connected to a regulator of a $^{13}CO_2$ 1L lecture bottle (Cambridge Isotope, >99% $^{13}$C) and the remaining branch to a rubber balloon tightly secured with tape and copper wire. The flask was cooled to −35 °C in a dry ice/iPrOH bath. The apparatus up to the regulator was evacuated and carefully back-filled with $^{13}CO_2$ gas until $Et_2O$ became saturated and the rubber balloon was slightly inflated. Then n-$C_8H_{17}MgBr$ (60.0 mL, 0.97 M in THF, 58.2 mmol)[28] was added dropwise with rapid stirring. The gas was continuously introduced into the flask as the balloon became deflated upon addition of n-$C_8H_{17}MgBr$ until all of the n-$C_8H_{17}MgBr$ was added and $^{13}CO_2$ gas consumed. The reaction mixture was warmed to room temperature. If the rubber balloon inflated upon warming, more n-$C_8H_{17}MgBr$ was added. The reaction was cooled to 0 °C and 5% $H_2SO_{4(aq)}$ was added until pH = 2. The ether layer was separated and the aqueous layer was extracted twice with $Et_2O$ (20 mL). The combined organic phase was washed with brine (20 mL), dried over $Na_2SO_4$, filtered, and evaporated to afford 7.11 g (99%) of the product as a yellow oil. The product was used in the next step without further purification. **$^1$H NMR** ($CDCl_3$, 500 MHz): δ 11.28 (br s, 1H), 2.35 (dt, 2H, *J* = 7.3 Hz), 1.63 (m, 2H), 1.38–1.23 (m, 10H), 0.88 (t, 3H, *J* = 7.1 Hz). **$^{13}$C{$^1$H}**

**NMR** ($CDCl_3$, 125 MHz): δ 180.30–179.80 (broad, $^{13}C$ label), 34.15 ($J_{CC}$ = 55.5 Hz), 31.95, 29.35, 29.25, 29.22 ($J$ = 3.6 Hz), 24.83 ($J$ = 1.5 Hz), 22.79, 14.24. **HRMS** (DART): *m*/*z* calculated for $C_8{}^{13}CH_{19}O_2^+$ $(M + H)^+$ 160.14131, found 160.14173.

**(1-$^{13}$C)-Nonanoic acid methyl ester**

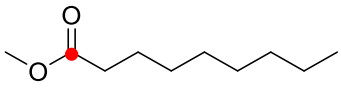

To a 50 mL round bottom flask equipped with a Teflon-coated stir bar, n-$C_8H_{17}{}^{13}CO_2H$ (1.18 g, 7.40 mmol) and anhydrous DMF (20 mL) were added. To the obtained solution $K_2CO_3$ (1.53 g, 11.1 mmol) was added followed by dropwise addition of methyl iodide (0.700 mL, 11.1 mmol). The flask was covered with aluminum foil and the reaction was stirred at room temperature in the dark for 15 hours (overnight). The mixture was poured into water (100 mL), transferred to a separatory funnel, and extracted with ethyl acetate (3 × 50 mL). The combined organic phase was washed with brine (50 mL), dried over $Na_2SO_4$, filtered, and concentrated *in vacuo*. The residue was purified by column chromatography ($SiO_2$, EtOAc/hexanes 1/4) affording 1.16 g (91%) of the title compound as a colorless oil. **$^1$H NMR** ($CDCl_3$, 500 MHz): δ 3.66 (d, 3H, $J$ = 3.8 Hz), 2.30 (dt, 2H, $J$ = 7.4 Hz), 1.62 (m, 2H) 1.34–1.21 (m, 10H), 0.88 (t, $J$ = 7.2 Hz). **$^{13}$C{$^1$H} NMR** ($CDCl_3$, 125 MHz): δ 174.49 ($^{13}C$ label), 51.57 ($J$ = 2.7 Hz), 34.27 ($J_{CC}$ = 57.4 Hz), 31.96, 29.37, 29.31 ($J$ = 3.7 Hz), 29.26, 25.12 ($J$ = 1.7 Hz), 22.79, 14.24. **HRMS** (DART): *m*/*z* calculated for $C_9{}^{13}CH_{21}O_2^+$ $(M + H)^+$ 174.15696, found 174.15724.

**1-(1-$^{13}$C)-Nonanol**

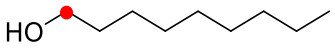


A flame dried 50 mL Schlenk flask equipped with Teflon-coated stir bar was transferred to the glove box and $LiAlH_4$ (589 mg, 14.7 mmol) was added. Outside the glove box, $Et_2O$ (10 mL) was added and the mixture was cooled to 0 °C. Then, a solution of n-$C_8H_{17}{}^{13}CO_2CH_3$ (1.16 g, 6.70 mmol) in $Et_2O$ (10mL) was added dropwise. The reaction mixture was stirred at 0 °C for 1 hour, warmed to room temperature, and stirred for an additional 2 hours. The reaction was cooled to 0 °C and MeOH (20 mL) was carefully added dropwise to quench unreacted $LiAlH_4$ followed by dropwise addition of $H_2O$ (50 mL). To the obtained mixture, potassium sodium tartrate tetrahydrate (approximately 1 g) was added and the organic phase was separated. The aqueous phase was extracted with $Et_2O$ (3 × 50 mL). The combined organic phase was washed with brine (50 mL), dried over $Na_2SO_4$, filtered, and concentrated *in vacuo* to afford 930 mg (96%) of the product as a colorless oil. The product was used in the next step without further purification. **$^1$H NMR** ($CDCl_3$, 500 MHz): δ 3.64 (d of br t, 2H, $J_{CH}$ = 141 Hz), 1.56 (m, 2H) 1.39–1.20 (m, 10H), 0.88 (t, 3H, $J$ = 7.1 Hz), hydroxyl proton not observed. **$^{13}$C{$^1$H} NMR** ($CDCl_3$, 125 MHz): δ 63.26 ($^{13}$C label), 32.97 ($J_{CC}$ = 37.2 Hz), 32.03, 29.73, 29.59 ($J$ = 4.2 Hz), 29.41, 25.89, 22.82, 14.25. **HRMS** (ESI) *m*/*z* calculated for $C_8{}^{13}CH_{18}{}^+$ $(M - H_2O)^+$ 127.1446, found 127.1442.

**(1-$^{13}$C)-Nonanal**

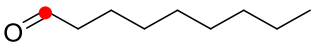

Pyridinium chlorochromate (PCC, 2.76 g, 12.8 mmol) was mixed with $SiO_2$ (2.76 g, 1 weight equiv. of PCC) in a mortar and pestle to a fine, fluffy powder. The obtained mixture was transferred to a 100 mL round bottom flask equipped with a Teflon-coated stir bar and suspended in $CH_2Cl_2$ (25 mL). To the obtained orange suspension, n-$C_8H_{17}{}^{13}CH_2OH$ (930 mg, 6.40 mmol) solution in $CH_2Cl_2$ (5 mL) was added dropwise. The mixture turned dark brown upon addition of alcohol. After 2 hours, Celite® was added and the resulting suspension was filtered through a glass frit. Solids were washed with $Et_2O$ (100 mL) and filtrate was concentrated *in vacuo*. The residue was purified by column chromatography on a short $SiO_2$ column (4/1 hexanes/EtOAc) affording 917 mg (99%) of a product. The product decomposes readily so it was *immediately* used in the next step. **$^1$H NMR** ($CDCl_3$, 400 MHz): δ 9.76 (dt, $J_{CH}$ = 170 Hz, $J$ = 1.9 Hz) 2.41 (m, 2H), 1.62 (m, 2H), 1.37–1.19 (m, 10H), 0.88 (t, 3H, J = 7.1 Hz). **$^{13}$C{$^1$H} NMR** ($CDCl_3$, 100 MHz): δ 203.17 ($^{13}$C label), 64.55, 31.94, 29.47, 29.34, 29.30, 29.24, 22.79, 22.23, 14.25. The product oxidized before an **HRMS** could be acquired.

**1-(2-$^{13}$C)-Decene**

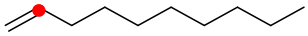

In a 100 mL Schlenk flask equipped with a Teflon-coated stir bar, $CH_3PPh_3Br$ (2.97 g, 8.32 mmol) was suspended in dry THF (25 mL). The resulting mixture was cooled to 0 °C and a solution of NaHMDS (1.53 g, 8.32 mmol) in dry THF (9 mL) was added *via* canula. The reaction mixture was stirred at 0 °C for 40 minutes. To the formed yellow mixture, n-$C_8H_{17}{}^{13}CHO$ (917 mg, 6.40 mmol) was added and the reaction

mixture was stirred at room temperature overnight. After completion as evident by TLC ($SiO_2$, hexanes, $R_f$ = 1, $KMnO_4$ stain) reaction was diluted with pentane (50 mL) and solids were filtered off. Collected solids were washed with pentane (2 × 50 mL). Washings and filtrate were combined and washed with sat. $NH_4Cl$ aqueous solution (50 mL) and water (50 mL). Organic phase was dried over $MgSO_4$, filtered, and concentrated *in vacuo* (bath temp. 40 °C). The resulting oil was purified by column chromatography (100% pentane) to afford 610 mg (68%) of the product as a colorless oil. **$^1$H NMR** ($CDCl_3$, 500 MHz): δ 5.82 (dm, 1H, $J_{CH}$ = 151 Hz, $^{13}$C-label), 5.02–4.90 (m, 2H), 2.04 (m, 2H), 1.38 (m, 2H), 1.33–1.21 (m, 10H), 0.88 (t, 3H, $J$ = 7.1 Hz). **$^{13}$C{$^1$H} NMR** ($CDCl_3$, 125 MHz): δ 139.43 ($^{13}$C-label), 114.16 ($J_{CC}$ = 69.1 Hz), 33.99 ($J_{CC}$ = 41.9 Hz), 32.06, 29.64, 29.45, 29.33 ($J$ = 3.6 Hz), 29.13 ($J$ = 2.1 Hz), 22.84, 14.27. **HRMS** (ESI) *m*/*z* calculated for $C_9{}^{13}CH_{20}{}^+$ $(M)^+$ 141.1599, found 141.1598.

### *3.5.5 Synthesis of $^{13}$C-Labeled 1-Dodecene (ω-position)*

**1-(12-$^{13}$C)-Dodecene**

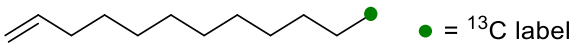


Magnesium turnings (1.08 g, 44.4 mmol) were charged into a 250 mL 3-neck round bottom flask equipped with a Teflon-coated stir bar, reflux condenser, nitrogen inlet, and rubber septum inlet. A small portion of 11-chloro-1-undecene (7.0 mL, 37.0 mmol) in dry $Et_2O$ (37 mL) was canula transferred onto the magnesium with vigorous stirring. A few drops of 1,2-dibromoethane were added to promote Grignard initiation. The rest of the $Et_2O$ solution was canula transferred into the round bottom flask and

refluxed for 15 hours. A small aliquot was removed from the reaction mixture, quenched with water, and analyzed by $^{1}H$ NMR and GC-MS to confirm complete formation of Grignard (via absence of 11-chloro-1-undecene). The reaction mixture was cooled to 22 °C and transferred via canula to a fresh 250 mL Schlenk flask under nitrogen. The reaction mixture was cooled to 0 °C, followed by syringe addition of $^{13}CH_3I$ (3.0 mL, 48.1 mmol). Then, careful addition of CuI (0.7 g, 3.7 mmol) as a solid (exothermic reaction) resulted in an immediate color change to dark brown/black. The reaction was warmed to room temperature and stirred for 1 hour. The reaction was quenched with water (40 mL) at 0 °C. The organic layer was separated and the aqueous layer was extracted with hexanes (3 x 30 mL). All organics were combined, washed with brine (1 x 80 mL), dried over $MgSO_4$, filtered, and concentrated. GC-MS analysis displayed minor impurities including 11-iodo-1-undecene. For purification, the resulting mixture was filtered through a short plug of silica (hexanes as eluent), dried in vacuo, redissolved in dry $Et_2O$ (30 mL), and stirred over a slight excess of magnesium turnings for 20 hours. The reaction mixture was quenched with water (30 mL) at 0 °C. Organics were separated and the aqueous layer extracted with hexanes (3 x 30 mL). The organics were combined, dried over MgSO4, filtered over a pad of Celite®, and concentrated in vacuo to afford the desired product as a colorless oil (42%). **$^{1}$H NMR** ($CDCl_3$, 500 MHz): δ 5.82 (m, 1H), 4.96 (m, 2H), 2.04 (m, 2H), 1.38 (m, 2H), 1.26 (m, 14H), 0.88 (dt, $J_{CH}$ = 125 Hz). **$^{13}$C{$^{1}$H} NMR** ($CDCl_3$, 125 MHz): δ 139.43, 114.22, 33.99, 32.08, 29.79, 29.68, 29.50 ($J$ = 4.0 Hz), 29.33, 29.12, 22.85 ($J_{CC}$ = 34.8 Hz), 22.82, 22.71, 14.27 ($^{13}$C label). **HRMS** (ESI) *m*/*z* calculated for $C_{11}{}^{13}CH_{22}{}^{+}$ $(M)^{+}$ 169.1913, found 169.1912.

### *3.5.6 General Procedure for the Polymerization of $^{13}C$-labeled and Unlabeled α-Olefins*

All reactions (aside from the 1.0 M concentration experiment) were performed in a 60 mL Fisher Porter tube (FPT) equipped with a magnetic stir bar and a Swagelock reactor head with a gas inlet and a rubber septum inlet for syringe injection. PMAO-IP (200 eq, 1.0 mmol) was charged into the FPT, followed by addition of PhCl and the appropriate α-olefin (300 eq, 1.49 mmol) via syringe. The reactor was sealed, and appropriate complex (1.0 eq, 5.0 μmol) was weighed into a 20 mL scintillation vial and dissolved in PhCl (2 mL). The complex solution was drawn into a gas tight syringe equipped with a stainless-steel needle which was sealed at the tip with a rubber septum. All materials were removed from the glovebox and the FPT placed into the appropriate bath for temperature regulation (cooling bath for 0 °C, water bath for 22 °C, oil bath for 50 °C). A nitrogen overpressure of ~ 1.0 atm was then charged into the reactor. After 15 minutes of stirring, the complex solution was directly injected into the FPT under positive pressure, sealed and allowed to stir for the appropriate time. Upon completion, the polymerization was quenched with a syringe injection of methanol (~2 mL), followed by precipitation into a 5% methanol/hydrochloric acid solution (~150 mL). The precipitated polymer was stirred for at least 3 hour, filtered over a Buchner funnel, washed with methanol, collected in a 20 mL scintillation vial and dried in vacuo until the sample was constant weight.

### 3.5.7 *General Procedure for the High Concentration Polymerization of $^{13}C$-Labeled and Unlabeled 1-Dodecene*

A 20 mL scintillation vial equipped with a Teflon-coated stir bar was charged with PMAO-IP (200 eq, 1.0 mmol) and appropriate α-olefin (300 eq, 1.49 mmol) inside a glove box. A separate 4 mL scintillation vial was charged with appropriate nickel complex (1.0 eq, 5.0 μmol) and dissolved in PhCl (1.18 mL). The slurry was injected via syringe directly into the 4 mL vial, sealed with a Teflon-lined cap and removed from the glovebox and stirred for the appropriate time. Upon completion, the reaction mixture was quenched with 1 mL of methanol and immediately poured into a solution of 5% methanol/hydrochloric acid and stirred for at least 3 hours. The resulting polymer was filtered over a Buchner funnel, washed with methanol, collected in a 20 mL scintillation vial, and dried in vacuo until constant weight.

### 3.5.8 *$^{13}C$ NMR Spectroscopy Signal Assignments*

All signals were assigned according to DEPT-135 analysis and various reports from the literature.[7,16e,17,18,29] Chemical shift values were normalized to the linear polyethylene signal $\delta^+$ at 29.19 ppm. A commonly used naming convention described in the literature for naming carbon signals originally developed by Usami and Takayama is listed below for comparison to our naming convention, albeit the sequence convention

is omitted. Our convention describes both the specific carbon and its proximity to other branches.

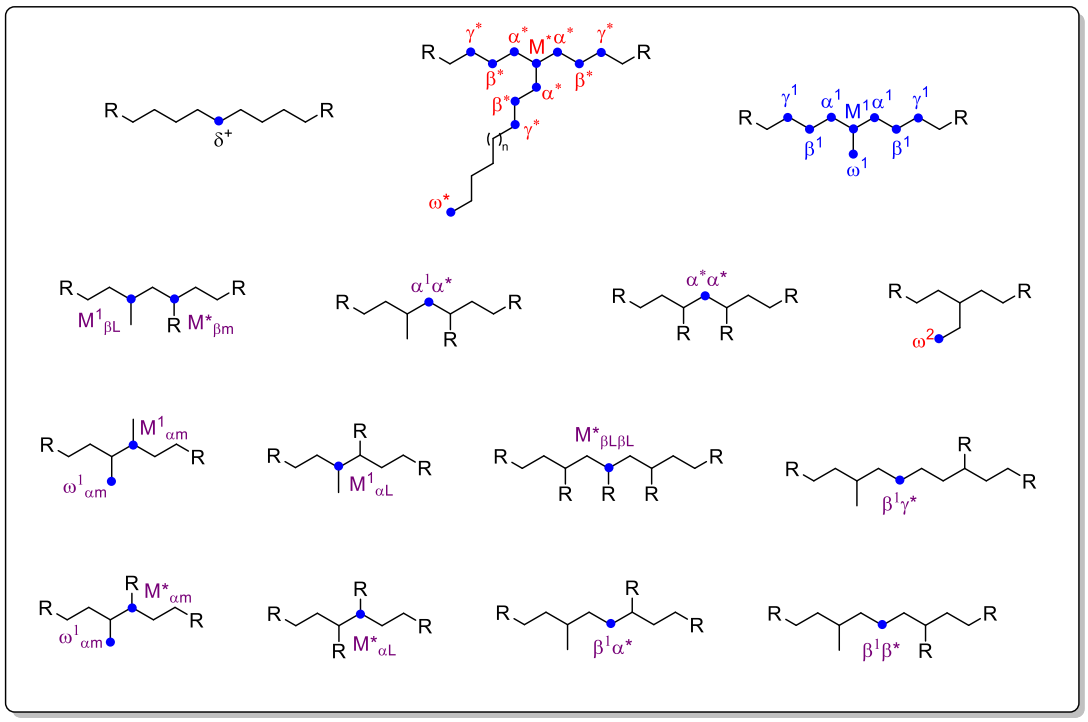


**Figure 3.11** Examples of polymer structures and their corresponding signal assignments. R indicates alkyl chain.

**Table 3.22** $^{13}$C NMR Signal Assignments for all Observable Structures

| Peak Number | Chemical Shift (ppm) | Assignment ($xB_n$) | Assignment ($M^1{}_{\alpha L}$) | $^{13}$C-Labeled Monomer | Reference |
|---|---|---|---|---|---|
| **1** | 10.53 | $1B_2$ | $\omega^2$ | ω | 16e |
| **2** | 11.87+12.05 | $1B_x$ | $\omega^x$ | ω | This Work |
| **3** | 13.42 | $1B_4 + 1B_n$ | $\omega^4 + \omega^*$ | ω | 7, 16e |
| **4** | 13.94 | $1B_3$ | $\omega^3$ | ω | 16e |
| **5** | 14.39 | $1B_1$ | $\omega^1{}_{\alpha m}$-*rac* | ω | 17 |
| **6** | 15.01+15.15 | $1B_x$ | $\omega^x$ | ω | This Work |
| **7** | 15.53 | $1B_1$ | $\omega^1{}_{\alpha m}$-*meso* | ω | 17 |
| **8** | 15.66 | $1B_x$ | $\omega^?$ | ω | This Work |
| **9** | 16.22 | $1B_1$ | $\omega^1{}_{\alpha m}$-*meso* | ω | 17 |
| **10** | 19.32 | $1B_1$ | $\omega^1$ | ω | 7, 16e |
| **11** | 19.81 | $1B_1$ | $\omega^1{}_{\beta L}$ | ω | 16e |
| **12** | 22.11 | $2B_n$ | $2^*$ | n/a | 7, 16e |
| **13** | 23.77+23.94 | $\beta\beta B_n$ | $\beta^1\beta^*$ or $\beta^*\beta^*$ | C2 | 16e |
| **14** | 24.99+25.18 | $\beta B_2$ | $\beta^2$ | C2 | 29 |
| **15** | 26.50 | $\beta B_{2\text{-}n}$ | $\beta^*$ | ω, C2 | 7, 16e |
| **16** | 26.64 | $\beta B_1$ | $\beta^1$ | ω, C2 | 7, 16e |
| **17** | 26.78 | $\beta B_x$ | $\beta^x$ | ω | – |
| **18** | 27.10-28.11 | $\beta B_x$ | $\beta^1\gamma^*$ or $\beta^*\gamma^*$ | ω, C2 | 17 |
| **19** | 27.50 | $brB_{1\text{-}n}$ | $M^x$ | C2 | 18 |
| **20** | 28.79 | $4B_n$ | $4^*$ | n/a | 7, 16e |
| **21** | 29.19 | $\delta B_{1\text{-}n}$ | $\delta^+$ | ω, C2 | 7, 16e, 17, 18 |
| **22** | 29.58 | $\gamma B_1$ | $\gamma^1$ | n/a | 7, 16e |
| **23** | 29.68 | $\gamma B_n$ | $\gamma^*$ | ω, C2 | 7, 16e |
| **24** | 30.19+30.59 | $brB_1$ | $M^1{}_{\beta L}$ | C2 | 18 |
| **25** | 30.99 | $\alpha B_1$ | $\alpha^*{}_{\beta m}$ | ω, C2 | 16e |
| **26** | 31.43 | $3B_n$ | $3^*$ | n/a | 7, 16e |
| **27** | 32.47 | $brB_1$ | $M^1$ | C2 | 7, 16e |
| **28** | 32.89 | $brB_n$ or $brB_1$ | $M^*{}_{\beta L\beta L}$ or $M^*{}_{\beta m\beta L}$ or $M^1{}_{\gamma L}$ | C2 | 16e, 18 |
| **29** | 33.32 | – | – | ω | – |
| **30** | 33.79 | $\alpha B_n$ | $\alpha^*$ | ω, C2 | 7, 16e |
| **31** | 33.89–34.39 | $\alpha B_{1\text{-}n}$ | $\alpha^x$ | ω | – |
| **32** | 34.82 | $brB_1$ | $M^1{}_{\alpha m}$ | C2 | This Work |
| **33** | 35.05 | $brB_n$ | $M^*{}_{\beta m}$ or $M^*{}_{\beta L}$ | C2 | 18 |
| **34** | 36.61 | $brB_1$ | $M^1{}_{\alpha L}$ | C2 | 18 |
| **35** | 36.77 | $\alpha B_1$ | $\alpha^1$ | ω | 7, 16e |
| **36** | 37.25 | $\alpha\alpha B_n$ | $\alpha^*\alpha^*$ | ω | 16e |
| **37** | 37.41 | $brB_n$ | $M^*$ | ω, C2 | 7, 16e |
| **38** | 39.34–40.37 | $brB_n$ | $M^*{}_{\alpha L}$ | C2 | 18 |
| **39** | 42.23 | $\alpha\alpha B_{1+n}$ | $\alpha^*\alpha^1$ | ω | 18 |
| **40** | 42.36 | $brB_n$ | $M^*{}_{\alpha m}$ | ω, C2 | 18 |

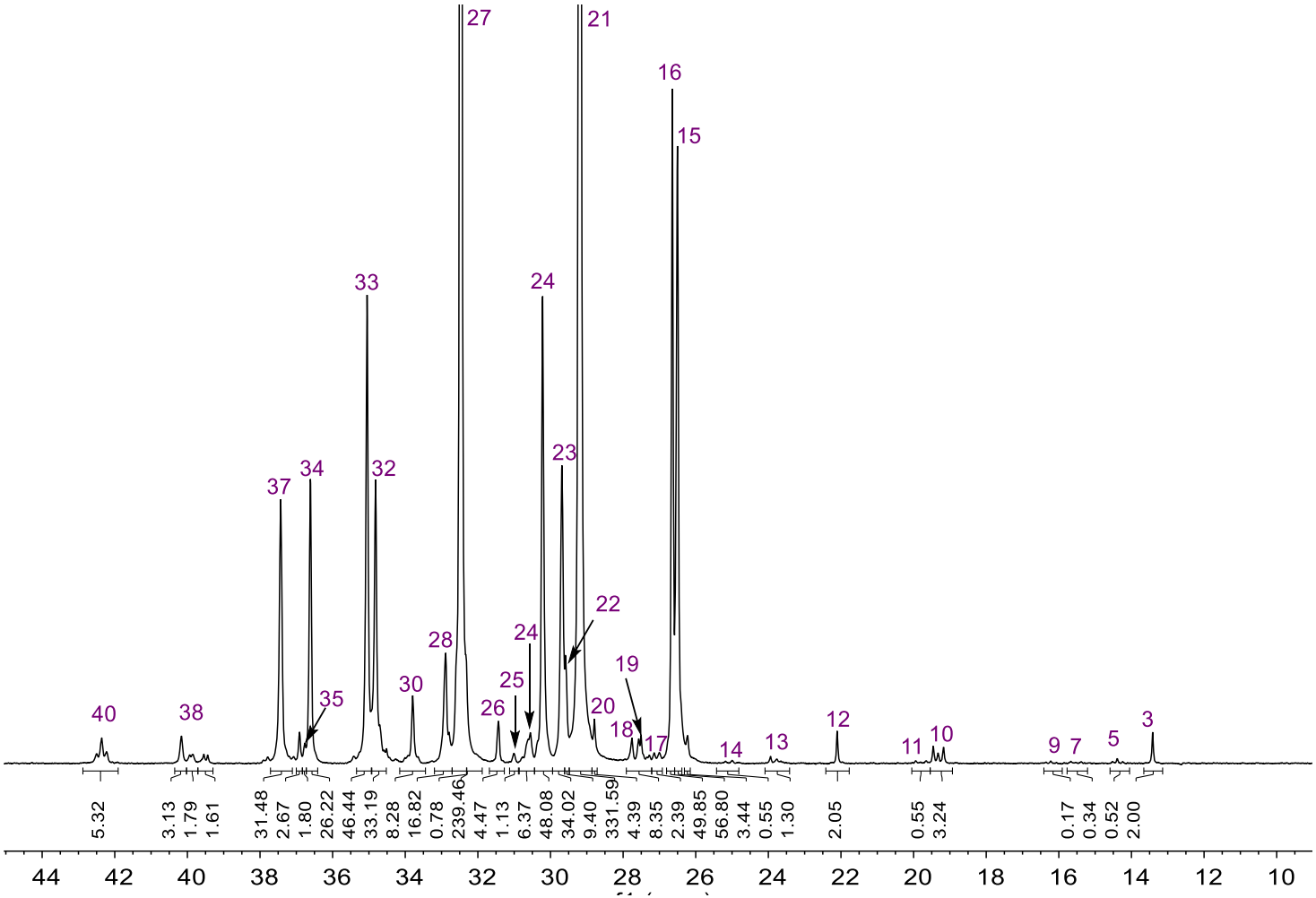


**Figure 3.12** $^{13}$C NMR signal assignments for sample $2_v$: C2-labeled poly(1-decene) from complex **1d**.

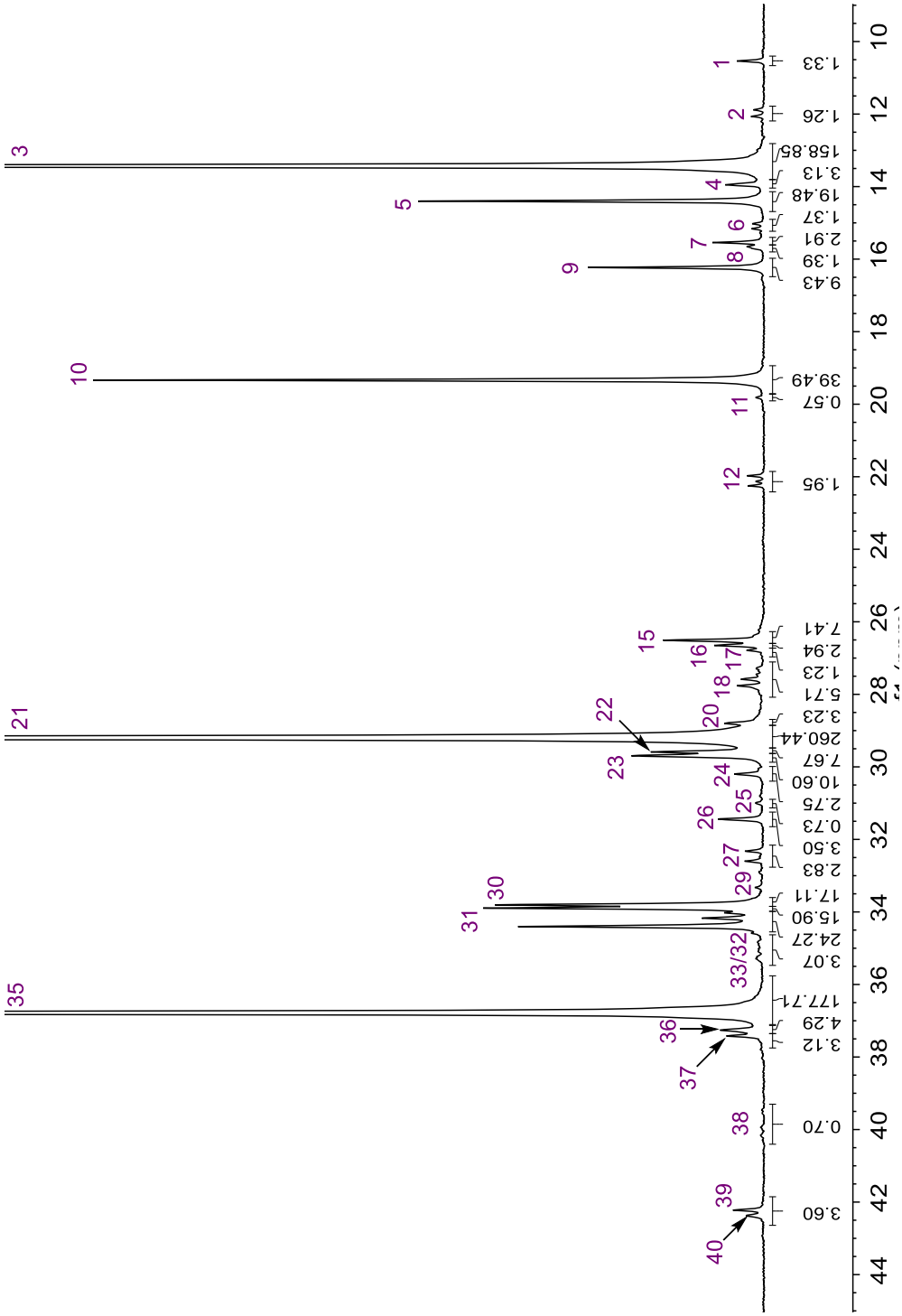

**Figure 3.13** $^{13}$C NMR signal assignments for sample $\omega_{ix}$: ω-labeled poly(1-dodecene) from complex **1d**.

## *3.6 Derivation of the Mechanistic Model*

### *3.6.1 C2-Labeled Monomer*

#### *3.6.1.1 Pathways that Cannot be Distinguished*

There are a few signals that arise from multiple pathways that cannot be distinguished. Scheme 3.10 shows the relevant pathways for multiple long branches in a row. It should be noted that **M*$_{\beta m}$** and **M*$_{\beta L}$** cannot be distinguished in the $^{13}$C NMR spectra due to identical chemical shifts. Likewise, **M*$_{\beta m\beta L}$** and **M*$_{\beta L\beta L}$** also cannot be distinguished from each other or from **M$^{1}_{\gamma L}$**. The latter signal can only arise from pathway B followed by a very specific chain walk and pathway E. This sequence of events seems highly improbable, and thus **M$^{1}_{\gamma L}$** is ignored in this analysis.

Due to our assumption that chain-walking is fast relative to insertion and that primary insertions occur more readily than secondary insertions, it seems unlikely that the sequences shown in Scheme 3.10A and B would occur. There is no driving force for the complex to continuously chain isomerize to the same secondary position before the next insertion. The pathways shown in Scheme 3.10C and D, on the other hand, generate signals through primary and penultimate insertion events which are more likely. Because **M*$_{\beta L}$(H) (**Scheme 3.10D) is only produced by the specific sequence C–H–G (as opposed to C–H–H or similar), it was deemed less likely than pathway B followed by pathway H (Scheme 3.10C). Therefore, we have assigned **M*$_{\beta m}$** and **M*$_{\beta L}$** to pathway B and **M*$_{\beta m\beta L}$** and **M*$_{\beta L\beta L}$** to pathway H. From the analysis derived from using the ω-labeled monomer, we do know that C–H–G (Scheme 3.10D) occurs even though we cannot correct for it. The error propagation of putting too much **M*$_{\beta L}$** into pathway

B and not enough into pathway H is a slight overestimation of **β*(C)** and a slight underestimation of **β*(E)**.

**Scheme 3.10** Pathway Sequences that Give Component Signals that Cannot be Differentiated for the C2-Labeled Monomer

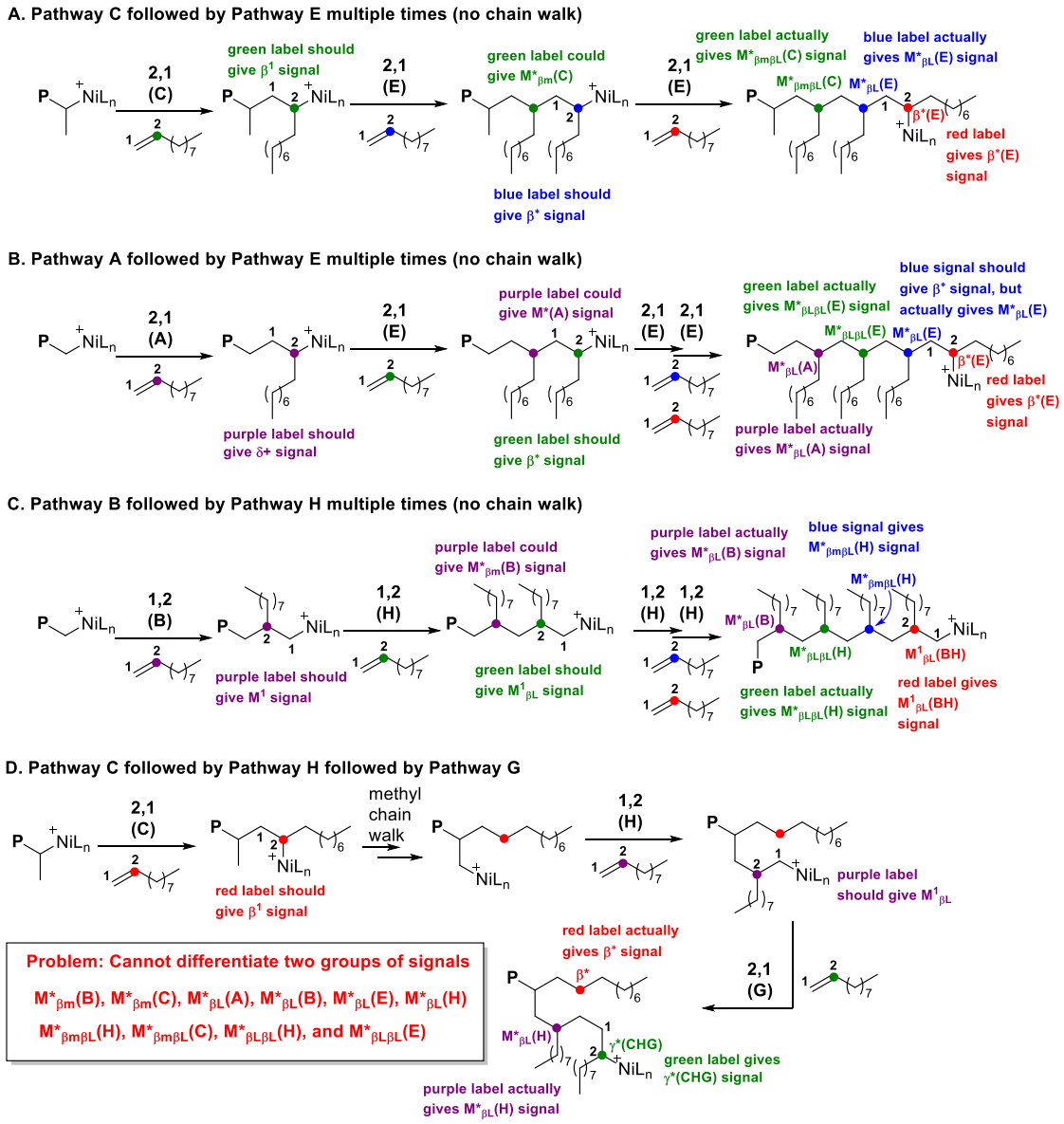


Scheme 3.11 shows three different pathways that can give $\mathbf{M^1_{\alpha L}}$. Scheme 3.11A is unlikely because it requires a secondary insertion next to a sterically congested

tertiary center. Scheme 3.11B and C, however, are both viable routes to $\mathbf{M^1_{\alpha L}}$. Pathway D followed by pathway G (Scheme 3.11B) is two steps but invokes energetically favorable primary and penultimate insertion events. Pathway F (Scheme 3.11C) accesses the signal in one step, but requires a 1,2 insertion from a secondary position which is energetically unfavorable. For this case, we decided to split the integration from the $\mathbf{M^1_{\alpha L}}$ signal evenly between pathway D and F, as shown in eqs (3.33) and (3.34). We recognize that error is inherently introduced from this assumption, but the relatively low integration of this, especially in competent chain straightening catalysts, means it will not significantly affect the calculations of the overall insertion pathways. For example, if the D:F split is instead set to 80:20, the ending pathways change up to 0.1% for **1a** and 0.6% for **1d**.

$$M^1_{\alpha L} = M^1_{\alpha L}(D) + M^1_{\alpha L}(F) \tag{3.32}$$

$$M^1_{\alpha L}(D) = \tfrac{1}{2}\, M^1_{\alpha L} \tag{3.33}$$

$$M^1_{\alpha L}(F) = \tfrac{1}{2}\, M^1_{\alpha L} \tag{3.34}$$

**Scheme 3.11** Pathways that Give $M^1{}_{\alpha L}$ Signal

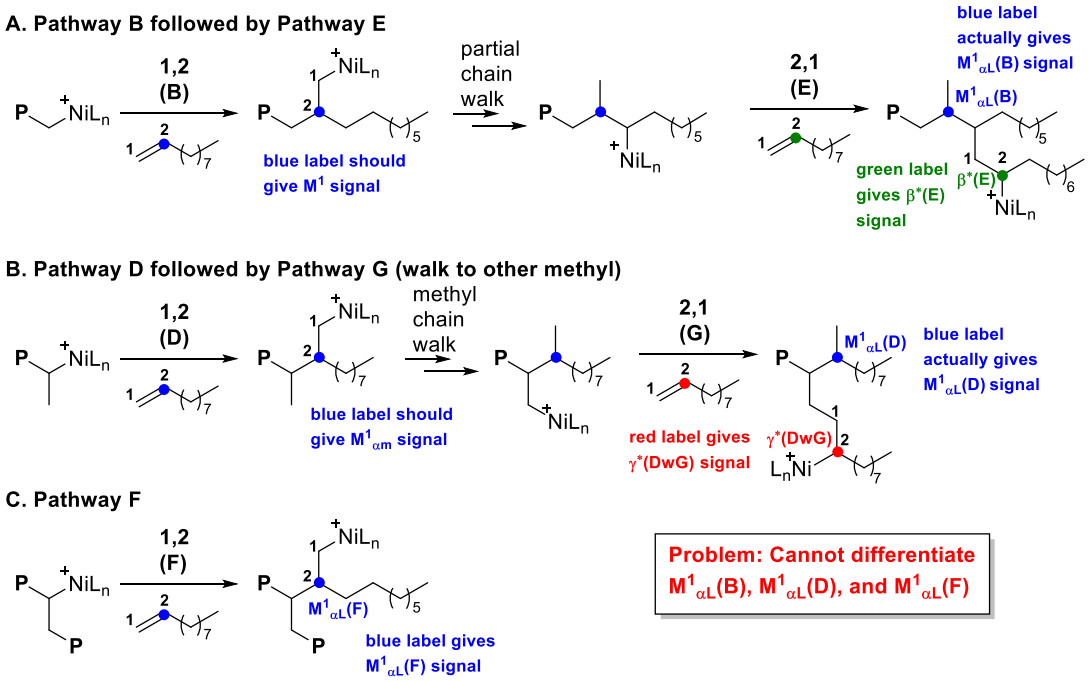


### *3.6.1.2 Derivation of Component Signals*

Since the same signal can arise from multiple pathways, a few signals were broken down into multiple components that contribute to different mechanistic pathways. For signals that have multiple components, parentheses are added after the position label to denote to which pathway that component contributes. For example, **β*(A)** denotes a **β*** signal derived from pathway A, whereas **β*(E)** denotes a **β*** signal derived from pathway E.

Scheme 3.12 shows one example of pathway A followed by E to give rise to **M***, **α***, **β***, and **γ*** signals. We assume that chain walking can equilibrate before the next insertion, such that it is equally likely for 2° insertion to occur off any backbone carbon distant from branching defects. Following this assumption, the **α***, **β*(A)**, and **γ*(A)** signals should be equivalent due to 2° insertion being equally likely 1, 2, or 3

carbons away from a label. Each of these insertion events should be twice as likely as 2° insertion from the labeled carbon itself, which would afford an **M*** signal. This is summarized in eq (3.35) below.

**Scheme 3.12** A Common Pathway Sequence that Gives Component Signals for C2-Labeled Monomer

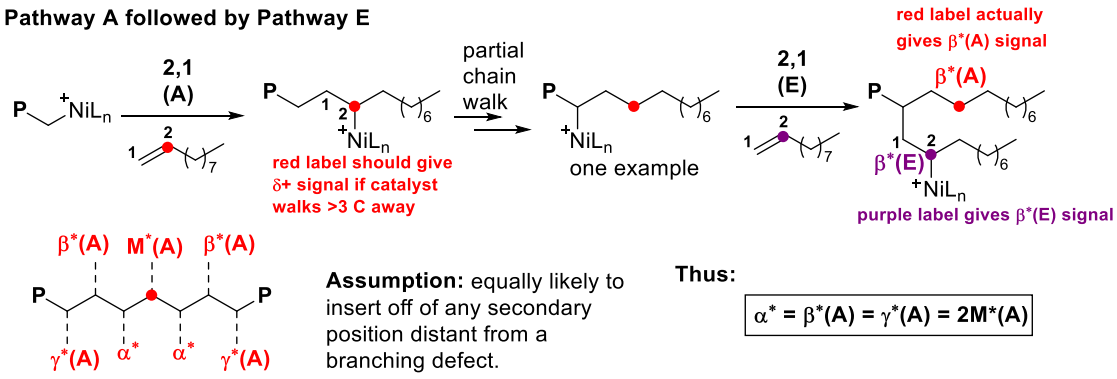


The other relevant pathways involve performing primary insertion off a methyl group instead of the end of the chain (pathways G and H). These convert a methyl branch into an alkyl branch. In the case of the **γ*** components, the sequence of pathways that originate each component is relevant when calculating the correction factors, which is denoted in the parentheses (e.g., **γ*(BG)** indicates **γ*** arising from pathway B followed by pathway G and contributes to G; **β*(C[G])** indicates **β*** arising from pathway C followed by pathway G but contributes to C).

The relevant sequences for pathway G are shown in Scheme 3.13. Scheme 3.13A shows pathway B followed by G with no chain walking. The label from pathway B that would normally give an $\mathbf{M^1}$ signal actually contributes to **M*** and the label from pathway G will contribute to **γ*(BG)**, described in eq (3.36). Scheme 3.13B shows

pathway C followed by chain walking to the 1° position of the methyl then pathway G. This results in the label from pathway C giving a **β*** signal (instead of $\boldsymbol{\beta^1}$) and a **γ*(CG)** signal from pathway G (eq (3.37)). Scheme 3.13C shows pathway D followed by G with no chain walking (similar to Scheme 3.13A), such that the signal from pathway D that would normally give an $\mathbf{M^1_{\alpha m}}$ signal actually contributes to $\mathbf{M^*_{\alpha m}}$ and the label from pathway G will contribute to **γ*(DG)** (eq (3.38)). Scheme 3.13D shows pathway D followed by chain walking from one methyl branch to the other, followed by pathway G, such that the signal from pathway D that would normally give an $\mathbf{M^1_{\alpha m}}$ signal actually contributes to $\mathbf{M^1_{\alpha L}(D)}$ and the γ* signal is labeled **γ*(DwG)** (eq (3.39)) for "pathway D, walk, pathway G" to differentiate it from **γ*(DG)** from Scheme 3.13C. Scheme 3.13E shows pathway F followed by pathway G with no chain walking, such that the signal from pathway F that would normally give an $\mathbf{M^1_{\alpha L}}$ signal actually contributes to $\mathbf{M^*_{\alpha L}}$ and the label from pathway G contributes to **γ*(FG)** (eq (3.40)).

**Scheme 3.13** Pathway G Sequences that Give Component Signals for C2-Labeled Monomer

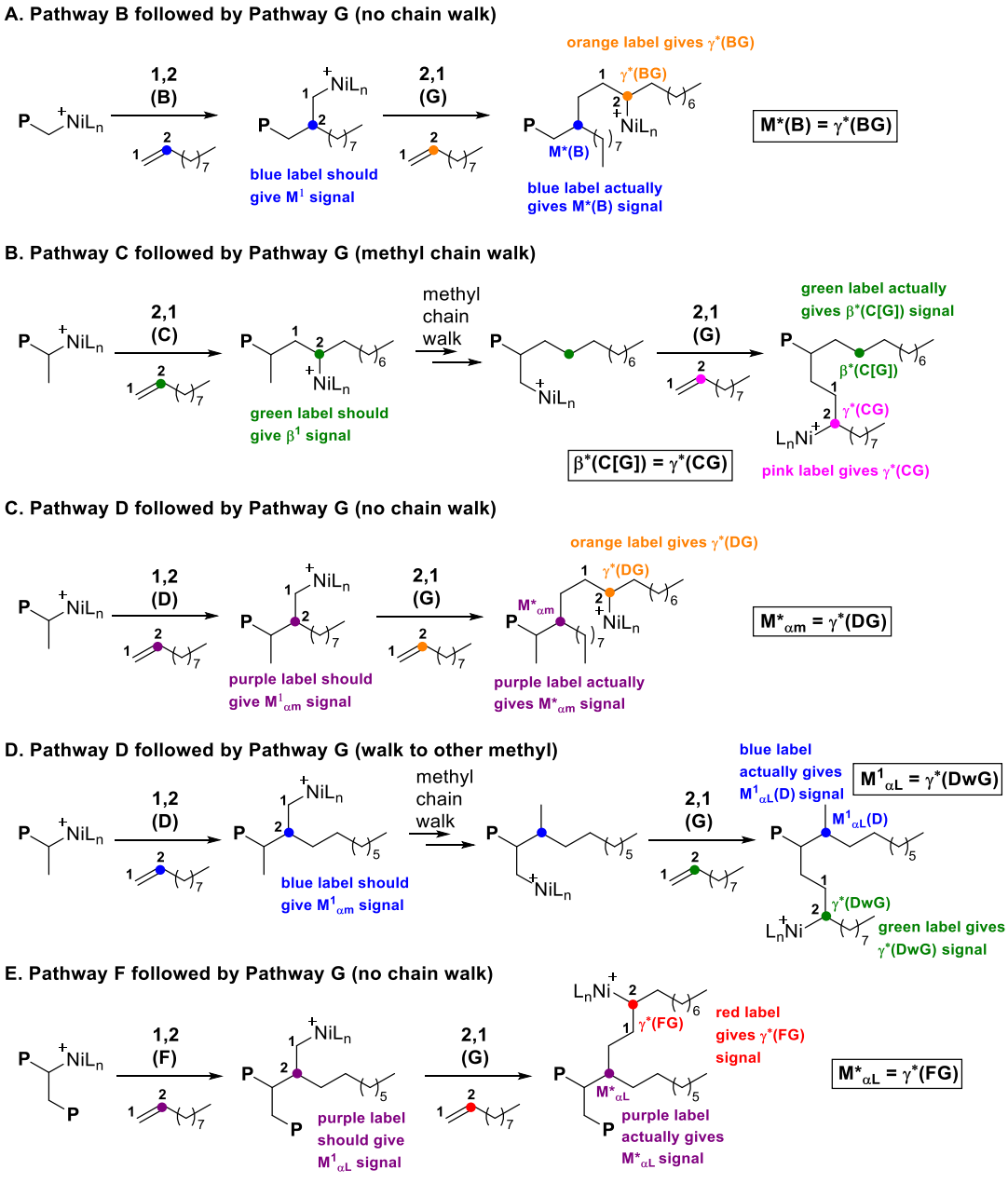


The relevant sequences for pathway H are shown in Scheme 3.14. Pathway H always gives the $\mathbf{M^1_{\beta L}}$ signal if only done once, but components are needed to calculate other correction factors. Whenever pathway H follows pathway B (Scheme 3.14A and

B), the signal from pathway B, which would normally give $\mathbf{M^1}$, actually contributes to $\mathbf{M^*_{\beta m}} + \mathbf{M^*_{\beta L}}$. This is reflected in eq (3.41). Scheme 3.14C shows pathway C followed by pathway H to give $\mathbf{M^1_{\beta L}}$ and **β*(C[H])**, as shown in eq (3.42). We do not observe any evidence of pathway H occurring off methyls from pathway D or F.

**Scheme 3.14** Pathway H Sequences that Give Component Signals for C2-Labeled Monomer

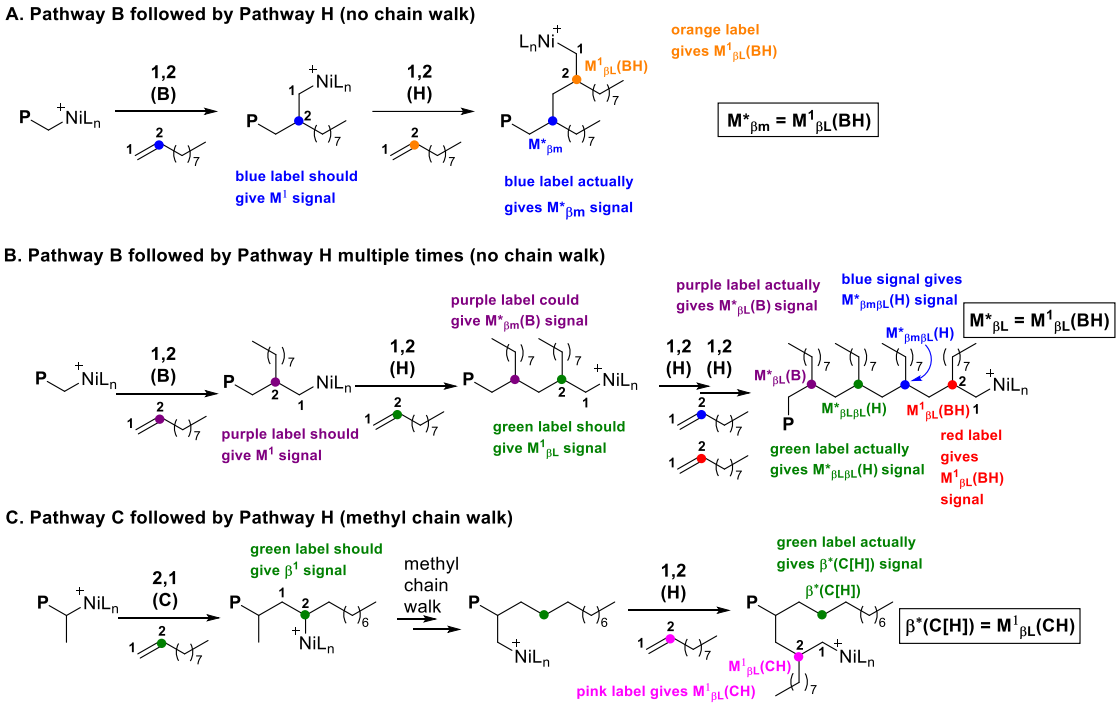


With these insertion pathways laid out, we can derive the following starting equations below, where symbols followed by parentheses are the various components described above and symbols without parentheses are the actual integration of the $^{13}C$ NMR signal observed (Note eq (3.47) is a simplified version of eq (3.46) since most **γ*** components contribute to pathway G):

$$\alpha^* = \beta^*(A) = \gamma^*(A) = 2M^*(A) \qquad (3.35)$$

$$M^*(B) = \gamma^*(BG) \tag{3.36}$$

$$\beta^*(C[G]) = \gamma^*(CG) \tag{3.37}$$

$$M^*_{\alpha m} = \gamma^*(DG) \tag{3.38}$$

$$M^1_{\alpha L}(D) = \gamma^*(DwG) \tag{3.39}$$

$$M^*_{\alpha L} = \gamma^*(FG) \tag{3.40}$$

$$M^1_{\beta L}(BH) = M^*_{\beta m} + M^*_{\beta L} \tag{3.41}$$

$$M^1_{\beta L}(CH) = \beta^*(C[H]) \tag{3.42}$$

$$M^* = M^*(A) + M^*(B) \tag{3.43}$$

$$M^1_{\beta L} = M^1_{\beta L}(BH) + M^1_{\beta L}(CH) \tag{3.44}$$

$$\beta^* = \beta^*(A) + \beta^*(C[G]) + \beta^*(C[H]) + \beta^*(E) \tag{3.45}$$

$$\gamma^* = \gamma^*(A) + \gamma^*(BG) + \gamma^*(CG) + \gamma^*(DG) + \gamma^*(DwG) + \gamma^*(FG) \tag{3.46}$$

$$\gamma^* = \gamma^*(A) + \gamma^*(G) \tag{3.47}$$

Because **α*** is the only signal that has a single component, the integration of that signal was assumed to be the "actual" value. *All correction factors are based on this assumption.* The **M*** components were calculated from eqs (3.35) and (3.43):

$$M^*(A) = \tfrac{1}{2}\alpha^* \tag{3.48}$$

$$M^*(B) = M^* - \tfrac{1}{2}\alpha^* \tag{3.49}$$

Even though the $\mathbf{M^1_{\beta L}}$ signal only contributes to pathway H, the components are necessary for the calculation of other correction factors. The $\mathbf{M^1_{\beta L}}$ components were calculated from eqs (3.41) and (3.44):

$$M^1_{\beta L}(BH) = M^*_{\beta m} + M^*_{\beta L} \quad (3.50)$$

$$M^1_{\beta L}(CH) = M^1_{\beta L} - M^1_{\beta L}(BH) = M^1_{\beta L} - M^*_{\beta m} - M^*_{\beta L} \quad (3.51)$$

Similarly, even though the **γ*** signal only contributes to pathways A and G, the individual components are necessary for the calculation of other correction factors. The **γ*(A)** component was taken from eq (3.35), shown in eq (3.52). The total **γ*(G)** component is found from eqs (3.47) and (3.52), shown below in eq (3.53). The **γ*(BG)** component was found by substituting eq (3.50) into eq (3.36), shown in eq (3.54). The **γ*(DG)** component was taken from eq (3.38), shown in eq (3.55). The **γ*(DwG)** component was taken from eqs (3.33) and (3.39), shown in eq (3.56). The **γ*(FG)** component was taken from eq (3.40), shown in eq (3.57).

$$\gamma^*(A) = \alpha^* \quad (3.52)$$

$$\gamma^*(G) = \gamma^* - \gamma^*(A) = \gamma^* - \alpha^* \quad (3.53)$$

$$\gamma^*(BG) = M^*(B) = M^* - \tfrac{1}{2}\alpha^* \quad (3.54)$$

$$\gamma^*(DG) = M^*_{\alpha m} \quad (3.55)$$

$$\gamma^*(DwG) = M^1_{\alpha L}(D) = \tfrac{1}{2} M^1_{\alpha L} \quad (3.56)$$

$$\gamma^*(FG) = M^*_{\alpha L} \quad (3.57)$$

For the **γ*(CG)** component: eq (3.46) was rearranged to give eq (3.58). Substituting in from eqs (3.52), (3.54), (3.55), (3.56), and (3.57) gives eq (3.59), which simplifies to eq (3.60).

$$\gamma^*(CG) = \gamma^* - \gamma^*(A) - \gamma^*(BG) - \gamma^*(DG) - \gamma^*(DwG) - \gamma^*(FG) \quad (3.58)$$

$$\gamma^*(CG) = \gamma^* - \alpha^* - (M^* - \tfrac{1}{2}\alpha^*) - M^*_{\alpha m} - \tfrac{1}{2}M^1_{\alpha L} - M^*_{\alpha L} \quad (3.59)$$

$$\gamma^*(CG) = \gamma^* - M^* - \tfrac{1}{2}\alpha^* - M^*_{\alpha m} - \tfrac{1}{2}M^1_{\alpha L} - M^*_{\alpha L} \quad (3.60)$$

The **β*(A)** component was taken from eq (3.35), shown in eq (3.61). The **β*(C[G])** component was found by substituting eq (3.60) into eq (3.37), shown in eq (3.62). The **β*(C[H])** component was found by substituting eq (3.51) into eq (3.42), shown in eq (3.63). The total **β*(C)** contribution is shown in eq (3.64).

$$\beta^*(A) = \alpha^* \quad (3.61)$$

$$\beta^*(C[G]) = \gamma^*(CG) = \gamma^* - M^* - \tfrac{1}{2}\alpha^* - M^*_{\alpha m} - \tfrac{1}{2}M^1_{\alpha L} - M^*_{\alpha L} \quad (3.62)$$

$$\beta^*(C[H]) = M^1_{\beta L}(CH) = M^1_{\beta L} - M^*_{\beta m} - M^*_{\beta L} \quad (3.63)$$

$$\beta^*(C) = \gamma^* - M^* - \tfrac{1}{2}\alpha^* - M^*_{\alpha m} - \tfrac{1}{2}M^1_{\alpha L} - M^*_{\alpha L} + M^1_{\beta L} - M^*_{\beta m} - M^*_{\beta L} \quad (3.64)$$

For the **β*(E)** component: eq (3.45) was rearranged to give eq (3.65). Substituting in from eqs (3.61), (3.62), and (3.63) gives eq (3.66), which simplifies down to eq (3.67).

$$\beta^*(E) = \beta^* - \beta^*(A) - \beta^*(C[G]) - \beta^*(C[H]) \quad (3.65)$$

$$\beta^*(E) = \beta^* - \alpha^* - (\gamma^* - M^* - \tfrac{1}{2}\alpha^* - M^*_{\alpha m} - \tfrac{1}{2}M^1_{\alpha L} - M^*_{\alpha L}) - (M^1_{\beta L} - M^*_{\beta m} - M^*_{\beta L}) \quad (3.66)$$

$$\beta^*(E) = \beta^* - \gamma^* + M^* - \tfrac{1}{2}\alpha^* + M^*_{\alpha m} + \tfrac{1}{2}M^1_{\alpha L} + M^*_{\alpha L} - M^1_{\beta L} + M^*_{\beta m} + M^*_{\beta L} \quad (3.67)$$

### *3.6.1.3 Additional Signals from Consecutive Pathways*

We also observed additional minor signals that arise from very specific insertion events not previously considered in our analysis. Fortunately, since if there is only one sequence of pathways that can contribute to this signal, component signals do not need to be calculated. The new signal just needs to be added to the numerator of the appropriate pathway. Scheme 3.15 shows a sequence of insertion events that contribute to pathway C.

**Scheme 3.15** Pathway Sequence that Gives Additional Observed Signals that Must be Added in for the C2-Labeled Monomer

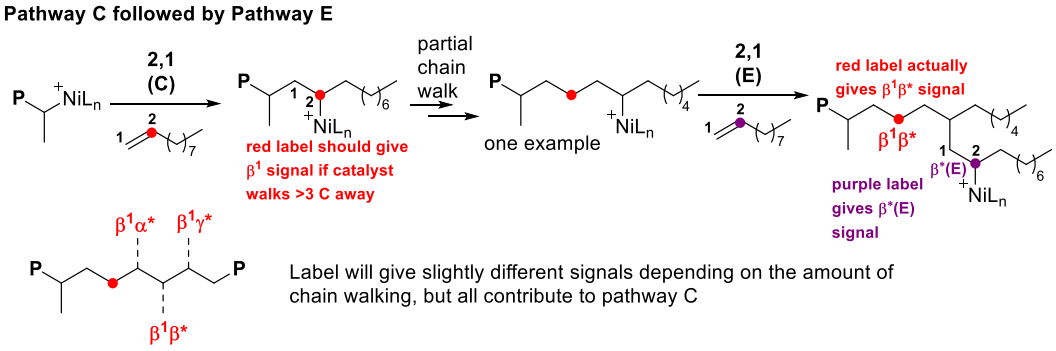

### *3.6.1.4 Summary of all Observed $^{13}C$ NMR Signals from C2-Labeled Monomer*

**Table 3.23** Summary of all Observed Signals and Corrections for Polymerization of the C2-Labeled Monomer

| Signal Label | Possible Pathways | Corrections |
|---|---|---|
| δ+ | A | |
| $M^1$ | B | |
| $\beta^1$ | C | |
| $M^1_{\alpha m}$ | D | |
| β* | A, C, E | β*(A) = α*,<br>β*(C) = γ* – M* – ½α* – $M^*_{\alpha m}$ – ½$M^1_{\alpha L}$ – $M^*_{\alpha L}$ + $M^1_{\beta L}$ – $M^*_{\beta m}$ – $M^*_{\beta L}$,<br>β*(E) = β* – γ* + M* – ½α* + $M^*_{\alpha m}$ + ½$M^1_{\alpha L}$ + $M^*_{\alpha L}$ – $M^1_{\beta L}$ + $M^*_{\beta m}$ + $M^*_{\beta L}$ |
| $M^1_{\alpha L}$ | B, D, F | Split the signal between D and F |
| $M^*_{\beta m}$ | B, C | All assigned to B |
| $M^*_{\beta L}$ | A, B, E, H | All assigned to B |
| $M^*_{\beta L \beta L}$ | E, H | All assigned to H |
| $M^*_{\beta m \beta L}$ | C, H | All assigned to H |
| $M^1_{\beta L}$ | H | |
| M* | A, B | M*(A) = ½α*, M*(B) = M* – ½α* |
| α* | A | |
| γ* | A, G | γ*(A) = α*, γ*(G) = γ* – α* |
| $M^*_{\alpha m}$ | D | |
| $M^*_{\alpha L}$ | F | |
| $\beta^1\alpha^*$ | C | |
| $\beta^1\beta^*$ | C | |
| $\beta^1\gamma^*$ | C | |

There were a few small signals in some $^{13}C$ NMR spectra that we were unable to assign. DEPT 135 was used to confirm that the signal at 27.50 ppm was from a methine and the signals at 24.99–25.18 and 26.23 ppm were from methylenes.

### *3.6.2 ω-Labeled Monomer*

#### *3.6.2.1 Pathways that Cannot be Distinguished*

There are a few signals that could arise from multiple pathways that cannot be distinguished. Scheme 3.16 shows sequences of pathways to **α*α*(B)** and **α*α*(C)**, which cannot be distinguished. The pathway sequence B–G–E (Scheme 3.16A) requires a highly specific chain walking event before the 2° insertion, but there is no obvious driving force for this to occur. The pathway sequence C–B–A (Scheme 3.16B) is more likely because it relies on the higher propensity for the complex to undergo 1° insertion off a methyl group over 2° insertion off the polymer backbone. In this situation, it is more likely that the complex would walk away and then return to the primary position before the next insertion. So, the entirety of the **α*α*** signal was assigned to pathway C.

Scheme 3.17 shows sequences of pathways to $\boldsymbol{\omega^{1}_{\alpha L}}$**(C)** and $\boldsymbol{\omega^{1}_{\alpha L}}$**(D)** that cannot be differentiated. Again, using our standard assumption that 1° insertion off a methyl branch is much more likely than 2° insertion, we attributed the entirety of the $\boldsymbol{\omega^{1}_{\alpha L}}$ signal to pathway D.

**Scheme 3.16** Pathway Sequences that Give α*α* Signals that Cannot be Differentiated for the ω-Labeled Monomer

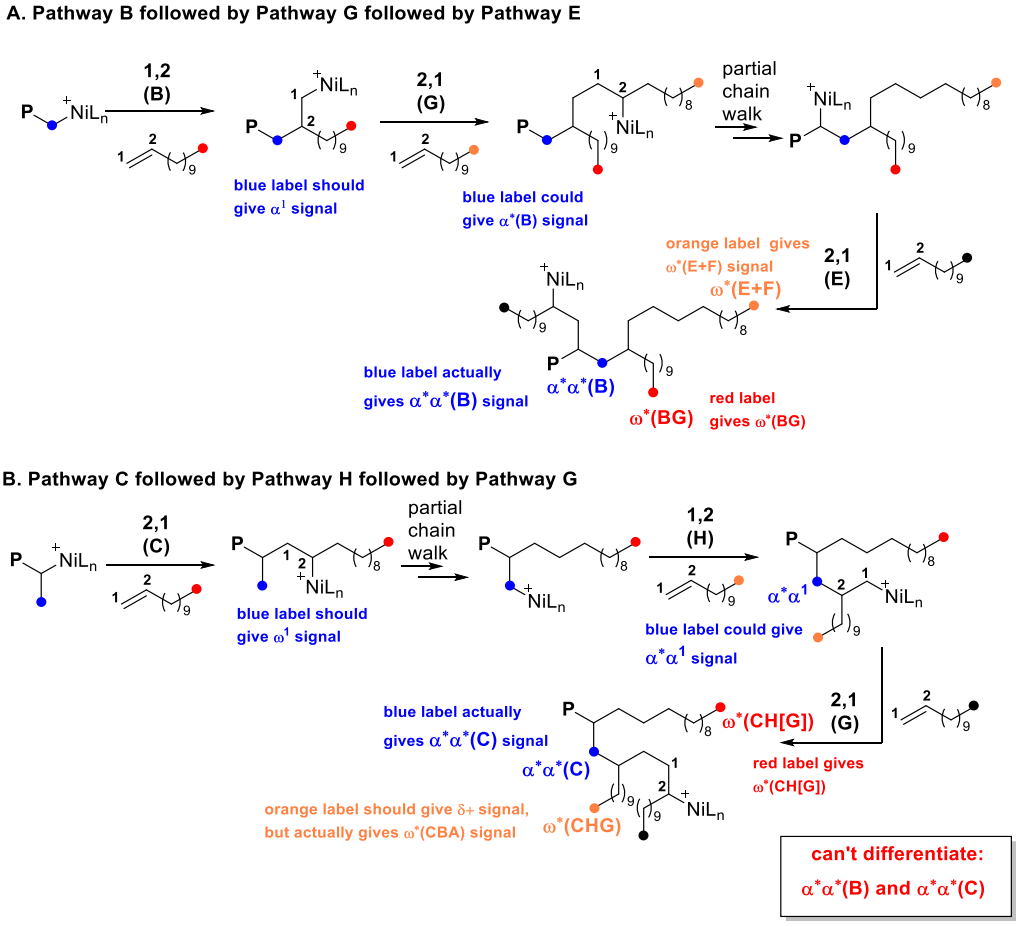


**Scheme 3.17** Pathway Sequences that Give $\omega^{1}{}_{\alpha l}$ Signals that Cannot be Differentiated for the ω-Labeled Monomer

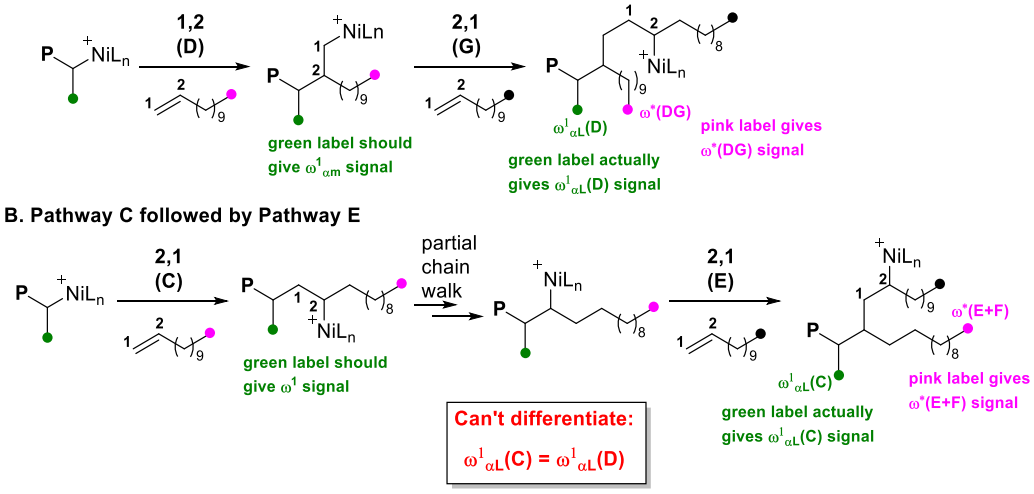

### *3.6.2.2 Derivation of Component Signals*

Since the same signal can arise from multiple pathways, a few signals were broken down into multiple components that contribute to different mechanistic pathways. For signals that have multiple components, parentheses are added after the position label to denote to which pathway that component contributes.

Scheme 3.18 shows one example of pathway A followed by E to give rise to **M***, **α***, **β***, and **γ*** signals. We assume that chain walking can equilibrate before the next insertion, such that it is equally likely for 2° insertion to occur at any backbone carbon far from any branching defects. Following this assumption, the **α*(A)**, **β***, and **γ*** signals should be equivalent due to 2° insertion being equally likely 1, 2, or 3 carbons away from a label. Each of these insertions should be twice as likely as 2° insertion from the labeled carbon itself, which would give rise to an **M*** signal. This is summarized in eq (3.68), below.

**Scheme 3.18** A Common Pathway Sequence that Gives Component Signals for the ω-Labeled Monomer

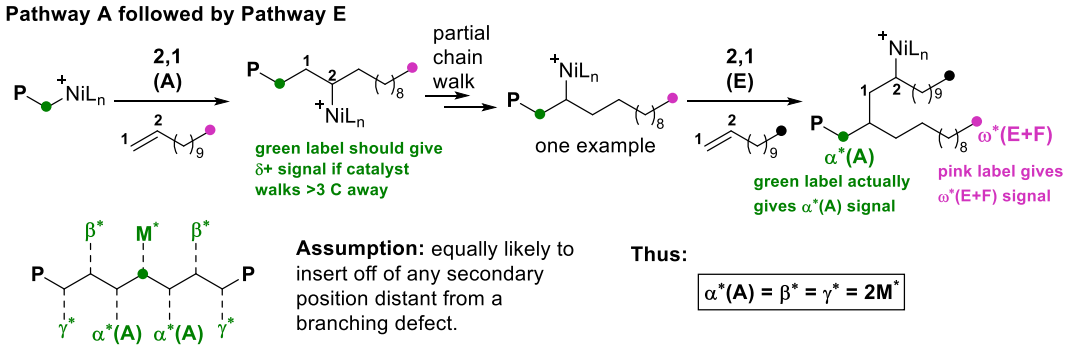


The relevant sequences for pathway G are shown in Scheme 3.19. Scheme 3.19A shows pathway B followed by pathway G with no chain walking. The label from

pathway B that would normally give an $\boldsymbol{\alpha^1}$ signal actually contributes to **α*(B)** and the label from pathway G will contribute to **ω*(BG)**¸ as shown in eq (3.69). Scheme 3.19B shows pathway C followed by chain walking to the 1° position of the methyl branch then pathway G. This sequence results in the label from pathway C giving an **α*(C)** signal (instead of $\boldsymbol{\omega^1}$) and a **ω*(CG)** signal from pathway G (eq (3.70), below).

Unfortunately, a variety of pathways were not able to be corrected for because of the limitations of the ω-labeled monomer. We understand by not correcting for these factors, too much of the **ω*** signal is attributed to pathway (E+F) and not enough to pathway G. **ω*(DG)** (Scheme 3.19C) cannot be corrected for because $\boldsymbol{\omega^1_{\alpha L}}$ cannot be distinguished from $\boldsymbol{\omega^1_{\alpha m}}$ in the $^{13}$C NMR spectra. Using information from the C2-labeled monomer, we could distinguish how much of the ($\boldsymbol{\omega^1_{\alpha L}}$ + $\boldsymbol{\omega^1_{\alpha m}}$) signal is from each label, but this will be highly dependent on the catalyst used and the rate of insertion versus chain walking. Therefore, we chose to set **ω*(DG)** to zero and is not included in the following derivations.

**ω*(DwG)** (from Scheme 3.19D) cannot be corrected for since the assignment for $\boldsymbol{\alpha^*_{\alpha m}}$ is not well-established. It is likely one of the signals in the 33.88–34.39 ppm region, but a specific signal was not able to be assigned to this specific label. Therefore, we chose to set **ω*(DwG)** to zero and is not included in the following derivations.

**ω*(FG)** (from Scheme 3.19E) cannot be corrected for since **ω*(E+F)** is observed regardless of the subsequent insertion. Therefore, **ω*(FG)** was set to zero and is not included in the following derivations. This assumption should not affect the model much because pathway F is a very small percentage of total insertions across many (if not most) nickel systems.

**Scheme 3.19** Pathway G Sequences that Give Component Signals for the ω-Labeled Monomer

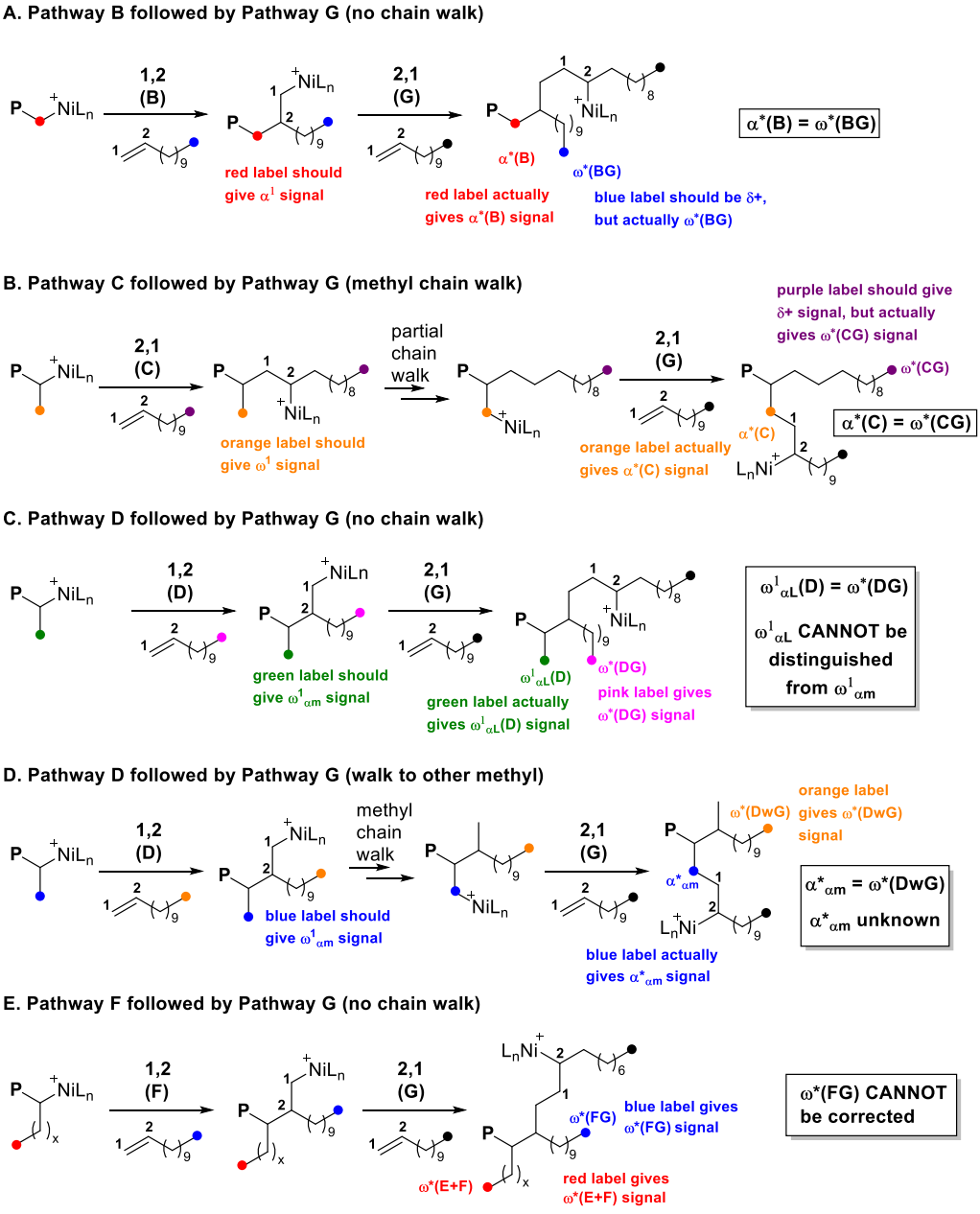


In addition, Scheme 3.20 shows additional relevant sequences for pathway H. Again, the weaknesses of the ω-labeled monomer are highlighted by these pathways. Scheme 3.20A and B show pathway B followed by pathway H, once (A) or multiple

times (B). These cannot be corrected for even though we know they are occurring from the C2-labeled monomer because assignments for the **α*βm** and **α*βL** signals are unknown. It is likely they are two of the signals in the 33.88–34.39 ppm region, but specific signals were not able to be assigned to these specific labels. The effect of not correcting for these signals is an overestimation of **ω*(E+F)** and an underestimation of **ω*(H)**.

**Scheme 3.20** Pathway H Sequences that Give Component Signals for the ω-Labeled Monomer

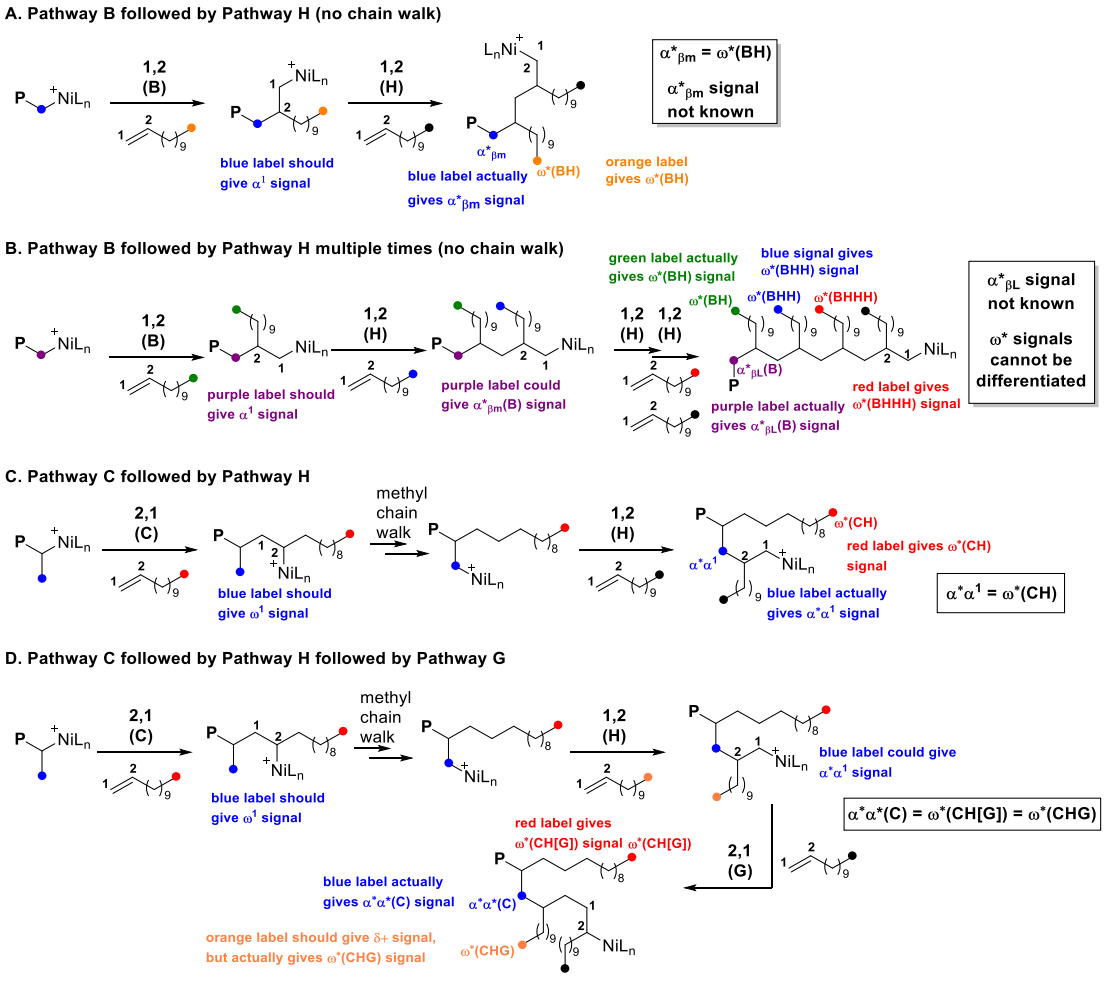

Scheme 3.20C shows pathway C followed by pathway H to give **α*α¹** and **ω*(CH)** signals, as shown in eq (3.71). Scheme 3.20D shows the same C–H sequence from Scheme 3.20C, but then with an additional pathway G, which changes the signals to **α*α***, **ω*(CH[G])**, and **ω*(CHG)**, as shown in eq (3.72).

From all of these pathways, we can derive the following starting equations:

$$\alpha^*(A) = \beta^* = \gamma^* = 2M^* \tag{3.68}$$

$$\alpha^*(B) = \omega^*(BG) \tag{3.69}$$

$$\alpha^*(C) = \omega^*(CG) \tag{3.70}$$

$$\alpha^*\alpha^1 = \omega^*(CH) \tag{3.71}$$

$$\alpha^*\alpha^*(C) = \omega^*(CH[G]) = \omega^*(CHG) \tag{3.72}$$

$$\alpha^* = \alpha^*(A) + \alpha^*(B) + \alpha^*(C) \tag{3.73}$$

$$\omega^* = \omega^*(BG) + \omega^*(CG) + \omega^*(CH) + \omega^*(CH[G]) + \omega^*(CHG) + \omega^*(E+F) \tag{3.74}$$

**α*(A)** can be taken from eq (3.68), noting that 2**M*** could also be substituted with **γ*** or **β***, though the **M*** signal was chosen because it was the most separated from other peaks and thus easiest to integrate accurately:

$$\alpha^*(A) = 2M^* \tag{3.75}$$

Unfortunately, **α*(B)** and **α*(C)** are not distinguishable from each other, which reveals another weakness of the ω-labeled monomer. Because the best chain straightening complexes have very few branching defects, we decided to estimate that half of the (**α*(B)** + **α*(C)**) signal arises from each pathway, believing that this would maintain the proper amount of branching and still yield useful information. This

assumption is used in eqs (3.77) and (3.78), below. We recognize the inherent error introduced by this estimation; however, we believe this to be the best method for correcting this drawback. If we set the B:C ratio to 80:20 instead, there is no discernable difference for **1a** and only a 0.4% difference for **1d**. Using this estimation method, the **α*** components of pathways B and C were calculated from substituting eq (3.75) into a rearranged eq (3.73).

$$\alpha^*(B) + \alpha^*(C) = \alpha^* - \alpha^*(A) = \alpha^* - 2M^* \tag{3.76}$$

$$\alpha^*(B) = \tfrac{1}{2}(\alpha^* - 2M^*) \tag{3.77}$$

$$\alpha^*(C) = \tfrac{1}{2}(\alpha^* - 2M^*) \tag{3.78}$$

The **ω*(BG)** and **ω*(CG)** components are taken from combining eqs (3.69) and (3.70) followed by substitution from eq (3.76), as shown in eq (3.79). **ω*(CHG)** is taken from eq (3.72) and is shown in (3.80). The total **ω*(G)** component is the sum of eqs (3.79) and (3.80), shown in eq (3.81). The **ω*** component for pathway H is shown in eq (3.82), calculated from eqs (3.71) and (3.72). As discussed above for Scheme 3.19 and Scheme 3.20, it is known that **ω*(G)** and **ω*(H)** are underestimated due to the number or sequences that are unable to be corrected for (Scheme 3.19C–E and Scheme 3.20A–B). This will propagate to overestimating **ω*(E+F)** in eqs (3.83)–(3.86), below.

$$\omega^*(BG) + \omega^*(CG) = \alpha^*(C) + \alpha^*(B) = \alpha^* - 2M^* \tag{3.79}$$

$$\omega^*(CHG) = \alpha^*\alpha^* \tag{3.80}$$

$$\omega^*(G) = \alpha^* - 2M^* + \alpha^*\alpha^* \tag{3.81}$$

$$\omega^*(H) = \omega^*(CH) + \omega^*(CH[G]) = \alpha^*\alpha^1 + \alpha^*\alpha^* \tag{3.82}$$

For the **ω*(E+F)** component: rearranging eq (3.74) gives eq (3.83), below. Substituting in from eqs (3.69)–(3.72) gives eq (3.84). Substituting in from eq (3.76) gives eq (3.85), which simplifies to eq (3.86).

$$\omega^*(E+F) = \omega^* - [\omega^*(BG) + \omega^*(CG) + \omega^*(CH) + \omega^*(CH[G]) + \omega^*(CHG)] \quad (3.83)$$

$$\omega^*(E+F) = \omega^* - [\alpha^*(B) + \alpha^*(C) + \alpha^*\alpha^1 + \alpha^*\alpha^*(C) + \alpha^*\alpha^*(C)] \quad (3.84)$$

$$\omega^*(E+F) = \omega^* - (\alpha^* - 2M^* + \alpha^*\alpha^1 + 2\alpha^*\alpha^*(C)) \quad (3.85)$$

$$\omega^*(E+F) = \omega^* - \alpha^* + 2M^* - \alpha^*\alpha^1 - 2\alpha^*\alpha^*(C) \quad (3.86)$$

### *3.6.2.3 Additional Signals from Consecutive Pathways*

Additional signals arising from specific insertion pathways previously not considered were also determined. The following pathways shown in Scheme 3.21 do not require calculation of component signals, therefore the new signals were simply added to the numerator of the appropriate pathway.

**Scheme 3.21** Pathway Sequence that Gives an Additional Observed Signal that Must be Added in for the ω-Labeled Monomer

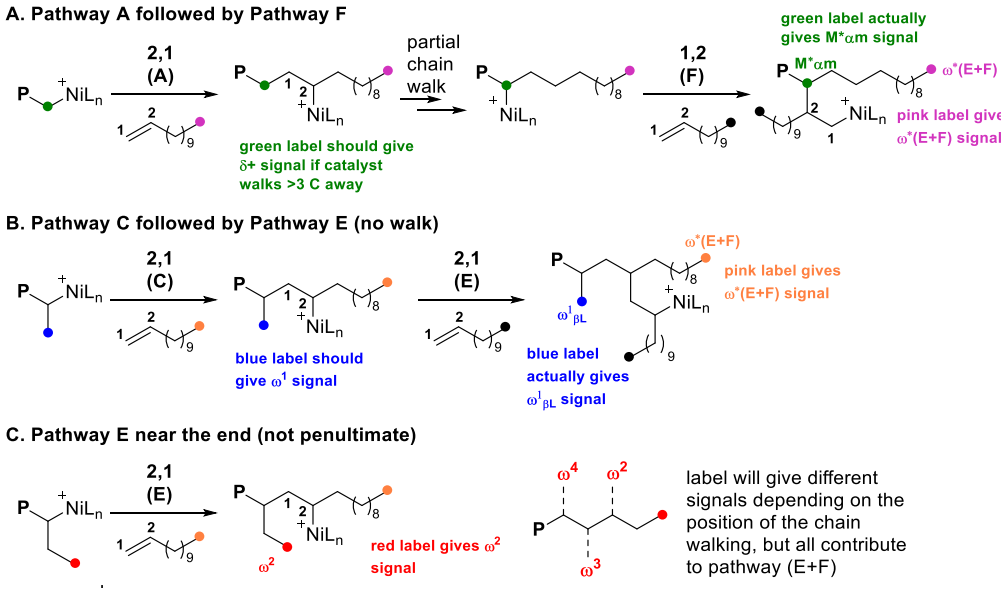

### *3.6.2.4 Summary of all Observed $^{13}C$ NMR Signals from ω-Labeled Monomer*

**Table 3.24** Summary of all Observed Signals for the ω-Labeled Monomer

| Signal Label | Possible Pathways | Corrections |
|---|---|---|
| δ+ | A | |
| $\alpha^1$ | B | |
| $\omega^1$ | C | |
| $\omega^1_{\alpha m}$ | D | Cannot be distinguished from $\omega^1_{\alpha L}$ |
| ω* | E, F, G, H | ω*(G) = α* – 2M* + α*α*, ω*(H) = α*$\alpha^1$ + α*α*, ω*(E+F) = ω*– α* + 2M* – α*$\alpha^1$ – 2α*α*, NOT corrected: ω*(DG), ω*(DwG), ω*(FG), ω*(BH) |
| α*α* | B, C | All assigned to pathway C |
| $\omega^1_{\alpha L}$ | C, D | All assigned to pathway D. Cannot be distinguished from $\omega^1_{\alpha m}$ |
| α* | A, B, C | α*(A) = 2M*, α*(B) = ½α* – M*, α*(C) = ½α* – M* |
| β* | A | |
| γ* | A | |
| M* | A | |
| $\alpha^1$α* | C | |
| $M^*_{\alpha m}$ | A | |
| $\omega^1_{\beta L}$ | C | |
| $\omega^2$ | E, F | |
| $\omega^3$ | E, F | |
| $\omega^4$ | E, F | |
| $\omega^x$ | E, F | |

There were a few small signals in some $^{13}C$ NMR spectra that we were unable to assign. DEPT 135 was used to confirm that the signals at 33.88, 34.01, 34.16, and 34.39 are methylenes likely corresponding to α positions near multiple branches (**$\alpha^x$**). There is one additional methylene signal at 33.32 ppm that we are unable to assign (**$CH_2^x$**).

## REFERENCES

(1) (a) Johnson, L. K.; Killian, C. M.; Brookhart, M. *J. Am. Chem. Soc.* **1995**, *117*, 6414–6415. (b) Pellecchia, C.; Zambelli, *Macromol. Rapid Commun.* **1996**, *17*, 333–338. (c) Musaev, D. G.; Froese, R. D. J.; Svensson, M.; Morokuma, K. *J. Am. Chem. Soc.* **1997**, *119*, 367–374. (d) Simon, L. C.; Soares, J. B. P.; de Souza, R. F. *AIChE J.* **2000**, *46*, 1234–1240. (e) Tempel, D. J.; Johnson, L. K.; Huff, R. L.; White, P. S.; Brookhart, M. *J. Am. Chem. Soc.* **2000**, *122*, 6686–6700. (f) Gates, D. P.; Svejda, S. A.; Oñate, E.; Killian, C. M.; Johnson, L. K.; White, P. S.; Brookhart, M. *Macromolecules* **2000**, *33*, 2320–2334. (g) Rose, J. M.; Cherian, A. E.; Coates, G. W. *J. Am. Chem. Soc.* **2006**, *128*, 4186–4187. (h) Santos, J. P. L.; Castier, M.; Melo, P. A. *Polymer* **2007**, *48*, 5152–5160. (i) Dai, S.; Sui, X.; Chen, C. *Angew. Chem. Int. Ed.* **2015**, *54*, 9948–9953. (j) Guo, L.; Dai, S.; Sui, X.; Chen, C. *ACS Catal.* **2016**, *6*, 428–441. (k) Wang, F.; Tanaka, R.; Cai, Z.; Nakayama, Y.; Shiono, T. *Macromol. Rapid Commun.* **2016**, *37*, 1375–1381. (l) Takeuchi, D.; Osakada, K. *Polymer* **2016**, *82*, 392–405.

(2) (a) Ye, Z.; Feng, W.; Zhu, S.; Yu, Q. *Macromol. Rapid Commun.* **2006**, *27*, 871–876. (b) Rose, J. M.; Cherian, A. E.; Lee, J. H.; Archer, L. A.; Coates, G. W.; Fetters, L. J. *Macromolecules* **2007**, *40*, 6807–6813. (c) Okada, T.; Park, S.; Takeuchi, D.; Osakada, K. *Angew. Chem. Int. Ed.* **2007**, *46*, 6141–6143. (d) Camacho, D. H.; Guan, Z. *Chem. Commun.* **2010**, *46*, 7879–7893. (e) Dong, Z.; Ye, Z. *Polym. Chem.* **2012**, *3*, 286–301. (f) Zhang, D.; Nadres, E. T.; Brookhart, M.; Daugulis, O. *Organometallics* **2013**, *32*, 5136–5143. (g) Ye, Z.; Xu, L.; Dong, Z.; Xiang, P. *Chem. Commun.* **2013**, *49*, 6235–6255. (h) Leone, G.; Mauri, M.; Bertini, F.; Canetti, M.; Piovani, D.; Ricci,

G. *Macromolecules* **2015**, *48*, 1304–1312. (i) Leone, G.; Mauri, M.; Pierro, I.; Ricci, G.; Canetti, M.; Bertini, F. *Polymer* **2016**, *100*, 37–44. (j) O'Connor, K. S.; Watts, A.; Vaidya, T.; LaPointe, A. M.; Hillmyer, M. A.; Coates, G. W. *Macromolecules* **2016**, *49*, 6743–6751.

(3) Small, B. L.; Brookhart, M. *J. Am. Chem. Soc.* **1998**, *120*, 7143−7144.

(4) Thomas, R. M.; Keitz, B. K.; Champagne, T. M.; Grubbs, R. H. *J. Am. Chem. Soc.* **2011**, *133*, 7490–7496.

(5) Stadler, F. J.; Piel, C.; Klimke, K.; Kaschta, J.; Parkinson, M.; Wilhelm, M.; Kaminsky, W.; Münstedt, H. *Macromolecules* **2006**, *39*, 1474–1482.

(6) Koivumäki, J.; Fink, G.; Seppälä, J. V. *Macromolecules* **1994**, *27*, 6254–6258.

(7) Vaidya, T.; Klimovica, K.; LaPointe, A. M.; Keresztes, I.; Lobkovsky, E. B.; Daugulis, O.; Coates, G. W. *J. Am. Chem. Soc.* **2014**, *136*, 7213–7216.

(8) Merna, J.; Hošt'álek, Z.; Peleška, J.; Roda, *Polymer* **2009**, *50*, 5016–5023.

(9) Wang, F.; Tanaka, R.; Cai, Z.; Nakayama, Y.; Shiono, T. *Polymers* **2016**, *8*, 160–175.

(10) (a) Liu, F.; Gao, H.; Hu, Z.; Hu, H.; Zhu, F.; Wu, Q. *J. Polym. Sci. A Polym. Chem.* **2012**, *50*, 3859–3866. (b) Liu, J.; Chen, D.; Wu, H.; Xiao, Z.; Gao, H.; Zhu, F.; Wu, Q. *Macromolecules* **2014**, *47*, 3325–3331.

(11) Camacho, D. H.; Guan, Z. *Macromolecules* **2005**, *38*, 2544–2546.

(12) Rose, J. M.; Deplace, F.; A. Lynd, N.; Wang, Z.; Hotta, A.; Lobkovsky, E. B.; Kramer, E. J.; Coates, G. W. *Macromolecules* **2008**, *41*, 9548–9555.

(13) Hu, H.; Gao, H.; Chen, D.; Li, G.; Tan, Y.; Liang, G.; Zhu, F.; Wu, Q. *ACS Catal.* **2015**, *5*, 122–128.

(14) Dai, S.; Sui, X.; Chen, C. *Chem. Commun.* **2016**, *52*, 9113–9116.

(15) In the context of this discussion, we consider branching to be a defect. However, there is indeed interest in targeting poly(α-olefin) materials with precision branching throughout the polymer structure. Our group has reported using nickel α-diimines for precise ω,2-enchainment of α-olefins to generate precision methyl branches (reference 1g and 12), and Kenneth Wagener's group has developed an ADMET strategy to access precision alkyl branches: Li, H.; Rojas, G.; Wagener, K. B. *ACS Macro Lett.* **2015**, *4*, 1225–1228.

(16) (a) Zhang, J.; Gao, H.; Ke, Z.; Bao, F.; Zhu, F.; Wu, Q. *J. Mol. Catal. A: Chem.* **2005**, *231*, 27–34. (b) Gao, H.; Pan, J.; Guo, L.; Xiao, D.; Wu, Q. *Polymer* **2011**, *52*, 130–137. (c) Losio, S.; Leone, G.; Bertini, F.; Ricci, G.; Sacchi, M. C.; Boccia, A. C. *Polym. Chem.* **2014**, *5*, 2065–2075. (d) Sokolohorskyj, A.; Mundil, R.; Lederer, A.; Merna, J. *J. Polym. Sci. A Polym. Chem.* **2016**, *54*, 3193–3202. (e) Azoulay, J. D.; Bazan, G. C.; Galland, G. B. *Macromolecules* **2010**, *43*, 2794–2800.

(17) Subramanyam, U.; Rajamohanan, P. R.; Sivaram, S. *Polymer* **2004**, *45*, 4063–4076.

(18) McCord, E. F.; McLain, S. J.; Nelson, L. T. J.; Ittel, S. D.; Tempel, D.; Killian, C. M.; Johnson, L. K.; Brookhart, M. *Macromolecules* **2007**, *40*, 410–420.

(19) There have been many detailed mechanistic studies of ethylene polymerization using both nickel and palladium α-diimine complexes, but for the purposes of this discussion we will focus specifically on efforts in α-olefin polymerization. For mechanistic evaluations of ethylene, please refer to: (a) Galland, G. B.; de Souza, R. F.; Mauler, R. S.; Nunes, F. F. *Macromolecules* **1999**, *32*, 1620–1625. (b) Leatherman, M. D.; Svejda, S. A.; Johnson, L. K.; Brookhart, M. *J. Am. Chem. Soc.* **2003**, *125*, 3068–3081.

(20) Complexes **1a**, **1b**, **1c**, and **1d** are technically pre-catalysts that require activation by methylaluminoxane (MAO) in order to generate the cationic, active catalytic species. During discussion, these complexes will directly be referred to as **1a**, **1b**, **1c**, and **1d** and assumed to be the activated species.

(21) Signal naming using the xBn convention developed by Usami and Takayama can be found in Section 3.5.8 for comparison. Refer to: Usami, T.; Takayama, S. *Macromolecules* **1984**, *17*, 1756–1761.

(22) Pentyl branches can generally be distinguished by the 2-position of the branch. However, it is not possible to install a $^{13}$C-label in this position with our system, so we cannot observe it. For assignment of the pentyl branch, refer to: Obuah, C.; Munyaneza, A.; Guzei, I. A.; Darkwa, J. *Dalton Trans.* **2014**, *43*, 8940–8950.

(23) Shultz, L. H.; Tempel, D. J.; Brookhart, M. *J. Am. Chem. Soc.* **2001**, *123*, 11539–11555.

(24) Gottfried, A. C.; Brookhart, M. *Macromolecules* **2003**, *36*, 3085–3100.

(25) Ittel, S. D.; Johnson, L. K. *Chem. Rev.* **2000**, *100*, 1169–1203.

(26) Prasad, J. V.; Rao, C.; Garg, V. N. *Eur. Polym. J.* **1991**, *27*, 251−254.

(27) Cherian, A. E.; Rose, J. M.; Lobkovsky, E. B.; Coates, G. W. *J. Am. Chem. Soc.* **2005**, *127*, 13770–13771.

(28) Peng, Z.; Haag, B. A.; Knochel, P. *Org. Lett.* **2010**, *12*, 5398 – 5401.

(29) Zhou, Z.; Kummerle, R.; Stevens, J. C.; Redwine, D.; He, Y.; Qiu, X. *J. Magn. Reson.* **2009**, *200*, 328–333.

# CHAPTER 4

# SYNTHESIS OF SEMI-CRYSTALLINE POLYOLEFIN MATERIALS: PRECISION METHYL BRANCHING USING CHIRAL ISOSELECTIVE α-DIIMINE NICKEL CATALYSTS

Adapted with permission from Vaccarello, D. N.; O'Connor, K. S.; Iacono, P.; Rose, J. M.; Cherian, A. E.; Coates, G. W. *J. Am. Chem. Soc.* **2017**, *Submitted*

## *4.1 Introduction*

Given the massive global production of polyethylene (PE) and isotactic polypropylene (*i*PP) and the importance of these materials to modern society, new semicrystalline polyolefins produced from readily available, inexpensive feedstocks would be of significant interest. The monomer 1-butene meets these criteria and can easily be accessed from both petroleum and biorenewable sources. 1-Butene can be synthesized through the dehydration of 1-butanol,[1] an emerging biomass fuel,[2] or by the dimerization of sugar-derived ethylene.[3] Polymerization of 1-butene using Ziegler-Natta catalysis results in isotactic 1,2-poly(1-butene) which exhibits superior mechanical properties relative to *i*PP and PE.[4] However, its complex crystallization hinders its use in many practical applications.[5] Crystallization from the melt gives a kinetically favored polymorph, which slowly transforms over several days at room temperature to yield a more thermodynamically stable structure resulting in dimensional changes of the material. Recent advances have attempted to address this issue, potentially allowing *iso*-1,2-poly(1-butene) to be more widely utilized.[5]

Since their discovery for olefin polymerization, α-diimine nickel(II) and palladium(II) catalysts have received considerable attention.[6] A unique mechanistic feature of these catalysts is their ability to undergo an isomerization event involving successive β-hydrogen eliminations followed by metal hydride reinsertions with opposite regiochemistry. Commonly known as "chain walking," this isomerization event places the active species at various positions along the polymer backbone, allowing for the preparation of numerous polymer topologies from simple olefin feedstocks.[7]

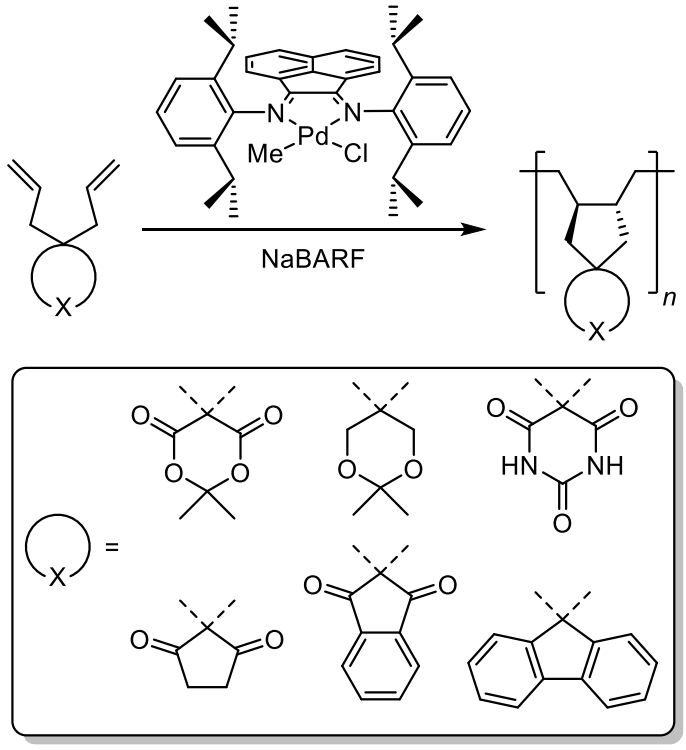


**Figure 4.1** Cyclopolymerization of non-conjugated dienes. Substrates were selected from a larger screen as performed in reference 9e.

Exhibiting control over polymer tacticity using late metal catalysts, however, is a challenge. By nature of the chain walking mechanism, previously installed stereocenters can easily be isomerized during polymerization. Notable advancements have been achieved, with Brookhart and DuPont reporting the polymerization of cyclopentene using α-diimine Ni(II) and Pd(II) complexes to form modestly isotactic *cis*-1,3-polycyclopentene.[8] Takeuchi and Osakada have accessed a variety of stereoregular structures through the polymerization of non-conjugated dienes and cycloolefins.[9] Additionally, Sigman and coworkers identified a rare example of enantioselective chain walking in a redox-relay oxidative Heck-arylation using chiral

palladium catalysts. After arylation, the catalyst walks through a branch point and maintains a high enantiomeric ratio of the original stereocenter.[10]

Despite this progress, there are very few reports for the chain walking polymerization of simple linear α-olefins into precision branched, stereoregular structures. Wagener and coworkers have pursued acyclic diene metathesis (ADMET) as a strategy for producing precision branched polyolefins, but this method does not provide inherent stereocontrol.[11] We previously reported the polymerization of *trans*-2-butene into *iso*-1,3-poly(2-butene);[12] however, the catalyst system was only modestly isoselective ([*mm*] = 0.41–0.64) with the resulting polymers exhibiting low melting temperatures ($T_m$ < 67 °C). Enchaining 1-butene with successive 4,2-units and isotacticity should lead to semicrystalline materials (Scheme 4.1). We believed a highly 1,2-regioselective and isoselective catalyst capable of preserving the stereochemistry from the initial insertion event could achieve this goal and produce isotactic materials with an improved melting temperature from 1-butene (Scheme 4.2). To the best of our knowledge, there have been no reports of late metal catalysts that can perform *both* isoselective monomer insertion *and* stereocontrolled chain walking polymerization in tandem.

**Scheme 4.1** Possible Enchainment Units for the Polymerization of 1-Butene Using α-Diimine Nickel Catalysts

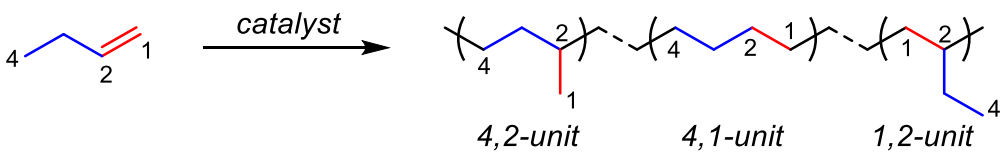

**Scheme 4.2** Comparison of Standard 1,2-Poly(1-Butene) Versus 4,2-Poly(1-Butene) Produced by Regio- and Stereoselective Chain Walking Catalysis

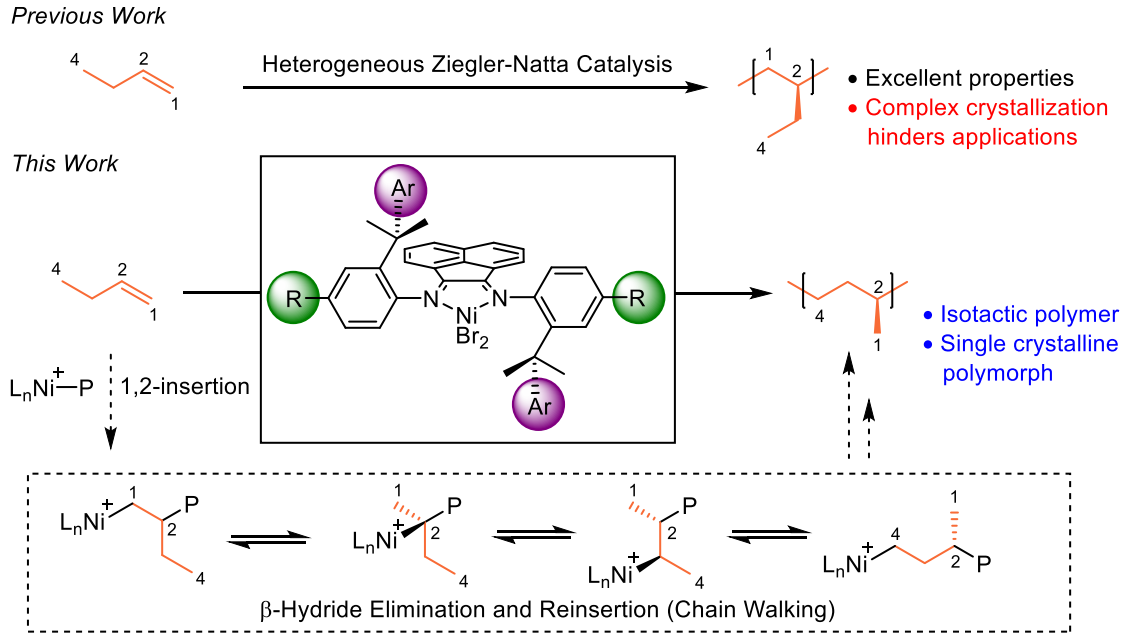


## *4.2 Results/Discussion*

### *4.2.1 Initial Polymerization Screen: Complexes **4.1** and **4.2***

Herein, we report on the synthesis and utilization of a family of α-diimine nickel complexes for the polymerization of 1-butene (Figure 4.2). Application of **4.1**/MAO to the polymerization of 1-butene resulted in amorphous material (Table 4.1, entry 1).[13] Analysis of the material by $^{13}$C NMR spectroscopy revealed a microstructure composed primarily of 4,2-poly(1-butene). However, a lack of stereocontrol as evidenced by a low [*mm*] triad value contributed to poor polymer thermal properties (Table 4.1, entry 1). We hypothesized that using a cumyl-derived complex (Figure 4.2, complex **4.2**) may be more effective for the regio- and stereoselective polymerization of 1-butene, with the

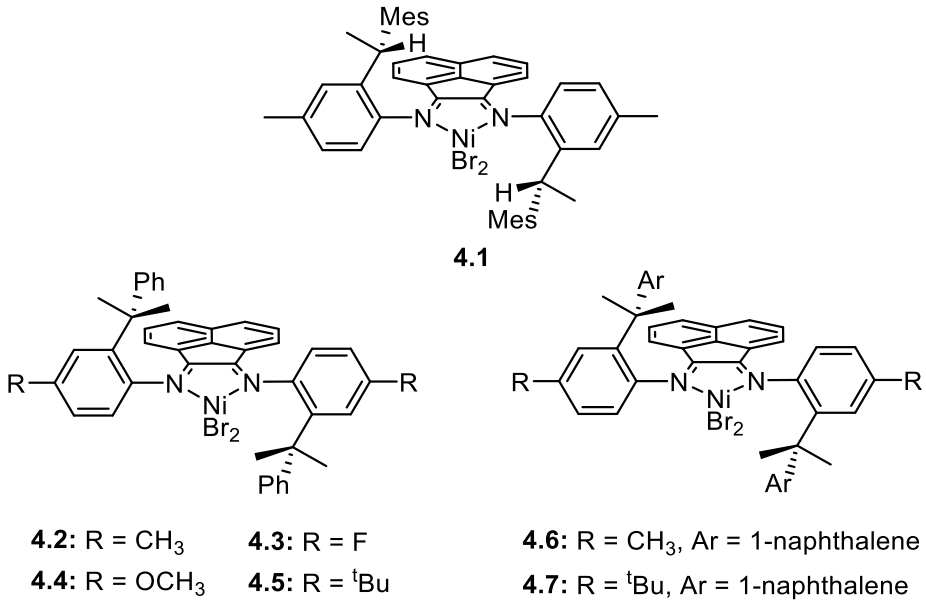


**Figure 4.2** α-Diimine nickel complexes used in this study.

additional steric bulk potentially preserving the stereochemical information imparted by the initial insertion event.

Activation of complex **4.2** with MAO in the presence of 1-butene resulted in the production of a white, powdery material. GPC and DSC analysis revealed a polymer with modest molecular weight (12.8 kDa), controlled unimodal molecular weight distribution (1.60), and a melting temperature ($T_m$) of 77 °C (Table 4.1, entry 2). Analysis by $^{13}C$ NMR spectroscopy revealed a microstructure composed primarily of 4,2-poly(1-butene) units arising from 4,2-enchainment (Scheme 4.1) and high amounts of isotacticity ([*mm*] = 0.75). The observed tacticity is considerably higher than that reported previously for the polymerization of *trans*-2-butene.[12]

**Table 4.1** Catalyst Screen for the Polymerization of 1-Butene.[a]

| entry | complex | yield (mg) | TOF[b] ($h^{-1}$) | $M_{n(theo)}$ (kDa) | $M_n$[c] (kDa) | $Đ$[c] ($M_w/M_n$) | enchainment type[d] (mole fraction) | | | [*mm*][d] | α[e] | $T_m$[f] (°C) |
|---|---|---|---|---|---|---|---|---|---|---|---|---|
| | | | | | | | 4,2 | 4,1 | 1,2 | | | |
| 1 | **4.1** | 598 | 44 | 59.8 | 70.0 | 1.26 | 0.88 | 0.06 | 0.02[h] | 0.43 | 0.74 | –[g] |
| 2 | **4.2** | 122 | 9 | 12.2 | 12.8 | 1.60 | 0.94 | 0.04 | 0.02 | 0.75 | 0.91 | 77 |
| 3 | **4.3** | 233 | 17 | 23.3 | 23.5 | 1.48 | 0.93 | 0.03 | 0.04 | 0.79 | 0.92 | 80 |
| 4 | **4.4** | 220 | 16 | 22.0 | 21.0 | 1.51 | 0.91 | 0.04 | 0.05 | 0.73 | 0.90 | 73 |
| 5 | **4.5** | 234 | 17 | 23.4 | 14.7 | 1.57 | 0.93 | 0.03 | 0.03[h] | 0.80 | 0.93 | 85 |
| 6 | **4.6** | 200 | 15 | 20.0 | 18.5 | 1.60 | 0.91 | 0.03 | 0.06 | 0.80 | 0.93 | 86 |
| 7 | **4.7** | 298 | 22 | 29.8 | 20.5 | 1.69 | 0.93 | 0.03 | 0.04 | 0.84 | 0.94 | 85 |

[a]Polymerization conditions: 3.0 ± 0.2 g 1-butene (53.5 mmol), 10 $\mu$mol Ni complex in 2 mL $CH_2Cl_2$, 1.0 mmol MAO; $t_{rxn}$ = 24 h, $T_{rxn}$ = −40 °C. [b]Determined using the equation (mol monomer consumed)(mol catalyst)$^{-1}$(time)$^{-1}$. [c]Determined by gel permeation chromatography at 150 °C in 1,2,4-trichlorobenzene versus polyethylene standards. [d]Determined using $^{13}$C NMR spectroscopy; equations can be found in Section 4.3.5. [e]Probability factor of three consecutive 4,2-units having the same relative stereochemistry, determined using the equation [*mm*] = $\alpha^3$+(1-$\alpha$)$^3$. [f]Determined by differential scanning calorimetry, endotherm from 2$^{nd}$ heating cycle. [g]No detectable $T_m$. [h]Additional signals can be observed corresponding to long chain branches.

### *4.2.2 Proposed Source of Stereoselectivity*

The addition of *ortho*-cumyl groups had a dramatic effect on the isoselectivity of the resulting 4,2-poly(1-butene). We believe that the steric environment created from this substitution pattern facilitates the necessary enantioface coordination event leading to stereoretentive chain isomerization. A π-stacking interaction with the ortho-aryl substituents and the acenaphthene backbone is consistently observed in the solid state for cumyl-derived complexes. We believe this π-stacking interaction persists in solution at low reaction temperature, causing the catalyst to maintain a very specific steric environment which contributes to the observed selectivity. We also cannot rule out the possibility that the catalyst structure may prevent racemization of the stereocenter after planarization from the chain walking mechanism.

### *4.2.3 Continued Polymerization Screen: Complexes **4.3**–**4.7***

To probe our assumptions regarding the source of selectivity for 1-butene polymerization, perturbations to the ligand framework were made. Electronic variants of the *ortho*-cumyl nickel complexes were first studied. It was found that MAO-activated **4.3** with electron withdrawing *para*-fluoro-substituents produced materials with higher molecular weight (23.3 kDa), slightly elevated $T_m$ (80 °C), and improved isotacticity ([*mm*]= 0.79) compared to **4.2**/MAO. MAO-activated **4.4**, with electron donating *para*-methoxy-substituents, however, produced materials with a decreased $T_m$ (73 °C) and lower isotacticity ([*mm*]= 0.73). Selectivity for 4,2-enchainment also decreased slightly for **4.4**/MAO (0.91). We also prepared and studied complex **4.5** with *para-tert*-butyl substituents that are slightly more electron donating than the methyl

substituents of complex **4.2**. To our surprise, **4.5**/MAO produced *iso*-4,2-poly(1-butene) with high levels of isotacticity ([*mm*] = 0.80) and an improved $T_m$ of 85 °C. One possibility is that the *tert*-butyl substituents in **4.5** affect the ion pairing interaction of the cationic nickel complex and the MAO activator such that an improvement in selectivity is observed.[14]

We continued probing the system by modifying the aryl substituent of the cumyl group from phenyl (**4.2**) to 1-naphthyl (**4.6**). Complex **4.6**/MAO produced polymer with similar tacticity to that of complex **4.5**/MAO ([*mm*] = 0.80) and a similar $T_m$ of 86 °C. We suspect the π-stacking interaction between the 1-naphthyl group and the acenapthene backbone is enhanced due to the additional π overlap, resulting in a more rigidified structure that contributes to the desired regio- and stereoselectivity. After observing the enhanced selectivities for materials produced by MAO-activated **4.5** and **4.6**, we attempted to increase the steric bulk of the system further by preparing complex **4.7**, bearing both *tert*-butyl and 1-naphthyl substituents (Figure 4.2). The polymer produced by **4.7**/MAO exhibited the highest isotacticity out of all samples previously generated ([*mm*] = 0.84). Interestingly, despite the increase in tacticity, there was no apparent improvement in the observed melting temperature of the resulting material (Table 4.1, entry 7).

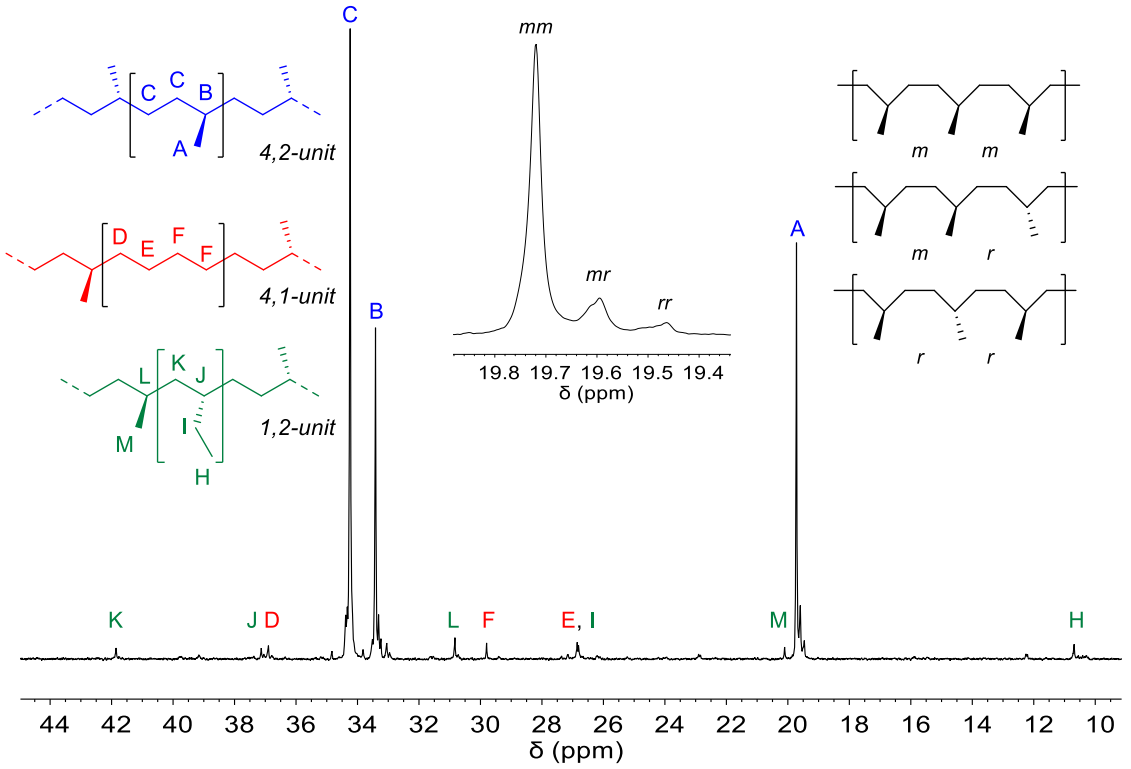


**Figure 4.3** $^{13}$C NMR spectrum of *iso*-4,2-poly(1-butene) produced by **4.5**/MAO (Table 4.1, entry 5).

### *4.2.4 Effect of Branch Composition on Thermal Properties*

The thermal properties of *iso*-4,2-poly(1-butene) are influenced not only by tacticity, but also by branch composition. A small percent of ethyl branches were detected in these systems which can be installed through 1,2-insertion of 1-butene without chain walking. Ethyl branches can considerably reduce $T_m$ and crystallinity compared to methyl branches.[15] Another defect observed in this system arises from 4,1-enchainment, where 2,1-insertion followed by complete chain walking produces a linear "polyethylene" segment. Due to the small amount of these units (< 5%), it is difficult to quantify its effect on the properties of the resulting *iso*-4,2-poly(1-butene).[16] Recent studies have shown that *i*PP with < 5% 3,1-insertions, made with related cumyl-

substituted catalysts retained most of its crystallinity, suggesting that the effect in this system may also be small.[17]

### *4.2.5 Effects of Reaction Conditions on the Resulting Polymer Thermal Properties and Catalyst Selectivity*

We further studied the effects of reaction conditions on the thermal properties and tacticity of the resulting polymers produced by **4.5**/MAO (Table 4.2 and Table 4.3) Reaction temperature had a dramatic effect on polymer thermal properties. By increasing the temperature from −40 °C to −30 °C, the melting temperature of the resulting material dropped considerably from 85 °C to 66 °C (Table 4.2, entry 2). corresponding to a significant loss in tacticity (Table 4.3, entry 2). Increasing the reaction temperature further to −10 °C resulted in a complete loss of crystallinity. Cooling the reaction further to −50 °C decreased the polymerization rate and polymer

**Table 4.2** Effects of Varying Reaction Conditions on the Polymerization of 1-Butene using **4.5**[a]

| entry | temp (°C) | conc (M) | yield (mg) | $M_n$[b] (kDa) | $Đ$[b] ($M_w/M_n$) | $T_m$[c] (°C) |
|---|---|---|---|---|---|---|
| 1 | −10 | 7.8 | 262 | 10.8 | 1.95 | –[d] |
| 2 | −30 | 7.8 | 420 | 23.7 | 1.80 | 66 |
| 3 | −40 | 7.8 | 234 | 14.7 | 1.57 | 85 |
| 4 | −50 | 7.8 | 173 | 10.6 | 1.81 | 85 |
| 5 | −40 | 6.0[e] | 163 | 12.4 | 1.46 | 80 |
| 6 | −40 | 9.1[f] | 464 | 16.3 | 2.17 | 73 |

[a]Polymerization conditions: 3.0 ± 0.2 g 1-butene (53.5 mmol), 10 μmol of complex **4.5** in 2 mL $CH_2Cl_2$, 100 equiv. MAO; $t_{rxn}$ = 24 h. [b]Determined by gel permeation chromatography at 150 °C in 1,2,4-trichlorobenzene versus polyethylene standards. [c]Determined by differential scanning calorimetry, endotherm from 2nd heating cycle. [d]No detectable $T_m$. [e]1.5 ± 0.2 g 1-butene (26.8 mmol). [f]6.0 ± 0.2 g 1-butene (107.0 mmol).

**Table 4.3** Effects of Varying Reaction Conditions on the Tacticity and Enchainment Ratios of 4,2-Poly(1-Butene) Produced using **4.5**[a]

| entry | temp (°C) | conc (M) | [*mm*][b] | enchainment pathways[b] | | |
|---|---|---|---|---|---|---|
| | | | | 4,1 | 4,2 | 1,2 |
| 1 | −10 | 7.8 | n.d.[c] | n.d.[c] | n.d.[c] | n.d.[c] |
| 2 | −30 | 7.8 | 0.53 | 0.17 | 0.79 | 0.04 |
| 3 | −40 | 7.8 | 0.80 | 0.03 | 0.93 | 0.03 |
| 4 | −50 | 7.8 | 0.80 | 0.02 | 0.96 | 0.02 |
| 5 | −40 | 6.0[d] | 0.70 | 0.05 | 0.91 | 0.04 |
| 6 | −40 | 9.1[e] | 0.59 | 0.14 | 0.83 | 0.03 |

[a]Polymerization conditions: 10 μmol of complex **4.5** in 2 mL $CH_2Cl_2$, 100 equiv. MAO; $t_{rxn}$ = 24 h. [b]Determined by $^{13}C$ NMR spectroscopy. [c]Not determined. [d]1.5 ± 0.2 g 1-butene (26.8 mmol). [e]6.0 ± 0.2 g 1-butene (107.0 mmol).

yield, and resulted in materials with similar thermal properties to those produced at −40 °C (Table 4.2, entry 3).

The effect of 1-butene concentration was also studied. Increasing the concentration from the standard 7.8 M to 9.1 M (Table 4.2 and Table 4.3, entry 6). resulted in higher polymer yield but a marked decrease in tacticity ([*mm*] = 0.59) and melting temperature ($T_m$ = 73 °C). A decrease in 4,2-enchainment in favor of 1,2-enchainment was also observed at a higher concentration of 1-butene. Decreasing the concentration of 1-butene to 6.0 M resulted in lower polymer yield, but also a slight decrease in tacticity ([*mm*] = 0.70) and melting temperature ($T_m$ = 80 °C) compared to the standard conditions (Table 4.2 and Table 4.3, entry 5). Lower 1-butene concentrations may increase the rate of chain isomerization relative to insertion, allowing additional time for stereoerrors to be introduced.

Reaction solvent also played an important role in the resulting material properties. Using aromatic solvents such as toluene and chlorobenzene resulted in materials with broader molecular weight distributions and decreased melting temperatures corresponding to decreased polymer tacticity (Table 4.4 and Table 4.5, entries 2 and 3). We suspect that aromatic solvents may participate in competitive interactions with the acenaphthene backbone, disrupting the π-stacking interaction with the cumyl side-chain. We also cannot rule out the possibility of changes in ion pairing interactions that affect the observed selectivity. Interestingly, polymerization in strongly polar 1,2-difluorobenzene resulted in polymer with a higher $T_m$ compared to the polymers produced in other aromatic solvents, despite a further decrease in tacticity (Table 4.4 and Table 4.5, entry 4). Ultimately, dichloromethane was found to be the most suitable solvent for this system in terms of producing *iso*-4,2-poly(1-butene).

**Table 4.4** Solvent Effects on the Polymerization of 1-Butene using **4.5**[a]

| entry | solvent | TOF ($h^{-1}$) | yield (mg) | $M_n$[b] (kDa) | $Đ$[b] | $T_m$[c] (°C) |
|---|---|---|---|---|---|---|
| 1 | DCM | 17 | 234 | 14.7 | 1.57 | 85 |
| 2 | PhMe | 15 | 198 | 12.2 | 1.96 | 79 |
| 3 | PhCl | 25 | 338 | 21.1 | 1.85 | 76 |
| 4 | 1,2-$F_2$Ph | 17 | 223 | 10.9 | 2.05 | 82 |

[a]Polymerization conditions: 3.0 ± 0.2 g 1-butene (53.5 mmol), 10 μmol of complex **4.5** in 2 mL solvent, 1.0 mmol MAO; $t_{rxn}$ = 24 h, $T_{rxn}$ = −40 °C. [b]Turnover frequency, TOF = (mol monomer consumed)(mol catalyst)$^{-1}$(time)$^{-1}$. [c]Determined by gel permeation chromatography at 150 °C in 1,2,4-trichlorobenzene versus polyethylene standards. [d]Determined by differential scanning calorimetry, endotherm from 2nd heating cycle.

**Table 4.5** Solvent Effects on the Tacticity and Enchainment Ratios of 4,2-Poly(1-Butene) Produced by **4.5**[a]

| entry | solvent | [*mm*][b] | enchainment pathways[b] | | |
|---|---|---|---|---|---|
| | | | 4,2 | 4,1 | 1,2 |
| 1 | DCM | 0.80 | 0.93 | 0.03 | 0.03[f] |
| 2 | PhMe | 0.79 | 0.95 | 0.02 | 0.03 |
| 3 | PhCl | 0.76 | 0.90 | 0.07 | 0.03 |
| 4 | 1,2-$F_2$Ph | 0.69 | 0.89 | 0.04 | 0.05[f] |

[a]Polymerization conditions: 3.0 ± 0.2 g 1-butene (53.5 mmol), 10 μmol of complex **4.5** in 2 mL solvent, 1.0 mmol MAO; $t_{rxn}$ = 24 h, $T_{rxn}$ = −40 °C. [b]Determined by $^{13}$C NMR spectroscopy.

### *4.2.6 Mechanical Properties of iso-4,2-Poly(1-Butene)*

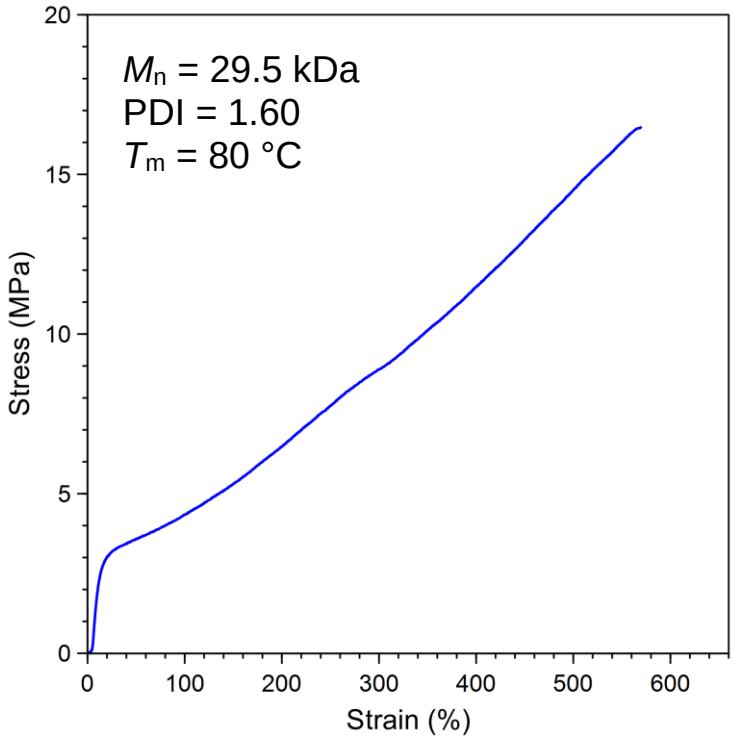


**Figure 4.4** Tensile strength curve of *iso*-4,2-poly(1-butene) produced by **4.5**/MAO. Reaction conditions: 3.0 ± 0.2 g 1-butene, 10 μmol of complex **4.5** in 2 mL $CH_2Cl_2$, 100 equiv. MAO; $t_{rxn}$ = 168 h, $T_{rxn}$ = −40 °C. Polymer data: yield = 3.52 g, $M_n$ = 29.5 kDa, $Đ$ = 1.60, $T_m$ = 80 °C.

We examined the mechanical properties of *iso*-4,2-poly(1-butene). Polymer films were melt-pressed directly into a tensile bar mold at 95 °C under a pressure of 5.2 MPa for 15 minutes and cooled at a rate of ~6 °C/min to 22 °C. The tensile bars were subsequently used for analysis of mechanical properties. Tensile strength was measured for a sample produced by **4.5** with Figure 4.4 showing a representative tensile strength curve. Interestingly, the resulting material experiences yielding at relatively low stress values (~5 MPa) in comparison to other thermoplastics such as *i*PP. After yielding, the material experiences high elongations up to 600% strain before breaking with a gradual increase in stress during elongation.

## *4.3 Conclusions*

In summary, we performed the iso- and regioselective polymerization of 1-butene using cationic α-diimine nickel(II) complexes to pro-duce semi-crystalline iso-4,2-poly(1-butene). The methyl substituents on the cumyl-groups of the ligand are crucial for the isoselective insertion and stereocontrolled chain walking. Furthermore, rigidifying the structure of the active catalyst through π-stacking interactions with the catalyst backbone was also beneficial for improving tacticity. This system allows access to isotactic polymers from a simple, inexpensive α-olefin feedstock. Additional catalyst development should be pursued to further increase the selectivity of this unique polymerization process.

## *4.4 Experimental*

### *4.4.1 General Considerations*

All manipulations of air- and/or water-sensitive compounds were carried out under dry nitrogen using a Braun UniLab drybox or standard Schlenk techniques. NMR spectra were acquired using either a Varian Mercury (300 MHz) or a Varian Inova (400 MHz) and were referenced versus residual nondeuterated solvent shifts ($^{1}$H, $^{13}$C). Polymer NMR spectra were acquired using a Bruker AV III HD with broadband Prodigy cryoprobe and were referenced versus residual nondeuterated solvent shifts ($^{1}$H, $^{13}$C). The mass spectrum was recorded using a Exactive Plus Orbitrap Mass Spectrometer with a DART SVP ion source from Ion Sense or a Waters MALDI Micro MX system. The sample was prepared by using the dried droplet method with no matrix present. Ionization was by a 257 nm UV nitrogen laser and the accelerating potential was 17.2 keV. The spectrum was recorded using the reflectron in positive ion mode. Molecular weights ($M_n$ and $M_w$) and dispersities ($M_w/M_n$) were determined by high temperature gel permeation chromatography (GPC) using a Waters Alliance GPCV 2000 GPC equipped with a Waters DRI detector and viscometer. The column set (four Waters HT 6E and one Waters HT2) was eluted with 1,2,4-trichlorobenzene containing 0.01 wt. % di-*tert*-butylhydroxytoluene (BHT) at 1.0 mL/min at 150 °C. Data were calibrated using monomodal polyethylene standards. Polymer melting points ($T_m$) and glass transition temperatures ($T_g$) were measured by differential scanning calorimetry (DSC) using a TA Instruments Q1000 calorimeter equipped with an automated sampler. Analyses were performed in crimped aluminum pans under nitrogen and data were collected from the

second heating run at a heating rate of 10 °C/min from −70 to 200 °C, and processed with TA Q series software.

### *4.4.2 Materials and Complex Synthesis*

Toluene and hexanes were purified over columns of alumina and copper (Q5). Methylene chloride was purified over an alumina column and degassed by three freeze-pump-thaw cycles before use. 1,2-Difluorobenzene, chloroform, dibromomethane, and chlorobenzene were dried over crushed $CaH_2$ for 24 hours and degassed by three freeze-pump-thaw cycles before use. Acenaphthenequinone (Aldrich), α-methylstyrene (Aldrich), 4-fluoroaniline (Aldrich), formic acid (Aldrich), trifluoromethanesulfonic acid ($CF_3SO_3H$, Aldrich), 1-butene (Aldrich), and (dimethoxyethane)$NiBr_2$ ((DME)$NiBr_2$, Strem) were used without further purification. Methylaluminoxane (MAO) was generously donated from Albemarle Corporation as a 30% wt solution in toluene which was dried by evaporation of volatiles giving a white powder. Complexes **4.1, 4.2** and **4.6** were synthesized as previously reported.[18]

**4-Fluoro-2-(2-phenylpropan-2-yl)aniline (AN-4.3).** $CF_3SO_3H$ (0.54 mL, 6.0 mmol) was added to a mixture of 4-fluoroaniline (2.85 mL, 30.0 mmol) and α-methylstyrene (3.90 mL, 30.0 mmol). The mixture was heated to 160 °C and allowed to react for 20 h. The reaction was quenched with a solution of saturated $NaHCO_3$, followed by an extraction with dichloromethane. Organics were combined, dried over $MgSO_4$, filtered, and concentrated. The crude product was chromatographed on silica (95:5 hexanes:ethyl acetate) and dried to give a light purple solid (2.98 g, 43%). **$^1$H NMR** (500 MHz, $CDCl_3$): δ 7.34–7.28 (m, 4H, ArH), 7.25–7.18 (m, 2H, ArH) 6.79 (m, 1H, ArH), 6.47

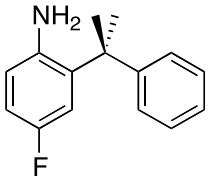

(dd, $J$ = 5.23 Hz, $J$ = 8.62 Hz, 1H, ArH), 3.02 (broad s, 2H, $NH_2$), 1.68 (s, 6H, $C(CH_3)_2$). **$^{13}C\{^1H\}$ NMR** (125 MHz, $CDCl_3$): δ 156.5 (d, $J_{CF}$ = 235.0 Hz), 148.6, 140.6 (d, $J_{CF}$ = 2.1 Hz), 135.3 (d, $J_{CF}$ = 5.7 Hz), 129.0, 126.5, 125.9, 118.0 (d, $J_{CF}$ = 7.7 Hz), 113.7 (d, $J_{CF}$ = 2.9 Hz), 113.5, (d, $J_{CF}$ = 1.4 Hz), 42.5 (d, $J_{CF}$ = 1.1 Hz), 28.9. **HRMS** (DART) *m/z* calc for $C_{15}H_{17}NF$ $(M+H)^+$: 230.1345, found 230.1345.

***rac*-ArN=C(An)C=NAr (Ar = 4-fluoro-2-(2-phenylpropan-2-yl)phenyl; An = acenaphthene) (L-4.3).** 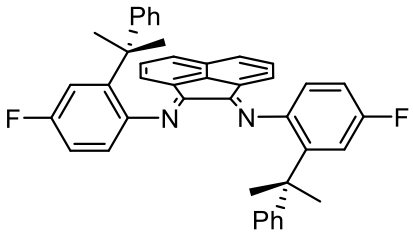

In a sealed vial a mixture of **AN-4.3** (0.504 g, 2.20 mmol), acenaphthenequinone (0.182 g, 1.00 mmol), and anhydrous $ZnCl_2$ (0.157 g, 1.15 mmol) in glacial acetic acid (2.2 mL) was heated to 130 °C with stirring for 1 h. Upon stirring, bright yellow solids precipitated. The solution was cooled briefly (5 minutes) and then filtered over a Buchner funnel. The yellow solids were washed with AcOH (3x2 mL) and then washed with $Et_2O$ (8x3 mL). Drying in vacuo afforded a yellow solid (58 %). A small portion was set aside, with the rest immediately used in the next step. The intermediate (0.317 g) was dissolved in DCM (100 mL) in an Erlenmeyer flask. A solution of excess potassium oxalate hydrate in water (4 mL) was added. The biphasic reaction was stirred vigorously for 1 h. The organic layer was separated and dried over $Na_2SO_4$, filtered, and concentrated to give a bright yellow solid (0.206 g, 80%, 69% over two steps). **$^1H$ NMR** (500 MHz, $d_2$-TCE, 100 °C): δ 7.77 (d, $J$ = 7.9 Hz, 2H, ArH), 7.39 (d, $J$ = 10.6 Hz, 2H, ArH), 7.28 (br s, 2H, ArH), 7.11 (d, $J$ = 7.5 Hz, 4H, ArH), 7.02 (m, 2H, ArH), 6.88–6.58 (m, 8H, ArH), 6.36 (br s, 2H, ArH), 1.85 (br s, 12H, $C(CH_3)_2$). **$^{13}C\{^1H\}$ NMR** (125 MHz, $d_2$-TCE, 100 °C): δ 159.9 (d, $J_{CF}$ = 241.8 Hz), 148.8, 141.2, 130.1, 127.7, 126.9, 126.6 (br s), 126.2, 124.2, 122.7 (br s), 119.3 (br s), 114.2 (d, $J_{CF}$ = 21.8 Hz),

112.9 (d, $J_{CF}$ = 21.8 Hz), 42.8, 28.4 (br s). **HRMS** (DART) *m/z* calc for $C_{42}H_{35}N_2F_2$ $(M+H)^+$: 605.2762, found 605.2762.

***rac*-(ArN=C(An)C=NAr)NiBr$_2$ (Ar = 4-fluoro-2-(2-phenylpropan-2-yl)phenyl; An = acenaphthene) (4.3). L-4.3** (0.388 g, 0.642 mmol) and (DME)$NiBr_2$ (0.198 g, 0.0.642 mmol) were combined under $N_2$. $CH_2Cl_2$ (ca. 15mL) was added to afford a dark red solution, which was allowed to stir for 18 h. The reaction mixture was filtered through Celite® under $N_2$ and volatiles were then removed *in vacuo*. The crude red solid was redissolved in $CH_2Cl_2$ and layered with hexanes to afford a dark red microcrystalline solid (0.092 g, 17%).

**4-OMe-2-(2-phenylpropan-2-yl)aniline (AN-4.4).** $CF_3SO_3H$ (0.30 mL, 3.38 mmol) was added to a mixture of *p*-anisidine (3.13 g, 25.4 mmol) and α-methylstyrene (2.20 mL, 16.9 mmol). The mixture was heated to 160 °C and allowed to react for 20 h. The crude product was chromatographed on silica (90:10 hexanes:ethyl acetate) and dried in vacuo to afford a light beige solid (2.77 g, 68%). **$^1$H NMR** (500 MHz, $CDCl_3$): δ 7.32–7.27 (m, 4H, ArH), 7.24–7.18 (m, 2H, ArH), 7.10 (d, *J* = 2.8 Hz, 1H, ArH), 6.67 (dd, *J* = 2.9 Hz, *J* = 8.5 Hz, 1H, ArH), 6.50 (d, *J* = 8.5 Hz, 1H, ArH) 3.81 (s, 3H, $OCH_3$), 2.90 (s, 2H, $NH_2$), 1.69 (s, 6H, $C(CH_3)_2$). **$^{13}$C{$^1$H} NMR** (125 MHz, $CDCl_3$): δ 152.6, 149.2, 138.3, 135.5, 128.9, 126.3, 126.0, 118.3, 114.0, 111.5, 55.8, 42.6, 29.1. **HRMS** (DART) *m/z* calc for $C_{16}H_{20}NO$ $(M+H)^+$: 242.1545, found 242.2544.

***rac*-ArN=C(An)C=NAr (Ar = 4-OMe-2-(2-phenylpropan-2-yl)phenyl; An = acenaphthene) (L-4.4).** 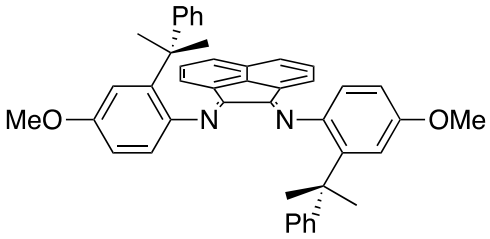

In a sealed vial a mixture of **AN-4.4** (0.600 g, 2.49 mmol), acenaphthenequinone (0.216 g, 1.18 mmol), and glacial acetic acid (0.43 mL, 7.58 mmol) in toluene (3.1 mL) was heated and stirred at 100 °C for 16 h. The solution was removed from heat for 5 minutes, followed by filtration over Celite® and washing with $CH_2Cl_2$. Volatiles were removed in vacuo until a sticky, orange solid was obtained. The crude mixture was triturated in cold hexanes (~20 mL), filtered, and then washed with copious cold hexanes (~100 mL). Drying in vacuo afforded a bright orange powder (0.191 g, 26%). **$^1$H NMR** (500 MHz, $d_2$-TCE, 100 °C): δ 7.74 (d, *J* = 7.1 Hz, 2H, ArH), 7.23 (br s, 4H, ArH), 7.15 (d, *J* = 6.7 Hz, ArH), (broad s, 12H, $C(CH_3)_2$). **$^{13}$C{$^1$H} NMR** (125 MHz, $d_2$-TCE, 100 °C): δ 158.9, 156.6, 149.4, 144.0, 140.6, 130.1, 128.9, 127.3, 126.8, 126.5, 126.3, 124.0, 122.6, 119.1, 114.4, 111.1, 55.5, 42.9, 28.6. **HRMS** (DART) *m/z* calc for $C_{44}H_{41}N_2O_2$ $(M+H)^+$: 629.3162, found 629.3177.

***rac*-(ArN=C(An)C=NAr)NiBr$_2$ (Ar = 4-OMe-2-(2-phenylpropan-2-yl)phenyl; An = acenaphthene) (4.4). L-4.4** 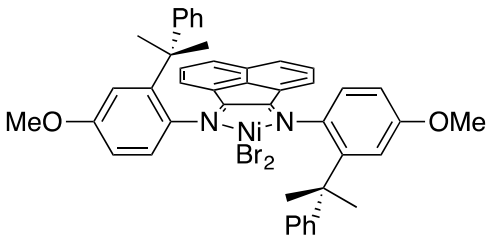

(0.191 g, 0.304 mmol) and (DME)$NiBr_2$ (0.092 g, 0.298 mmol) were combined under $N_2$ in a Schlenk flask. $CH_2Cl_2$ (7 mL) was added to afford a dark red solution, which was allowed to stir at 22 °C for 18 hours. The reaction mixture was filtered through Celite® under $N_2$ and volatiles were removed *in vacuo*. The crude red solid was redissolved in $CH_2Cl_2$ and layered with hexanes to afford dark red blocky

crystals (0.155 g, 62%).

**4-$^t$Bu-2-(2-phenylpropan-2-yl)aniline (AN-4.5).** $CF_3SO_3H$ (0.10 mL, 1.1 mmol) was added to a mixture of 4-*tert*-butyl-aniline (2.52 g, 16.9 mmol) and α-methylstyrene (0.40 g, 3.4 mmol). The mixture was heated to 160 °C and allowed to react for 20 hours before it was diluted with EtOAc and washed with a saturated solution of $NaHCO_3$. The organic solution was dried over $Na_2SO_4$, filtered, and concentrated to give a crude brown oil. The crude product was chromatographed on silica (95:5 hexanes/ethyl acetate) to give a pale yellow oil (0.399 g, 44%). **$^1$H NMR** (400 MHz, $CDCl_3$): δ 7.45 (d, *J* = 2.3 Hz, 1H), 7.30 – 7.21 (m, 4H), 7.19 – 7.11 (m, 1H), 7.06 (dd, *J* = 8.2, 2.3 Hz, 1H), 6.44 (d, *J* = 8.2 Hz, 1H), 2.98 (br s, 2H), 1.65 (s, 6H), 1.30 (s, 9H). **$^{13}$C{$^1$H} NMR** (125 MHz, $CDCl_3$): δ 149.6, 141.9, 140.9, 133.0, 128.8, 126.1, 125.9, 124.0, 123.3, 117.1, 42.6, 34.2, 31.8, 29.2. **HRMS** (DART) *m/z* calc for $C_{19}H_{26}N$ $(M+H)^+$: 268.2065, found 268.2061.

***rac*-ArN=C(An)C=NAr (Ar = 4-$^t$Bu-2-(2-phenylpropan-2-yl)phenyl; An = acenaphthene) (L-4.5).** In a sealed vial a mixture of **AN-4.5** (0.399 g, 1.5 mmol), acenaphthenequinone (0.108 g, 0.60 mmol), and $ZnCl_2$ (0.092 g, 0.67 mmol) in glacial acetic acid (3 mL) was heated to 130 °C with stirring for 2 h. Upon cooling to room temperature, a brown solid crashed out. The solid was filtered and washed with $Et_2O$. The solid was then dissolved in DCM (5 mL) and added to a solution of water (5 mL) and excess potassium oxalate hydrate. The biphasic reaction was stirred vigorously for 12 h. The organic layer was separated and dried over $Na_2SO_4$, filtered, and concentrated to give a red orange solid (0.260 g, 64%). **$^1$H NMR** (400 MHz, $CDCl_3$): δ 7.71 – 7.60 (m, 4H),

7.28 (s, 2H), 7.14 (t, *J* = 7.7 Hz, 2H), 7.06 (d, *J* = 7.9 Hz, 4H), 6.71 (d, *J* = 8.1 Hz, 2H), 6.48 (d, *J* = 8.3 Hz, 4H), 6.14 (s, 2H), 1.82 (s, 12H), 1.44 (s, 18H). **$^{13}C\{^{1}H\}$ NMR** (125 MHz, $CDCl_3$): δ 158.8, 150.0, 148.1, 146.93, 141.1, 138.1, 130.1, 129.1, 127.5, 126.9, 126.7, 126.6, 124.0, 123.8, 123.6, 123.1, 117.9, 43.0, 34.8, 31.9. **HRMS** (DART) *m/z* calc for $C_{50}H_{53}N_2$ $(M+H)^+$: 681.4209, found 681.4208.

***rac*-(ArN=C(An)C=NAr)NiBr$_2$ (Ar = 4-$^t$Bu-2-(2-phenylpropan-2-yl)phenyl; An = acenaphthene) (4.5). L-5** (0.260 g, 0.38 mmol) and (DME)$NiBr_2$ (0.117 g, 0.38 mmol) were combined under $N_2$. $CH_2Cl_2$ (~ 5 mL) was added to afford a dark red solution, which was allowed to stir for 18 h. The reaction mixture was filtered through Celite® under $N_2$ and volatiles were then removed *in vacuo*. The crude red solid was redissolved in a minimum amount of $CH_2Cl_2$ and layered with hexanes (4 x the volume of DCM) to afford a dark red crystalline solid (0.226 g, 66%).

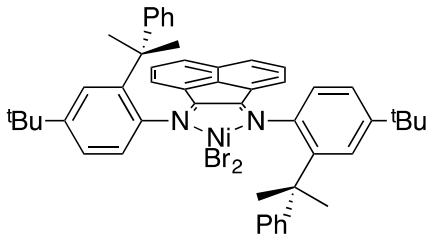


**4-$^t$Bu-2-(2-(naphthalen-1-yl)propan-2-yl)aniline (AN-4.7).** $CF_3SO_3H$ (0.40 mL, 4.5 mmol) was added to a mixture of 4-*tert*-butyl-aniline (12.0 g, 80.4 mmol) and 1-(prop-1-en-2-yl)naphthalene (2.54 g, 15.1 mmol) and 2 mL xylenes. The mixture was heated to 160 °C and allowed to react for 20 h. The material was then cooled to room temperature and washed with a saturated solution of $NaHCO_3$ and dried over $Na_2SO_4$. The crude product was chromatographed on silica (95:5 hexanes:ethyl acetate) to give an off-white solid (596 mg, 12%). **$^1$H NMR** (500 MHz, $CDCl_3$): δ 7.90 (d, *J* = 8.8 Hz, 1H), 7.84 – 7.81 (m, 2H), 7.80 (d, *J* = 8.2 Hz, 1H), 7.73 (d, *J* = 2.3 Hz, 1H), 7.52 (t, *J* = 7.8 Hz, 1H), 7.36 (ddd, *J* = 8.0, 6.7, 1.1 Hz, 1H), 7.13 (ddd, *J* = 8.5, 6.8, 1.4 Hz, 1H),

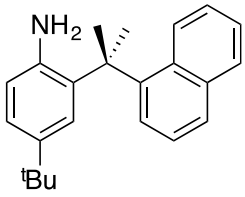

7.08 (dd, *J* = 8.2, 2.3 Hz, 1H), 6.35 (d, *J* = 8.1 Hz, 1H), 3.03 (s, 2H), 1.94 (s, 6H), 1.44 (s, 9H). **$^{13}C\{^{1}H\}$ NMR** (125 MHz, $CDCl_3$): δ 145.3, 142.0, 141.7, 134.9, 133.3, 131.4, 129.0, 128.2, 125.9, 125.5, 125.4, 125.0, 123.8, 123.1, 122.6, 117.1, 43.2, 34.4, 31.9. **HRMS** (DART) *m/z* calc for $C_{23}H_{28}N$ $(M+H)^+$: 318.2222, found 318.2215.

***rac*-ArN=C(An)C=NAr (Ar = 4-$^{t}$Bu-2-(2-(naphthalen-1-yl)propan-2-yl)aniline; An = acenaphthene) (L-4.7).** 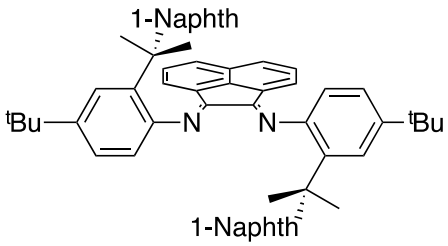

In a sealed vial a mixture of **AN-4.7** (0.597 g, 1.9 mmol), acenaphthenequinone (0.114 g, 0.62 mmol), glacial acetic acid (0.244 g, 4.1 mmol) were dissolved in anhydrous PhMe (3 mL). 4Å mol sieves were added and the solution was heated to 130 °C with stirring for 12 h. After cooling to room temperature, a crude solution was purified by column chromatography (95:5 hexanes/ethyl acetate) with no additional workup. Analytical samples were prepared by dissolving the purified material in a minimum amount of DCM and layering with MeOH, producing orange needles upon crystallization (180 mg, 37%). **$^{1}H$ NMR** (500 MHz, $d_2$-TCE, 100 °C): δ 8.01 (d, *J* = 8.6 Hz, 2H), 7.85 (br s, 2H), 7.58 (d, *J* = 7.4 Hz, 2H), 7.45 (br s, 2H), 7.32 (d, *J* = 8.1 Hz, 2H), 7.12 – 6.96 (m, 8H), 6.92 – 6.70 (m, 6H), 6.25 (br s, 2H), 2.10 (br s, 12H), 1.50 (br s, 18H). **$^{13}C\{^{1}H\}$ NMR** (125 MHz, $d_2$-TCE, 100 °C): δ 157.7, 147.1, 146.9, 145.5, 140.1, 138.3, 134.2, 131.0, 129.5, 128.3, 126.8, 126.4, 125.9, 124.3, 124.3, 123.8, 123.4, 123.4, 122.7, 121.8, 117.7, 43.8, 34.3, 31.4, 29.2. **HRMS** (DART) *m/z* calc for $C_{58}H_{57}N_2$ $(M+H)^+$: 781.4522, found 781.4532.

***rac*-(ArN=C(An)C=NAr)NiBr$_2$ (Ar = 4-$^t$Bu-2-(2-(naphthalen-1-yl)propan-2-yl)aniline; An = acenaphthene) (4.7). L-4.7** 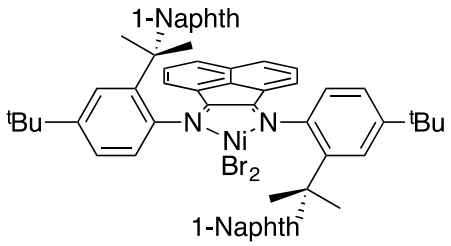

(0.180 g, 0.231 mmol) and (DME)NiBr$_2$ (0.071 g, 0.231 mmol) were combined under $N_2$. $CH_2Cl_2$ (~ 15 mL) was added to afford a dark red solution, which was allowed to stir at 23 °C for 18 h. The reaction mixture was filtered through Celite® under $N_2$ and volatiles were then removed *in vacuo*. The crude red solid was then dissolved in a minimum amount of DCM and layered with 4x the volume of hexanes to afford red needles (0.116 g, 50%).

### *4.4.3 General Procedure for the Polymerization of 1-Butene*

A 60 mL Fisher Porter tube was charged with a stir bar and d-MAO (0.060 g, 1.0 mmol) under $N_2$. 1-Butene (3.0 g ± 0.2 g, 0.05 mol) was condensed into the vessel at −78 °C. The reaction vessel was then transferred to a cooling bath at −40 °C and the solution was allowed to equilibrate at this temperature for 15 min. The appropriate pre-catalyst (10 $\mu$mol) was dissolved in 2 mL of DCM, drawn into a gas-tight syringe and then injected to initiate the polymerization. The reaction was stirred at −40 °C for 24 h before quenching with ~2 mL MeOH. The polymer was precipitated with copious amounts of acidic methanol (5% HCl/MeOH), followed by stirring of the suspension until the color faded, giving a white suspension. The polymer was filtered, washed with methanol, and dried to constant weight *in vacuo.*

### *4.4.4 $^{13}C$ NMR Assignments*

Signals were assigned based on DEPT-135 and previous assignments performed in the literature.[19] Chemical shifts were normalized to the residual nondeuterated tetrachloroethane signal at 73.78 ppm. The naming convention developed by Usami and Takayama is listed in the table below.[20] Common structural motifs found in these polymers are also drawn below with their respective peak assignments for clarity.

**Table 4.6** Signal Assignments for Poly(Butene) Produced in this Study

| Peak Letter | Chemical Shift (ppm) | Assignment (xBn) | Reference |
|---|---|---|---|
| **A** | 19.26–19.76 | $1B_1$ | 19a |
| **B** | 32.71–33.49 | $brB_1$ | 19a |
| **C** | 33.78–34.36 | $\alpha\beta B_1$ | 19a |
| **D** | 36.48–37.54 | $\alpha B_1$ | 19b |
| **E** | 26.25–27.30 | $\beta B_1$ | 19c |
| **F** | 25.65 | $\gamma B_1$ | 19c |
| **G** | 29.25 | $\delta B_{1\text{-}n}$ | 19b, 19c |
| **H** | 10.22–10.68 | $1B_2$ | 19b |
| **I** | 26.25–27.30 | $2B_2$ | 19b |
| **J** | 36.97 | $brB_2$ | This Work |
| **K** | 41.70 | $\alpha\alpha B_1B_2$ | 19c |
| **L** | 30.68 | $brB_1$ | 19d |
| **M** | 19.96 | $1B_1$ | 19d |
| **N** | 39.01 | $brB_2$ | 19c |

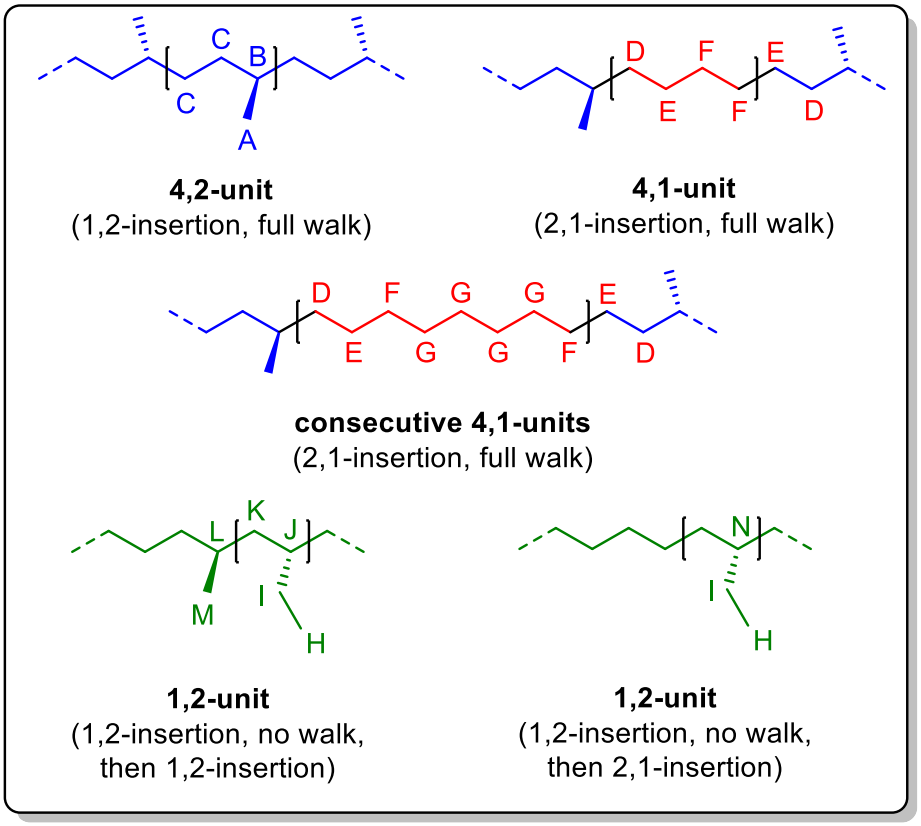


**Figure 4.5** Branching structures found in poly(1-butene) produced in this study.

### *4.4.5 Derivation of Equations for Calculating Enchainments*

Signals A, B, and C all arise from the main 4,2-poly(1-butene) structure which comes from ω,2-enchainment. Signals L and M are included as part of ω,2-enchainment because they are part of a 4,2-unit. If ω,1-enchainment occurs after ω,2-enchainment, signals D, E, and F are installed. However, this enchainment causes signals C from the 4,2-unit to change into D and E. When ω,2-enchainment occurs after ω,1-enchainment, additional D and E signals are observed which are associated with the 4,1-unit. This means that half of the signals from D and E are associated with a 4,2-unit and the other half with a 4,1-unit. Thus. we split the integrations for these signals between ω,2 and ω,1-enchainment. Successive ω,1-enchainments lead to signal G in the 4,1-unit. Signals

H, I, J, K and N all arise solely from 1,2-enchainment. There is evidence of a small portion of isolated ethyl branches in these materials which give signals H, I, N, and D. We chose not to correct for D in this situation since the effect of the correction is very small. In some cases, there are signs of longer chain branches that arise from multiple insertion pathways. These are small and not included in the main calculations.

$$(\omega,2) = \frac{[A+B+C+0.5(D+E)+L+M]}{\Sigma(A–N)}$$

$$(\omega,1) = \frac{[0.5(D+E)+F+G]}{\Sigma(A–N)}$$

$$(1,2) = \frac{[H+I+J+K+N]}{\Sigma(A–N)}$$

**Figure 4.6** Equations used to calculate values for enchainment pathways.

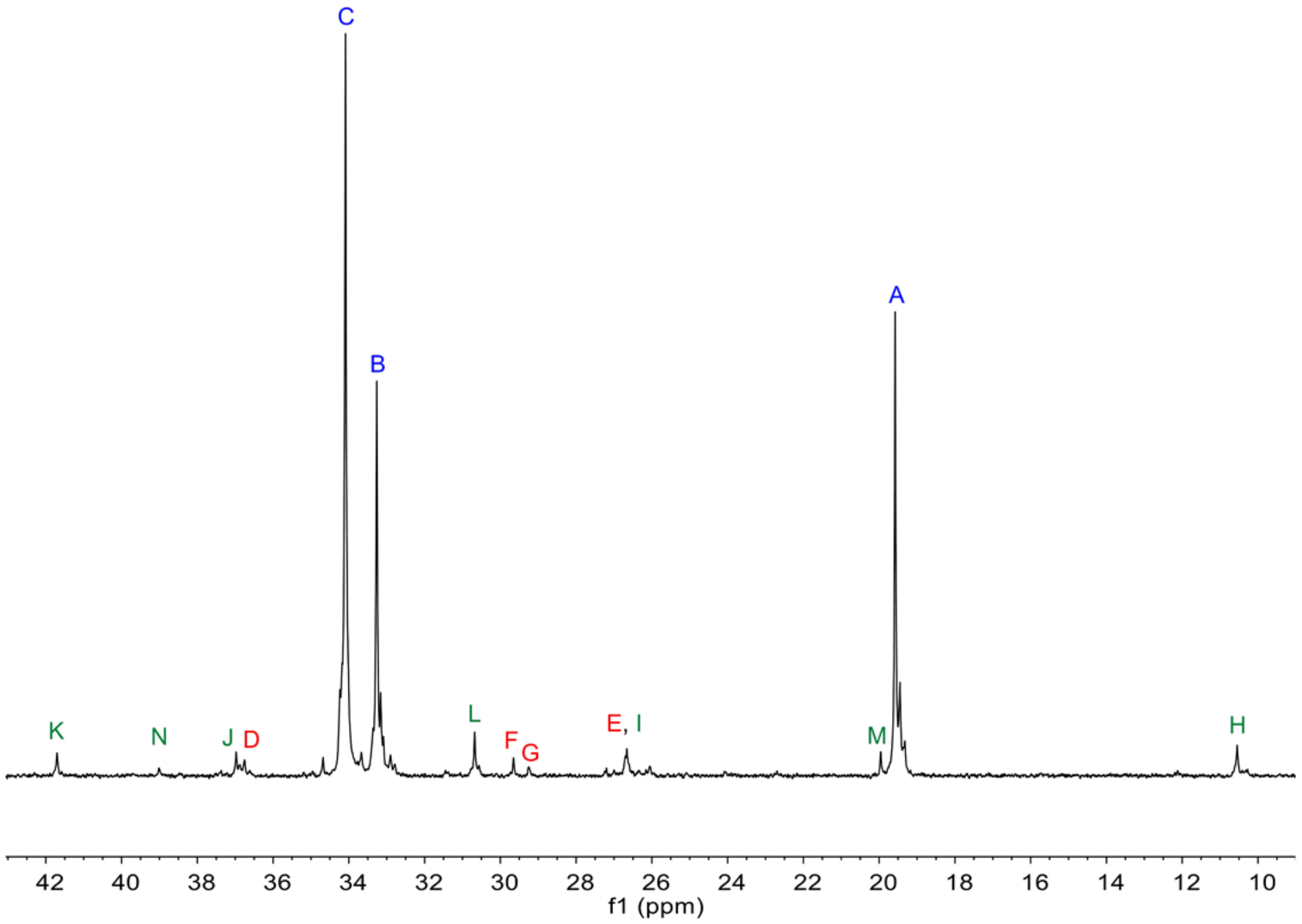


**Figure 4.7** $^{13}$C NMR spectrum of 4,2-poly(1-butene) produced by complex **4.4** (Table 4.1, entry 4).

### *4.4.6 Differential Scanning Calorimetry Traces of Select 4,2-Poly(1-Butene) Samples*

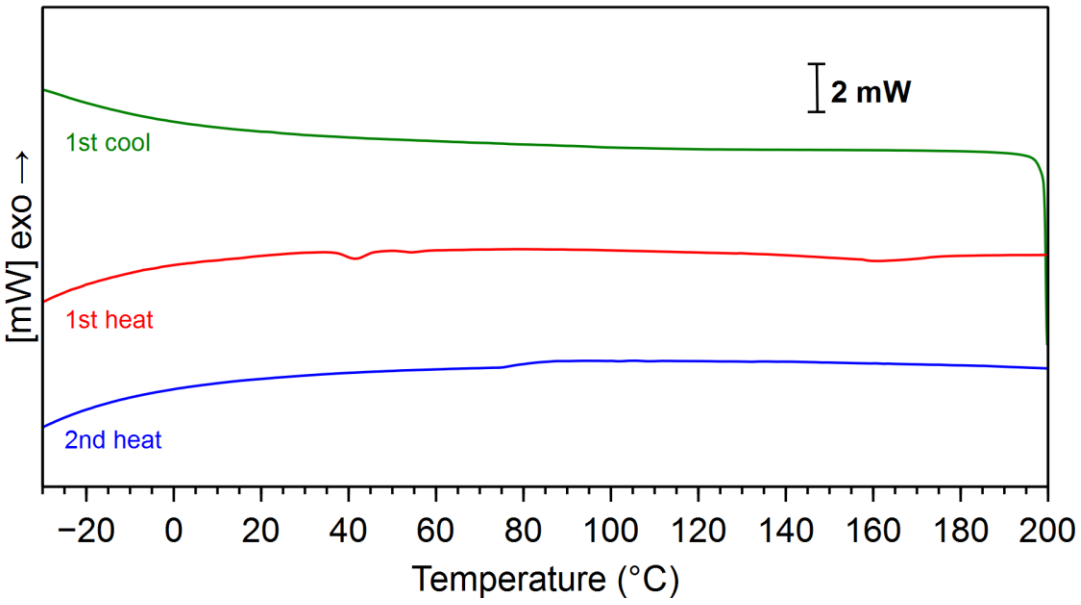


**Figure 4.8** DSC trace of atactic 4,2-poly(1-butene) produced by complex **4.1** (Table 4.1, entry 1).

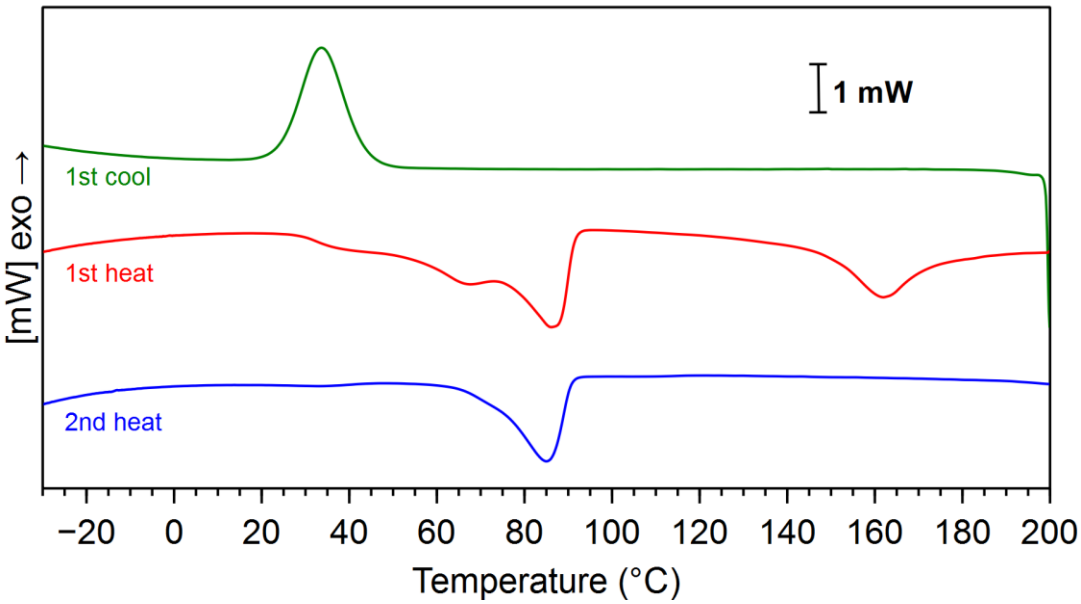


**Figure 4.9** DSC trace of *iso*-4,2-poly(1-butene) produced by complex **4.5** (Table 4.1, entry 5).

### *4.4.7 Crystal Structure Data for Complex **4.5***

**Front View**

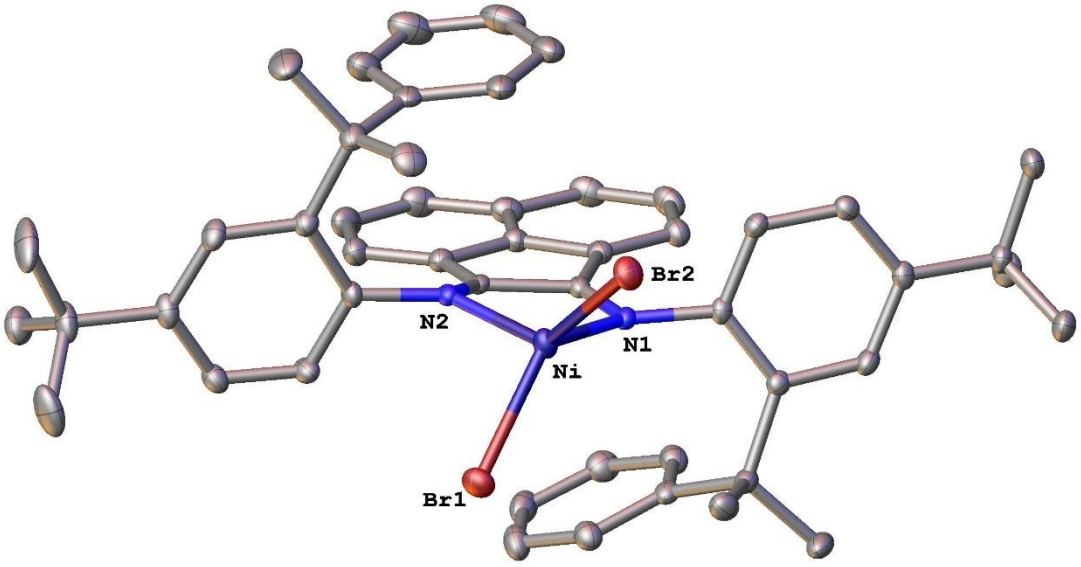


**Side View**

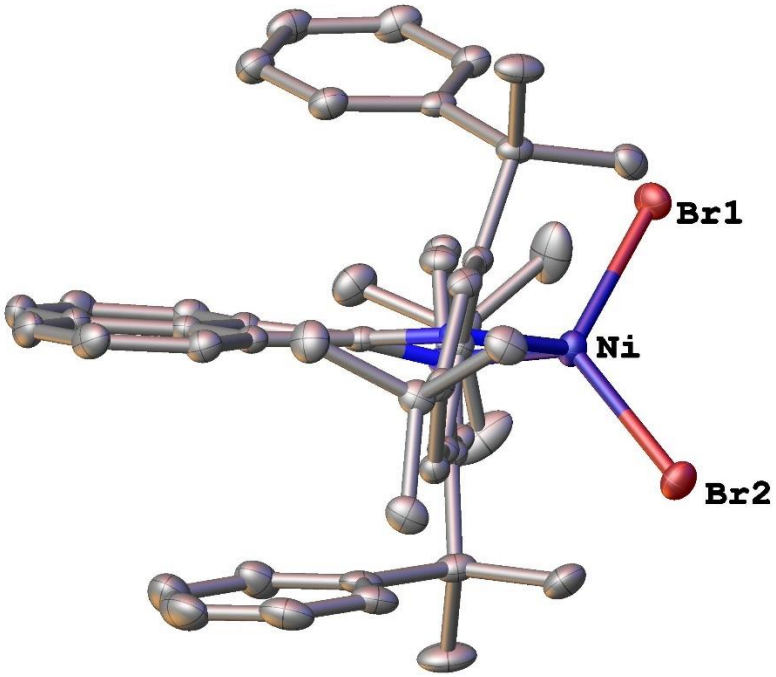

**Table 4.7** Crystal Data and Structure Refinement for **4.5**

| | | |
|---|---|---|
| Identification code | rdv1_abs2 | |
| Empirical formula | C50 H52 Br2 N2 Ni | |
| Formula weight | 899.46 | |
| Temperature | 100.01(10) K | |
| Wavelength | 1.54184 Å | |
| Crystal system | Monoclinic | |
| Space group | P 1 21/c 1 | |
| Unit cell dimensions | a = 9.04574(5) Å | a= 90°. |
| | b = 25.29692(13) Å | b= 103.1909(5)°. |
| | c = 19.03833(11) Å | g = 90°. |
| Volume | 4241.58(4) $Å^3$ | |
| Z | 4 | |
| Density (calculated) | 1.409 $Mg/m^3$ | |
| Absorption coefficient | 3.134 $mm^{-1}$ | |
| F(000) | 1856 | |
| Crystal size | 0.198 x 0.08 x 0.019 $mm^3$ | |
| Theta range for data collection | 2.956 to 70.075°. | |
| Index ranges | -11<=h<=8, -26<=k<=30, -22<=l<=23 | |
| Reflections collected | 36578 | |
| Independent reflections | 8040 [R(int) = 0.0259] | |
| Completeness to theta = 67.684° | 100.0 % | |
| Absorption correction | Gaussian | |
| Max. and min. transmission | 1.000 and 0.628 | |
| Refinement method | Full-matrix least-squares on $F^2$ | |
| Data / restraints / parameters | 8040 / 0 / 506 | |
| Goodness-of-fit on $F^2$ | 1.036 | |
| Final R indices [I>2sigma(I)] | R1 = 0.0254, wR2 = 0.0661 | |
| R indices (all data) | R1 = 0.0274, wR2 = 0.0671 | |
| Extinction coefficient | n/a | |
| Largest diff. peak and hole | 0.673 and -0.416 $e.Å^{-3}$ | |

**Table 4.8** Atomic Coordinates ( x $10^4$) and Equivalent Isotropic Displacement Parameters ($Å^2$x $10^3$) for **4.5**, where U(eq) is Defined as One Third of the Trace of the Orthogonalized $U^{ij}$ Tensor

| | x | y | z | U(eq) |
|---|---|---|---|---|
| Br(1) | 4210(1) | 2760(1) | 7917(1) | 24(1) |
| Br(2) | 7352(1) | 3023(1) | 6740(1) | 23(1) |
| Ni | 4806(1) | 2930(1) | 6803(1) | 18(1) |
| N(1) | 4012(1) | 2490(1) | 5904(1) | 14(1) |
| N(2) | 2941(1) | 3385(1) | 6386(1) | 14(1) |
| C(1) | 2067(2) | 1746(1) | 6909(1) | 22(1) |
| C(2) | 585(2) | 1925(1) | 6848(1) | 27(1) |
| C(3) | -476(2) | 1877(1) | 6203(1) | 26(1) |
| C(4) | -58(2) | 1639(1) | 5622(1) | 26(1) |
| C(5) | 1415(2) | 1460(1) | 5683(1) | 22(1) |
| C(6) | 2509(2) | 1519(1) | 6322(1) | 18(1) |
| C(7) | 4137(2) | 1330(1) | 6358(1) | 18(1) |
| C(8) | 4721(2) | 1548(1) | 5716(1) | 16(1) |
| C(9) | 5310(2) | 1212(1) | 5267(1) | 18(1) |
| C(10) | 5984(2) | 1385(1) | 4715(1) | 16(1) |
| C(11) | 6134(2) | 1926(1) | 4635(1) | 16(1) |
| C(12) | 5513(2) | 2275(1) | 5053(1) | 16(1) |
| C(13) | 4761(2) | 2092(1) | 5564(1) | 14(1) |
| C(14) | 5274(2) | 1502(1) | 7050(1) | 23(1) |
| C(15) | 4098(2) | 721(1) | 6358(1) | 26(1) |
| C(16) | 6451(2) | 978(1) | 4208(1) | 20(1) |
| C(17) | 4992(2) | 736(1) | 3742(1) | 26(1) |
| C(18) | 7419(2) | 537(1) | 4643(1) | 24(1) |
| C(19) | 7356(2) | 1227(1) | 3704(1) | 24(1) |
| C(20) | 2776(2) | 2691(1) | 5527(1) | 14(1) |
| C(21) | 1765(2) | 2572(1) | 4826(1) | 16(1) |
| C(22) | 1805(2) | 2231(1) | 4267(1) | 19(1) |
| C(23) | 544(2) | 2223(1) | 3670(1) | 24(1) |
| C(24) | -705(2) | 2539(1) | 3628(1) | 24(1) |
| C(25) | -773(2) | 2898(1) | 4191(1) | 21(1) |

| | | | | |
|---|---|---|---|---|
| C(26) | -1973(2) | 3254(1) | 4221(1) | 25(1) |
| C(27) | -1870(2) | 3584(1) | 4806(1) | 26(1) |
| C(28) | -588(2) | 3591(1) | 5394(1) | 21(1) |
| C(29) | 592(2) | 3251(1) | 5376(1) | 17(1) |
| C(30) | 484(2) | 2906(1) | 4778(1) | 17(1) |
| C(31) | 2095(2) | 3152(1) | 5842(1) | 14(1) |
| C(32) | 2327(2) | 3823(1) | 6715(1) | 16(1) |
| C(33) | 1291(2) | 3693(1) | 7126(1) | 19(1) |
| C(34) | 680(2) | 4079(1) | 7489(1) | 21(1) |
| C(35) | 1106(2) | 4606(1) | 7455(1) | 20(1) |
| C(36) | 2112(2) | 4727(1) | 7023(1) | 20(1) |
| C(37) | 2745(2) | 4350(1) | 6638(1) | 17(1) |
| C(38) | 3863(2) | 4517(1) | 6176(1) | 22(1) |
| C(39) | 3339(2) | 4292(1) | 5409(1) | 22(1) |
| C(40) | 1959(2) | 4458(1) | 4979(1) | 31(1) |
| C(41) | 1447(2) | 4274(1) | 4280(1) | 39(1) |
| C(42) | 2311(3) | 3914(1) | 3995(1) | 38(1) |
| C(43) | 3676(2) | 3742(1) | 4414(1) | 32(1) |
| C(44) | 4194(2) | 3930(1) | 5115(1) | 25(1) |
| C(45) | 453(2) | 5029(1) | 7876(1) | 26(1) |
| C(46) | 1143(2) | 5576(1) | 7822(2) | 44(1) |
| C(47) | 755(2) | 4867(1) | 8675(1) | 40(1) |
| C(48) | -1262(2) | 5066(1) | 7575(1) | 29(1) |
| C(49) | 5454(2) | 4334(1) | 6562(1) | 28(1) |
| C(50) | 3957(2) | 5124(1) | 6104(1) | 35(1) |

**Table 4.9** Lengths [Å] and Angles [°] for **4.5**

| | | | |
|---|---|---|---|
| Br(1)-Ni | 2.3446(3) | C(12)-C(13) | 1.387(2) |
| Br(2)-Ni | 2.3449(3) | C(14)-H(14A) | 0.9600 |
| Ni-N(1) | 2.0310(13) | C(14)-H(14B) | 0.9600 |
| Ni-N(2) | 2.0473(13) | C(14)-H(14C) | 0.9600 |
| N(1)-C(13) | 1.4460(19) | C(15)-H(15A) | 0.9600 |
| N(1)-C(20) | 1.288(2) | C(15)-H(15B) | 0.9600 |
| N(2)-C(31) | 1.282(2) | C(15)-H(15C) | 0.9600 |
| N(2)-C(32) | 1.4442(19) | C(16)-C(17) | 1.539(2) |
| C(1)-H(1) | 0.9300 | C(16)-C(18) | 1.538(2) |
| C(1)-C(2) | 1.395(2) | C(16)-C(19) | 1.533(2) |
| C(1)-C(6) | 1.393(2) | C(17)-H(17A) | 0.9600 |
| C(2)-H(2) | 0.9300 | C(17)-H(17B) | 0.9600 |
| C(2)-C(3) | 1.381(3) | C(17)-H(17C) | 0.9600 |
| C(3)-H(3) | 0.9300 | C(18)-H(18A) | 0.9600 |
| C(3)-C(4) | 1.385(3) | C(18)-H(18B) | 0.9600 |
| C(4)-H(4) | 0.9300 | C(18)-H(18C) | 0.9600 |
| C(4)-C(5) | 1.387(2) | C(19)-H(19A) | 0.9600 |
| C(5)-H(5) | 0.9300 | C(19)-H(19B) | 0.9600 |
| C(5)-C(6) | 1.390(2) | C(19)-H(19C) | 0.9600 |
| C(6)-C(7) | 1.535(2) | C(20)-C(21) | 1.467(2) |
| C(7)-C(8) | 1.540(2) | C(20)-C(31) | 1.506(2) |
| C(7)-C(14) | 1.538(2) | C(21)-C(22) | 1.377(2) |
| C(7)-C(15) | 1.540(2) | C(21)-C(30) | 1.421(2) |
| C(8)-C(9) | 1.396(2) | C(22)-H(22) | 0.9300 |
| C(8)-C(13) | 1.408(2) | C(22)-C(23) | 1.414(2) |
| C(9)-H(9) | 0.9300 | C(23)-H(23) | 0.9300 |
| C(9)-C(10) | 1.400(2) | C(23)-C(24) | 1.371(3) |
| C(10)-C(11) | 1.386(2) | C(24)-H(24) | 0.9300 |
| C(10)-C(16) | 1.536(2) | C(24)-C(25) | 1.417(2) |
| C(11)-H(11) | 0.9300 | C(25)-C(26) | 1.420(2) |
| C(11)-C(12) | 1.391(2) | C(25)-C(30) | 1.402(2) |
| C(12)-H(12) | 0.9300 | C(26)-H(26) | 0.9300 |
| C(26)-C(27) | 1.380(3) | C(45)-C(48) | 1.529(2) |

| | | | |
|---|---|---|---|
| C(27)-H(27) | 0.9300 | C(46)-H(46A) | 0.9600 |
| C(27)-C(28) | 1.415(2) | C(46)-H(46B) | 0.9600 |
| C(28)-H(28) | 0.9300 | C(46)-H(46C) | 0.9600 |
| C(28)-C(29) | 1.378(2) | C(47)-H(47A) | 0.9600 |
| C(29)-C(30) | 1.419(2) | C(47)-H(47B) | 0.9600 |
| C(29)-C(31) | 1.466(2) | C(47)-H(47C) | 0.9600 |
| C(32)-C(33) | 1.392(2) | C(48)-H(48A) | 0.9600 |
| C(32)-C(37) | 1.403(2) | C(48)-H(48B) | 0.9600 |
| C(33)-H(33) | 0.9300 | C(48)-H(48C) | 0.9600 |
| C(33)-C(34) | 1.383(2) | C(49)-H(49A) | 0.9600 |
| C(34)-H(34) | 0.9300 | C(49)-H(49B) | 0.9600 |
| C(34)-C(35) | 1.393(2) | C(49)-H(49C) | 0.9600 |
| C(35)-C(36) | 1.393(2) | C(50)-H(50A) | 0.9600 |
| C(35)-C(45) | 1.533(2) | C(50)-H(50B) | 0.9600 |
| C(36)-H(36) | 0.9300 | C(50)-H(50C) | 0.9600 |
| C(36)-C(37) | 1.401(2) | | |
| C(37)-C(38) | 1.543(2) | Br(1)-Ni-Br(2) | 119.735(13) |
| C(38)-C(39) | 1.537(2) | N(1)-Ni-Br(1) | 123.48(4) |
| C(38)-C(49) | 1.531(2) | N(1)-Ni-Br(2) | 100.04(4) |
| C(38)-C(50) | 1.545(2) | N(1)-Ni-N(2) | 83.07(5) |
| C(39)-C(40) | 1.391(3) | N(2)-Ni-Br(1) | 96.59(4) |
| C(39)-C(44) | 1.397(2) | N(2)-Ni-Br(2) | 131.01(4) |
| C(40)-H(40) | 0.9300 | C(13)-N(1)-Ni | 130.34(10) |
| C(40)-C(41) | 1.385(3) | C(20)-N(1)-Ni | 110.41(10) |
| C(41)-H(41) | 0.9300 | C(20)-N(1)-C(13) | 117.45(13) |
| C(41)-C(42) | 1.389(3) | C(31)-N(2)-Ni | 109.97(10) |
| C(42)-H(42) | 0.9300 | C(31)-N(2)-C(32) | 119.06(13) |
| C(42)-C(43) | 1.378(3) | C(32)-N(2)-Ni | 128.84(10) |
| C(43)-H(43) | 0.9300 | C(2)-C(1)-H(1) | 119.6 |
| C(43)-C(44) | 1.394(3) | C(6)-C(1)-H(1) | 119.6 |
| C(44)-H(44) | 0.9300 | C(6)-C(1)-C(2) | 120.87(16) |
| C(45)-C(46) | 1.530(3) | C(1)-C(2)-H(2) | 119.8 |
| C(45)-C(47) | 1.540(3) | C(12)-C(11)-H(11) | 119.9 |
| C(3)-C(2)-H(2) | 119.8 | C(11)-C(12)-H(12) | 119.5 |
| C(2)-C(3)-H(3) | 120.4 | C(13)-C(12)-C(11) | 121.01(14) |

| | | | |
|---|---|---|---|
| C(2)-C(3)-C(4) | 119.21(16) | C(13)-C(12)-H(12) | 119.5 |
| C(4)-C(3)-H(3) | 120.4 | C(8)-C(13)-N(1) | 123.45(13) |
| C(3)-C(4)-H(4) | 119.8 | C(12)-C(13)-N(1) | 115.84(13) |
| C(3)-C(4)-C(5) | 120.39(17) | C(12)-C(13)-C(8) | 120.69(14) |
| C(5)-C(4)-H(4) | 119.8 | C(7)-C(14)-H(14A) | 109.5 |
| C(4)-C(5)-H(5) | 119.4 | C(7)-C(14)-H(14B) | 109.5 |
| C(4)-C(5)-C(6) | 121.16(16) | C(7)-C(14)-H(14C) | 109.5 |
| C(6)-C(5)-H(5) | 119.4 | H(14A)-C(14)-H(14B) | 109.5 |
| C(1)-C(6)-C(7) | 122.75(15) | H(14A)-C(14)-H(14C) | 109.5 |
| C(5)-C(6)-C(1) | 117.96(15) | H(14B)-C(14)-H(14C) | 109.5 |
| C(5)-C(6)-C(7) | 119.29(14) | C(7)-C(15)-H(15A) | 109.5 |
| C(6)-C(7)-C(8) | 110.61(13) | C(7)-C(15)-H(15B) | 109.5 |
| C(6)-C(7)-C(14) | 113.39(13) | C(7)-C(15)-H(15C) | 109.5 |
| C(6)-C(7)-C(15) | 106.85(13) | H(15A)-C(15)-H(15B) | 109.5 |
| C(14)-C(7)-C(8) | 107.19(13) | H(15A)-C(15)-H(15C) | 109.5 |
| C(14)-C(7)-C(15) | 107.03(14) | H(15B)-C(15)-H(15C) | 109.5 |
| C(15)-C(7)-C(8) | 111.77(13) | C(10)-C(16)-C(17) | 107.91(13) |
| C(9)-C(8)-C(7) | 121.05(13) | C(10)-C(16)-C(18) | 110.71(13) |
| C(9)-C(8)-C(13) | 115.98(14) | C(18)-C(16)-C(17) | 109.27(14) |
| C(13)-C(8)-C(7) | 122.91(13) | C(19)-C(16)-C(10) | 112.30(13) |
| C(8)-C(9)-H(9) | 117.9 | C(19)-C(16)-C(17) | 108.18(14) |
| C(8)-C(9)-C(10) | 124.19(14) | C(19)-C(16)-C(18) | 108.40(13) |
| C(10)-C(9)-H(9) | 117.9 | C(16)-C(17)-H(17A) | 109.5 |
| C(9)-C(10)-C(16) | 119.36(14) | C(16)-C(17)-H(17B) | 109.5 |
| C(11)-C(10)-C(9) | 117.45(14) | C(16)-C(17)-H(17C) | 109.5 |
| C(11)-C(10)-C(16) | 123.12(14) | H(17A)-C(17)-H(17B) | 109.5 |
| C(10)-C(11)-H(11) | 119.9 | H(17A)-C(17)-H(17C) | 109.5 |
| C(9)-C(8)-C(13) | 115.98(14) | H(17B)-C(17)-H(17C) | 109.5 |
| C(3)-C(2)-C(1) | 120.34(16) | C(16)-C(18)-H(18A) | 109.5 |
| C(10)-C(11)-C(12) | 120.17(14) | C(16)-C(18)-H(18B) | 109.5 |
| C(16)-C(18)-H(18C) | 109.5 | C(29)-C(28)-H(28) | 120.9 |
| H(18A)-C(18)-H(18B) | 109.5 | C(28)-C(29)-C(30) | 119.48(15) |
| H(18A)-C(18)-H(18C) | 109.5 | C(28)-C(29)-C(31) | 135.14(15) |
| H(18B)-C(18)-H(18C) | 109.5 | C(30)-C(29)-C(31) | 105.34(13) |
| C(16)-C(19)-H(19A) | 109.5 | C(25)-C(30)-C(21) | 122.92(15) |

| | | | |
|---|---|---|---|
| C(16)-C(19)-H(19B) | 109.5 | C(25)-C(30)-C(29) | 122.91(15) |
| C(16)-C(19)-H(19C) | 109.5 | C(29)-C(30)-C(21) | 114.17(14) |
| H(19A)-C(19)-H(19B) | 109.5 | N(2)-C(31)-C(20) | 117.10(13) |
| H(19A)-C(19)-H(19C) | 109.5 | N(2)-C(31)-C(29) | 135.23(14) |
| H(19B)-C(19)-H(19C) | 109.5 | C(29)-C(31)-C(20) | 107.36(13) |
| N(1)-C(20)-C(21) | 135.07(14) | C(33)-C(32)-N(2) | 115.94(13) |
| N(1)-C(20)-C(31) | 117.73(13) | C(33)-C(32)-C(37) | 121.03(14) |
| C(21)-C(20)-C(31) | 107.18(12) | C(37)-C(32)-N(2) | 123.02(13) |
| C(22)-C(21)-C(20) | 135.36(15) | C(32)-C(33)-H(33) | 119.6 |
| C(22)-C(21)-C(30) | 119.26(15) | C(34)-C(33)-C(32) | 120.71(15) |
| C(30)-C(21)-C(20) | 105.38(13) | C(34)-C(33)-H(33) | 119.6 |
| C(21)-C(22)-H(22) | 120.9 | C(33)-C(34)-H(34) | 119.8 |
| C(21)-C(22)-C(23) | 118.12(15) | C(33)-C(34)-C(35) | 120.48(15) |
| C(23)-C(22)-H(22) | 120.9 | C(35)-C(34)-H(34) | 119.8 |
| C(22)-C(23)-H(23) | 118.6 | C(34)-C(35)-C(45) | 119.97(15) |
| C(24)-C(23)-C(22) | 122.77(15) | C(36)-C(35)-C(34) | 117.51(14) |
| C(24)-C(23)-H(23) | 118.6 | C(36)-C(35)-C(45) | 122.52(15) |
| C(23)-C(24)-H(24) | 119.8 | C(35)-C(36)-H(36) | 118.0 |
| C(23)-C(24)-C(25) | 120.50(16) | C(35)-C(36)-C(37) | 124.06(15) |
| C(25)-C(24)-H(24) | 119.8 | C(37)-C(36)-H(36) | 118.0 |
| C(24)-C(25)-C(26) | 127.02(16) | C(30)-C(25)-C(26) | 116.56(15) |
| C(30)-C(25)-C(24) | 116.42(15) | C(25)-C(26)-H(26) | 119.9 |
| C(27)-C(26)-H(26) | 119.9 | C(27)-C(26)-C(25) | 120.30(16) |
| C(26)-C(27)-H(27) | 118.7 | C(37)-C(38)-C(50) | 112.24(13) |
| C(26)-C(27)-C(28) | 122.58(16) | C(39)-C(38)-C(37) | 109.89(13) |
| C(28)-C(27)-H(27) | 118.7 | C(39)-C(38)-C(50) | 107.09(15) |
| C(27)-C(28)-H(28) | 120.9 | C(49)-C(38)-C(37) | 108.09(14) |
| C(29)-C(28)-C(27) | 118.17(16) | C(49)-C(38)-C(39) | 113.36(14) |
| C(49)-C(38)-C(50) | 106.17(15) | H(47A)-C(47)-H(47B) | 109.5 |
| C(40)-C(39)-C(38) | 119.27(15) | H(47A)-C(47)-H(47C) | 109.5 |
| C(40)-C(39)-C(44) | 117.76(17) | H(47B)-C(47)-H(47C) | 109.5 |
| C(44)-C(39)-C(38) | 122.96(16) | C(45)-C(48)-H(48A) | 109.5 |
| C(39)-C(40)-H(40) | 119.2 | C(45)-C(48)-H(48B) | 109.5 |
| C(41)-C(40)-C(39) | 121.55(18) | C(45)-C(48)-H(48C) | 109.5 |
| C(41)-C(40)-H(40) | 119.2 | H(48A)-C(48)-H(48B) | 109.5 |

| | | | |
|---|---|---|---|
| C(40)-C(41)-H(41) | 120.0 | H(48A)-C(48)-H(48C) | 109.5 |
| C(40)-C(41)-C(42) | 120.0(2) | H(48B)-C(48)-H(48C) | 109.5 |
| C(42)-C(41)-H(41) | 120.0 | C(38)-C(49)-H(49A) | 109.5 |
| C(41)-C(42)-H(42) | 120.3 | C(38)-C(49)-H(49B) | 109.5 |
| C(43)-C(42)-C(41) | 119.43(19) | C(38)-C(49)-H(49C) | 109.5 |
| C(42)-C(43)-H(43) | 119.8 | H(49A)-C(49)-H(49B) | 109.5 |
| C(42)-C(43)-C(44) | 120.48(18) | H(49A)-C(49)-H(49C) | 109.5 |
| C(44)-C(43)-H(43) | 119.8 | H(49B)-C(49)-H(49C) | 109.5 |
| C(39)-C(44)-H(44) | 119.6 | C(38)-C(50)-H(50A) | 109.5 |
| C(43)-C(44)-C(39) | 120.78(18) | C(38)-C(50)-H(50B) | 109.5 |
| C(43)-C(44)-H(44) | 119.6 | C(38)-C(50)-H(50C) | 109.5 |
| C(35)-C(45)-C(47) | 109.15(15) | H(50A)-C(50)-H(50B) | 109.5 |
| C(46)-C(45)-C(35) | 112.58(15) | H(50A)-C(50)-H(50C) | 109.5 |
| C(46)-C(45)-C(47) | 108.89(17) | H(50B)-C(50)-H(50C) | 109.5 |
| C(48)-C(45)-C(35) | 109.04(14) | C(45)-C(46)-H(46A) | 109.5 |
| C(43)-C(42)-H(42) | 120.3 | C(45)-C(46)-H(46B) | 109.5 |
| C(48)-C(45)-C(46) | 108.31(16) | C(45)-C(46)-H(46C) | 109.5 |
| C(48)-C(45)-C(47) | 108.79(15) | H(46A)-C(46)-H(46B) | 109.5 |
| C(32)-C(37)-C(38) | 123.09(13) | | |
| C(36)-C(37)-C(32) | 116.11(14) | | |
| C(36)-C(37)-C(38) | 120.78(14) | | |
| H(46A)-C(46)-H(46C) | 109.5 | | |
| H(46B)-C(46)-H(46C) | 109.5 | | |
| C(45)-C(47)-H(47A) | 109.5 | | |
| C(45)-C(47)-H(47B) | 109.5 | | |
| C(45)-C(47)-H(47C) | 109.5 | | |

## REFERENCES

(1) Takai, T.; Mochizuki, D.; Umeno, M. Method of Producing Propylene Containing Biomass-Origin Carbon. Patent WO2007/55361, 2008.

(2) (a) Dürre, P. *Biotechnol. J*. **2007**, *2*, 1525–1534. (b) Kohse-Höinghaus, K.; Oßwald, P.; Cool, T. A.; Kasper, T.; Hansen, N.; Qi, F.; Westbrook, C. K.; Westmoreland, P. R. *Angew. Chem. Int. Ed.* **2010**, *49*, 3572–3597.

(3) Komon, Z. J. A.; Bu, X.; Bazan, G. C. *J. Am. Chem. Soc.* **2000**, *122*, 1830–1831.

(4) Freeman, A.; Mantell, S. C.; Davidson, J. H., *Solar Energy* **2005**, *79*, 624–637.

(5) (a) De Rosa, C.; Auriemma, F.; Resconi, L. *Angew. Chem. Int. Ed*. **2009**, *48*, 9871–9874. (b) De Rosa, C.; Auriemma, F.; Ruiz de Ballesteros, O.; Esposito, F.; Laguzza, D.; Di Girolamo, R.; Resconi, L. *Macromolecules* **2009**, *42*, 8286–8297.

(6) (a) Johnson, L. K.; Killian, C. M.; Brookhart, M. *J. Am. Chem. Soc.* **1995**, *117*, 6414–6415. (b) Gates, D. P.; Svejda, S. A.; Oñate, E.; Killian, C. M.; Johnson, L. K.; White, P. S.; Brookhart, M. *Macromolecules* **2000**, *33*, 2320–2334. (c) Ittel, S. D.; Johnson, L. K.; Brookhart, M. *Chem. Rev.* **2000**, *100*, 1169–1203. (d) Subramanyam, U.; Rajamohanan, P. R.; Sivaram, S. *Polymer* **2004**, *45*, 4063–4076. (e) Bomfim, J. A. S.; Dias, M. L.; Filgueiras, C. A. L.; Peruch, F.; Deffieux, A. *Catal. Today* **2008**, *133–135*, 879–885. (f) Camacho, D. H.; Guan, Z. *Chem. Commun.* **2010**, *46*, 7879–7893. (g) Liu, J.; Chen, D.; Wu, H.; Xiao, Z.; Gao, H.; Zhu, F.; Wu, Q. *Macromolecules* **2014**, *47*, 3325–3331. (h) Vaidya, T.; Klimovica, K.; LaPointe, A. M.; Keresztes, I.;

Lobkovsky, E. B.; Daugulis, O.; Coates, G. W. *J. Am. Chem. Soc.* **2014**, *136*, 7213–7216. (i) Wang, F.; Tanaka, R.; Cai, Z.; Nakayama, Y.; Shiono, T. *Macromol. Rapid Commun.* **2016**, *37*, 1375–1381. (j) Dai, S.; Sui, X.; Chen, C. *Chem. Commun.* **2016**, *52*, 9113–9116.

(7) (a) Tempel, D. J.; Johnson, L. K.; Huff, R. L.; White, P. S.; Brookhart, M. *J. Am. Chem. Soc.* **2000**, *122*, 6686–6700. (b) Leatherman, M. D.; Svejda, S. A.; Johnson, L. K.; Brookhart, M. *J. Am. Chem. Soc.* **2003**, *125*, 3068–3081. (c) Wang, J.; Ye, Z.; Joly, H. *Macromolecules* **2007**, *40*, 6150–6163. (d) Sun, G.; Guan, Z. *Macromolecules* **2010**, *43*, 4829–4832. (e) Xu, Y.; Xiang, P.; Ye, Z.; Wang, W.-J. *Macromolecules* **2010**, *43*, 8026–8038.

(8) McLain, S. J.; Feldman, J.; McCord, E. F.; Gardner, K. H.; Teasley, M. F.; Coughlin, E. B.; Sweetman, K. J.; Johnson, L. K.; Brookhart, M. *Macromolecules* **1998**, *31*, 6705–6707.

(9) (a) Okada, T.; Park, S.; Takeuchi, D.; Osakada, K. *Angew. Chem. Int. Ed.* **2007**, *46*, 6141–6143. (b) Okada, T.; Takeuchi, D.; Shishido, A.; Ikeda, T.; Osakada, K. *J. Am. Chem. Soc.* **2009**, *131*, 10852–10853. (c) Okada, T.; Takeuchi, D.; Osakada, K. *Macromolecules* **2010**, *43*, 7998–8006. (d) Park, S.; Okada, T.; Takeuchi, D.; Osakada, K., *Chem. Eur. J.* **2010**, *16*, 8662–8678. (e) Takeuchi, D.; Osakada, K., *Polymer* **2016**, *82*, 392–405.

(10) Mei, T.-S.; Werner, E. W.; Burckle, A. J.; Sigman, M. S. *J. Am. Chem. Soc.* **2013**, *135*, 6830–6833 (b) Mei. T.-S.; Patel, H. H.; Sigman, M. S. *Nature* **2014**, *508*, 340–344.

(11) (a) Li, H.; Rojas, G.; Wagener, K. B. *ACS Macro Lett.* **2015**, *4*, 1225–1228. (b) Rojas, G.; Berda, E.; Wagener, K. *Polymer*, **2008**, *49*, 2985–2995. (c) Sworen, J. C.; Smith, J. A.; Berg, J. M.; Wagener, K. B. *J. Am. Chem. Soc.* **2004**, *126*, 11238–11246.

(12) Cherian, A. E.; Lobkovsky, E. B.; Coates, G. W. *Chem. Commun*. **2003**, 2566–2567.

(13) We previously reported the polymerization of 1-butene using complex **1.1** activated by PMAO-IP and observed amorphous 4,2-poly(1-butene) with low tacticity: Rose, J. M.; Cherian, A. E.; Coates, G. W. *J. Am. Chem. Soc.* **2006**, *128*, 4186–4187.

(14) Detailed studies on ion paring in late transition metal complexes are limited, but ion pairing in early transition metal complexes are well documented. For a review on this topic, please refer to: Macchioni, A. *Chem. Rev*. **2005**, 105, 2039–2074.

(15) (a) Starck, P.; Rajanen, K.; Löfgren, B. *Thermochim. Acta* **2003**, *395*, 169–181. (b) Isasi, J. R.; Haigh, J. A.; Graham, J. T.; Mandelkern, L.; Alamo, R. G. *Polymer* **2000**, *41*, 8813–8823.

(16) Analogously, it has been shown that a small percentage (<5%) of branches (C1 to C4 in length) can be masked in the highly crystalline portion of high-density polyethylene. Cutler, D. J.; Hendra, P. J.; Cudby, M. E. A.; Willis, H. A. *Polymer* **1977**, *18*, 1005–1008.

(17) Ruiz-Orta, C.; Fernandez-Blazquez, J. P.; Anderson-Wile, A. M.; Coates, G. W.; Alamo, R. G. *Macromolecules* **2011**, *44*, 3436–3451.

(18) Rose, J. M.; Deplace, F.; A. Lynd, N.; Wang, Z.; Hotta, A.; Lobkovsky, E. B.; Kramer, E. J.; Coates, G. W. *Macromolecules* **2008**, *41*, 9548–9555.

(19) (a) Leatherman, M. D.; Brookhart, M. *Macromolecules* **2001**, *34*, 2748–2750. (b) Endo, K.; Kondo, Y. *J. Polym. Sci. Part A: Polym. Chem.* **2008**, *46*, 2858–2846. (c) Azoulay, J. D.; Bazan, G. C.; Galland, G. B. *Macromolecules* **2010**, *43*, 2794–2800. (d) McCord, E. F.; McLain, S. J.; Nelson, L. T. J.; Ittel, S. D.; Tempel, D.; Killian, C. M.; Johnson, L. K.; Brookhart, M. *Macromolecules* **2007**, *40*, 410–420.

(20) Usami, T.; Takayama, S. *Macromolecules* **1984**, *17*, 1756–1761.

# APPENDIX

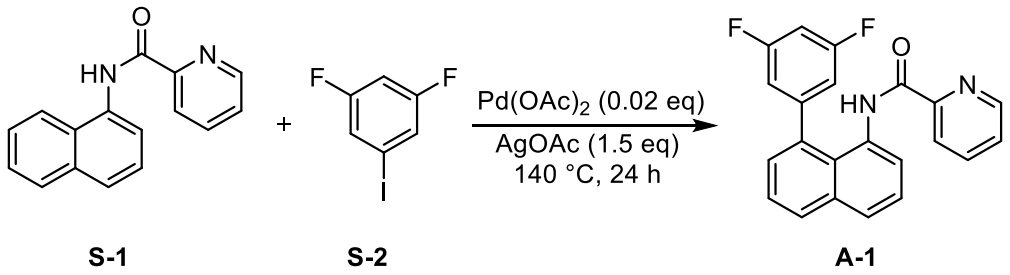


***N*-(8-(3,5-bis(fluoro)phenyl)naphtalen-1-yl)picolinamide (A-1).** *N*-(Naphthalen-1-yl)picolinamide (**S-1**) (2.0 g, 8.06 mmol), $Pd(OAc)_2$ (36.1 mg, 0.16 mmol), AgOAc (2.02 g, 12.1 mmol), and 3,5-difluoroiodobenzene (7.73 g, 32.22 mmol) were combined in a 20 mL scintillation vial equipped with a Teflon stir bar. The vial was sealed with a Teflon-coated cap, and submerged in an oil bath set to 145 °C. The reaction was stirred for 25 hours and removed from the oil bath. After cooling for 10 minutes, the mixture was filtered over a fritted funnel packed with Celite® and solids were washed with DCM until the filtrate was mostly clear (~100 mL). Volatiles were removed in vacuo, and the crude dark oil was purified by chromatography (90:10 hexanes:EtOAc). Recrystallization from hexanes afforded analytically pure material (1.90 g, in 65%). **$^1$H NMR** (400 MHz, $CDCl_3$): δ 9.50 (br s, 1H), 8.33 (d, *J* = 4.5 Hz, 1H), 8.15 (dd, *J* = 5.1, 2.1 Hz, 2H), 7.93 (d, *J* = 8.0 Hz, 1H), 7.82 (m, 2H), 7.60 (dd, *J* = 7.9 Hz, 1H), 7.49 (dd, *J* = 7.6 Hz, 1H), 7.41 (m, 1H), 7.29 (d, *J* = 7.0 Hz, 1H), 6.93 (m, 1H), 6.39 (m, 1H). **$^{13}$C{$^1$H} NMR** (125 MHz, $CDCl_3$): **δ** 163.75 ($J_{CF}$ = 13.2 Hz), 162.09, 161.77 ($J_{CF}$ = 13.2 Hz), 149.66, 147.45, 146.37 (t, *J* = 9.7 Hz), 137.45, 135.56, 135.42 (t, *J* = 2.2 Hz), 132.44, 130.16, 129.77, 127.00, 126.39 (*J* = 1.1 Hz), 125.41, 124.97, 123.96, 122.27, 112.49 (m), 102.08 (t, *J* = 25.2 Hz).

**8-(3,5-(bisfluoro)phenyl)-1-naphthalen-1-amine (A-2).** Potassium hydroxide (1.51 g, 27.0 mmol) and **A-1** (0.97 g, 2.7 mmol) were added to a round bottom flask. A solution of absolute ethanol (14 mL) and $H_2O$ (1.4 mL) were added and a reflux condenser was attached. The mixture was heated at 130 °C for 24 hours. Afterwards, the solution was cooled to room temperature, and water (~40 mL) was added. The mixture was extracted with DCM (~30 mL x3). Organics were washed with $H_2O$, combined, dried over $MgSO_4$, filtered and concentrated in vacuo. The crude product was chromatographed 95:5 hexanes:$Et_2O$, affording a red oil (0.493 g, 72%). A light purple powder was achieved upon complete removal of residual solvent. **$^1$H NMR** (400 MHz, $CDCl_3$): δ 7.82 (dd, *J* = 8.4, 1.2 Hz), 7.43–7.27 (m, 3H), 7.14 (dd, *J* = 7.0, 1.3 Hz, 1H), 7.00 (m, 2H), 6.88, (tt, *J* = 9.0, 2.3 Hz, 1H), 6.69 (dd, *J* = 7.0, 1.7 Hz, 1H), 3.69 (br s, 2H). **$^{13}$C{$^1$H} NMR** (125 MHz, $CDCl_3$): δ 163.40 (d, $J_{CF}$ = 13.0 Hz), 161.41 (d, $J_{CF}$ = 13.0 Hz), 146.85 (t, *J* = 9.4 Hz), 143.30, 135.98 (t, *J* = 2.3 Hz), 135.95, 129.69, 128.24, 126.97, 124.61, 120.35, 119.40, 112.79 (m), 111.94, 103.10 (t, *J* = 25.2 Hz).

**Bis[(8-(3,5-bisfluorophenyl)naphthylimino)acenaphthene] (A-3).** A 4 mL scintillation vial was charged with a magnetic stir bar, **A-2** (0.150 g, 0.59 mmol), acenaphthenequinone (0.049 g, 0.27 mmol), anhydrous zinc chloride (0.42 g, 0.31 mmol) and glacial acetic acid (0.5 mL). The vial was sealed with a Teflon cap, submerged in a 130 °C oil bath and stirred for 1 hour. The reaction was removed from the oil bath and cooled for ~15 minutes, revealing bright red precipitate. Solids were filtered over a Buchner funnel, washed with glacial acetic acid (3 x 3 mL)

and diethyl ether (8 x 3 mL). The red precipitate was dried in vacuo and used immediately in the next step, where it was dissolved in DCM (75 mL) in an Erlenmeyer flask. A solution of excess potassium oxalate ($K_2C_2O_4$) in $H_2O$ (~3 mL) was added to the DCM solution with vigorous stirring. After 1 hour, $H_2O$ was added (~50 mL) and the organic layer was separated, dried over MgSO4, filtered and concentrated in vacuo, affording an orange powder (0.090 g, 52%). **$^1$H NMR** (400 MHz, $CDCl_3$) δ 7.97 (dd, *J* = 8.2, 1.0 Hz, 2H), 7.84 (d, *J* = 8.1 Hz, 2H), 7.81 (d, *J* = 8.3 Hz, 2H), 7.67 (m, 2H), 7.44 (m, 2H), 7.19 (m, 2H), 7.07–6.97 (m, 6H), 6.44 (tt, *J* = 9.0, 2.4 Hz, 2H), 6.39 (d, *J* = 7.1 Hz, 2H), 5.45 (br d, *J* = 8.8 Hz).

**Bis[(8-(3,5-bisfluorophenyl)naphthylimino)acenaphthene-nickel-dibromide] (A-4).** $NiBr_2$(DME) (0.041 g, 0.13 mmol), A-3 (0.090 g, 0.14 mmol) and anhydrous DCM (5 mL) were combined in a Schlenk tube under nitrogen. The solution was stirred at 22 °C for 18 hours. A dark red solution with precipitate formed during the course of the reaction. Volatiles were removed in vacuo, followed by addition of ~10 mL anhydrous DCM. The slurry was filtered under nitrogen over a frit filter. The vessel was evacuated and pumped directly into a dry box, where the product was isolated as a dark red powder (0.065 g, 57%).

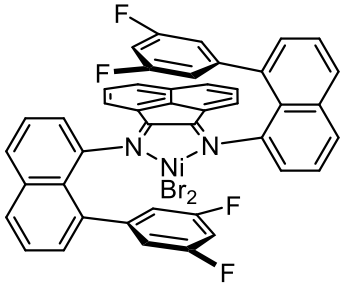


**Synthesis of Triblock Copolymer using A-4**

Similar to the procedure used in Chapter 2, section 2.4.4, a triblock copolymer from 1-decene (0.2 M) and ethylene (16 psig) was produced in chlorobenzene (40.5 mL) with **A-4** (16.2 mg, 18.5 μmol) activated with MAO (0.215 g, 3.7 mmol). The

polymerization was quenched with MeOH and precipitated into acidic MeOH. The resulting polymer was filtered, dried, and analyzed.

**Table A1.** Triblock Copolymer Data for Complex **A-4**

| entry[a] | $t_{(total)}$ (h) | $t_1$–$t_2$–$t_3$ (h) | $M_n$ total[b] (kDa) | block sizes[b] (kDa) | $M_w/M_n$[b] | hard content (%) | $T_m$[c] (°C) |
|---|---|---|---|---|---|---|---|
| 1 | 11.3 | 4–0.8–6.5 | 114 | 16–76–21 | 1.10 | 32 | 94 |
| 2[d] | 8.8 | 3–0.8–5 | 78 | 13–53–12 | 1.30 | 32 | 25, 98 |

[a]Conditions: catalyst = 1 eq, MAO = 200 eq, [1-decene] = 0.2 M, ethylene = 1.1 atm, PhCl = 78 mL. [b]Determined by high temperature gel permeation chromatography (GPC). [c]Determined by differential scanning calorimetry (DSC). [d]Synthesized with complex **2.2** from Chapter 2 under identical conditions.

**Table A2.** Mechanical Properties of Triblock Copolymers

| entry | cat. | E[a] (MPa) | ε[b] (%) | σ[c] (MPa) | SR[d] *(%)* |
|---|---|---|---|---|---|
| 1 | **A-4** | 8.7 | 783 | 12.7 | 92 |
| 2 | **2.2** | 14.4 | 710 | 23.9 | 80 |

[a]E = Young's Modulus. [b]ε = Strain at break. [c]σ = Stress at break. [d]SR = strain recovery after 10 cycles of 300% strain.

Complex **A-4** activated with MAO produces triblock copolymers with improved elastic strain recovery compared to materials produced by complex **2.2**/MAO discussed in chapter 2. We hypothesize that the more amorphous midblock generated by this system limits strain-induced crystallization, thus giving materials with improved recovery. The stress at break of the new material is half of the materials produced by complex **2.2**. This suggests that the crystallinity present in the midblock produced by **2.2** provides additional structural integrity. Complex **A-4**/MAO also exhibits highly

living behavior (PDI of triblock copolymer = 1.1), allowing for discrete block materials to be accessed. This complex requires characterization and should be pursued further.

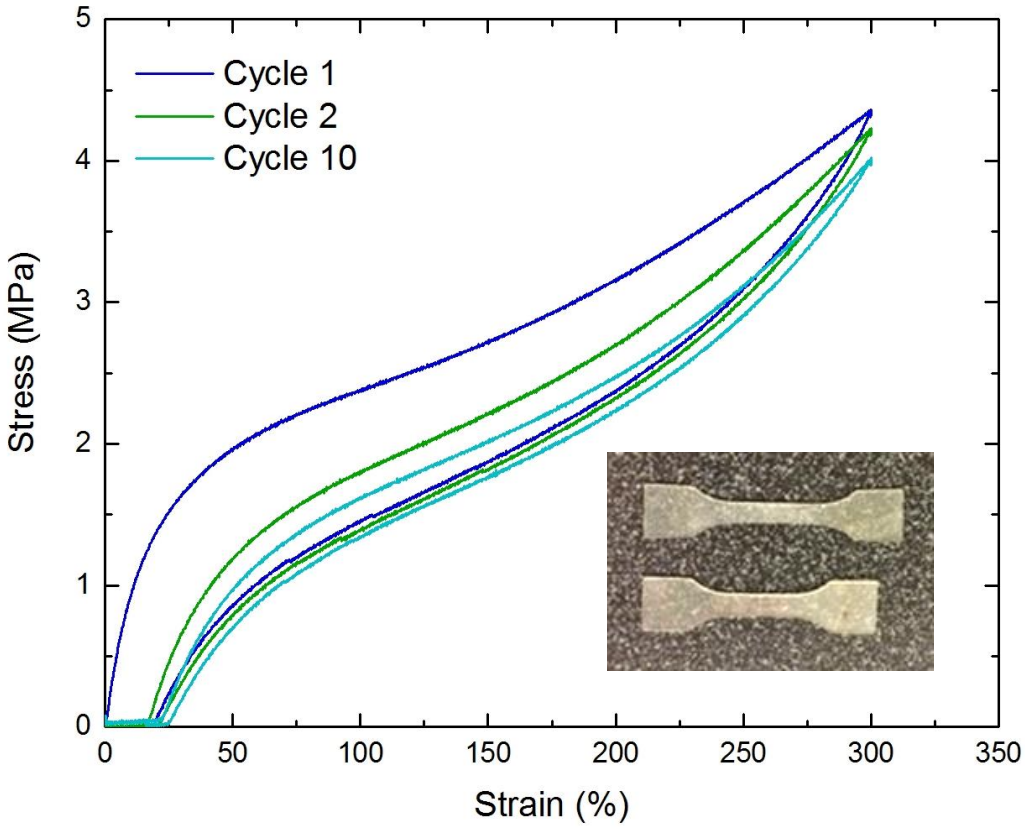


**Figure A1.** Hysteresis curve for triblock copolymer produced by complex **A-4**/MAO. The material was cycled 10 times to 300% strain at a rate of ~100% strain/min. The calculated strain recovery for this material is 92%. The top tensile bar depicted has undergone strain-induced deformation, while the bottom tensile bar is before deformation.